Vol. 128, Nos. 1–6

September–October, 1959

PROCEEDINGS OF THE ACADEMY OF SCIENCES

OF THE USSR

(DOKLADY AKADEMII NAUK SSSR)

Physical Chemistry Section

A publication of the Academy of Sciences of the USSR

IN ENGLISH TRANSLATION

Year and issue of first translation:
Vol. 112, Nos. 1-6 Jan.-Feb. 1957

Annual subscription	*$160.00*
Single issue	*35.00*

Copyright 1960
CONSULTANTS BUREAU ENTERPRISES, INC.
227 West 17th Street, New York, N. Y.

A complete copy of any paper in this issue may be purchased from the publisher for $5.00

Note: The sale of photostatic copies of any portion of this copyright translation is expressly prohibited by the copyright owners.

Printed in the United States of America

PROCEEDINGS OF THE ACADEMY OF SCIENCES OF THE USSR

Physical Chemistry Section

Volume 128, Numbers 1-6 September-October, 1959

CONTENTS

	PAGE	RUSS. ISSUE	RUSS. PAGE
Peculiarities of Anodic Oxidation on Germanium. E. A. Efimov and I. G. Erusalimchik	743	1	124
The Effects of High Pressure on the Dielectric Loss in Polymers. L. A. Igonin, Yu. V. Ovchinnikov, and V. A. Kargin	747	1	127
The Standard Entropies of Certain Lactams. V. P. Kolesov, L. E. Paukov, S. M. Skuratov, and É. A. Seregin	751	1	130
A Study of Capillary Osmosis in Gases. B. V. Deryagin and G. A. Batova	755	2	323
Molecular Energies of Alkaline Earth Halides Calculated on the Basis of an Ionic Model. K. S. Krasnov	759	2	326
Diffusion and Solubility of Tantalum in Germanium. A. V. Sandulova and He Yu-Liang	763	2	329
The Dielectric Properties of Netted Rubberlike Swollen High Polymers in Solvent–Nonsolvent Binary Systems. G. L. Starobinets and V. F. Tikavyi	767	2	333
The Appearance of Thixotropic Structure in Solutions and in Two-Sided Films Containing Sucrose and Aerosol-OT and the Effect of this Structure on the Stability of Foams. A. A. Trapeznikov and K. V. Zotova	771	2	337
The Kinetics of Acid-Catalyzed Decomposition of Arylalkyl Hydroperoxides. V. A. Shushunov and Yu. A. Shlyapnikov	775	2	341
Cation Mobility in Molten Phosphates. O. A. Esin and G. A. Teterin	779	3	567
The Problem of Chain Interaction in Complex Chain Reactions. V. F. Tsepalov	785	3	571
The Effect of Alloying Elements on the Corrosion and Electrochemical Behavior of Titanium. V. V. Andreeva and V. I. Kazarin	791	4	748
The Law of Darkening of the Photographic Emulsion in the Region of Solarization. E. A. Galashin	795	4	752
The Kinetic Laws of Autocatalytic Reactions in Open Systems. E. T. Denisov, Z. K. Maizus, I. P. Skibida and N. M. Émanuél'	799	4	755
The Measurement of the Electrical Conductivity of KI in Nonaqueous Solutions at High Pressures. Yu. A. Ershov, M. G. Gonikberg, M. B. Neiman, and A. A. Opekunov	803	4	759
The Null-Charge Potentials of Tellurium–Thallium Alloys. V. A. Kuznetsov, V. I. Aksenov and M. P. Kletsova	807	4	763
The Rapid Addition of Chlorine to a Double Bond at Low Temperatures. V. A. Lishnevskii and G. B. Sergeev	811	4	767

CONTENTS (continued)

	PAGE	RUSS. ISSUE	RUSS. PAGE
The Adsorption Characteristics of High-Molecular Hydrocarbons of Composite Structure. S. R. Sergienko, L. N. Kvitkovskii, Yu. T. Gordash and Al. A. Petrov	813	4	769
A Study of the Rates of Simultaneous Electrochemical Reactions. T. A. Fatueva and A. T. Vagramyan.	817	4	773
The Influence of Surface Active Lubricants on Frictional Shear Resistance. I. S. Avetisyan and G. I. Epifanov	821	5	973
The Mechanism of the Vaporization of Beryllium in High Vacuum. V. M. Amonenko, L. N. Ryabchikov, G. F. Tikhinskii and V. A. Finkel'	825	5	977
Measurements of the Vapor Pressure of Solid Beryllium Oxide. L. P. Belykh and A. N. Nesmeyanov	827	5	979
An Investigation of the Interaction of Crossed Polarized Metallic Filaments in Electrolytic Solutions for the Simulation of Coagulation Effects, and the Determination of Null-Charge Potentials and the Van Der Waals' Force Constant. T. N. Voropaeva, B. V. Deryagin and B. N. Kabanov	829	5	981
Consecutive Electrochemical Reactions in Oscillographic Polarography. Ya. P. Gokhshtein and A. Ya. Gokhshtein.	833	5	985
The Detonation Wave Parameters of Trotyl, Hexogen, Nitroglycerin and Nitromethane. A. N. Dremin and P. F. Pokhil	839	5	989
The Zinc Tungstate, Hydrogen Equilibrium and the Thermodynamic Properties of $ZnWO_4$. L. A. Zharkova, Ya. I. Gerasimov, T. N. Rezukhina and Yu. P. Simanov	843	5	992
The Theory of Thermal Chain Flame Propagation in Systems with Branching Chain Reactions. L. A. Lovachev	847	5	995
The Theory of Catalytic Selectivity and Bond Energies. V. Kh. Matyushenko	851	5	999
The Mechanism of the Action of Low Melting Alloys on the Mechanical Properties of Metals of Higher Melting Point. N. V. Pertsov, Yu. V. Goryunov, L. A. Kochanova and V. I. Likhtman	855	5	1003
The Mechanism of Electroreduction of the $Fe(CN)_6^{3-}$ Anion of the Dropping Mercury Electrode. A. N. Frumkin, O. A. Petrii and N. V. Nikolaeva-Fedorovich	859	5	1006
The Equilibrium Distribution of Deuterium during Hydrogen Exchange with Liquid Deuterium Iodide. P. P. Alykhanov and Ya. M. Varshavskii.	863	6	1214
The Solution of Metallic Magnesium in Fused Chlorides. N. G. Bukun and E. A. Ukshe	867	6	1217
Turbulent Combustion in an Enclosed Space. V. P. Karpov, E. S. Semenov and A. S. Sokolik	871	6	1220
The Spectra of Paramagnetic Electron Resonance and the Kinetics of the Accumulation of Radicals Formed during the Irradiation of Frozen Aqueous Solutions of Sodium Nitrate by Fast Electrons. Yu. N. Molin, V. A. Sharpatyi and N. Ya. Buben	875	6	1224
A Study of Absorption Layers on Liquid Metal Surfaces. N. L. Pokrovskii and D. S. Tissen	879	6	1228

CONTENTS (continued)

	PAGE	RUSS. ISSUE	RUSS. PAGE
Copolymerization of Parachlorostyrene with α-Methylstyrene and Styrene under the Action of Alkali Catalysts. Ya. L. Spirin, A. R. Gantmakher and S. S. Medvedev	883	6	1232
Molecular Orbitals of $Cr(C_6H_6)_2$ (Dibenzenechromium) $Fe(C_5H_5)_2$ (Ferrocene or Biscyclopentadienyliron) and $Co(C_5H_5)_2^+$ (Biscyclopentadienylcobalt Ion). E. M. Shustorovich and M. E. Dyatkina	885	6	1234
Critical Conditions for the Thermal Explosion of Tetryl. A. G. Merzhanov, V. G. Abramov and F. I. Dubovitskii	889	6	1238

PECULIARITIES OF ANODIC OXIDATION ON GERMANIUM

E. A. Efimov and I. G. Erusalimchik

(Presented by A. N. Frumkin, May 6, 1959)

At present we can assume as proven the fact that the rate determining step in the anodic dissolution of N-type germanium is the diffusion of holes from inside the semiconductor toward the surface [1-5]. One would therefore expect the semiconductors to have similar effects on other anode reactions. Meanwhile a study of the electrolytic oxidation of divalent vanadium on a rotating N-type germanium electrode [6] showed that the V^{++} ions were freely oxidized in that range of potentials where the rate of germanium solution was retarded by the shortage of holes. It was also shown that the rate of vanadium oxidation greatly exceeded that of hole diffusion and was only limited by the electrolytic diffusion processes.

Consequently it was interesting to establish whether this phenomenon was also typical of other oxidation reactions carried out on germanium anodes, or whether it was a property specific only for the electrolytic oxidation of vanadium. In the way of examples we picked the oxidation of oxalate and iodide anions, the kinetics of which had been well studied on platinum electrodes.

The standard oxidation potential of oxalate ($C_2O_4^{2-} = 2CO_2 + 2e^-$) is -0.49 v [7].

The end reaction product, carbon dioxide, is not a good oxidizing agent, and uplike potassium ferricyanide it cannot be reduced on germanium at high anodic potentials and remove electrons from the valence band [4].

In Fig. 1 we have plotted the potentials of N-and P-type germanium electrodes (with reference to a standard hydrogen electrode) against the current density; the specific resistivity of the electrodes was 1.5 ohm · cm and the diffusion length 0.4-0.5 mm. The curves were recorded at 20°C in 0.1 N HCl solutions free of, or containing some potassium oxalate and over a range of current densities from 10^{-4} to $2 \cdot 10^{-2}$ amp/cm^2. The technique used in our polarization measurements was similar to that described in [3].

Introduction of potassium oxalate into the solution decreased the potential on P-type germanium anodes over the entire investigated current density range. This effect was particularly pronounced at high current densities, where we were measuring the limiting hole diffusion current during the anodic dissolution of P-type germanium (Fig. 1, 1). This limiting hole diffusion current disappeared after oxalate was introduced into solution (Fig. 1, 3). When the electrode (P-type germanium) was illuminated with a 100-candle power lamp placed 20 cm away the anode potential decreased by approximately 20 mv.

Curve 3 in Fig. 1 represents a case where we have two electrochemical processes going on simultaneously on the germanium anode—the oxidation of oxalate and anodic solution of germanium. The measured current output at $I = 10^{-2}$ amp/cm^2 and $2 \cdot 10^{-2}$ amp/cm^2 showed that in both cases the fraction of charge used to oxidize the oxalate was the same and equal to 25-28%.

Figure 1 shows that the oxidation of the oxalate which proceeded simultaneously with the solution of germanium greatly enhanced the rate of the latter in the range of potentials where the electrode reaction was kinetically limited by the diffusion of holes from inside the semiconductor to the surface. One gets the impression that the anodic oxidation of $C_2O_4^{2-}$ somehow increased the concentration of holes at the germanium surface, and thus facilitating the solution process.

In our opinion this effect was connected with the following phenomena. In the first place, the oxidation

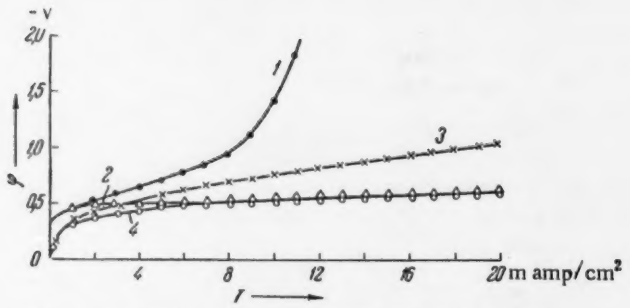

Fig. 1. Polarization of a germanium anode in the presence of $K_2C_2O_4$. 1) N-type germanium in 0.1 N HCl; 2) P-type germanium in 0.1 N HCl; 3) N-type germanium in 0.1 N HCl + 1.0 N $K_2C_2O_4$; 4) P-type germanium in 0.1 N HCl + 1.0 $K_2C_2O_4$.

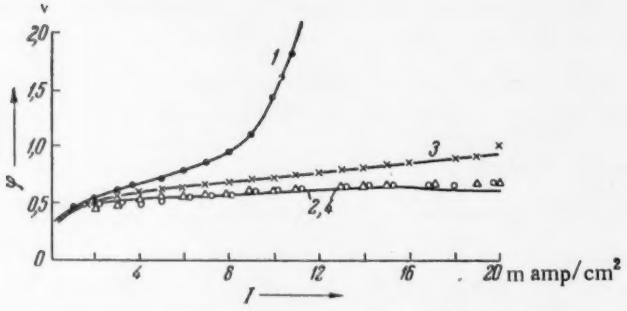

Fig. 2. Polarization of a germanium anode in the presence of KI. 1) N-type germanium in 0.1 N HCl; 2) P-type germanium in 0.1 N HCl; 3) N-type germanium in 0.1 N HCl + 1.0 N KI; 4) P-type germanium in 0.1 N HCl + 1.0 N KI.

of oxalate did not involve the use of holes, but an injection of electrons into the germanium anode, or else Curve 3 would have given us the hole saturation current. Therefore this process could not be limited by the diffusion of holes from inside the electrode. In the second place, as a result of oxalate oxidation the injection process would tend to increase sharply the electron concentration on the germanium electrode surface. This turns out to be quite reasonable if we consider the fact that within the studied current density range the germanium surface was positively charged [8], i.e., that the energy bands were convex toward the surface and hence the electron concentration at the surface was much lower than inside the semiconductor. Electron injection would give rise to strong electric fields inside the surface layers of germanium; these fields would in turn promote the formation of even more holes on account of drifting or local generation. All this accelerated the anodic solution of germanium, which involved the participation of holes and was only limited by their concentration at the germanium–electrolyte interface.

On P-type germanium (Fig. 1, 4) only at low current densities (up to $6 \cdot 10^{-3}$ amp/cm^2) was the potential decreased by the oxidation of the oxalate. At higher current densities, where (as the measured current yields have shown) only the anodic solution of germanium occurred, the presence of $C_2O_4^{2-}$ in solution had no effect on the anode potential.

It should be noted that the pock marks usually formed during anodic solution of germanium at high current densities were much less pronounced when oxalate was present in solution. This once again confirmed the fact that in this case the number of holes on the germanium surface had increased.

Similar phemonena were also observed after potassium iodide was introduced into solution (Fig. 2). Here again we failed to observe the limiting hole diffusion current during the oxidation of iodide ions due to the injection of electrons into germanium. Besides, it seems that in this case we also had an additional process which helped accelerate the anodic dissolution of germanium.

The oxidation of iodide is a thermodynamically reversible process. The standard electrode oxidation potential for this reaction is +0.53 v. Hence, it is reasonable to assume that iodine (the end reaction product) could undergo reduction on the anode by capturing electrons from the valence band. As was shown by Gerischer and Beck [4] this should create an additional number of holes in the surface layer of germanium and consequently help depolarize the anodic dissolution.

Visual observations supported the possibility of iodine reduction . Thus, we did not detect the deep yellow coloration characteristic of iodine solutions during electrolysis. Besides, in this case we had an almost 100% current output from the anodic dissolution of germanium. Evidently the iodide acted solely as a "charge carrier" promoting the exchange of electrons between the valence band on the conduction band.

Thus on the basis of the data found in the literature [1-6] and the experimental results obtained in our work it was possible to conclude that only one electrochemical reaction—the anodic dissolution of germanium (which destroyed the crystal lattice) was limited by the diffusion of holes from inside the semiconductor to the electrode surface. Other oxidation reactions proceed not by the use of holes, but through the injection of electrons. In such cases, due to the specific properties of semiconductor electrodes, the concurrent reaction of anodic dissolution of germanium will be accelerated.

LITERATURE CITED

[1] W. Brattain and C. Garrett, Bell. Syst. Tech. J. 34, 129 (1955).

[2] D. Turner, J. Electrochem. Soc. 103, 252 (1956).

[3] E. A. Efimov and I. G. Erusalimchik, J. Phys. Chem. 32, 413 (1958).

[4] H. Gerischer and F. Beck, Z. Phys. Chem. 13, 389 (1957).

[5] J. Flynn, J. Electrochem. Soc. 105, 715 (1958).

[6] Yu. V. Pleskov and B. N. Kabanov, Proc. Acad. Sci. USSR 123, 884 (1958).*

[7] W. Latimer, Oxidation Potentials (IL, 1954), pp. 65, 136 [Russian translation].

[8] E. A. Efimov and I. G. Erusalimchik, J. Phys. Chem. 33, 441 (1959).

Received May 4, 1959

* Original Russian pagination. See C. B. Translation.

THE EFFECTS OF HIGH PRESSURE ON THE DIELECTRIC LOSS IN POLYMERS

L. A. Igonin, Yu. V. Ovchinnikov, and Academician V. A. Kargin

State Scientific Research Institute of Plastics

In a previously published paper [1] it was shown that over a certain temperature range a high compression of granulated or powdered polymers produced certain vitrification phenomena. Consequently, at any single compression temperature there will be two pressure limits defining the range of pressures at which polymer grains are fused together and the boundary of separation disappears. We proposed a theory that this phenomenon should be attributed to a reduced mobility of polymeric molecular chain segments under the applied high pressure.

It was interesting to try and detect such a change in the polymeric chain mobility under high pressures by using another independent method. For this purpose we picked the method involving a determination of the temperature dependence of the dielectric loss (tan δ) in polymers under various external pressures. At the present time it is well established that many polar polymers exhibit two dielectric loss maxima, which are due to two relaxation processes [2]. G. P. Mikhailov [3] described these two maxima as due to dipole–radical and dipole–elastic losses. The dipole–radical loss, which takes place at temperatures below the T_g for the polymer, is caused by the thermal motion of the radicals (polar monomeric chains, side groups) attached to the polymer chains. The dipole–elastic loss observed above T_g is connected with the thermal movement of individual polymeric chain segments, i.e., with extreme elastic properties of polymers. It is noteworthy that when plasticizers are introduced into a polymer the dipole–elastic loss maximum becomes displaced toward lower temperatures [4] as the elasticity of the polymer increases. Therefore when high pressure is applied to a polymer, one would expect just the opposite effect–displacement of the dipole–elastic loss maximum toward higher temperatures. At the same time we could conduct a general study of polymers in a hard solid state.

To measure the temperature dependence of the dielectric loss in polymers we constructed a specially designed press-forge (Fig. 1), which enabled us to determine tan δ over a wide range of temperatures and pressures. A polymer sample (a) in the form of a flat disc 38 mm in diameter and 0.2-0.3 mm thick was placed over the measuring electrode (b), and was insulated from the press material (c) by means of a Teflon jacket (d). The wire connecting this electrode to the measuring bridge was insulated with a quartz sleeve and a Teflon jacket (d). The upper punch (a) was grounded and served as the other electrode. The sample temperature was measured with a thermocouple introduced through the channel (f) of the upper punch. The sample was compressed through hydraulic pressure applied to the upper punch. We heated the press by placing it inside of a cylindrical electric heating mantle. Before each measurement the sample was maintained for 30 min under the required pressure at the experimental temperature. The dielectric loss was measured directly on a MLE-1 bridge at frequencies of 400, 1000, and 5000 hertz. The study was carried out on polyvinylchloride, polymethyl acrylate, and polymethyl methacrylate. The first two polymers showed pronounced and well resolved dipole–elastic loss maxima within the range of our frequencies, whereas in polymethyl methacrylate the two maxima overlapped and one could observe only a single spread-out strong maximum [5]. In Fig. 2 we have plotted our experimentally determined tan δ as a function of temperature for polymethyl acrylate under various pressures at a frequency of 5000 hertz. We can see that as the pressure on the sample was increased the tan δ maximum in the region of the dipole–elastic loss shifted over toward higher temperatures. A similar relationship was observed with polyvinyl chloride.

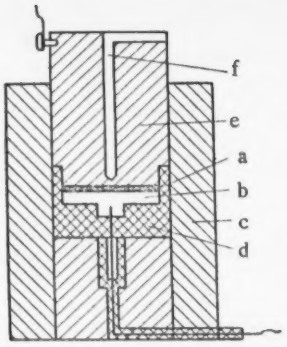

Fig. 1. The press-forge used for measuring the temperature dependence of tan δ in polymers under various pressures.

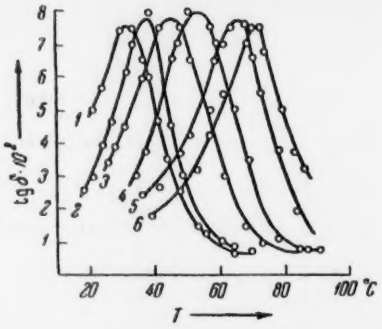

Fig. 2. Tan δ of polymethyl acrylate as a function of temperature at a frequency of 5000 hertz and various pressures. 1) Atm. pressure; 2) 306 kg/cm²; 3) 612 kg/cm²; 4) 1224 kg/cm²; 5) 1836 kg/cm²; 6) 2448 kg/cm².

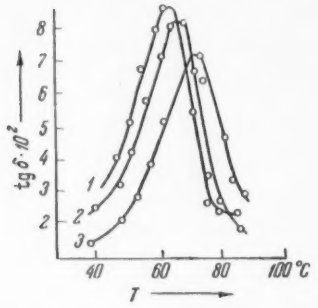

Fig. 3. Tan δ of polymethacrylate under a pressure of 2448 kg/cm² as a function of temperature and frequency: 1) 400 cps; 2) 1000 cps; 3) 5000 cps.

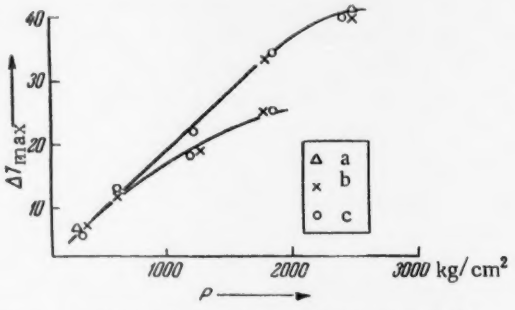

Fig. 4. Shift of the maximum dipole–elastic loss temperature as a function of pressure for polymethyl acrylate (upper curve) and polyvinyl chloride. a) 400 hertz; b) 1000 hertz; c) 5000 hertz.

In Fig. 3 we plotted the temperature dependence of tan δ of polymethyl acrylate at various frequencies under 2448 kg/cm². At each fixed pressure the dipole–elastic loss maximum would shift toward higher temperatures with increasing frequencies. In other polymers studied by us we observed a similar temperature and frequency dependence. In Fig. 4 we have shown the shift of the maximum dipole–elastic loss temperatures as the pressure on polymethyl acrylate and polyvinyl chloride was increased. For polymethacrylate over a wide range of pressures we found the ΔT_{max} shift to be a linear function of pressure, while nonlinearity appeared only above 2000 kg/cm². With polyvinyl chloride this nonlinearity was detected above 1000 kg/cm². It seems that the nonlinear relationship between ΔT_{max} and pressure is a general effect and is connected with the increasing influence of elastic (Hook's) deformations in polymers at high pressures. In polymers containing more rigid chains the vitrification effects were detected at lower pressures [6]. Presumably this may be responsible for the fact that the attenuation of the shift in maximum ΔT as a function of pressure was more rapid in polyvinyl chloride than in polymethyl acrylate. Thus the data obtained in this work confirm the fact that under an all-sided compression the molecular chains in polymers lose some of their mobility. It seems that the principal cause of this effect is the increasingly tight packing of polymers resulting from the applied pressure. The effects of any internal changes in chain flexibilities should also have shown up, but they probably played a secondary role.

In concluding we wish to express our gratitude to Prof. P. G. Mikhailov for discussing with us the experimental results and giving us valuable advice, and to S. P. Kabin for assisting us with the experimental work.

LITERATURE CITED

[1] L. A. Igonin, Yu. V. Ovchinnikov, and S. A. Arzhakov, Proc. Acad. Sci. USSR 120, 5 (1958).*

[2] P. P. Kobeko, G. P. Mikhailov, and Z. I. Novikova, J. Tech. Phys. 14, 24 (1944).

[3] G. P. Mikhailov, J. Tech. Phys. 21, 1395 (1951).

[4] G. P. Mikhailov, T. I. Borisova, and D. A. Dmitrochenko, J. Tech. Phys. 26, 1924 (1956).

[5] G. P. Mikhailov, Progr. Chem. 24, 875 (1955).

[6] L. A. Igonin and Yu. V. Ovchinnikov, Chemistry and Chemical Technology, Coll. Works, Gor'kii, 1959.**

Received June 9, 1959

*Original Russian pagination. See C. B. Translation.

**In Russian.

THE STANDARD ENTROPIES OF CERTAIN LACTAMS

V. P. Kolesov, I. E. Paukov, S. M. Skuratov, and

E. A. Seregin

M. V. Lomonosov Moscow State University

(Presented by Academician P. A. Rebinder, May 13, 1959)

Although in recent years there has been a great increase in the number of papers dealing with the determination of heat capacities at low temperatures for the purpose of calculating the absolute entropies of compounds, still the data available for organic compounds is very scant. Alkanes and alkenes have been most thoroughly investigated. Among the various series of cyclic compounds the only reliable data are available for rings from 3 to 8 members. No absolute entropy data are available for any heterocyclic compounds. Meanwhile these data are essential for calculating the free energy changes in various reactions involving heterocyclic compounds, particularly in polymerization reactions. Attempts to calculate absolute entropies from semiempirical equations did not yield sufficiently precise results. Thus, for example, when Dainton [1] calculated the absolute entropies of liquid cycloheptane and cyclooctane at 298.16°K by what appeared to be a very fundamental method, he obtained 54.8 and 53.0 e.u. respectively, while the values calculated from experimental heat capacities were 57.97 and 62.62 e.u. [2]. Small's [3] attempts to calculate the entropies of heterocyclic compounds did not yield any reliable results either. In the present communication we have reported the results of our heat capacity measurements at low temperatures (in the 60-350° K temperature range) and the melting points of 5 to 8 membered lactams, i.e., α-pyrrolidone, α-piperidone, ε-caprolactam, ζ-enantholactam. We also calculated the absolute entropies of these compounds at 298.16°K and 350°K.

The method used for determining the heat capacities of lactams has already been described in detail before [4].

All the lactams were purified by repeated distillation under nitrogen.* Before being placed in the calorimeter the compounds were dried for several days over phosphorus pentoxide. Unfortunately, despite careful purification some compounds were still insufficiently pure. During the heat capacity determination we detected the following amounts (in mole %) of impurities; 0.12 in α-pyrrolidone, 0.98 in α-piperidone, 0.05 in ε-caprolactam, and 0.29 in ζ-enantholactam. All the operations involved in filling the calorimeter with the compounds were performed inside a drybox. In order to prevent exposing the lactams to air, the calorimeter with the sample inside was taken out of the box in a special airtight apparatus fitted out with a small soldering bit. The calorimeter was weighed in this same apparatus, filled with helium, and soldered tight. The experimentally determined heat capacities of lactams at low temperatures were used for plotting C_p vs T curves; the smoothed curve values are presented (in brief) in Table 1. The experimental points over the entire temperature range did not deviate by more than 0.1% from the smoothed curve. We used the conversion factor 1 calorie = = 4.1840 joules.

From the C_p vs T curves in Fig. 1, one can see that above approximately 150° K the heat capacity of α-piperidone increased much faster than that of other lactams. Additional measurements carried out on purer samples of α-piperidone (with 0.65 mole % impurities) confirmed the previous results. Figure 1 also shows that within the range of our measurements the heat capacities of liquid lactams were linear functions of temperature, but their slopes differed somewhat.

* The lactams were synthesized and purified at the All-Union Scientific Research Institute of Synthetic Fibers by N. F. Erofeeva and V. N. Topchebasheva.

TABLE 1

Temp., °K	Smoothed curve C_p values (cal/mole · deg)				Temp., °K	Smoothed curve C_p values (cal/mole · deg)			
	α-pyrrolidone	α-piperidone	ε-caprolactam	ζ-enantholactam		α-pyrrolidone	α-piperidone	ε-caprolactam	ζ-enantholactam
60	8,56	9,87	10,73	11,60	290	32,40	45,36	36,35	46,86
80	11,04	12,44	13,36	14,66	310	41,46		39,20	
100	12,94	14,46	15,55	17,36	320	42,43	51,19	40,83	61,62
150	16,89	19,51	20,52	23,51	335	43,90	53,19	44,82	64,02
200	21,26	26,66	25,50	30,17	350		55,20	58,43	66,42
250	26,02	34,73	31,27	37,96	370			60,89	
270	28,35	38,36	33,73	41,56					

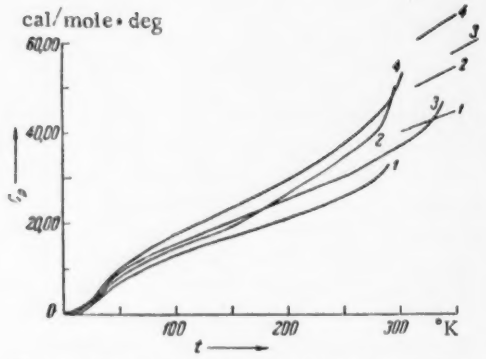

Fig. 1. Heat capacities of lactams. 1) α-Pyrrolidone; 2) α-piperidone; 3) ε-caprolactam; 4) ζ-enantholactam.

TABLE 2

Compound	Melting point* °K	Heat of fusion cal/mole
α-Pyrrolidone	299.082 ± 0.014	3327 + 19 (from 3 expts)
α-Piperidone	311.85 ± 0.05	2508 + 15 (from 3 expts)
ε-Caprolactam	342.305 ± 0.002	3847 + 7 (from 4 expts)
ζ-Enantholactam	310.295	3197 (from 1 expt)

*The melting points in this table are given for absolutely pure compounds.

TABLE 3

Compound	$S^\circ_{298.16}$	S_{350}
α-Pyrrolidone	32.7	50.7
α-Piperidone	39.4	55.5
ε-Caprolactam	40.3	58.4
ζ-Enantholactam	45.4	65.3

The melting points and heats of fusion of our lactams are given in Table 2.

Until recently there was no literature data on the heats of fusion of lactams. Only the value for ε-caprolactam had appeared in print while this work was in progress; it was given as 3856 cal/mole [5].

In order to calculate the absolute entropies we extrapolated the heat capacity curves of our lactams from 60° K to 0° K by using the equations shown below, which were derived by selecting an arbitrary number of Debye-Einstein functions:

for α-pyrrolidone

$$c = D\left(\frac{125}{T}\right) + E_1\left(\frac{182}{T}\right) + E_2\left(\frac{314}{T}\right) + 5E_3\left(\frac{1000}{T}\right); \quad (1)$$

for α-piperidone

$$c = D\left(\frac{125}{T}\right) + E_1\left(\frac{155}{T}\right) + E_2\left(\frac{261}{T}\right) + E_3\left(\frac{651}{T}\right) + 3E_4\left(\frac{890}{T}\right) + 5E_5\left(\frac{1275}{T}\right); \quad (2)$$

for ε-caprolactam

$$c = D\left(\frac{110}{T}\right) + E_1\left(\frac{140}{T}\right) + E_2\left(\frac{244}{T}\right) + E_3\left(\frac{560}{T}\right) + E_4\left(\frac{654}{T}\right) + E_5\left(\frac{845}{T}\right) + 20E_6\left(\frac{1785}{T}\right); \quad (3)$$

for ζ-enantholactam

$$c = D\left(\frac{124}{T}\right) + E_1\left(\frac{148}{T}\right) + E_2\left(\frac{184}{T}\right) + 2E_3\left(\frac{505}{T}\right) + E_4\left(\frac{688}{T}\right) + \\ + E_5\left(\frac{960}{T}\right) + 10E_6\left(\frac{1485}{T}\right). \quad (4)$$

The agreement between Eqs. 1-4 and the experimental heat capacity curves for our lactams was better than ± 0.2% in the 60-170° K temperature range. In Table 3 we have listed the standard absolute entropies of solid lactams at 298.16° K and of liquid lactams at 350° K. We believe that these entropies are not off by more than 0.4 e.u.

The data obtained in this work constitute the only case of experimentally determined absolute entropies for a series of heterocyclic compounds, and in that sense deserve a special attention. Currently it is still difficult to use them to calculate the ΔF for lactam polymerization, for the simple reason that we do not as yet have a sufficient amount of data on the entropies of linear polyamides.

LITERATURE CITED

[1] F. S. Dainton and K. J. Ivin, Quart. Rev. 12, No. 1, 61 (1958).

[2] H. L. Finke, D. W. Scott, and M. E. Gross, J. Am. Chem. Soc. 78, 5469 (1956).

[3] P. A. Small, Trans. Farad. Soc. 51, 1717 (1955).

[4] M. M. Popov and V. P. Kolesov, J. Gen. Chem. 26, 2385 (1956).*

[5] S. V. R. Mastrangelo, Anal. Chem. 29, 841 (1957).

Received May 12, 1959

*Original Russian pagination. See C. B. Translation.

A STUDY OF CAPILLARY OSMOSIS IN GASES

Corresponding Member Academy of Sciences, USSR

B. V. Deryagin and G. A. Batova

Institute of Physical Chemistry of the Academy of Sciences, USSR

The existence of osmotic pressure in gases can be demonstrated in the oxygen–hydrogen system if we separate the two gases by a platinum partition which at high temperatures is permeable to hydrogen but not to oxygen.

In contrast to such classical osmosis, by the term of capillary osmosis we mean the appearance of a drop in the total pressure across a porous partition which separates a mixture of two gases (or vapors) at various concentrations and is fully permeable to any one type of molecule. In this case after the equilibrium is established the mixtures assume equal concentrations on both sides of the partition, and consequently we can only speak of a nonequilibrium, quasi-osmotic pressure which only persists until the thermodynamic equilibrium is established and remains constant as long as there is any process which may continually compensate the concentration changes in one of the mixture components by diffusion through the partition. As an example we can use two cells in one of which a constant vapor pressure is maintained (by means of a drying agent or liquid water), while the other is open to the air.

One of the first to discover capillary osmosis in gases was Shidlovskii (1886), an Army doctor and a travel companion of Admiral Makarov; his particular contribution was the application of the above-mentioned methods as a means of "stabilizing" the total pressure drop on both sides of the partition. At the same time he attributed the appearance of a pressure drop, where at first there wasn't any, to a difference between the diffusion rates of molecules with different molecular weights.

It is quite obvious that, strictly speaking, such a simplified treatment of this effect would only be reasonable if both kinds of molecules diffused through the partition independently of each other, and this would only be feasible if $\lambda >> d$, where λ is the mean free path, and d the pore diameter (that is under conditions of Knudsen's flow). In such a case by using the laws for Knudsen's flow one can easily calculate the increase in the pressure drop with time. More often, however, one achieves the reverse conditions, $\lambda << d$, where, in the first place, the "mixing" of gas molecules in the partition pores will occur through a free diffusion mechanism obeying Fick's law

$$Q = D_{12} S \operatorname{grad} C,$$

where S is the total cross-sectional area of the pores, Q the diffusion current of one gas in moles/sec · cm^2, D_{12} a mutual diffusion coefficient, and grad C the water vapor concentration gradient across the partition; in the second place, we can have in such a case a convection current of the gaseous mixture in the pores, which would (in the first approximation) obey Poiseuille's law for viscous flow through a capillary

$$Q = \frac{S\beta\Delta P_1}{\eta V \Delta h},$$

where Q is the convection current, β a filtration coefficient, η air viscosity, V volume of the gaseous mixture

containing a mole of the given gas, ΔP_1 the hydrostatic pressure drop across the porous partition, Δh the width of the porous partition.

The theory of diffusion instruments (hygrometers [2]) developed at the Physical Chemistry Institute of the Acad. Sci. USSR was based on a simultaneous consideration of Fick's and Poiseuille's Laws. At the same time we ignored the possibility that in presence of a concentration gradient down the pore length the gaseous mixture may slide by the walls; Epstein [3] and other workers found that a temperature gradient may cause thermal sliding and produce thermophoresis of aerosol particles. In other words, we ignored any surface phenomena connected with the collisions of gas-vapor molecules on the walls which might have caused similar effects. The additional convection current resulting from this may influence not only the instrument parameters but also its lag. The study and calculation of this current is not only important for the perfection of the diffusion hygrometer theory, but also for the study of aerosols.

Actually, when an aerosol particle finds itself in a diffusion current it may undergo some sliding relative to the gaseous mixture on account of the tangential concentration gradients on the particle surface, in other words, the particle will acquire a motion relative to the center of gravity of the surrounding gas molecules in the reverse or the same direction as the diffusion current. Thus the theory derived by Deryagin and Dukhin [4] for the movement of aerosol particles in diffusion fields, which was based on convective diffusion equations and also took into account the carrying of particles in a Stefan's current, requires a certain correction for the sliding effects caused by concentration gradients.

Deryagin and Bakanov [5] calculated the exact movement of aerosol particles relative to a Stefan's current for particles smaller than the mean free path of gas molecules. The velocity of particles will be reduced to zero when the following conditions are fulfilled simultaneously: 1) all molecules in the mixture have the same mass, and 2) the number of molecules per unit volume when multiplied by their effective diameters gives the same product throughout the gas.

They also examined the case where a very porous partition separated two vessels containing gaseous mixtures at different concentrations. To be more precise, they were able to solve the case of gas flow under pseudo-molecular conditions, which required the use of partitions with a high porosity coefficient δ and a fixed ratio between the specific partition surface S and the mean free path of gas molecules

$$\frac{4(1-\delta)}{S_0} < \delta < \frac{4\delta}{S_0}.$$

So far no measurements have been carried out under these conditions, hence a quantitative comparison with the theory is not possible.

As a result of the capillary-osmotic flow caused by the sliding of the gaseous mixture relative to the pore walls the pressure in one chamber increases and in another decreases. Gradually the increase in the pressure drop will be slowed down due to a convection counter-current caused by the absolute pressure drop which had arisen. Finally, we will achieve a quasi-stationary state where the two currents will be mutually compensating. Meanwhile, however, the concentrations on each side of the partition will become equal. Consequently the pressure drop will gradually begin to decline, eventually approaching zero.

The purpose of the current work was to experimentally study the flow of gaseous mixtures through a porous partition (in the absence of any initial pressure difference) and the pressure drop which later appears on account of this flow.

The apparatus used for studying the capillary osmosis (Fig. 1) consisted of two cells (1 and 2) separated by a 9 mm thick (9 pieces) microporous rubber partition (P) with a 56-60% porosity and 0.2-0.4 micron average pore diameter. The cells were first evacuated then filled with the studied gases (Fig. 2) through appropriate inlets. A mercury seal (Fig. 1, 7) separated the two cells while they were being filled. By means of a magnetic stirrer (M) the gas distribution was maintained even throughout each cell. The cells were connected via a U-shaped manometer (3) which measured the absolute pressure drop across the porous partition and were also attached to mercury manometers (4, 5) which measured the pressure in each cell when the experiment was carried out at pressures below atmospheric. In order to maintain the same pressure in both cells while they were being filled

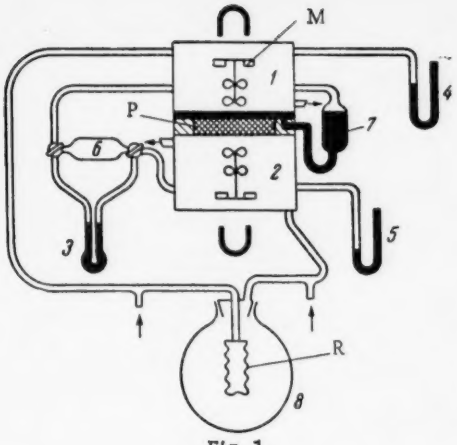

Fig. 1

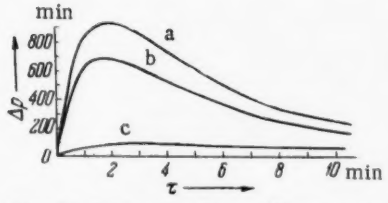

Fig. 2. Curves for the capillary-osmotic effect. a) Argon–helium b) nitrogen–helium; c) argon – nitrogen.

we made use of a glass bulb (8) which was partitioned in two by a loosely hanging rubber membrane (R). Both sides of this vessel were connected to the gas lines. In addition to this appliance, stopcocks were used to adjust the final pressure after the cells had been filled. A cylinder (6) was placed between the two stopcocks so as to avoid mixing the gases in the cells (1 and 2) during the final adjustment.

After this the mercury seals were opened, the stirrers were turned on, and measurements were begun. We investigated systems containing gases of different molecular weights: nitrogen–argon, nitrogen–helium, and argon–helium.

Throughout the experiment the temperature was maintained at 21-22°C.

The resultant curves (Fig. 2) were characteristic for the capillary- osmotic effect. The greater the difference between the gas masses the larger the effect. It is also possible to study a case of mutual diffusion between two gases with equal molecular weights, where there is no Stefan's current and the capillary osmosis arises because of a difference between the molecular radii of the two gases. We studied in this way the ethylene–nitrogen system. Preliminary results indicate that the effect is also present in this case, although to a lesser extent.

LITERATURE CITED

[1] F. Shidlovskii, J. Russ. Phys. Chem. Soc. Phys. Series 18, 182 (1886).

[2] B. V. Deryagin P. S. Prokhorov, et al., J. Tech. Phys. 26, 887 (1956).

[3] P. Epstein, Zs. Phys. 54, 537 (1929).

[4] B. V. Deryagin and S. S. Dukhin, Proc. Acad. Sci. USSR 106, 851 (1956).

[5] B. V. Deryagin and S. P. Bakanov, Proc. Acad. Sci. USSR 117, 959 (1957).*

Received June 5, 1959

*Original Russian pagination. See C. B. Translation.

MOLECULAR ENERGIES OF ALKALINE EARTH HALIDES CALCULATED ON THE BASIS OF AN IONIC MODEL

K. S. Krasnov

Ivanov Institute of Chemical Technology

(Presented by Academician A. A. Grinberg, May 11, 1959)

The chemical bond in alkaline earth metal halides (denoted below by MeX_2) is of an intermediate type between purely ionic (NaF type) and ultimate covalent (Cl_2 type). The analysis of properties and structural parameters of molecules possessing such bonds can be achieved by approaching the problem from the covalent or ionic standpoint. There is ample evidence in the literature [1-4] that both treatments are possible. "If the predominant interaction is ionic then it is advisable to represent the bond in terms of electrostatic and polarization effects" [2]. The percent ionic character of a bond is usually the best criterion for deciding to which of the two limiting cases should the true bond be referred. The percent ionic character of bonds in MeX_2 molecules (determined from the difference in electronegativities by Pauling's or Gordy's methods) vary from ~ 50% in BeI_2 and MgI_2 to 200% in BaF_2.

This extremely crude approximation still tells us that most MeX_2 molecules can be treated from an ionic standpoint.

In order to determine the nature of the predominant interaction in a given bond it is extremely important to calculate the bond energy by starting from a definite model. In the present communication we will derive an equation for the bond energies in MeX_2 molecules on the basis of an ionic model (with the ionic polarization taken into account), and we will show that the calculated results are in good agreement with thermal data.

By molecular energy of MeX_2 we mean the energy change which occurs when a MeX_2 molecule is formed (at 0°K) by bringing a Me^{++} and two X^- ions from infinity to the equilibrium distance M−X, equal to r_0.

According to Böttcher [5] the electrostatic interaction energy between two polarizable ions, Me^{++} and X^-, is

$$W' = -\frac{Ze^2}{r} - \frac{4\alpha_1\alpha_2/r^3 + Z^2\alpha_2 e^2 + \alpha_1 e^2}{2r^4(1 - 4\alpha_1\alpha_2/r^6)}. \qquad (1)$$

where Z is the ionic charge (in our case 2), α_1 and α_2 the polarizabilities of the cation and anion respectively. The MeX_2 molecules are linear and symmetrical [6]. Therefore for the entire molecule Eq. (1) has to be doubled. From this, after taking into account the electrostatic repulsion between the two anions (equal to $+e^2/2r$) and neglecting the polarizability of the cation and the repulsion between the dipoles induced in the anions ($+\alpha_2^2 e^2/16r^7$), we will get the electrostatic interaction energy in a MeX_2 molecule:

$$W = -\frac{3{,}5e^2}{r} - \frac{4\alpha_2 e^2}{r^4}. \qquad (2)$$

The total molecular energy will be

$$U = W + 2Ae^{-r/\rho} - \frac{c}{r^6} + \sum \frac{h\nu_0}{2} . \quad (3)$$

The second term in Eq. (3) gives the quantum-mechanical repulsion between the Me^{++} cation and X^- anions; the third gives the van der Waal's attraction energy between ions. The last term gives the zero vibrational energy. The c/r^6 term can be dropped since we have disregarded the polarizability of the cation. Hence we will get

$$U = W + 2Ae^{-r/\rho} + \sum \frac{h\nu_0}{2} . \quad (4)$$

Determining the constant A from the equilibrium condition $[du/dr]_{r = r_0} = 0$, for the equilibrium distance R_0 we will get an energy

$$V_0 = -\frac{3,5}{r_0}\left(1 - \frac{\rho}{r_0}\right) - \frac{4\alpha_2 e^2}{r_0^4}\left(1 - \frac{4\rho}{r_0}\right) + \sum \frac{h\nu_0}{2} . \quad (5)$$

In calculating V_0 by means of Eq. (5) we used the Me–X bond length determined by electron diffraction with an accuracy of 0.02-0.03 A (1%) [6].

The value of ρ was the same (0.338 A) as that used for alkali halides [7]. The values of α were taken from Pauling [8]. The zero energies can be neglected since their values for $BeCl_2$ and $MgCl_2$ (whose vibrational frequencies are known [4]) constitute only 0.6 and 0.3% of V_0. For the remaining heavier molecules it should be even less.

TABLE 1

Molecular Energies

Molecule	$-V_0$	V_0 (thermal)	Δ	$\frac{\Delta}{V_0\text{(thermal)}}$ %
1	2	3	4	5
$BeCl_2$	654	687	—33	4,8
$BeBr_2$	640	661	—21	3,2
BeI_2	637	637	—0	4,3
MgF_2	564	595	—31	5,2
$MgCl_2$	532	541	— 9	1,7
CaF_2	490	513	—23	4,5
$CaCl_2$	457	478	—21	4,4
BaF_2	447	447	0	0
$BaCl_2$	403	418	—15	3,6

The calculated values of V_0 are given in the second column of Table 1. The validity of Eq. (5) can be verified by comparing the calculated with the thermal values of V_0 (Column 3, Table 1).

From the thermal data we calculated the change in enthalpy ΔH_{298} for the reaction $Me^{++}_{(g)} + 2\,X^-_{(g)} = MeX_{2(g)}$:

$$\Delta H_{298} = \Delta H_{MeX_2(s)} - \Delta H_{Me^{++}(g)} - 2\Delta H_{X^-(g)} + \Delta H_s, \quad (6)$$

where ΔH is the heat of formation at 298° K, ΔH_s the heat of sublimation at the same temperature. ΔH for the fluoride ion was taken from [9], while the remaining ones from [10]; we also converted the heat of sublimation to 298° K. By means of Kirchhoff's equation we computed the molecular energy at 0° K ($V_{0(\text{thermal})}$) from ΔH_{298}. Heat capacities were taken from [10], while those not available were calculated from approximate quantum-mechanical equations.

Calculations were done for 9 molecules, for which we had accurate values of all the terms in Eq. (6). The absolute error, $\Delta = V_0 - V_{0(\text{thermal})}$, varied from 33 kcal for $BeCl_2$ to 0 kcal for BaF_2, or from 5% to 0% respectively. The average deviation was 3.0%, which, one has to admit, was a very satisfactory result.*

In all except two (BeI_2 and BaF_2, $\Delta = 0$) cases Δ was negative. This indicates a systematic error which seems to be connected with the determination of Me–X distance at high temperatures. (It probably reflects the known covalent character of the bonds). A recalculation of r to absolute zero temperature will decrease the deviations from thermal data. As our calculations have shown, any approximations made in deriving Eq. (5) had very little effect on the value of V_0 (the changes either way were of the order of 0.5-1%).

When Eq. (5) was used to calculate V_0 for $HgCl_2$, where the covalent character of the bonds is much more pronounced than in MeX_2 molecules, Δ was about -100 kcal/mole, or 16%.

* The error in determination of r was 1%, which would result in a 1.5% error for V_0. The error in the determination of $V_{0(\text{thermal})}$ was also about 2%.

This confirms our opinion that the good results obtained for MeX_2 molecules were not fortuitous, and that it was possible to adequately analyze the properties of these molecules by using ionic representations.

LITERATURE CITED

[1] B. V. Nekrasov, General Chemistry, Moscow, 1948.*

[2] A. A. Grinberg, Introduction to the Chemistry of Complexes, Moscow, 1951.*

[3] E. Cartmell and G. Fowles, Valency and Molecular Structure, London, 1956.

[4] A. Büchler and W. Klemperer, J. Chem. Phys. 29, No. 1, 121 (1958).

[5] C. I. F. Böttcher, Theory of Electric Polarization, Houston, 1952.

[6] P. A. Akishin and V. P. Spiridonov, Crystallography 2, 475 (1958).

[7] K. S. Krasnov and V. T. Antoshkin, J. Inorg. Chem. 3, No. 7, 1490 (1958).

[8] H. Landolt-R. Bomstein, Zahlenwerte und Funktionen, 1, T. 1 1950.

[9] A. F. Kapustinskii and K. B. Yatsimirskii, J. Gen. Chem. 26, No. 4, 941 (1956).*

[10] F. D. Rossini, D. D. Wagman et al., Selected Values of Chemical Thermodynamics, Properties, Washington, 1952.

Received May 11, 1959

* In Russian.

** Original Russian pagination. See C. B. Translation.

Card 1. Photo

DIFFUSION AND SOLUBILITY OF TANTALUM IN GERMANIUM

A. V. Sandulova and He Yu-Liang

L'vov Polytechnical Institute

(Presented by Academician A. F. Ioffe, May 11, 1959)

We are presenting in this paper the results of an experimental study of the temperature dependence of the diffusion coefficient and solubility of tantalum in germanium samples with various specific resistivities.

The diffusion was studied by removing successively thin layers of the sample and using a radioactive Ta^{182} isotope. In our study we used single germanium crystals with the specific resistivities of 60, 1, and 0.5 ohm · cm, and also polycrystalline germanium with a specific resistivity of 20 ohm · cm. Germanium was used in the form of rectangular rods with the dimensions being 0.5 × 0.4 × 0.3 cm. Before diffusion the germanium samples were filed down, polished, and etched in boiling 30% hydrogen peroxide. In all of our experiments the radioactive tantalum was deposited only on one surface of each sample.

The initial diffusion tempering of our samples was done in evacuated sealed quartz tubes in the temperature interval from 671 to 899°, with the temperature regulated to within ± 1°. The thickness of removed layers was determined by weighing. The activity of these layers was then determined by measuring the γ-radiation. The concentrations of tantalum in the stripped layers were computed by comparing their radiation intensity with that of calibrated samples prepared separately from radioactive tantalum [1]. The diffusion coefficient was calculated by means of Fick's Diffusion Equation

$$C = \frac{Q}{\sqrt{\pi D t}} \exp\left[-\frac{x^2}{4Dt}\right],$$

where C is the concentration, D the diffusion coefficient, t the diffusion time, and x the penetration depth of the diffusing atom.

Our experimental data were used to plot the graphs of log C against x^2 shown in Fig. 1. We then calculated the diffusion coefficients at various temperatures. On the basis of our diffusion coefficients we constructed curves for the function $\log D = f(\frac{1}{T})$, i.e., curves for the temperature dependence of the diffusion coefficients.

In Fig. 2 we have plotted curves showing the temperature of the diffusion coefficient in monocrystalline (1 and 2) and polycrystalline (3) germanium. One can see in Fig. 2 that when the function is plotted as log D vs 1/T we get straight lines, which confirms the exponential character of the diffusion coefficient equation. From these graphs we determined the sintering energy Q and the preexponential coefficient in the diffusion equation D_0. On the basis of our data it can be shown that the diffusion coefficients of tantalum in monocrystalline and polycrystalline germanium can be expressed by the following equations:

$$D_{\text{m}_{60}} = 623{,}16 \exp\left[-\frac{64904}{RT}\right];$$

$$D_{m_{0.5-1}} = 8{,}49 \cdot 10^{-5} \exp\left[-\frac{21948}{RT}\right];$$

$$D_{p_{20}} = 2{,}97 \cdot 10^{-6} \exp\left[-\frac{19382}{RT}\right].$$

The first equation corresponds to a single germanium crystal with a specific resistivity of 60 ohm·cm, the second to a single crystal with a specific resistivity of 0.5-1 ohm·cm, and the third to polycrystalline germanium with a specific resistivity of 20 ohm·cm.

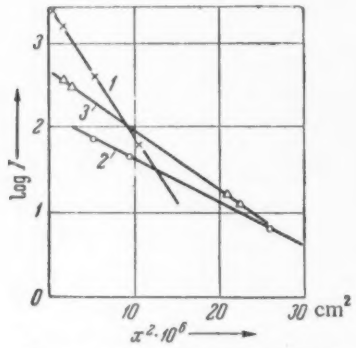

Fig. 1. Log I as a function of x^2 for the diffusion of tantalum in: 1) a single germanium crystal with a specific resistivity of 60 ohm·cm; 2) a single germanium crystal with a specific resistivity of 0.5 ohm·cm; 3) polycrystalline germanium with a specific resistivity of 20 ohm·cm.

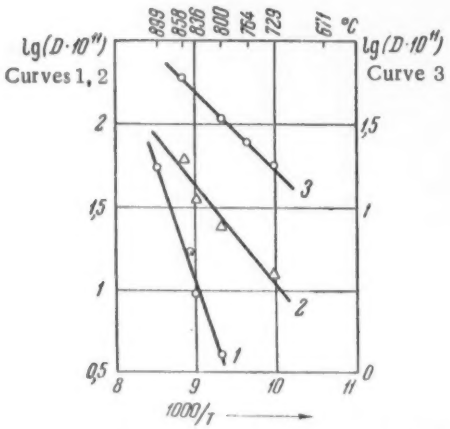

Fig. 2. Temperature dependence of the diffusion coefficient of tantalum in: 1) a single germanium crystal with a specific resistivity of 60 ohm·cm; 2) a single germanium crystal with a specific resistivity of 0.5-1 ohm·cm; 3) polycrystalline germanium with a specific resistivity of 20 ohm·cm.

The graphs in Fig. 2 indicate that the Ta diffusion rate depends on the purity of monocrystalline germanium, while the sintering energy in the high-resistance samples (i.e., purer ones) is larger (almost by a factor of three) than in the low-resistance ones. The equations presented above show that the diffusion parameters in polycrystalline germanium and in single crystals of low purity were very similar in their absolute values, although the polycrystalline samples possessed a higher degree of purity than the comparable single crystals.

In the solubility determinations, just as in the case of diffusion rate experiments, the germanium was only coated on one side with the radioactive tantalum, except that the initial radiation intensity was much higher. The diffusion tempering was extended from 20 to 60 hrs. After the tempering we filed off successive layers and determined their activities. As can be seen in Fig. 3, at a certain depth all the germanium layers had the same activity. The figure shows data obtained on P-type and N-type germanium, both of which were tempered under similar conditions. The horizontal segments on the I = f (x) curves give the maximum solubility of tantalum in germanium at the diffusion tempering temperature.

We determined the solubility of tantalum in germanium at various diffusion tempering temperatures; the solubility diagram shown in Fig. 4 was constructed on the basis of our experimental data. The maximum solubility of tantalum in both N-and P-type germanium occurred at the same temperature, 880 ± 3°. However, the solubilities in the two types were slightly different, and the solubility was greater in the P-type over the entire temperature range covered by us.

The solubility determination method described by us has certain advantages over other methods. Thus, for example, one does not have to deposit the radioisotope on all sides of the sample and then cut it into sections, which can become very cumbersome when small samples are used in experiments.

In Table 1 we have presented the comparative data for the diffusion coefficients and sintering energies of group-V elements diffusing into germanium.

Table 1 shows that the diffusion coefficients of $Ta_{m_{0.5-1}}$ and $Ta_{m_{60}}$ differ by one order of magnitude,

TABLE 1

Element	D at 800°, cm^2/sec	E, cal/mole	Element	D at 800°, cm^2/sec	E, cal/mole
$Ta^*_{P_{20}}$	$3{,}38 \cdot 10^{-10}$	19382	P**	$6{,}5 \cdot 10^{-12}$	57000
$Ta^*_{m_{0.51}}$	$2{,}43 \cdot 10^{-10}$	21948	As**	$4{,}0 \cdot 10^{-11}$	57000
$Ta^*_{m_{60}}$	$4{,}05 \cdot 10^{-11}$	64904	Sb**	$2{,}0 \cdot 10^{-11}$	57000

* Our measurements.

** Data in [2-5].

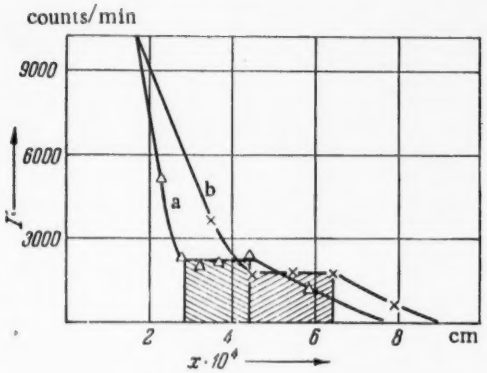

Fig. 3. I as a function of x for the solubility of tantalum in germanium. a) N-type; b) P-type germanium.

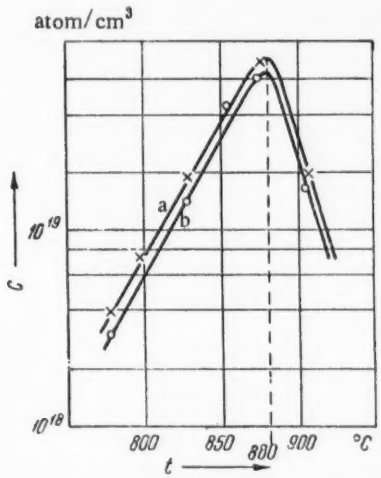

Fig. 4. The solubility of tantalum in germanium as a function of temperature. 1) P-type; 2) N-type germanium.

while the sintering energy of $Ta_{m_{60}}$ is almost three times greater than that of $Ta_{m_{0.5\text{-}1}}$ It is worth noting that the diffusion coefficient and sintering energy of $Ta_{m_{60}}$ are similar in magnitude to the corresponding parameters of other group-V elements: P, As, Sb.

If we accept the hypothesis that the group-V elements (P, As, and Sb) diffuse into germanium through the crystal lattice nodes [2, 5, 6], then we can assume a similar diffusion mechanism for tantalum, considering how similar its parameters are to those of the other elements of this group.

LITERATURE CITED

[1] A. V. Sandulov and A. I. Andrievskii, Radiotechnology and Electronics 1, 12, 1492 (1956).

[2] W. C. Dunlap, Phys. Rev. 99, 6, 1531 (1954).

[3] C. S. Fuller, Phys. Rev. 86, 1, 136 (1952).

[4] J. S. Saly and C. Dunlap, Phys. Rev. 90, 4, 630 (1953).

[5] B. I. Boltaks, J. Tech. Phys. 26, 2, 457 (1956).

[6] W. Jost, Diffusion in Solids, Liquids, Gases, N. Y., 1952.

Received May 5, 1959

THE DIELECTRIC PROPERTIES OF NETTED RUBBERLIKE SWOLLEN HIGH POLYMERS IN SOLVENT – NONSOLVENT BINARY SYSTEMS

G. L. Starobinets and V. F. Tikavyi

V. I. Lenin Belorussian State University

(Presented by Academician V. N. Kargin, May 4, 1959)

When compared to the great success achieved in recent years in determining the dielectric properties of high polymers and copolymers [1], the study of swollen polymers appears to be very neglected. There are only isolated bits of information on the dielectric constants of high polymers swollen in individual low molecular weight compounds [2], but no such data are available for polymers swollen in binary and more complex mixtures of low molecular weight components. At the same time the study of dielectric constants and dielectric polarization of such systems makes it possible to obtain new information about the structure of swollen polymers, about the adsorption of low molecular weight compounds by high polymers, and about the changes in the dielectric properties of high polymers in mixed systems.

In the present paper we will discuss our experimental data on the dielectric constants and dielectric polarizations of netted rubberlike high polymers, swollen in solvent–nonsolvent binary systems over the entire range of binary mixture compositions. Benzene and carbon tetrachloride served as solvents, low molecular weight aliphatic alcohols as nonsolvents. The polymer consisted of a vulcanized butadiene–styrene copolymer, which contained 10 parts by weight of styrene and the following ingredients in 100 parts (by weight) of the copolymer: 2 parts sulfur, 5 parts ruberax, 1.25 parts captax, 1.5 parts stearic acid, 0.5 parts diphenylguanidine, and 5 parts zinc oxide. The dielectric constants of swollen samples were measured by the beat heterodyne method at a frequency of 568 kcycles/min in a tightly sealed Nernst-type condenser at 25°C. At the same time, by using a method developed in our laboratory [3], we measured the effective adsorption isotherms of both low molecular weight components, as well as their distribution between the polymer and binary solution phases.

In Fig. 1 we have plotted the dielectric constant curve for a polymer–benzene–methyl alcohol ternary system. The dotted lines link the concentrations of swollen polymers and binary solutions in equilibrium. This figure is typical for the systems studied in our work. As the molecular weight of the alcohol increased so did the dashed area representing the swollen polymer phase. The connection between the dielectric constant isotherm and the effective adsorption isotherm for the nonsolvent is very apparent in Fig. 2, where the dielectric constants and effective adsorption of alcohol are represented as a function of the alcohol mole fractions in the binary solutions at equilibrium for the polymer–carbon tetrachloride–ethyl alcohol system. In the same figure we have plotted the equilibrium curve for the polymer + binary solution system (i.e., a curve showing the mole fraction of alcohol in the polymer phase vs. the mole fraction of alcohol in the equilibrium solution).

In all the systems investigated the dielectric constant isotherm and the effective adsorption isotherm of the nonsolvent passed through a maximum, and both isotherms were symbatic, i.e., to the first approximation we could assume that the dielectric constant of the swollen polymer would be determined by the dielectric constant and the nonsolvent concentration in the polymer. However, as may be seen in Fig. 2, the dielectric constant and the effective adsorption isotherms of the alcohol could not be superimposed, i.e., the dielectric constant of the ternary system also depended (though to a lesser extent) on the solvent properties.

While studying the relationship between the dielectric polarization and the composition of swollen polymers we found that it could be satisfactorily described by applying the form of Onsager–Kirkwood theory for

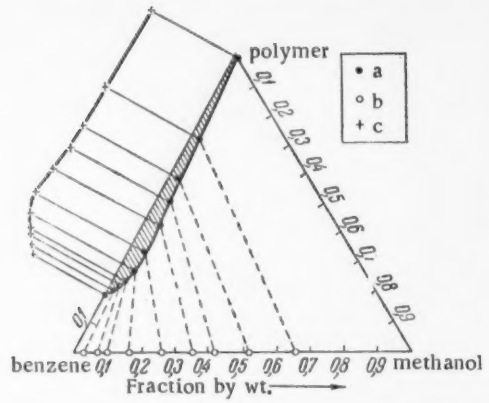

Fig. 1. The high polymer–benzene–methyl alcohol system. a) Composition of the swollen polymer; b) the equilibrium binary solution; c) dielectric constant of the swollen polymer.

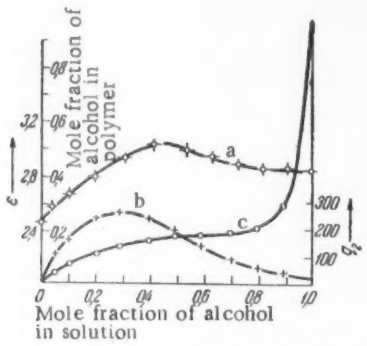

Fig. 2. The high polymer–carbon tetrachloride–ethyl alcohol system. a) Dielectric constant of the swollen polymer (E); b) effective adsorption isotherm of alcohol in mg/g of rubber (q_2); c) low molecular weight component distribution between the polymer and solution phases.

solutions of polar molecules in nonpolar solvents [4]. This seemingly unexpected result is in full accord with the nature of the systems studied in our work. As a matter of fact, according to the contemporary statistical thermodynamics of high polymer solutions one could assume [5] that in the presence of a solvent (i.e., a compound whose cohesive energy is close to that of the polymer), chain segments equal in size to the solvent molecule would constitute the macromolecular kinetic units. On top of that, in one of our papers [6] it was experimentally established that rubberlike high polymers adsorbed the alcohol not in the form of molecular aggregates, but as individual molecules. Consequently, a rubberlike high polymer–solvent–nonsolvent ternary system is equivalent in its properties to a binary system composed of monomeric alcohol molecules dissolved in a hypothetical solvent whose cohesive energy is the same as in rubber and whose molecular weight is equal to that of polymeric chain segments. One can easily see that Onsager's dielectric polarization theory would be applicable to such systems [7]. And in fact the theory does cover polar liquids in which there aren't any dielectric nonhomogeneities next to the molecules under consideration, which is equivalent to assuming the existence of a monomolecular polar liquid. The dielectric polarization of swollen polymers was calculated with the help of the Onsager-Kirkwood equation, which was applicable to binary solutions of polar molecules in nonpolar solvents and assumed the form [4]

$$\frac{(\varepsilon-1)(2\varepsilon+1)}{9\varepsilon}V=\frac{(\varepsilon_1-1)(2\varepsilon_1+1)}{9\varepsilon_1}X_1V_1+\frac{(\varepsilon_2-1)(2\varepsilon_2+1)}{9\varepsilon_2}X_2V_2=X_1P_1+X_2P_2, \quad (1)$$

where X is the mole fraction, V the molar volume, while indices 1 and 2 refer to the hypothetical solvent and nonsolvent respectively; P_1 is the molar polarization of the hypothetical solvent (a polymer swollen to its maximum in the solvent), and P_2 the polarization of a monomolecular alcohol whose dielectric constant was calculated by means of the Onsager equation [7]. The molar volume of the system was calculated from the equation

$$V=\frac{X_1M_1+X_2M_2}{d}, \quad (2)$$

where M_1 and M_2 are the respective component molecular weights, and d the densities of swollen polymers determined by the hydrostatic suspension in equilibrium binary solutions. The validity of Eq. (1) for the systems studied in this paper can be demonstrated in the following manner. Since the alcohol concentration in the polymer phase was small, if we replaced the mole fraction of the nonsolvent by its concentration in moles per liter, Eq. (1) would assume the form

$$\frac{(\varepsilon-1)(2\varepsilon+1)}{9\varepsilon} = \frac{(\varepsilon_1-1)(2\varepsilon_1+1)}{9\varepsilon_1} + KC. \quad (3)$$

K was calculated from the equation,

$$K = \left[\frac{(\varepsilon_2-1)(2\varepsilon_2+1)}{9\varepsilon_2} - \frac{(\varepsilon_1-1)(2\varepsilon_1+1)}{9\varepsilon_1}\right]\frac{V_2}{1000}. \quad (4)$$

V_2 in Eq. (4) denotes the molar volume of the nonsolvent.

Figure 3, where the experimental polarizabilities are compared with those calculated for the polymer–benzene–n-butyl alcohol system, illustrates the applicability of the Onsager-Kirkwood polarization theory to the systems studied in our work.

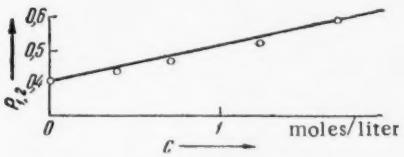

Fig. 3. The high polymer–benzene–n-butyl alcohol system. The polarizability $P_{1,2}$ as a function of the bulk concentration of alcohol. Circles denote experimental points, the line is calculated.

It would be interesting to find out whether the monomeric nonsolvent molecules are randomly oriented in the polymeric phase, or whether they exhibited a certain degree of order, expressed in some preferable orientation around the polar groups (double bonds) in the polymer. The question can be answered by studying the orientation polarization component of P_2, which was computed from Eq. (1). According to Kirkwood,

$$P_2 = P_{el} + P_{at} + \frac{4}{3}\pi N\frac{\mu^2 g}{3kT}, \quad (5)$$

where P_{el} and P_{at} are the electron and the atom polarizations respectively, μ the dipole moment, and g Kirkwood's correlation parameter, determined by the number and relative configurations of nearest neighbors around the molecule under consideration. The polarization of alcohols, computed from the data on polymers in equilibrium with binary solutions of a composition to the left of critical (i.e., composition up to which the solvent–nonsolvent mixture would still dissolve the polymer), was in the range from 120-130 cm^3. The maximum on the effective adsorption isotherm of the nonsolvent corresponds to the critical composition [8]. The dipole moment of the alcohol when calculated by assuming a random orientation for alcohol molecules in the polymer (g = 1) proved to be too large. If we assume that g = 2 we will get a normal value (1.7 debyes) for the dipole moments of our alcohols. Since the correlation parameter is determined from the equation

$$g = 1 + Z\cos\gamma, \quad (6)$$

where Z is the number of nearest neighbors around the molecule under consideration, and cos γ the mean cosine of the angle formed by the dipole moment of the molecule and the moments of its nearest neighbors, then g = 2 corresponds to the formation of dimers with a parallel orientation of dipoles. It seems that the orderly alcohol orientation in the polymeric phase should be represented as a "dimerization" between the alcohol molecules and the polymer double bonds. At the same time the alcohol and the double bond dipoles assume a parallel orientation, while the carbon chains of the alcoholic molecules "dissolve" among the polymeric chain segments. One of us arrived at a similar conclusion by applying the method of modeling [9] to the study of adsorption on high polymers.

LITERATURE CITED

[1] G. P. Mikhailov, Progr. Chem. 24, 875 (1955).

[2] H. Veith, Koll. Zs. 152, 36 (1957).

[3] G. L. Starobinets and V. S. Komarov, Proc. Acad. Sci. USSR 86, 771 (1952).

[4] G. Oster, J. Am. Chem. Soc. 68, 2036 (1946).

[5] G. Gee, Coll. Chemistry of Large Molecules, (IL, 1948, p. 152) [Russian translation].

[6] G. L. Starobinets, Dissertation, Minsk, 1955; Sci. Rep. V. I. Lenin Belorussian State University, No. 42, Chem. Ser. 151 (1958).

[7] L. Onsager, J. Am. Chem. Soc. 58, 1486 (1936).

[8] G. L. Starobinets and V. S. Komarov, J. Phys. Chem. 30, 1771 (1956).

[9] G. L. Starobinets, J. Phys. Chem. 30, 2029 (1956).

Received May 2, 1959

THE APPEARANCE OF THIXOTROPIC STRUCTURE IN SOLUTIONS AND IN TWO-SIDED FILMS CONTAINING SUCROSE AND AEROSOL-OT* AND THE EFFECT OF THIS STRUCTURE ON THE STABILITY OF FOAMS

A. A. Trapeznikov and K. V. Zotova

Institute of Physical Chemistry of the Academy of Sciences, USSR

(Presented by Academician P. A. Rebinder, April 22, 1959)

The study of two-sided** films formed in soaplike solutions presents considerable interest not only from the point of view of structural determinations but also as a means of measuring foam stabilities. Many workers attributed the high stability of foams and films exclusively to the improved mechanical properties of adsorption layers. However, other views are also possible regarding this problem. Several papers have reported investigations of the mechanical properties of surface layers in solutions [1], but the study of these properties in films should be considered more significant. Work along these lines has already led to some interesting new results. It was shown that the properties and structure of the adsorption layers in films were different from those in the surface layers of soap and saponin solutions [2].

A study of the mechanical properties of films makes it possible to explain the film structure throughout its width and to separate the effective role of the adsorption layers from that of the internal film portions whose structure in semicolloidal solutions may have an entirely different origin and exert an independent effect on the film stability. The viscosity and strength of films and surface layers in solutions were studied by means of a previously described method [2] which involved the use of horizontal concentric rings. We found that the surface layers in commercial aerosol (esters of sulfosuccinic acid) possessed a relatively low surface viscosity, while the viscosity of adsorption layers on the film was even lower. The latter fact was particularly well pronounced in 1-5% solutions of aerosol-OT (dioctyl ether). The absolute viscosity of an aerosol-OT film (computed for the full film thickness in 1-5% solutions) varied from $0.5\text{-}0.9 \times 10^{-4}$ surface poises, which was close to that of sodium oleate films [2]. Aerosol films were quite stable in horizontal rings (especially at high concentrations).

It is well known that glycerine and sucrose tend to increase the stability of films and bubbles by retarding the downward flow of liquids. Therefore it was very interesting to examine the mechanical properties of films formed in a solution to which a foam-stabilizer has been added. As an example we took a solution of aerosol-OT to which some sucrose had been added (0.045 moles/liter of aerosol-OT, 1.4 moles/liter of sucrose) and which was prepared according to recommendations given by Kuchner [3] who had studied the effects of such substances on the stability of films and bubbles. Viscosity was calculated from the equation: $\eta = K \cdot P_s$, where $K = \frac{1}{4\pi}\left(\frac{1}{a^2} - \frac{1}{b^2}\right)$; a the outside radius of the inner ring, b the inside radius of the outer ring (a = 2.755 cm, b = 3.00 cm, wire diameter = 0.15 cm), P_s the damping moment calculated from

$$P_s = 2M\left(\frac{\lambda_s}{T_s} - \frac{\lambda_0}{T_0}\right),$$

where λ_s is the logarithmic damping decrement in the surface layer or film, T_s the corresponding oscillation

*OT stands for dioctyl ether.

**From now on, for the sake of brevity, we will use the word film to denote a two-sided film.

period, λ_0 and T_0 the damping decrement and oscillation period in air. (In this case $\lambda_0 = 0.0185$, $T_0 = 36.66$ sec). The film viscosity η_s^f can be regarded approximately as a sum of two viscosities, $\eta_s^f = 2\eta_s^{f\delta} + \eta_s^{fh}$, where $\eta_s^{f\delta}$ is the viscosity of the adsorption layer on the film, and η_s^{fh} the viscosity of the film's interior inclosed between two adsorption layers [2].

Investigation has shown that film properties depend greatly on the solution aging. Table 1 shows that the films made in freshly prepared solutions had a low η_s^f, as did also films in sucrose-free solutions of aerosol-OT. This indicates that a simple addition of sucrose had practically no effect on the properties of the surface layers in aerosol-OT solutions or on the gross viscosity of the film's interior. Films formed from solutions at various stages of aging already exhibited a 100-300 times larger viscosity η_s^f, and at the same time there appeared some elastic shear, reflected in decreased T; this makes it possible to calculate the effective shearing coefficient E_s^f from the equation $E_s^f = K\Delta C$, where K is the instrument constant, ΔC the moment of the elastic forces in the film, $\Delta C = 4\pi^2 M(T_s^{-2} - T_0^{-2})$.

TABLE 1

Aging time of solution, in days	λ	T_s, sec	$\eta_s^f \cdot 10^4$, surface poises	$E_s^f \cdot 10^4$, dynes/cm
Freshly prepared	0,027	37,76	0,72	
34	0,575	32,75	58,3	13,0
87	1,550	31,80	164,0	17,0
101	1,675	27,0	209,0	42,0

TABLE 2

Film No.	λ	T_s, sec	$\eta_s^f \cdot 10^4$, surface poises	$E_s^f \cdot 10^4$, dynes/cm
1	1,550	31,80	164,0	17,0
2	0,141	35,80	11,7	2,7
3	0,075	36,31	7,1	1,3
6	0,053	36,08	3,3	1,7

Note. Solution aged for 87 days.

Thus, when the film was formed in aged solutions it absorbed certain components which increased its viscosity. By relying on some previous data on the formation of highly viscous adsorption layers in certain films, we could assume that the aging process gave rise to some new surface-active components which produced viscous adsorption layers, i.e., increased $\eta_s^{f\delta}$ and consequently the over-all film viscosity η_s^f. However, subsequent experiments have shown that something else was responsible for the increase in η_s^f.

First of all, the surface tensions of fresh and aged solutions (determined by the methods of counterpoised leafs [4]) were identical and equal to 25.5 dynes/cm. In the second place, when several films were repeatedly formed in the same aged solution η_s^f and E_s^f systematically declined from film to film, approaching their values in fresh solutions (Table 2). This was connected with the fact that the repeated formation of each new film was accompanied by additional mixing and destruction of the three-dimensional thixotropic structure which had arisen in solution during aging. Formation of the latter was confirmed through direct measurements in an Ubbelohde capillary viscosimeter at various pressures as the solution was aged for 87 days. From the data in Table 3 it follows that the volume viscosity decreases from 0.0720 poise at P = 105 mm water column to 0.0661 poise at P = 690 mm of water. A repeated measurement at P = 109 mm gave a lower η_v which indicated structural deformation. When the solution was subsequently allowed to rest, the viscosity increased again. Similar behavior could also be observed in films formed from aged solutions. In Table 4 it is shown that in solutions aged for two different periods of time a repeated vibrational agitation of any one film systematically reduced its η_s^f and E_s^f to almost the same value as that observed in films formed from corresponding unaged solutions. After the film was allowed to rest its viscosity increased again, but the structure was restored much more slowly in the film than in the bulk of solution. No extensive destruction followed by comparatively slow restoration of the film structure has been previously detected in adsorption layers containing spontaneously adsorbed particles possessing high two-dimensional mobility. Therefore it would be difficult to ascribe such a structure to the two monolayers which bound the film. The above described destruction of the colloidal structure inside the solution could not have been reflected in the structure of the adsorption layers either, since these, as a rule, are formed from particles of molecular dimensions. We have, therefore, concluded that the film structure detected in our case and the surface viscosity and elasticity connected with it were all caused by particles of the three-dimensional colloidal structure, which had fallen into the film (out of the bulk of solution) during its formation. Such particles seem to distribute themselves inside the film, between the adsorption layers, forming a three-

TABLE 3

Increase in P		Decrease in P	
P, mm of H_2O	η_v, poise	P, mm of H_2O	η_v, poise
105	0,0720	614	0,0662
206	0,0704	516	0,0677
300	0,0690	396	0,0680
410	0,0684	306	0,0677
512	0,0671	213	0,0690
616	0,0675	109	0,0699
690	0,0661	After a 90 minute rest	
		110	0,0719

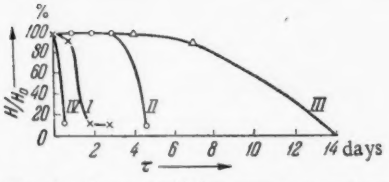

Fig. 1. Foam stability curves at various aging times of solutions. I) 3 days; II) 19 days; III) 49 days; IV) 49 days, but the solution vigorously agitated.

dimensional overlapping structure and increasing its η_s. The viscosity of the adsorption layers themselves (denoted by $\eta_s^{f\delta}$) retained the same low value as that in fresh or in sucrose-free solutions of aerosol-OT. Consequently we could assume that the adsorption layers in aged films with disrupted or undisrupted structures were essentially formed by the same aerosol particles as those which were also adsorbed in films made from sucrose-free solutions. From this it also follows that in our case the high viscosity of aged films was not the result of a diffused structure which extended from a "gellike" adsorption layer in the film's interior or deep into the solution surface layer, and which has generally been assigned to all kinds of surface layers (in our case the adsorption layer wasn't even gellike). Finally, it is also possible that the polar groups in the adsorbed layer interact somehow with the colloidal particles which had fallen from inside the solution into the interior portions of the film, but still the primary cause and origin of such particles would not be in the adsorption layer but in the bulk of solution.

A mechanical disruption of the film structures does not necessarily lead to an immediate disruption (break) of the film itself. It does not follow, however, that the formation of a three-dimensional structure in the film's interior should have no definite effect on the stability of films and foams. The experimental heights of foam columns determined under standard (not too vigorous) agitation of solution and at various aging stages indicated that aging increased the stability of foams. This can be seen from the curves of foam-column height versus time (Fig. 1). Consequently, the growth of colloidal structure (increasing η_s^f and E_s^f) in foam films is accompanied by increased stability of foams. Besides this, when an aged solution (in which structure had formed) was vigorously agitated and the three-dimensional structure destroyed (i.e., structure extending into the foam film), the stability of foam columns was considerably reduced (1 day instead of 14). At the same time the initial column height remained practically unchanged. This proves unequivocally that the existence of a three-dimensional structure in the film greatly increases the stability of foams as a whole. The stabilization in this case probably involved a sharp retardation of the downward flow of liquids and of the decline in film thickness. This was confirmed by the fact that films formed from aged solutions in horizontal rings were almost colorless, i.e., about 1 μ thick. They also

TABLE 4

Agit. Nos.	Film No. 1, solution aged 34 days				Film No. 2, solution aged 87 days				Film No. 3, solution aged 101 days				
	λ	T_s, sec	$\eta_s^f \cdot 10^4$ surface poise	$E_s^f \cdot 10^4$ dyne/cm	λ	T_s, sec	$\eta_s^f \cdot 10^4$ surface poise	$E_s^f \cdot 10^4$ dyne/cm	T** days	λ	T_s, sec	$\eta_s^f \cdot 10^4$ surface poise	$E_s^f \cdot 10^4$ dyne/cm
1	0,575	32,75	58,3	13	1,550	30,80	169,0	21		1,675	27,0	209,0	42,0
2	0,444	32,37	45,0	14	1,380	29,50	157,0	28	P*	0,063	37,29	4,1	
3	0,367	33,00	36,2	12	1,350	30,33	152,0	22	14	0,335	32,55	33,5	13,6
4	0,233	34,60	21,2	6,4	1,250	30,00	140,8	25	23	0,328	32,65	32,6	13,2
15	0,175	35,58	15,2	3,7	1,060	28,65	124,0	32	33	0,324	32,58	34,2	13,6
18	0,154	36,36	14,4	1,3					39	0,312	32,44	33,0	13,9
P*	0,058	36,86	3,3		0,060	36,26	3,4	1,2					

* The ring turned through 360° destroying the film structure.

** Film structure restoration time after destruction.

preserved this state for a long time without any change; i.e., while in solutions freshly prepared or containing just the aerosol-OT the film rapidly grew thinner (acquired colored interference lines), in our case there was practically no change. When, however, such a film was rapidly and strongly deformed by twisting the inside ring through 360°, for example, then due to the disruption of the film structure the liquid would rapidly run down rendering the film thinner and giving rise to interference colors. It follows from these experiments that the three-dimensional structure inside the film prevented the liquid from running down and the film from getting thinner by forming a rigid skeleton. The retarded flow may have resulted not only from the fact that the liquid would flow slower in the tiny capillaries of the structure, but also from a reverse capillary suction into the capillaries which had become exposed after the liquid had flown down. We can also assume that the mechanical strengthening of the film may have a direct and substantial effect on its stability.

LITERATURE CITED

[1] Platean, Ann. phys. 141, 44 (1870); R. E. Wilson and E. D. Ries, Coll. Symp. Monogr. 1, 145 (1923); N. M. Lubman, J. Phys. Chem. 1, 721 (1930); P. A. Rebinder and A. A. Trapeznikov, J. Phys. Chem. 12, 573 (1938); Proc. Acad. Sci. 18, 421 (1938); A. A. Trapeznikov, J. Phys. Chem. 14, 821 (1940); A. G. Broun, W. Thuman and W. C. McBain, J. Coll. Sci. 8, 491 (1953); J. T. Davies, Second International Congress of Surface Activity, 1, London, 1957, p. 220.

[2] A. A. Trapeznikov, Coll. Viscosities of Liquids and Colloidal Solutions, 1, 67, 87, 1941;* Colloid. J. 19, 252 (1957);* Second International Congress of Surface Activity, 1, London, 1957, p. 242; K. V. Zotova and A. A. Trapeznikov, Proc. Acad. Sci. 117, 883 (1957).**

[3] A. L. Kuchner, J. Chem. Education 25, 3, 210 (1948).

[4] A. A. Trapeznikov, J. Phys. Chem. 19, 228 (1945).

Received April 23, 1959

* In Russian.

** Original Russian pagination. See C. B. Translation.

THE KINETICS OF ACID-CATALYZED DECOMPOSITION OF ARYLALKYL HYDROPEROXIDES

V. A. Shushunov and Yu. A. Shlyapnikov

Chemical Scientific Research Institute at the N. I. Lobachevskii Gor'kii State University

(Presented by Academician V. N. Kondrat'ev, May 14, 1959)

As far as we know, the literature contains no references to any systematic study of the kinetics of acid-catalyzed decomposition of arylalkyl hydroperoxides. We can only mention a couple of papers in which the decomposition of cumene hydroperoxide in an acetic acid–water mixture [1, 2], in an ethyl alcohol–water mixture [3], and in glacial acetic acid [4] were studied. A possible mechanism for such decompositions of the arlyalkyl hydroperoxides was discussed in papers [1, 5, 6].

When first the hydroperoxides of cumene, diphenyl methane, and tetralin [7], then later those of other arylalkyl derivatives [5, 6, 8] were heated with strong acids ($HClO_4$, H_2SO_4) they yielded the corresponding phenols, and ketones or aldehydes.

Our paper is devoted to the study of acid-catalyzed decomposition kinetics of arylalkyl hydroperoxides. The kinetic regularities we established were found to be generally applicable to the decomposition of all the arylalkyl hydroperoxides studied by us.

In the absence of any complicating processes, the reaction under investigation exhibited first order kinetics with respect to both the hydroperoxide (HP) and the acid (HA).

$$-\frac{d[\mathrm{HP}]}{dt} = k[\mathrm{HA}][\mathrm{HP}]. \qquad (1)$$

The first order decomposition rate with respect to the acid was retained over a considerable range of acid concentrations, regardless of the nature of the arylalkyl hydroperoxide or of the solvents used (dioxane, glacial acetic acid, and their mixtures with water). We have also established that the acid concentration remained constant throughout the reaction. Consequently, the acid acted solely as a catalyst.

When the initial hydroperoxide concentration was low (0.01-0.05 mole /liter) the first order with respect to the hydroperoxide would, as a rule, be conserved to a considerable degree of conversion (until 70-90% of the hydroperoxide had been decomposed). When the initial hydroperoxide concentration was varied, the reaction rate constant (k) remained constant. As an example we will list the values of k for the decomposition of cumene hydroperoxide at 50° in dioxane, catalyzed by sulfuric acid:

Initial hydroperoxide conc. moles/liter	0,02	0,02	0,05	0,10	0,20
$k \cdot 10^2$ liter/mole sec	2,48	2,38	2,35	2,45	2,35

The decomposition products of arylalkyl hydroperoxides had different effects on the reaction rate. The type of effect would also depend on the nature of the solvent. Thus, the addition of acetone greatly enhanced

the acid-catalyzed decomposition of cumene hydroperoxide in glacial acetic acid, but it slightly retarded the same reaction in dioxane. Traces of phenol, on the other hand, would somewhat enhance the reaction in dioxane but show no visible effect on the rate in glacial acetic acid.

Traces of water or acetic anhydride had a particularly strong effect on the rate of acid-catalyzed decomposition of hydroperoxides.

TABLE 1

Hydroperoxide of:	$C_{H_2O} \cdot 10^2$ moles/liter					
	0,00*	0,32	1,76	3,52	5,62	11,80
	$k \cdot 10^3$ liters/moles · sec					
Cumene	9,8	8,8	6,1	--	3,2	1,7
p-Tert-butyl cumene	39,0	36,1	26,1	--	14,0	7,0
1,1-Diphenyl ethane	29,4	25,6	--	11,0	--	4,1
Diphenyl ethane	4,4	--	--	2,9	--	1,3

*Obtained by extrapolation.

When small amounts of water were added to the dioxane or glacial acetic acid (whichever was used as a solvent) the reaction rate was greatly reduced. In Table 1 we have compiled the results of some experiments carried out at 40° with water added to a solution of hydroperoxide in dioxane.

When the water concentration in the reaction mixture did not exceed 0.05-0.1 mole /liter, 1/k increased linearly with the H_2O content in solution. Additional increase in the water concentration caused a deviation from the linear relationship toward slower decomposition rate.

TABLE 2

Hydroperoxide of:	K_1, k_2, liter /mole · sec	k_1 / k_2, liter/mole	E, kcal	log k_0
Cumene	9,8	36	20,7	12,5
p-Tert-butyl cumene	39,0	30	19,6	12,6
p-Hydroxycumene	500	100	18	12,3
Sec-butyl benzene	10	55	21,0	12,7
Cyclohexyl benzene	5	26	18,2	9,0
Diphenyl methane	4,4	20	22,8	13,6
1,1-Diphenyl ethane	29,4	45	18,0	11,0
Dihydroperoxide of p-diisopropyl benzene	48	20	19,5	12,3

Traces of acetic anhydride greatly accelerated the acid-catalyzed decomposition of arylalkyl hydroperoxides. We studied these effects by using the decomposition of cumene hydroperoxide in dioxane (catalyzed by sulfuric acid) as an example. Figure 1 shows the results of several experiments in this series. Experiments carried out in the absence of acetic anhydride are shown in Fig. 1, 1; Fig. 1, 2 refers to experiments where one of the initial solutions (the hydroperoxide solution) contained some acetic anhydride while sulfuric acid contained a trace of water. At first the anhydride showed almost no effect (curves 1 and 2 are almost parallel), but later on acceleration was observed. Figure 1, 3 shows how the reaction proceeded when the anhydride was added to both the hydroperoxide and the sulfuric acid solutions before they were mixed. Here the anhydride accelerated the reaction right from the beginning. Figure 1, 4 refers to an experiment carried out under conditions similar to those of curve 3, but where 3 minutes after mixing the solutions, we added to the reaction mixture a small amount (up to 0.02 mole /liter) of water plus an equivalent amount of acetic anhydride. The figure shows that the addition of water sharply reduced the rate of the acid-catalyzed decomposition of hydroperoxide. The addition of acetone (up to 0.1 mole /liter) under similar experimental conditions and in the presence of acetic anhydride (0.1 mole /liter) reduced quite noticeably the decomposition rate of the hydroperoxide.

Thus we can attribute the spontaneous acceleration of the reaction in the presence of acetic anhydride to the fact that it would remove not only the water originally present in the solution but also any that might have formed during the reaction.

When the acetic acid was placed beforehand into the reaction mixture (up to 0.1 mole /liter), unlike acetic anhydride, it had no effect on the reaction rate. Traces of α,α-diphenyl-β-picrylhydrazil added to the reaction mixture had no effect on the reaction rate either, while the concentration of this compound remained constant throughout the reaction. This is a fairly convincing proof that the acid-catalyzed decomposition of arylalkyl hydroperoxides does not proceed through a free radical mechanism.

The temperature variation of the decomposition rate obeyed Arrhenius' Law. From the temperature dependence of k we computed the apparent activation energies (E) and the logarithms of the frequency factors (log k_0), both of which are shown in Table 2.

The experimental regularities which we detected in the reaction kinetics could be readily explained if we assumed the following mechanism for the acid-catalyzed decomposition of arylalkyl hydroperoxides (for example, cumene hydroperoxide):

$$C_6H_5(CH_3)_2COOH + HA \underset{k'_1}{\overset{k_1}{\rightleftarrows}} [C_6H_5(CH_3)_2COOH_2]^+A^-; \quad (I)$$

$$[C_6H_5(CH_3)_2COOH_2]^+A^- \xrightarrow{k_2} [C_6H_5(CH_3)_2CO]^+A^- + H_2O; \quad (II)$$

$$[C_6H_5(CH_3)_2CO]^+A^- \xrightarrow{k_3} [C_6H_5OC(CH_3)_2]^+A^-; \quad (III)$$

$$[C_6H_5OC(CH_3)_2]^+A^- + C_6H_5(CH_3)_2COOH \xrightarrow{k_4} \rightarrow C_6H_5OC(CH_3)_2OH + [C_6H_5(CH_3)_2CO]^+A^-; \quad (IV)$$

$$[C_6H_5(CH_3)_2CO]^+A^- + H_2O \xrightarrow{k'_2} [C_6H_5(CH_3)_2COOH_2]^+A^-; \quad (V)$$

$$[C_6H_5OC(CH_3)_2]^+A^- + H_2O \xrightarrow{k_5} [C_6H_5OC(CH_3)_2OH_2]^+A^-; \quad (VI)$$

$$[C_6H_5OC(CH_3)_2OH_2]^+A^- \rightarrow C_6H_5OC(CH_3)_2OH^+ + HA; \quad (VII)$$

$$C_6H_5OC(CH_3)_2OH \rightarrow C_6H_5OH + CH_3COCH_3. \quad (VIII)$$

Separate assumptions about individual steps have been postulated in earlier papers [1, 5, 6].

Reactions I, VII, and VIII may involve several elementary steps. Reaction I forms a compound structurally similar to an oxonium salt. Reaction II gives a perester of a strong acid. According to [9, 10] similar peresters of even such a weak acid as benzoic structurally resembled ion pairs or were readily transformed into such, although there was no dissociation into free ions [11, 12]. A rearrangement takes place in the positive ion of the pair (Reaction III) leading to the formation of still another kind of ion pair (one containing a carbonium ion). The data from several papers [1, 11, 13] show that this reaction proceeds very readily. In Reaction IV the carbonium ion in the ion pair reacts with a molecule of hydroperoxide giving a hemiketal and an ion pair similar to that in Reaction II.

Hence Steps III and IV can be regarded as a sort of chain propagation, with ions as the active species, and the entire process as an ionic chain reaction. Reactions I and II constitute the chain initiation while V and VI constitute the chain break.

By using the stationary state approximation we derived the following equation for the rate at which the hydroperoxide concentration declined:

$$-\frac{d[HP]}{dt} = \frac{K_1 k_2 [HA][HP]}{1 + \frac{k'_2}{k_3}[H_2O] - \frac{k_4[HP]}{k_4[HP] + k_5[H_2O]}}, \quad (2)$$

where K_1, is the equilibrium constant Reaction I, and k'_2, k_2,... the rate constants of the respective reactions. When $k_4[HP] << k_5[H_2O]$ the third term in the denominator may be neglected and we will get

$$-\frac{d[HP]}{dt} = \frac{K_1 k_2 [HA][HP]}{1 + \frac{k'_2}{k_3}[H_2O]} = k[HA][HP]. \quad (3)$$

In Table 3 we compiled the values of K_1k_2 and k'_2/k_3 calculated by means of Eq. (3) for the decomposition of various hydroperoxides in dioxane at 40° and in the presence of sulfuric acid as catalyst.

One can detect in Table 3 certain relationships between the structure and the decomposition rate of the hydroperoxides.

The ionic chain mechanism was proven by decomposing cumene hydroperoxide in acetic anhydride, so that all the water formed in Step II would be removed by reacting with the anhydride. Experiment showed that in this case the reaction rate was 10^4 times greater than in dioxane, and that the reaction went to completion even when we had a 300 fold excess of hydroperoxide over the acid. This could not be explained unless we postulated Step IV, i.e., a chain reaction.

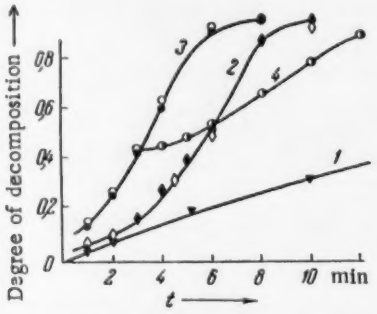

Fig. 1. Acid-catalyzed decomposition of cumene hydroperoxide at 50°. The initial concentration of the hydroperoxide was 0.02 moles/liter; catalyst 0.03 moles/liter; acetic anhydride 0.1 moles/liter; t was the reaction time.

LITERATURE CITED

[1] F. H. Seubold and W. E. Vaughan, J. Am. Chem. Soc. 75, 3790 (1953).

[2] O. Wichterle and P. Cefelin, Collect. 22, 1083 (1933).

[3] A. W. de Ruyter van Steveninck, J. Chem. Soc. 1958, 2066.

[4] V. A. Shushunov and Yu. A. Shlyapnikov, Reports on Chem. and Chem. Tech., Gor'kii 1958, p. 50.

[5] M. Kharasch, A. Fono, and W. Nudenberg, J. Org. Chem. 15, 748 (1950); 16, 128 (1951).

[6] M. S. Kharasch and J. G. Burt, J. Org. Chem. 16, 150 (1951).

[7] H. Hock and S. Lang, Ber. 77, 257 (1944).

[8] P. G. Sergeev and A. M. Sladkov, J. Gen. Chem. 27, 538, 540 (1957).*

[9] K. Criegee and R. Kaspar, Ann. 560, 127 (1948).

[10] P. D. Bartlett and B. T. Story, J. Am. Chem. Soc. 80, 4954 (1958).

[11] P. D. Bartlett and J. L. Kice, J. Am. Chem. Soc. 75, 559 (1953).

[12] D. B. Denney and D. G. Denney, J. Am. Chem. Soc. 79, 4806 (1957).

[13] H. Hock and H. Kropf, Ber. 88, 1544 (1955).

Received May 12, 1959

* Original Russian pagination. See C. B. Translation.

CATION MOBILITY IN MOLTEN PHOSPHATES

O. A. Esin and G. A. Teterin

The Institute of Metallurgy of the Ural Branch of the Academy of Sciences, USSR

(Presented by Academician A. N. Frumkin, May 21, 1959)

Measurements of the transference number (n) [1-8] have shown that the principal contribution to the transfer of electricity through molten silicates comes from the modifier cations (Na^+, Ca^{2+}, Co^{2+} etc.) rather than from the silicon ions. The low mobility of these latter ions is reflected in the low value of their diffusion coefficient [9]. On the other hand, the diffusion coefficient of phosphorus in $CaO-P_2O_5$ melts (D_p) is considerably greater than the diffusion coefficient of calcium (D_{Ca}) [10] even though its transfer number (np) is equal to zero [11].

It is possible that such inconsistencies could be explained in terms of differences in the mechanism of particle migration in diffusion and electrolysis [10, 12], but additional experimental work is still needed. It is for this reason that we have measured electrical conductivities, transference numbers, ionic mobilities, and mass-transfer coefficients in $CaO-P_2O_5$ and $CaO-CoO-P_2O_5$ melts. The radioactive isotopes Ca^{45}, Co^{60}, and P^{32} were used in this work.

The method of determining the transference number was not essentially different from that described earlier in [2]. A graphite crucible was used as the cathode and a graphite rod as the anode; this last was replaced by a rod of phosphor bronze (an alloy of Cu with 10% P) in latter experiments. Special experiments showed that there was only an insignificant loss of radioactive phosphorus by volatilization from the electrolyte at the working temperatures. Aluminum filters were used for separating the radiations from Ca^{45}, Co^{60}, and P^{32}. Transference numbers were evaluated from the equation:

$$n = \frac{26{,}8z}{Q} \frac{\nu_c}{\nu_a} \frac{p_c k}{M}, \qquad (1)$$

in which Q is the amount of electricity in ampere-hours, ν_c and ν_a are the activities of the central, and the anode, regions, respectively (counts/min·g), ρ_c is the weight of the middle region (g), $\underline{k}$ is the weight fraction of the oxide and M is the molecular weight.

Certain results are given in Tables 1 and 2 and in Figs. 1 and 2. The transference numbers of Ca and P were determined individually in the first two experiments (see Table 1, Experiments 1, 2) the results being $n_{Ca} = 0.8$ and $n_P = 0.3$. It was possible, however, that the hydraulic vibrations from the evolution of oxygen on the graphite electrode could give rise here to an additional transfer of activity from the anolyte into the central region. This effect was eliminated in subsequent measurements by using a soluble anode of phosphor bronze.

The simultaneous transfer of the calcium and phosphorus isotopes was studied in Experiment 4 (Table 1), the concentration of phosphorus in the anolyte being made considerably greater than that of the Ca^{45}. This last condition made it possible to measure the two activities in the central region to the same degree of precision. The transference numbers which were obtained here (see Table 1) show that the cations of phosphorus participate in the transfer of the electrical current. The value $n_P = 0.3$ is in good agreement with the results obtained in Experiments 2 and 3 where the transfer of phosphorus alone was studied.

TABLE 1

Transference Numbers of the Cations Ca^{2+}, Co^{2+}, and P^{5+} in $CaO-P_2O_5$ and $CaO-CoO-P_2O_5$ Melts at 1160°

Expt. No.	Melt composition, %			Radioactive indicator	Transference No.			Notes
	CaO	P_2O_5	CoO		n_{Ca}	n_{Co}	n_P	
1	27	73	—	Ca^{45}	0,8	—	—	Graphite anode, 1060°
2	53	68	—	P^{32}	—	—	0,3	The same, 1160°
3	30	70	—	P^{32}	—	—	0,3	Phosphor bronze anode
4	30	70	—	Ca^{45}, P^{32}	0,6	—	0,3	The same
5	14	68	18	Ca^{45}, P^{32}, Co^{60}	0,5	0,4	0,2	" "
6	30	70	—	P^{32}	—	—	0,3	Activity in catholyte

TABLE 2

The Alteration in the Concentrations of Ca^{45} and P^{32} in the Central and the Anode Regions During Electrolysis of a $CaO \cdot P_2O_5$ Melt

Specimen No.	Time of removal of specimen, min	Total activity of specimen	Intensity of radiation transmitted through filter	Activity P^{32},	Activity Ca^{45}
		counts/min			
Central region*					
1	0	8	0	0	8
2	5	32	10	14	18
3	15	73	32	46	27
4	22	106	40	58	48
5	29	170	66	94	76
6	35	236	88	126	110
7	41	282	100	143	139
8	47	354	120	170	184
Anode region					
1	0	—	—	—	—
2	5	8970	4390	6280	1960
3	15	7740	4090	5840	1900
4	22	7040	3640	5200	1840
5	29	6070	3020	4320	1730
6	35	5490	2710	3870	1620
7	41	5240	2560	3640	1600
8	47	5100	2450	3500	1600

*Experimental conditions: $P_{anolyte}$ = 7.0 g, $P_{central}$ = 11.6 g, $P_{catholyte}$ = 24.1 g, I = 0.6 amp, T = 1160°, circuit closed at 22 minutes.

A study of the possibility of the electrical migration of complex phosphorus-oxygen anions acquires interest here in view of the reticulated form of the P^{5+} cation. For this purpose, radioactive phosphorus was introduced into the cathode region instead of the anode region. Figure 1 shows that the slope of the ν vs τ curve did not increase when the electrical field was applied (Point a), but diminished. This indicates that phosphorus does not migrate as anions but is transferred into the catholyte in cation forms. The transference number of the phosphorus cation can be evaluated from a knowledge of the activity of one part by weight of the central region (ν_c) and the alteration of this activity ($\Delta \nu_c$) which results from the electrolysis. Thus the passage of Q ampere-hours of electricity is accompanied by the transfer of $Q_n M \nu_c / Fz$ activity units, or QnM / Fz gram-equivalents, of phosphorus from the central region into the catholyte. This alteration is also equal to the total diminution in the intensity of radiation of the central region, $p_c \cdot k \cdot \Delta \nu_c$, resulting from loss of the P^{5+} cation. From this it follows that:

$$n = \frac{p_c k \Delta \nu_c F z}{Q M \nu_c} . \qquad (2)$$

Calculations give the result $n_P = 0.2$ which is close to the value obtained earlier.

The effect of a third cation was traced out by determining simultaneously the transference numbers of calcium, cobalt and phosphorus in a $CoO \cdot 2P_2O_5$ melt which was held at 1120° in a neutral atmosphere in a corundum crucible with a phosphor bronze anode. The value of n for calcium (0.5) proved to be somewhat greater than that for cobalt (0.4) (Table 1, Exp. 5; Fig. 2). Similar relationships were observed earlier in silicate melts [13]. In enlarging on the interpretation advanced by this latter work, it should be noted that the lower mobility of the Co^{2+} could result from the fact that there is a higher degree of covalent binding in Co–O (43%) than in Ca–O (20%) [14, 15]. The transference number of the phosphorus was reduced from 0.3 to 0.2 by the introduction of cobalt, even though the mole fraction of the P_2O_5 remained constant. This confirms the existence of a reciprocal cation effect in ionic mobilities in oxide melts [16].

A combination of the moving-boundary method and the method of "tagged" atoms was used in determining the mobility (U) of the Ca^{2+} ion. These experiments were carried out simultaneously in two corundum

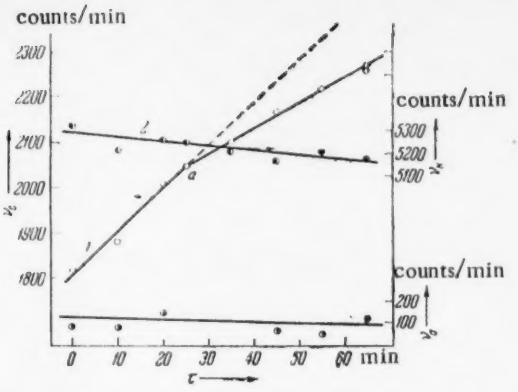

Fig. 1. Alteration in the P^{32} activity during electrolysis of $CaO \cdot P_2O_5$ (radioactive phosphorus introduced into catholyte): 1) in central region; 2) in catholyte; 3) in anolyte.

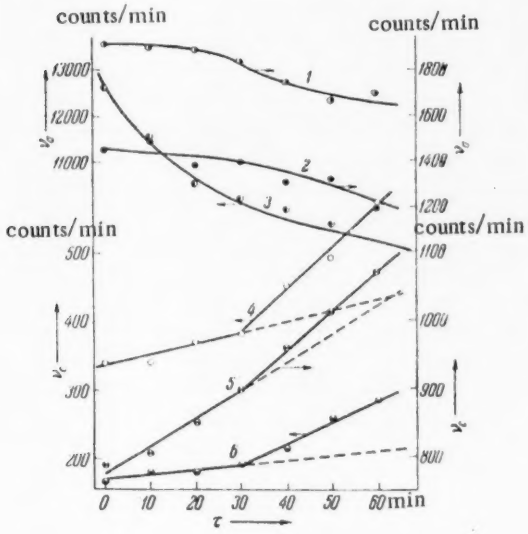

Fig. 2. Concentration of radioactive indicators in the anolyte (1, 2, 3) and in the central region of the cell (4, 5, 6) during electrolysis of $CaO \cdot CoO \cdot 2P_2O_5$: 1, 3) Ca^{45}; 2,6) Co^{60}; 3,5) P^{32}.

crucibles, each 0.38 cm in diameter, the electric current being passed through one of these and the isotope being transferred into the other by self-diffusion alone. The distance between the tungsten electrodes (L) was 6.3 cm, the time of electrolysis, one hour, the potential gradient (E), 30 volts, and the current, 0.15 amperes. Figure 3, 1 and 2 shows the distribution of the radiation intensity along the tube, during the passage of the current and in the absence of the current. The displacement of the radioactive calcium as a result of electrolysis was here $(\Delta l)_{\nu = 0} = 0.14$ cm. The transference number of the Ca^{2+} was calculated from this figure, using the equation:

$$n = \frac{\pi d^2 \cdot \Delta l \cdot \rho k F}{2QM}, \qquad (3)$$

in which ρ is the density of the $CaO-P_2O_5$ melt (2.5 g/cm^3, according to our data) and F is the value of the Faraday. The resulting value (n = 0.7) proved to be close to that which was obtained earlier. This again indicates considerable electrolytic mobility in the phosphorus of $CaO-P_2O_5$ melts. The mass-transfer coefficient of the calcium (D_{Ca}) can be evaluated from a knowledge of the activity distribution along the tube in the absence of a current:

$$D_{Ca} = \frac{l_2^2 - l_1^2}{4\tau \ln(\nu_1 / \nu_2)}. \qquad (4)$$

Here ν_1 and ν_2 are the intensities of radiation from Ca^{45} at the distances l_1 and l_2, respectively. The resulting value, $D_{Ca} = 6.5 \cdot 10^{-5}$ $cm^2 \cdot sec^{-1}$ was somewhat greater than that obtained earlier [10], a fact which is clearly to be explained by the presence of microconvection currents in the liquid. The absolute mobility of the Ca^{2+} was finally calculated from:

$$U = \frac{\Delta l L}{\tau E}. \qquad (5)$$

Its value is 0.00008 $cm^2/v \cdot sec$. By making use of this value and the transference number of calcium (n_{Ca}), and applying the defining equation for n, the absolute mobility of phosphorus (U_P) can be obtained:

$$U_P = \frac{U_{Ca} - n_{Ca} U_{Ca}}{n_{Ca}}. \qquad (6)$$

From the value of the phosphorus mobility (0.000034 $cm^2/v \cdot sec$) and the experimentally determined U_{Ca}, a specific conductivity of 0.16 $ohm^{-1} \cdot cm^{-1}$ (at 1150° ± 20°) was obtained for the $CaO \cdot P_2O_5$ melt. For comparison, the actual conductivity of molten $CaO \cdot P_2O_5$ was measured by the method of [17]. These measurements led to a specific conductivity of 0.168 $ohm^{-1} \cdot cm^{-1}$ at 1160°, a result which is satisfactorily close to the calculated value:

Temperature, °C	840	860	880	900	920	960	980	1000	1040	1060	1100	1140	1160	1200
κ, ohm^{-1}, cm^{-1}	0,0009	0,0015	0,0030	0,0043	0,005	0,010	0,015	0,019	0,030	0,040	0,082	0,136	0,168	0,172

It can thus be considered that both the calcium ions (n_{Ca} = 0.7) and the phosphorus ions (n_P = 0.3) contribute to the transfer of electricity in a $CaO-P_2O_5$ melt. Here the phosphorus migrates in the form of a cation rather than as a complex anion.

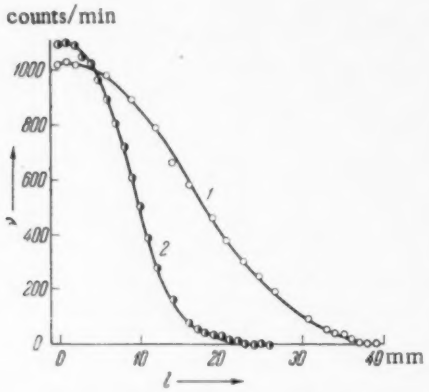

Fig. 3. Distribution of radioactive calcium along the tube, with an applied electric field (1) and without the field (2).

When the degree of covalent binding in Ca–O and P–O is evaluated from the data of Pauling and Haissinsky [14, 15], it is found that there is very little difference between the charges of the calcium and phosphorus ions ($Ca^{1.6+}$, $P^{1.9+}$). This difference would be still further diminished in the formation of a phosphate since the phosphorus ion attracts the ionic cloud of the oxygen in passing from the P–O–P grouping into the Ca–O–P combination. On the other hand, the radius of the calcium ion (1.06) is almost three times as large as that of the phosphorus ion (0.35) [18] so that from this point of view the probability of a displacement of P^{5x+} should not merely equal but even exceed that of Ca^{2x+}. It must also be taken into account, however, that there is more rigid homopolar binding in P–O than in Ca–O and that this will impede transfer of the phosphorus. It is for this reason that the electrolytic mobility of the smaller phosphorus ion is less than that of Ca^{2+}, despite the fact that these ions have approximately the same charge. This relation between the mobilities is not, however, maintained in diffusion processes [10]. It is clear that diffusion involves not only a transfer of the cations of phosphorus but also an additional movement of the phosphorus with the oxygen anions [19] which is similar to the paired ion diffusion in molten NaCl [12].

LITERATURE CITED

[1] J. Bockris, J. A. Kitchener, and A. Davies, Trans. Farad. Soc. 48, 536 (1952).

[2] O. A. Esin and A. K. Kir'yanov, Bull. Acad. Sci. USSR, Div. Tech. Sci. 12, 28 (1955).

[3] O. A. Esin and A. K. Kir'yanov, Bull. Acad. Sci. USSR, Div. Tech. Sci. 8, 20 (1956).

[4] T. Bååk, Acta Chem. Scand. 8, 166 (1954).

[5] M. Simnad, G. Derge, and J. George, J. Metals, 6, 1386 (1954).

[6] V. I. Malkin, S. F. Khokhlov, and L. A. Shvartsman, Proc. Acad. Sci. USSR 106, 491 (1956).

[7] V. I. Malkin, S. F. Khokhlov, and L. A. Shvartsman, J. Phys. Chem. 21, 11, 2485 (1957).

[8] V. I. Malkin and S. F. Khokhlov, Bull. Acad. Sci. USSR, Div. Tech. Sci. 3, 108 (1958).

[9] H. Towers and J. Chipman, J. Metals 9, 6, 769 (1957).

[10] O. A. Esin, E. S. Vorontsov, and S. K. Chuchmarev, J. Phys. Chem. 21, 10, 2322 (1957).

[11] V. I. Malkin and L. A. Shvartsman, Proc. Acad. Sci. USSR 102, 5, 961 (1955).

[12] A. Z. Borucka, J. Bockris, and J. A. Kitchener, J. Chem. Phys. 24, 6, 1282 (1956).

[13] V. I. Malkin and V. V. Pokadyshev, Bull. Acad. Sci. USSR, Div. Tech. Sci. 5, 129 (1958).

[14] L. Pauling, The Nature of the Chemical Bond (in Russian), Moscow, 1947.

[15] M. Haissinsky, J. Chim. Phys. 54, 9, 655 (1957).

[16] V. I. Malkin, Prog. Chem. 27, 3, 306 (1958).

[17] G. A. Teterin, O. A. Esin, and B. M. Lepinskikh, Proc. Institute of Metallurgy, Ural Branch, Acad. Sci. USSR, 4, 145 (1958).

[18] V. M. Gol'dshmidt, Crystallochemistry (in Russian), United Sci.-Tech. Press, Leningrad, 1937.

[19] E. S. Vorontsov and O. A. Esin, Scientific Reports, Higher Schools, Metallurgy, 2, 16 (1958)

Received May 21, 1959

THE PROBLEM OF CHAIN INTERACTION IN COMPLEX CHAIN REACTIONS

V. F. Tsepalov

The Institute of Physical Chemistry of the Academy of Sciences, USSR

(Presented by Academician V. N. Kondrat'ev, June 18, 1959)

Chain interaction arises in composite chain reactions involving several substances and can result in initiation, propagation or rupture of chains. Such interaction can exert a marked influence on the rate of reaction of each substance and on the over-all reaction rate, as well. Consideration of this problem has been limited for the most part to the literature on the kinetics of copolymerization in binary [1] and ternary [2] systems. Type curves showing the relation between the total rate and the mixture composition have been established for the special case of the binary system [1] and a condition developed for the existence of a minimum in the ratio of total rate to concentration of one component [3]. The results of these investigations can be applied not only to copolymerizations but also to other chain reactions such as the oxidation of hydrocarbons [4-6]. The present work will attempt a general solution of the problem of the kinetics of a chain reaction in a complex mixture and will discuss the most interesting of the special cases. The theory which is outlined below is applicable to reactions of copolymerization, oxidation, cracking, and so forth.

The scheme of a complex chain reaction can be represented in the form:

$$\text{Chain initiation, rate } W_l$$

$$\text{Chain propagation, } A_i + n_j \xrightarrow{K_{pij}} n_i + \text{inactive product}$$

$$\text{Linear rupture, } M_i + n_j \xrightarrow{K_{sij}} \text{inactive product}$$

$$\text{Second power rupture, } n_i + n_j \xrightarrow{K_{tij}} \text{inactive product}$$

Here, $\underline{n}$ is an active center, A is the substance which is participating in the chain reaction and M is the substance on which linear rupture takes place. These same symbols will be used in what follows for designating the corresponding concentrations.

The following equations can be written for a stationary approximation in the case of sufficiently long chains where diffusion is neglected:

$$-\frac{dA_i}{dt} = \sum_j K_{pij} A_i n_j, \tag{1}$$

$$\sum_l K_{pij} A_i n_j = \sum_j K_{pij} A_l n_i, \tag{2}$$

$$W_l = \sum_{ij} K_{sij} M_i n_j + \sum_{ij} K_{tij} n_i n_j. \tag{3}$$

Here, (1) gives the rate of consumption of the i-th component (2), the condition for equality between the rates of formation and consumption of the i-th active center, and (3), the condition for equality between the rates of formation and destruction of the active centers. An expression for $-dA_i/dt$ as a function of the concentrations of the reacting substances alone is obtained by solving (2) and (3) for n_j and setting the result into (1):

$$-\frac{dA_i}{dt} = C_{st} D_{ki} \sum_j K_{pji} A_j, \tag{4}$$

here C_{st} is a constant which is to be evaluated from the relation:

$$C_{st} = \pm \left[\frac{1}{4} \left(\frac{\sum_{ij} K_{sij} M_i D_{kj}}{\sum_{ij} K_{tij} D_{ki} D_{kj}} \right)^2 + \frac{W_I}{\sum_{ij} K_{tij} D_{ki} D_{kj}} \right]^{1/2} - \frac{1}{2} \frac{\sum_{ij} K_{sij} M_i D_{kj}}{\sum_{ij} K_{tij} D_{ki} D_{kj}}; \tag{5}$$

and D_{kl} is the adjunct of the i-th element of the k-th row of the determinant of the system of homogeneous linear equations which results from condition (2). For convenience, this determinant can be written as:

$$|K_{pij} - a_j \delta_{ij}|$$
$$\left(\delta_{ij} = 1 \text{ when } j = i;\ \delta_{ij} = 0 \text{ when } j \neq i;\ a_i = \sum_j K_{pji} A_j / A_i\right). \tag{6}$$

Eq. (4) is the general solution of the above-formulated problem. This expression gives the rate of chain consumption of a multicomponent system. Pure linear, or pure second-power, rupture can be accounted for by changing the quantity C_{st} in (4):

$$C_s = W_I \Big/ \sum_{ij} K_{sij} M_i D_{kj} \qquad \text{linear rupture,} \tag{7}$$

$$C_t = \pm \left(W_I \Big/ \sum_{ij} K_{tij} D_{ki} D_{kj} \right)^{1/2} \text{ second-power rupture.} \tag{8}$$

We will now treat the influence of the mixture composition on the rate of chain reaction of each of the components, and on the total reaction rate, using the simplest instances of binary systems by way of examples. For a binary system with pure linear rupture (rupture on a single component), a combination of (4) with (7) gives:

$$-\frac{dA_1}{dt} = W_I \frac{r_1 A_1^2 + A_1 A_2}{\lambda_1 A_1 + \lambda_2 A_2}, \tag{9}$$

$$-\frac{d(A_1 + A_2)}{dt} = W_I \frac{r_1 A_1^2 + 2A_1 A_2 + r_2 A_2^2}{\lambda_1 A_1 + \lambda_2 A_2}, \tag{10}$$

where

$$r_1 = \frac{K_{p11}}{K_{p21}}, \quad r_2 = \frac{K_{p22}}{K_{p12}}, \quad \lambda_1 = \frac{K_{s11}}{K_{p21}} M_1, \quad \lambda_2 = \frac{K_{s12}}{K_{p12}} M_1.$$

A similar result is obtained from (4) and (8) for the case of second-power rupture:

$$-\frac{dA_1}{dt} = W_I \frac{r_1 A_1^2 + A_1 A_2}{(\alpha_1 A_1^2 + 2\beta A_1 A_2 + \alpha_2 A_2^2)^{1/2}}, \tag{11}$$

$$-\frac{d(A_1+A_2)}{dt} = W^{1/2}\frac{r_1A_1^2+2A_1A_2+r_2A_2^2}{(\alpha_1A_1^2+2\beta A_1A_2+\alpha_2A_2^2)^{1/2}}, \tag{12}$$

$$\alpha_1 = \frac{K_{t11}}{K_{p21}^2}, \quad \alpha_2 = \frac{K_{t22}}{K_{p12}^2}, \quad \beta = \frac{K_{t12}}{K_{p12}K_{p21}}.$$

We will now introduce the notation: $-dA_1/dt = W_1$, $-d(A_1 + A_2)/dt = W$, $-dA_2/dt = W_2$ and develop the relation between the mixture composition and the rate W_1. We will consider that an increase in the A_2 concentration of the mixture will increase or diminish the rate W_1 when

$$\left|\frac{\partial W_1}{\partial A_1}dA_1\right| < \left|\frac{\partial W_1}{\partial A_2}dA_2\right| \tag{13}$$

an increase in the rate resulting with the condition

$$dW_1 > 0, \tag{14}$$

and a decrease, with the condition

$$dW_1 < 0, \tag{15}$$

where dW_1 is the complete differential of the rate W_1.

1. Effect of A_2 on the initial rates (9)-(12). It will be assumed that W = const and $A_1 + A_2 = A_0$ (A_0 = const). For linear rupture in the neighborhood of $A_2 = 0$, use of (13) with (14), and (13) with (15), shows that addition of A_2 to A_1 will increase W_1 when the condition

$$1/r_1 - \lambda_2/\lambda_1 > 1 \qquad \text{criterion for acceleration} \tag{16}$$

is fulfilled, and diminish W_1 when the condition

$$\lambda_2/\lambda_1 - 1/r_1 > 1 \qquad \text{criterion for retardation} \tag{17}$$

is fulfilled.

The criteria of Expressions (16) and (17) involve only the kinetic constants. The effect of an addition of A_2 on the rate W_1 can be predicted from the values of these criteria. The possibility of maxima or minima which will appear with further increase in the concentration of A_2 is fixed by the condition $dW_1 = 0$, from which it follows that:

$$\lambda_2\left(\frac{A_2}{A_1}\right)^2 + 2r_1\lambda_2\frac{A_2}{A_1} + (r_1\lambda_1 - \lambda_1 + r_1\lambda_2) = 0. \tag{18}$$

The positive roots of (18) will give the maxima or minima if any such exist. Criteria for the effect of addition of A_2 on W in the neighborhood of $A_2 = 0$ can be obtained in a similar fashion:

$$2/r_1 - \lambda_2/\lambda_1 > 1 \tag{19}$$

$$\lambda_2/\lambda_1 - 2/r_1 > 1 \tag{20}$$

Maxima and minima are to be found from Eq. (21):

$$(r_2\lambda_1 - 2\lambda_2 + r_2\lambda_2)\left(\frac{A_2}{A_1}\right)^2 - 2(r_1\lambda_2 - r_2\lambda_1)\frac{A_2}{A_1} - (r_1\lambda_1 - 2\lambda_1 + r_1\lambda_2) = 0. \quad (21)$$

For the case of second-power rupture, the criteria for acceleration or retardation of W_1 in the neighborhood of $A_2 = 0$ take the form

$$1/r_1 - \beta/\alpha_1 > 1 \quad \text{criterion for acceleration} \quad (22)$$

$$\beta/\alpha_1 - 1/r_1 > 1 \quad \text{criterion for retardation} \quad (23)$$

Similarly for W

$$2/r_1 - \beta/\alpha_1 > 1 \quad \text{criterion for acceleration} \quad (24)$$

$$\beta/\alpha_1 - 2/r_1 > 1 \quad \text{criterion for retardation} \quad (25)$$

The maxima and minima of W_1 are to be located from the equation:

$$\alpha_2\left(\frac{A_2}{A_1}\right)^3 + (2r_1\alpha_2 + \beta)\left(\frac{A_2}{A_1}\right)^2 + (r_1\alpha_2 - \beta + 3r_1\beta)\frac{A_2}{A_1} + (r_1\alpha_1 - \alpha_1 + r_1\beta) = 0 \quad (26)$$

and those of W, from the equation

$$(r_2\alpha_2 - 2\alpha_2 + r_2\beta)\left(\frac{A_2}{A_1}\right)^3 - (2r_1\alpha_2 + 2\beta - r_2\alpha_1 - 3r_2\beta)\left(\frac{A_2}{A_1}\right)^2 + (2r_2\alpha_1 + 2\beta - r_1\alpha_2 - 3r_1\beta)\frac{A_2}{A_2} - (r_1\alpha_1 - 2\alpha_1 + r_1\beta) = 0. \quad (27)$$

2. The alteration in the composition of a multicomponent mixture in the course of a composite chain reaction. The reaction kinetics determine the concentration ratios of the several substances which participate in a composite chain reaction. These concentration ratios can be obtained in differential form from (4) as ratios of the corresponding rates.* This involves cancellation of the constant so that the ratios contain the rate constants for chain propagation but not those for chain initiation or rupture. We will now consider the example of a composite chain reaction of two substances proceeding according to the scheme:

$$A_1 \rightarrow A_2 \rightarrow \text{inactive product}$$

$$\frac{dA_2}{dA_1} = \frac{W_1 - W_2}{-W_1} = -\frac{r_1A_1^2 - r_2A_2^2}{r_1A_1^2 + A_1A_2}. \quad (28)$$

Integration of (28) gives the two solutions:

1) $\gamma > 0$:

$$\frac{\left\{\left[1 + \frac{2\varkappa}{1r_1 - \sqrt{\gamma}}\left(\frac{A_2}{A_1}\right)\right] \Big/ \left[1 + \frac{2\varkappa}{r_1 + \sqrt{\gamma}}\left(\frac{A_2}{A_1}\right)\right]\right\}^{r_1(r_2-\varkappa)/\gamma}}{1 + \frac{A_2}{A_1} + \frac{\varkappa}{r_1}\left(\frac{A_2}{A_1}\right)^2} = \left(\frac{A_1}{A_0}\right)^{2\varkappa}; \quad (29)$$

2) $\gamma < 0$

$$\frac{r_1}{\sqrt{-\gamma}}(r_2 - \varkappa)\operatorname{arc\,tg}\frac{\frac{2\varkappa}{r_1}\left(\frac{A_2}{A_1}\right)}{\frac{\sqrt{-\gamma}}{r_1} + \frac{2\varkappa}{\sqrt{-\gamma}}\left(\frac{A_2}{A_1}\right) + \frac{r_1}{\sqrt{-\gamma}}} = \frac{1}{2}\ln\left\{\left(\frac{A_1}{A_0}\right)^{2\varkappa}\left[1 + \frac{A_2}{A_1} + \frac{\varkappa}{r_1}\left(\frac{A_2}{A_1}\right)^2\right]\right\}; \quad (30)$$

*These ratios can be obtained in another form by the use of determinants [7].

$\gamma = r_1^2 - 4r_1\kappa$, $\kappa = 1 - r_2$; and A_0 is the initial concentration of A. It can be shown that the above criteria for the acceleration and retardation of W_1 in the neighborhood of $A_2 = 0$ remain valid for the case in which the rate of initiation is constant. This shows that it is always possible to employ these criteria for determining the effect of the formation of the substance A_2 on the rate of the chain reaction of A_1. Similar criteria for the total reaction rate can be obtained from (13), (14) and (13), (15).

LITERATURE CITED

[1] H. W. Melville, B. Noble, and W. F. Watson, J. Polym. Sci. 2, 229 (1947).

[2] D. C. Blackley, H. W. Melville, and L. Valentine, Proc. Roy. Soc. A, 227, 10 (1954).

[3] S. R. Palit, Trans. Farad. Soc. 51, 1129 (1955).

[4] G. Russel, J. Am. Chem. Soc. 77, 4583 (1955).

[5] T. A. Ingles and H. W. Melville, Proc. Roy. Soc. A, 218, 163 (1953).

[6] G. M. Burnett and L. D. Loan, Trans. Farad. Soc. 51, 214 (1955).

[7] C. Walling and E. R. Briggs, J. Am. Chem. Soc. 67, 1774 (1945).

Received May 13, 1959

THE EFFECT OF ALLOYING ELEMENTS ON THE CORROSION AND ELECTROCHEMICAL BEHAVIOR OF TITANIUM

V. V. Andreeva and V. I. Kazarin

The Institute of Physical Chemistry of the Academy of Sciences, USSR

(Presented by Academician A. N. Frumkin, April 28, 1959)

Our preceding papers [1, 2] have dealt with the corrosional stability and electrochemical properties of titanium. The surface films which are formed in air and in liquid media have been shown to play an important role in determining the corrosional behavior of this metal [3-6].

The present communication will consider the effect of various alloying metals on the corrosion and electrochemical behavior of titanium, and the mechanism of the protective action shown by these metals. The effect of alloying with Cu, Zr, Nb, Mo, Ta, V, Al, Cr, Fe, Ni, Mn, Si, and B has been studied. The alloys did not contain more than 10% of the alloying component. The titanium–zirconium alloys were exceptional in that the concentration of zirconium reached 50%. Through the study and analysis of the characteristics of pure titanium, and of those metals which alloy with titanium, it was possible to obtain binary and ternary alloys which had better physicochemical and mechanical properties than unalloyed titanium [7-9].

Unalloyed titanium exists in two allotropic modifications; the α (stable up to 882°, hexagonal lattice) and the β (stable above 882°, body-centered cubic lattice). The single-phase alloys could be supposed to have the higher corrosional stabilities. It was for this reason that the systems selected for study were principally ones having a rather wide field of solid solutions of the alloying component in α-titanium, or ones in which a solid solution of the alloying element in β-titanium could be fixed by quenching.

Optimal procedures were developed for the thermal treatment of the titanium based alloys. The most favorable thermal treatment from the standpoint of corrosional stability was that which promoted the formation of a single-phase alloy with a fully recrystallized structure.

The experimental data showed that the titanium alloys could be divided into three principal groups on the basis of corrosional stability. The first of these groups contained those alloys in which the alloying element markedly increased the corrosional stability of titanium in a given aggressive medium. Mo, Ta, Nb, Zr, and V are elements of this type. The second group contained the alloys in which the alloying element did not alter the corrosional stability of titanium. Si is such an element. The third group contained the titanium alloys in which the corrosional stability of the titanium had been sharply impaired by alloying with such elements as Fe and Mn.

The curves of Fig. 1 show the relation between the content of the alloying component and the rate of corrosion in sulfuric acid for the case of the titanium alloys of the first group. These curves show that the rate of dissolution of titanium in this medium can be sharply reduced by the addition of relatively small amounts (from 1 to 2.5%) of such alloying components as Mo, Ta, Nb or Zr. There is either no further increase in the corrosional stability of the alloy, or only an infinitesimal increase (in comparison with the effect observed with from 1 to 2.5% of this additive), when the amount of the alloying component is raised to approximately 10%. It is only when the concentration of the alloying component becomes quite high (> 20%) that a further increase in the corrosional stability of the alloy is observed. A titanium–zirconium alloy containing 50% of zirconium

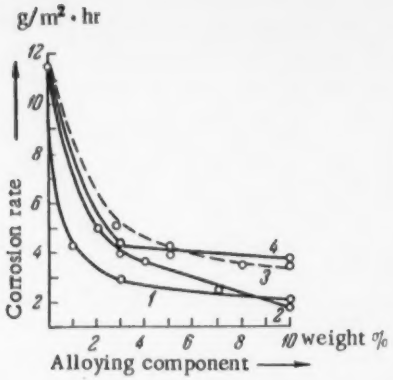

Fig. 1. The relation between the percentage of alloying elements in titanium based alloys and the rate of corrosion in 10% H_2SO_4 solution at 40°: 1) Ta, 2) Mo, 3) Nb, 4) Zr.

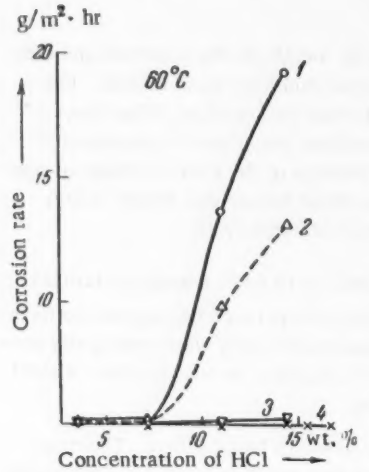

Fig. 2. The relation between the rates of corrosion of Ti, Zr, and titanium alloys containing 5 and 50% zirconium, and the concentration of HCl at 60°: 1) Ti, 2) Ti + 5% Zr, 3) Ti + 50% Zr, 4) Zr.

can serve as an example (Fig. 2). The corrosional resistance of this alloy to solutions of H_2SO_4 and HCl is just as high as that of pure Zr, which is practically uncorroded by these solutions.

The added components decrease in their effectiveness in raising the corrosional stability of the alloys of the first group in the order Mo, Ta, Zr, Nb, Cu, V. The corrosional stability of titanium is increased to such a degree by the addition of Mo and Ta that the resulting alloys show high corrosional stability in those solutions in which titanium is usually unstable.

Anodic and cathodic polarization curves for titanium and for binary alloys of titanium with Mo, Nb, and Ta, in 40% H_2SO_4, are given in Fig. 3. These curves show that the "critical" anodic current density is lowest for a Ti + 10% Ta alloy and highest for the unalloyed titanium. The curves for the Ti + 10% Mo and the Ti + 10% Nb alloys occupy intermediate positions.

The relation between the temperature and the rate of corrosion in 40% H_2SO_4 for the cases of titanium, and Ti + 10% Ta, Ti + 10% Mo, and Ti + 10% Nb alloys, is shown in Fig. 4. This figure indicates that there is a linear relationship between T^{-1} and the logarithm of the corrosion rate. Calculations give a value of 16.7 kcal/mole for the energy of activation for the ionization of titanium and its alloys with Mo and Nb, and a value of 13.5 kcal/mole for the titanium alloy with 10% Ta [2].

The addition of 3 or 5% iron, or manganese, to the titanium sharply reduces its corrosional stability in H_2SO_4 and in HCl solutions.

These experimental results lead to the following general rule. An alloying metal will increase the corrosional stability of titanium by participating in the formation of a surface film if the stability of this metal in the given medium is fixed by the properties of the protective film which is formed on its surface and this stability is greater than that of titanium.

It is clear that the experimental results can be explained in the light of the theory of Wagner [10-12] and Hauffe and his collaborators [13-16]. This theory makes it possible to pick out of the periodic system those elements which can form more perfect protective films on titanium and thus increase the corrosional stability of this metal. It will be remembered that the diffusion of ions and electrons through a protective film has been related to the semiconducting properties of the film by a recently advanced theory of chemical corrosion. This mechanism supposes an independent migration of ions and electrons along the lattice defects, or between the lattice positions, with a resultant formation of concentration gradients of those particles which act as driving forces. The theory of semiconduction is known to be based on a model of the real crystal lattice. The degree of departure of the actual lattice from the ideal is decisive in fixing the characteristics of semiconductors. Each dislocation or breakdown of the ideal crystal lattice exerts its influence on the mechanical properties of the crystal, and on its growth and activity. There is a very great difference between the chemical activity of the perfect structure and the activity of a structure in which there is a large number of dislocations [17].

Only in those cases where TiO_2 plays a decisive role in fixing the passivity, i.e., where a compact, nonporous, protective oxide layer of infinitesimal solubility in the given medium forms on the metallic surface, is it possible to think of applying the above mechanism to explain the corrosional stability of titanium and its

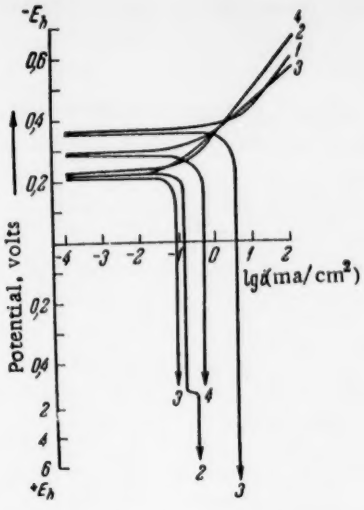

Fig. 3. Anodic and cathodic polarization curves for titanium and its alloys in 40% HCl at 40°: 1) Ti, 2) Ti + 10% Ta, 3) Ti + 10% Mo, 4) Ti + 10% Nb.

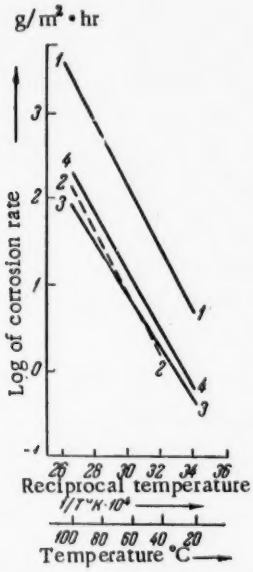

Fig. 4. The relation between T^{-1} and the rate of corrosion of titanium and its alloys in 40% H_2SO_4: 1) Ti, 2) Ti + 10% Mo, 3) Ti + 10% Ta, 4) Ti + 10% Nb.

alloys. Titanium dioxide is known to show electronic conduction. The measurements of various investigators on the electrical conductivity of TiO_2 [18-20] have shown that there is an excess of titanium ions and electrons (in comparison with the stoichiometric formula for the compound) at the metal–oxide film boundary, this excess being due to oxygen ion vacancies rather than to an excess of cations in the interstices in the titanium oxide lattice.

Because of these oxygen vacancies, the rate of diffusion of oxygen into TiO_2 is higher than the rate of diffusion into titanium, and the diffusion of oxygen through the TiO_2 layer to the titanium can thus be considered to be the factor which determines the rate of oxidation of the titanium when the film growth follows a parabolic law. The Wagner – Hauffe theory predicts that it is possible to displace the equilibrium in one direction or the other, i.e., to increase or diminish the number of defects, by introducing a second metal into the titanium. This second metal must participate in the formation of an oxide film on the alloy. The introduction of a metal of higher valence than titanium should lead to a diminution of the number of oxygen ion vacancies because of the resultant increase of free electrons, whereas addition of a second metal of lower valence than titanium should increase the number of oxygen ion vacancies by decreasing the number of free electrons. In the symbolism of Schottky, the formation of oxygen ion vacancies in the titanium dioxide lattice would be represented by:

$$TiO_2 \rightleftarrows O^{\square\cdot\cdot} + 2\ominus + \tfrac{1}{2}O_2^{gas} \qquad (1)$$

The oxygen deficit results in the formation of an equivalent number of vacancies, $O^{\square,\cdot\cdot}$, and free electrons, $\ominus$. The following reactions would represent the dissolving of niobium, tantalum, or molybdenum oxides (Nb_2O_5, Ta_2O_5 and MoO_3) in titanium dioxide during the alloying of titanium with these elements:

$$Nb_2O_5 \rightleftarrows 2Nb_{Ti}^{\bullet} + 2\ominus + 2TiO_2 + \tfrac{1}{2}O_2^{(gas)}$$

or (2)

$$O^{\square\cdot\cdot} + Nb_2O_5 \rightleftarrows 2Nb_{Ti}^{\bullet} + 2TiO_2 + 2\ominus$$

and

$$MoO_2 \rightleftarrows Mo_{Ti}^{\bullet\bullet} + 2\ominus + TiO_2 + \tfrac{1}{2}O_2^{(gas)}$$

or (3)

$$O^{\square} + MoO_2 \rightleftarrows Mo_{Ti}^{\bullet\bullet} + \ominus + TiO_2 + \tfrac{1}{2}O_2^{(gas)}$$

here the symbols $Nb_{Ti}^{\bullet}$ and $Mo_{Ti}^{\bullet\bullet}$ indicate those ions of Nb and Mo, respectively, which replace titanium ions in the oxide lattice.

Equations (2) and (3) show that pentavalent niobium ions, or the hexavalent molybdenum ions, increase the number of free electrons and thereby diminish the number of oxygen ion vacancies. The rate of corrosion of titanium should be increased by the introduction of ions of lower valence than titanium (Fe^{+3}, Mn^{+2}, for

example) into the oxide film of the titanium. The replacement of certain tetravalent titanium ions by trivalent ions, or by other metal ions of lower valence, must increase the number of oxygen ion vacancies and at the same time diminish the number of electrons, if the Law of Mass Action remains valid.

Zirconium dioxide will predominate in the formation of a protective film on the alloy surface when large amounts of this element (up to 50%) are introduced into titanium, so that the corrosional stability of a 50% Ti, 50% Zr alloy will be more nearly the same as that of pure zirconium.

LITERATURE CITED

[1] V. V. Andreeva and V. I. Kazarin, Inst. Tech.-Econ. Information, Acad. Sci. USSR, Project 23, No. I-56-159 (1956).

[2] V. V. Andreeva and V. I. Kazarin, Proc. Acad. Sci. USSR 121, No. 5, 875, 1958.*

[3] V. V. Andreeva and V. I. Kazarin, Proc. Acad. Sci. USSR 123, No. 6, 1048 (1958).*

[4] V. V. Andreeva, Proc. Inst. Phys. Chem., Acad. Sci. USSR, Vol. 6, 79 (1957).

[5] V. V. Andreeva, Inst. Tech. Econ. Information, Acad. Sci. USSR, Project 9, PS-55-503, Moscow, 1955.

[6] V. V. Andreeva and N. A. Shishakov, J. Phys. Chem 32, 7 (1958).

[7] V. V. Andreeva, G. P. Danilova, and Ya. M. Lipkes, State Comm. of the Council of Ministers of the USSR for New Tech. Methods, Advanced Technical Production Experiments, Series 19, No. T-56-452/9, Moscow 1956.

[8] V. V. Andreeva, V. I. Kazarin, G. P. Danilova, et al. State Rare Metals Sci. Res. Inst., Moscow, 1958.

[9] V. V. Andreeva, G. P. Danilova, I. P. Druzhinina, E. A. Kamenskaya, and M. V. Mal'tsev, State Scientific-Technical Committee of the Council of Ministers of the USSR, Acad. Sci. USSR, Project 18, M-58-274/15, Moscow, 1958.

[10] C. Wagner, J. Chem. Phys. 18 b. 2 (1950).

[11] C. Wagner, Thermodynamics of Alloys, Cambridge, 1952.

[12] C. Wagner, J. Electrochem. Soc. 99, 346 (1952).

[13] K. Hauffe, Progress in Metal Physics, London, 1953.

[14] K. Hauffe, Werkstoffe u. Korrosion, No. 3, 117 (1955).

[15] K. Hauffe, Passivierende Filme u. Deckschichten anlaufschichten Heidelberg, Berlin, Gottingen, 1956.

[16] P. Kofstad and K. Hauffe, Werkstoffe u. Korrosion, No. 11, 642 (1956).

[17] A. Ris, Chemistry of Crystals with Defects [Russian translation], IL, 1956.

[18] M. D. Earle, Phys. Rev. 61, 61 (1942).

[19] P. Ehrlich, Z. Elektrochem. 45, 362 (1939).

[20] K. Hauffe and H. Pfeiffer, Z. Elektrochem. 56, 390 (1952).

Received April 15, 1959

*Original Russian pagination. See C. B. Translation.

THE LAW OF DARKENING OF THE PHOTOGRAPHIC EMULSION IN THE REGION OF SOLARIZATION

E. A. Galashin

(Presented by Academician P. A. Rebinder, May 25, 1959)

Photographic reduction has been neglected in the attempted derivations of an analytical expression for the law of blackening [1]. A new equation for the characteristic curve which will give a satisfactory first approximation of the region of reduction can be readily obtained from the coagulation theory of photographic reduction and the ideas of K. V. Chibisov and E. A. Kirillov [2] concerning the inactivation of silver centers.

We will follow Volmer and Schaum [3] in distinguishing three steps in the photolysis of the silver halides.

$$\underset{\text{Silver halide}}{A} \longrightarrow \underset{\text{Latent image center}}{B} \longrightarrow \underset{\text{Solarized image center}}{C} \qquad (1)$$

We will depart from the views of Volmer and Schaum in treating the photolysis of the silver halides in the ordinary photographic emulsion as an irreversible process, i.e., we will consider that there is little likelihood of a recombination of the silver latent image centers, or of a transformation of the "solarized" image centers into active centers, under the "dispersive" action of radiation of long wavelength.

It is clear that the photolysis of the silver halides should be looked upon as the result of many sequential reactions involving numerous intermediate steps. A first approximation can be had by limiting the discussion of the kinetics to the case of the simplest of sequential reactions with a single intermediate step, as in the scheme of Volmer and Schaum.

We will suppose further that both of the reactions, $A \rightarrow B$ and $B \rightarrow C$, will take place under the action of light of any wavelength. The effectiveness of the $B \rightarrow C$ reaction rises with an increase in the wavelength while that of the $A \rightarrow B$ reaction diminishes.

Let the photolayer be acted on by a heterogeneous bundle of rays of both short and long wavelengths. The rate of transformation of the substance A will then be given by

$$dx/dt = k_1 I_1 (a - x) + k_2 I_2 (a - x) = (k_1 I_1 + k_2 I_2)(a - x)$$

or

$$dx/dt = k(a - x), \qquad (2)$$

where $k = k_1 I_1 + k_2 I_2$; $\underline{x}$ is the number of moles of AgBr which have undergone decomposition, $\underline{a}$ is the number of moles of AgBr initially present, I_1 is the intensity of the light of short wavelength, I_2 is the intensity of the light of long wavelength, and k_1 and k_2 are the rate constants for photolysis.

The rate of transformation of B is given by

$$dy/dt = l_1 I_1 (x - y) + l_2 I_2 (x - y) = (l_1 I_1 + l_2 I_2)(x - y)$$

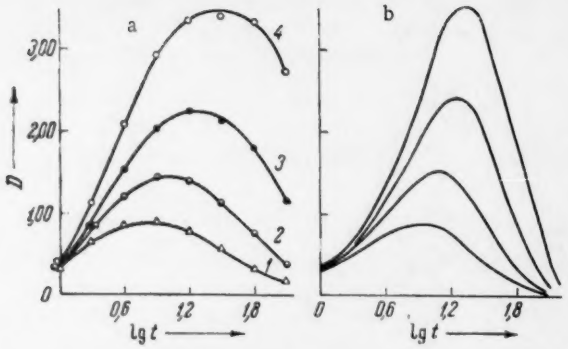

Fig. 1. a) Reduction in the action of mixed blue and red rays on a diapositive emulsion. Relative intensity of the red rays; 1) 1, 2) 0.5, 3) 0.25, 4) 0.125. b) Theoretical curves obtained from Eq. (5). Constant 1 (sec^{-1}) equal to: 1) 0.60, 2) 0.30, 3) 0.15, 4) 0.075; K = 0.072 sec^{-1}; D_m = 10.

or

$$dy / dx = l(x - y), \tag{3}$$

where $l_1 = l_{1}I_1 + l_{2}I_2$; $\underline{y}$ is the number of gram-equivalents of Ag converted into the inactive form and l_1 and l_2 are the rate constants for the inactivation of the latent image.

The integration of Eqs. (2) and (3) leads to the following expression for the amount of the intermediate product, i.e., for the number of gram-equivalents of metallic silver in the active form of the latent image [4]:

$$x - y = \frac{ka}{k - l}(e^{-lt} - e^{-kt}). \tag{4}$$

Supposing the optical density of the developed image to be proportional to the surface concentration of the photolytically formed active silver, we finally obtain:

$$D = D_m \frac{k}{k - l}(e^{-lt} - e^{-kt}), \tag{5}$$

where D is the optical density of blackening for an exposure time $\underline{t}$ and D_m is the maximum blackening.

Equation (5) proves to be in good agreement with certain experimental data:

1. The rate of photolysis is markedly increased by having a large excess of bromine acceptors in the film [5]. In this case $k \gg l$ and (5) goes over into the well-known equation of Elder [6]:

$$D = D_m(1 - e^{-kt}).$$

Photographic reduction is no longer observed here and this is consistent with the fact that bromine acceptors eliminate solarization.

2. We can see that the height of the maximum on the (D, t) curve is determined by the ratio of the rate constants for photolysis and for inactivation of the resultant development centers

$$r = k / l.$$

A decrease in the k/l ratio must lead to a diminution of the optical density of blackening of the photographic plate at the maximum point. A decrease in the k/l ratio, i.e., a relative increase in the rate of

inactivation of the centers with respect to the rate of photolysis, can be brought about by introducing an excess of bromides and desensitizers into the emulsion. A similar effect could be expected to result from an increase in the wavelength of the exposure radiation. The theoretically predicted diminution of the maximum density of blackening is actually observed here [8].

3. An increase in the intensity of the long-wave components of the heterogeneous radiation should result in a corresponding increase in the constant l. The constant $\underline{k}$ will remain unchanged if the long waves are not appreciably photochemically active.

The experimental (D, t) curves for this case are compared in Fig. 1 with theoretical curves which were obtained from Eq. (5). The figure shows the theoretical and the experimental curves to be in agreement. Ordinary diapositive films were used in these experiments. Exposure was carried out under a mixture of red (> 650 mμ) and blue (360-450 mμ) rays. The intensity of the long waves was altered by the introduction of neutral-gray filters.

I wish to express my indebtedness to K. V. Chibisov, Corresponding Member of the Academy of Sciences of the USSR, to Professor V. I. Tatevskii, and to V. P. Lebedev for their interest in this work and for their valuable advice.

LITERATURE CITED

[1] S. P. Shuvalov, J. Phys. Chem. 8, 387, 514 (1936); 11, 384 (1939); J. H. Webb, J. Opt. Soc. Am. 29, 309, 314 (1939); 38, 312 (1947); Kh. S. Bagdasar'yan, J. Tech. Phys. 16, 703 (1946).

[2] K. V. Chibisov, Prog. Chem. 22, 1222 (1953); E. A. Kirillov, Fine Structure of the Absorption Spectra of Photochemically Colored Silver Halides [in Russian], Acad. Sci. USSR, Press, 1954.

[3] M. Volmer and K. Schaum, Z. wiss. Photogr. 14, 1 (1914).

[4] A. V. Rakovskii, Chemical Kinetics and Catalysis [in Russian], Moscow, 1931, p. 24.

[5] W. Meidinger, Phys. Z. 38, 905 (1937).

[6] H. M. Elder, J. of the Camera Club, London, 7, 131 (1893).

[7] Lüppo-Cramer, Das latente Bild, Halle, 1911, S. 37.

[8] E. A. Galashin and V. M. Tatevskii, Proc. Acad. Sci. USSR 109, 347 (1956); J. Phys. Chem. 31, 1426 (1957).

Received May 12, 1959

THE KINETIC LAWS OF AUTOCATALYTIC REACTIONS IN OPEN SYSTEMS

E. T. Denisov, Z. K. Maizus, I. P. Skibida, and N. M. Émanuél', Corresponding Member, Academy of Sciences, USSR

The Institute of Physical Chemistry of the Academy of Sciences, USSR

Continuous chemical processes are widely used throughout modern chemical industry. The changes which occur in such processes are instances of reactions in so-called open systems, that is to say these reactions occur in systems in which there is an exchange of matter through the boundary. The study of such systems is of interest for both chemical kinetics and biochemistry [1].

Relatively little work has been done on the theory of continuous processes. The kinetic laws applying to the continuous operation of certain simple types of reactions have been considered in [2-4]. No treatment of this aspect of the practically important autocatalytic reactions, in general, or of the degenerative-branching chain reactions of oxidation of organic substances, in particular, has been given as yet. The available literature on the continuous oxidation of organic substances [5-6] fails to touch on the kinetic laws of such processes.

The present work is devoted to a study of the kinetic laws applying to the continuous operation of degenerative-branching chain reactions of oxidation. The rates of such reactions are fixed by the concentration of the intermediate products (peroxides) which arise from the chain branching.

Cyclohexanone was selected as the working material. Oxidation was carried out in a glass oxidation cell which had the form of an ideal mixing reactor, the temperature of oxidation being 130° and the rate of introduction of the oxygen, 1.6 liter/hour. The process was carried out continuously by running the cyclohexanone into the reactor, and withdrawing a part of the reacting mixture, at a constant rate. The construction of the reactor was such as to assure equality between the rate of feed of the reactant materials and the rate of removal of the products. We will now introduce the concept of the "specific rate", $\underline{v}$, defined as the volume of the initial liquid component entering unit volume of the reactor in unit time. The quantity $\underline{v}$ has the dimensions of reciprocal time. The value of $1/v$ represents the mean time of retention of the liquid in the reactor.

The amounts of peroxide, adipic acid, and CO_2 were determined in the reaction products from the continuous process carried out at various specific rates. A stationary state is set up some time after passing from the periodic oxidation to the continuous reaction, i.e., the rate of formation of the products then becomes equal to the rate at which these products are withdrawn from the reacting mixture.

The equilibrium concentration of the hydroperoxides proved to be low and only very slightly dependent on the specific rate of feed of the cyclohexanone.

v 1/hr		0	0,079	0,353	0,583	0,785	1,175
$[ROOH]_{eg}$	mole %	0,308	0,298	0,285	0,272	0,262	0,243

The following considerations are sufficient for explaining this insignificant variation in the equilibrium concentration of the hydroperoxide. The rate of change of the concentration of the hydroperoxide can be expressed through the following equation:

$$\frac{d[\mathrm{ROOH}]}{dt} = W\text{for} - k_M[\mathrm{ROOH}] - v[\mathrm{ROOH}],$$

in which k_M is the rate constant for the breakdown of this compound. In the stationary state

$$\frac{d[\mathrm{ROOH}]}{dt} = 0 \text{ and } [\mathrm{ROOH}]_{\text{стац}} = \frac{w\text{ for}}{v + k_M}.$$

The quantity k_M can be evaluated from the kinetic curves for the accumulation of adipic acid, if the rate of formation of this acid is assumed to be proportional to the hydroperoxide concentration.

The resultant value of $k_M = \frac{w_{\text{acid}}}{[\mathrm{ROOH}]}$ is considerably larger than $\underline{v}$ and it is for this reason that the equilibrium hydroperoxide concentration is affected only weakly by an alteration in the specific rate of feed of the cyclohexanone. The equilibrium concentration of the adipic acid is much more strongly dependent on the specific rate of withdrawal of the products.

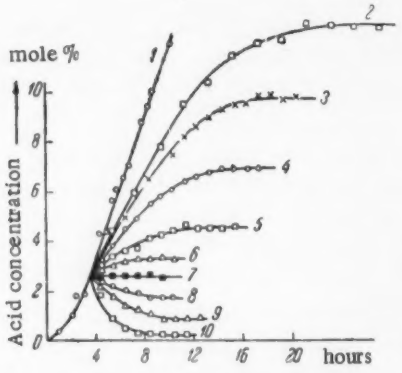

Fig. 1. Kinetic curves for the formation of adipic acid in the oxidation of cyclohexanone at 110° by a periodic process (1), and by a continuous process, with various specific rates of withdrawal of the products ($\underline{v}$, hours^{-1}): 2) 0.0392, 3) 0.0785, 4) 0.1175, 5) 0.235, 6) 0.353, 7) 0.471, 8) 0.548, 9) 0.785, 10 1.175.

The equilibrium concentration of the acid is the higher, $\underline{v}$ the lower, when passage to the continuous process is always made at the same initial acid concentration (Fig. 1).

It is characteristic that the kinetic-equilibrium concentrations of the reaction products do not depend on the initial conditions, i.e., these concentrations are independent of the state of the reaction at the instant of passage into the continuous regime. The rate of formation, or consumption, of any one substance in a homogeneous reaction is fully determined by the flow concentrations of those materials which are present in the mixture. It is thus possible to write the following system of differential equations for any reaction which is proceeding in an open system with the participation of the initial, intermediate, and final substances $A_1, A_2, \ldots A_k$:

$$\frac{d[A_i]}{dt} = w_i \text{ for } ([A_1] \ldots [A_k]) - w_i \text{ con } ([A_1] \ldots . \ldots . [A_k] + v[A_{i0}]) - v[A_i] \quad (i = 1, 2, \ldots k), \tag{1}$$

$[A_{i0}]$ being the concentration of A_1 in the liquid which is entering the reactor.

When the stationary state is established, $\frac{d[A_i]}{dt} = 0$, and the system of differential equations (1) then passes into a system of algebraic equations:

$$0 = w_i \text{ for } ([A_1] \ldots [A_k]) - w_i \text{ con } ([A_1] \ldots [A_k]) + v[A_{i0}] - v[A_i]. \tag{2}$$

The stationary concentrations, $[A_i]$, can be found by solving this system. It is essential here that these concentrations be determined by the instantaneous concentrations of the products alone, i.e., that they be independent of the product concentrations at the moment of passage into the continuous process.

Our experiments actually give kinetic curves for the change in the adipic acid concentration which show an equilibrium concentration characteristic of the given $\underline{v}$ value, regardless of the extent of oxidation at the instant of passage to the continuous process (Fig. 2). The system of Eq. (1) also shows that the rate of change of the concentrations of the reacting substances in the continuous process will be less than the rate of accumulation of substances in the periodic process, when $[A_{i0}] < [A_i]$.

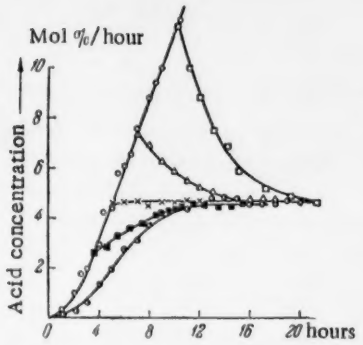

Fig. 2. Kinetic curves for the formation of adipic acid in the continuous oxidation of cyclohexanone at 110° with v = 0.265 hours^{-1}. Passage to the continuous process was made at various degrees of oxidation in the periodic oxidation of the cyclohexanone.

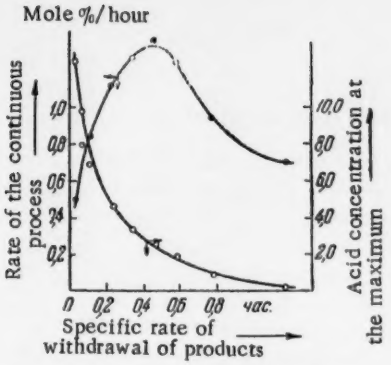

Fig. 3. The relation between the specific rate of withdrawal of the products in the continuous oxidation of cyclohexanone at 110° and the equilibrium concentration of adipic acid (1), and the rate of its formation (2).

The question of the relation between the rate of the continuous oxidation, w_C, and the specific rate of withdrawal of the products is an important one. The rate of a simple type of process increases monotonically with $\underline{v}$. A different kind of relation applies to autocatalytic reactions since the rates of such reactions depend not only on the concentrations of the reactant substances but also on the concentrations of the reaction products. The process rates of such special degenerative-branching chain reactions as are under consideration here prove to be functions of both the concentration of the reacting hydrocarbon, RH, and the concentration of the intermediate hydroperoxide, ROOH.

As $\underline{v}$ rises, RH increases because of the diminution of the degree of oxidation, and the concentration of the hydroperoxide decreases. Thus it would be anticipated that w_C would pass through a maximum as $\underline{v}$ increases.

Figure 3 shows the $w_C = vC_{eq}$ versus $\underline{v}$ relation which was obtained from experiments on the oxidation of cyclohexanone. This figure indicates that the rate of formation of adipic acid in the continuous oxidation of cyclohexanone actually increases with $\underline{v}$, reaching a maximum and then falling off. The curves for the relation between $\underline{w}$ and the equilibrium acid concentration (C_{eq}) are similar. On this basis it could be expected that the continuous oxidation could be carried out under optimal conditions so that the rate of formation of the products would be at a maximum.

We will now consider the general form of the condition required for giving a maximum rate in a continuous autocatalytic reaction.

The rate of change of the concentration of the final product of the reaction will be $\frac{dC}{dt} = w_{ac}(C) - vC$. In the stationary state of the continuous process

$$w_{ac}(C) = vC,$$

i.e., $w_c = vC$, a function of C, will have a maximum whenever $w_{ac}(C)$ passes through a maximum. At the maximum point:

$$\frac{dm_{ac}(C)}{dC} = \frac{d}{dC}\left(\frac{dC}{dt}\right) = \left(\frac{d^2C}{dt^2}\right) \Big/ \frac{dC}{dt} = 0;$$

since

$$\frac{dC}{dt} \neq 0, \text{then } \frac{dw_{ac}(C)}{dC} = 0, \text{ when } \frac{d^2C}{dt^2} = 0.$$

This condition is always met when the curve for the accumulation of reaction products is S-shaped.

The continuous oxidation has the advantage of reducing the combustion of the oxygen-containing reaction products to CO_2 and water by shortening the time of retention of these products in the reaction zone as compared with the case of the periodic process. We present the relation between the rate of withdrawal of the products and the amount of CO_2 per mole of adipic acid formed in the oxidation of cyclohexanone.

v 1/hr	0	0,0392	0,235	0,470
$[CO_2]$mole	0,1236	0,0584	0,0320	0,0246

LITERATURE CITED

[1] H. Bray and K. White, Kinetics and Thermodynamics in Biochemistry, London, 1957.

[2] N. I. Kirillov, J. Appl. Chem. 13, vol. 7, 978 (1940).

[3] A. N. Planovskii, Chem. Ind. 5, 5 (1944).

[4] W. Jost, Zs. phys. Chem. 195, 317 (1950).

[5] H. J. Aroyan, USA Pat. 2, 762, 893 (1956).

[6] V. K. Tsyskovskii, E. M. Nebylova, and Ts. N. Shcheglova, J. Appl. Chem. 30, 493 (1957).*

Received June 22, 1959

*Original Russian pagination. See C. B. Translation.

THE MEASUREMENT OF THE ELECTRICAL CONDUCTIVITY OF KI IN NONAQUEOUS SOLUTIONS AT HIGH PRESSURES

Yu. A. Ershov, M. G. Gonikberg, M. B. Neiman, and A. A. Opekunov

The N. D. Zelinskii Institute of Organic Chemistry of the Academy of Sciences, USSR

The Institute of Physical Chemistry of the Academy of Sciences, USSR

(Presented by Academician N. N. Semenov, April 27, 1959)

The results of an investigation of the effect of the solvent (ethyl alcohol or acetone) on the rate of the $n\text{-}C_3H_7I + \overset{*}{I}^-$ isotopic exchange at pressures up to 2500 kg/cm^2 have been published earlier by three of the present authors [1]. This study showed that the rate of the exchange reaction in ethyl alcohol solution increased markedly as the pressure rose, whereas the rate in acetone solution essentially diminished. This earlier paper postulated [1] that a partial desolvation resulting from the formation of active complexes was responsible for the observed change in the sign of the pressure effect when one solvent was replaced by the other. On the other hand, the evaluation of the rate constant for the exchange reaction gave no consideration to the pressure dependent degree of ionization of KI in these various solvents. It has seemed desirable to fill up this gap in the work. It was decided to use measurements of the electrical conductivity for this purpose. This method is known to yield good results when applied to the determination of the degree of dissociation of weak electrolytes. The data of the literature [2, 3] indicate that solutions of KI in ethyl alcohol, and acetone, differ from aqueous KI solutions in that the variation of the electrical conductivity with concentration at atmospheric pressure is quite different from that which is characteristic of strong electrolytes, even at low concentrations. It is clear that KI solutions in these solvents occupy a position intermediate between solutions of strong, and solutions of weak electrolytes. It was for this reason that we have assumed a portion of the KI ions in the investigated solutions to be associated and have approximated the degree of dissociation of KI from the $\lambda : \lambda_\infty$ ratio.

An apparatus similar to that used in the work of Buchanan and Hamann [4] was constructed for measuring the electrical conductivity of solutions under pressure. The design of the high pressure vessel and its glass cell is shown in Fig. 1. The cell 4 was prepared from Pyrex. The lower portion of the cell was closed by a ground glass joint containing a canal which was so bent as to prevent mercury from passing from the steel cup 3 into the electrode space when the pressure was raised. Two blacked platinum electrodes, 5, 4 cm^2 on a side, were sealed into the upper part of the cell at a distance of 0.9 cm from one another. The cell constant was determined from the conductivity of a standard aqueous KCl solution [5], and was equal to 0.1325 cm^{-1}. The electrodes were soldered to the ends of the leads 6 which were insulated from the body of the apparatus by mica. The cell 4 and the cup 3 with the mercury were affixed in the high-pressure steel vessel 2 which was then filled with transformer oil and set into a constant temperature bath. The measuring temperature was held constant to within ± 0.05°. The pressure was raised by feeding transformer oil from a pressure multiplier through the connector 1. The pressure was measured on a manometer having a scale calibrated to 4000 kg/cm^2, the accuracy of determination being ± 40 kg/cm^2.

The electrical conductivity was measured in a Shedlovskii circuit [6] using an ÉO-7 oscillograph as the null-indicator, this circuit being fed with current of 1000 kc/sec from a ZG-10 generator. The accuracy of the resistance measurements was 0.1-0.4% and varied with the resistance. The arms of the bridge were balanced

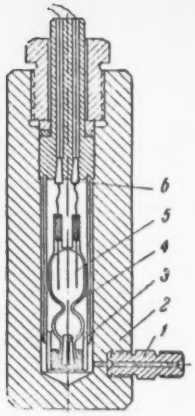

Fig. 1. High pressure vessel with cell.

up by an R-58 noninductive resistance box. A second R-58 box was used as a shunt in measuring resistances above 30000 ohms. The application of pressure resulted in a certain momentary increase in the temperature of the test liquid and this led to a diminution in the electrical conductivity. For this reason, measurements were continued at 10-15 minute intervals after applying the pressure until the resistance became constant.

All of these measurements were carried out at 20.0°, this being the temperature of the kinetic studies of [1]. The calculation of the conductivity of the solution involved a correction for the conductivity of the solvent itself (at atmospheric pressure). We estimate the total error of the measurements under pressure to be 1.5-2%.

The solvents were dried and redistilled through a rectifying column with an efficiency of 40 theoretical plates; their constants agreed with the values given in the literature. In the calculation of the concentration we assumed the compressibility of the solution to be the same as the compressibility of the pure solvent. The results are compiled in Table 1.

The data of Table 1 show the equivalent conductivity of the test solutions to diminish with increasing pressure and the degree of dissociation of the KI, (α) calculated as the ratio $\lambda : \lambda_{\infty}$, to increase. Table 2 presents the results of an evaluation of α and k_{α}, the ionization constant, for 0.005 M solutions of KI in ethyl alcohol and in acetone.

TABLE 1

The Electrical Conductivity of KI Solutions at 20°

P, kg·cm^{-2}	In ethyl alcohol		In acetone	
	c·10^3, moles·liter^{-1}	λ, ohms^{-1}·cm^2·moles^{-1}	c·10, moles·liter^{-1}	λ, ohms^{-1}·cm^2·moles^{-1}
1	0,100	45,4		
	0,500	42,3	0,500	158,5
	1,265	40,0	1,25	146,2
	2,53	37,7	2,50	137,7
	5,00	34,8	5,00	125,6
	99,9	20,6	10,0	111,3
	$\lambda_{\infty} = 47,5$		$\lambda_{\infty} = 178,5$	
1500	0,110	28,1		
	0,552	25,7	0,555	85,0
	1,395	25,7		
	2,79	24,7	2,77	79,8
	5,52	23,8	5,55	77,5
	110,3	15,8	11,07	72,8
	$\lambda_{\infty} = 28,5$		$\lambda_{\infty} = 89,0$	
2500	0,115	21,1		
	0,574	20,1	0,580	62,2
	1,452	20,3	1,444	62,6
	2,90	19,8	2,89	59,6
	5,74	18,7	5,77	59,4
	114,7	13,3	11,55	56,5
	$\lambda_{\infty} = 21,5$		$\lambda_{\infty} = 63,5$	

Table 2 shows that the ionization constant of KI in acetone increases much more rapidly with pressure than does the constant for KI in ethyl alcohol. This is consistent with the data of [1] which indicate that the contraction due to the dissolving of KI in acetone is greater than that due to the dissolving of this salt in ethyl alcohol. This clearly explains the observed difference in the sign of the pressure effect in the earlier mentioned study of the kinetics of isotopic exchange in ethyl alcohol and in acetone (see below). It can be supposed that the ionization constant actually increases more rapidly with pressure than would appear from the measurements

TABLE 2

The Degree of Dissociation and the Ionization Constant of KI Solutions (0.005 M)

P, kg · cm^{-2}	In ethyl alcohol			In acetone		
	α	$k_\alpha \cdot 10^5$	$\frac{k_{\alpha\,(p)}}{k_{\alpha\,(1\text{ атм.})}}$	α	$k_\alpha \cdot 10^5$	$\frac{k_{\alpha\,(p)}}{k_{\alpha(1\text{ атм.})}}$
1	0,733	10,05	1	0,705	8,43	1
1500	0,835	21,1	2,10	0,873	30,0	3,56
2500	0,888	35,2	3,50	0,935	67,2	7,97

TABLE 3

The Rate Constant for the Isotopic Exchange n-$C_3H_7I + \overset{*}{I}^-$ at 20°

Solvent	Source	k · 10, liters · moles^{-1}			$\Delta v^{\neq}$
		1 kg/cm^2	1500 kg/cm^2	2500 kg/cm^2	cm^3 · moles^{-1}
Ethyl alcohol	our data	16,6	23,8	27,7	— 7
	(*)	10	18	23,5	—12,5
Acetone	our data	3300	1500	850	+13
	(*)	2300	1300	800	+10

of the coefficient of conductivity. This is shown by the fact that the directly measured values of the contractions accompanying the dissolving of one gram-equivalent of KI in ethyl alcohol, and in acetone, at atmospheric pressure [1] are greater than those calculated from the data of Table 2.

The results of the present work make it possible to correct the earlier published [1] values of the rate constant for the n-$C_3H_7I + \overset{*}{I}^-$ reaction in these two solvents at various pressures for the degree of dissociation. Table 3 gives the values published earlier and the values corrected for the degree of dissociation. This table shows that the introduction of such corrections lead to no alteration in type of the pressure dependence of the rate constant for this reaction in acetone and in ethyl alcohol.

The last column of Table 3 gives values of the volume change accompanying the formation of one mole of the active complexes from the reacting substances. $\Delta v^{\neq}$, for this reaction in the absence of the solvent can be approximated from the model of the transition state (see [7], in this regard), the values thus obtained ranging from −10 to −14 cm^3/mole.

LITERATURE CITED

[1] M. G. Gonikberg, V. B. Miller, et al., J. Phys. Chem. 30, 784 (1956).

[2] H. Landolt and R. Börnstein, Phys. chem., Tab. 2, Erg. B. II, 1931, S. 1067.

[3] I. Dippy and S. Hughes, J. Chem. Soc. 1954, 953.

[4] I. Buchanan and S. D. Hamann, Trans. Farad. Soc. 49, 1425 (1953).

[5] G. Jones, J. Am. Chem. Soc. 55, 1780 (1933).

[6] A. Weisberger, Phys. Methods of Organic Chemistry 2, 1949, p. 1022.

[7] M. G. Gonikberg and A. I. Kitaigorodskii, Proc. Acad. Sci. USSR 122, 231 (1958).*

Received April 24, 1959

*Original Russian pagination. See C. B. Translation.

THE NULL-CHARGE POTENTIALS OF TELLURIUM–THALLIUM ALLOYS

V. A. Kuznetsov, V. I. Aksenov, and M. P. Kletsova

The A. M. Gor'kii Ural State University

(Presented by Academician A. N. Frumkin, April 13, 1959)

The relation between the null-charge potential and the composition of an alloy appears most clearly when the components of the alloy themselves have markedly different null-charge potentials. It was for this reason that the tellurium – thallium alloys were chosen for study in the present work. The data of S. Karpachev and A. Stromberg [1] show the null-charge potentials of these metals to differ by about 1.2 volts.

The null-charge potentials of liquid metals and alloys can be determined from a study of electrocapillary effects. A LiCl – KCl eutectic mixture was used as the electrolyte in the present work. The potential of the capillary electrode was measured against a molten lead electrode. These experiments were carried out at 475°. Details of the experimental technique are to be found in [2].

Electrocapillary curves for tellurium, thallium, and the tellurium – thallium alloys, are shown in Fig. 1. Alloys containing more than 65.2 atom percent were not investigated because two layers form in this range of concentrations [3]. A portion of the electrocapillary curve of thallium is shown in Fig. 1. The dashed extension of the anodic branch of this curve was obtained by extrapolating values of the interfacial tension of thallium into the potential region where direct measurements could not be made. Figure 1 shows that the addition of thallium to tellurium (up to approximately 25 atom percent) lowers the interfacial tension at the maximum on the electrocapillary curve (σ_{max}). The σ_{max} values of alloys more concentrated in thallium increase as the thallium content rises. The electrocapillary curves intersect almost exactly in one common point. Such an arrangement of electrocapillary curves was first observed by A. N. Frumkin and A. B. Gorodetskaya [4] who interpreted this as indication that the field of the electrical double-layer exerts an influence on the adsorption of the components in the surface layer of the alloy.

From the relation between the null-charge potential and the alloy composition as shown in Fig. 2, it follows that the potential moves in the direction of negative values when the thallium content of the alloy is increased. A qualitative explanation of this displacement can be given readily. A. N. Frumkin [4] has shown that the null-charge potential of an alloy is determined by the composition of the surface layer and by the null-charge potentials of the components. The value of σ_{max} is reduced by the addition of thallium to tellurium (up to 25 atom percent of tellurium). This indicates that the thallium is positively adsorbed in the surface layer of the alloy. The null-charge potential of the alloy is thus displaced in the negative direction and approaches the thallium value. The null-charge potentials of alloys containing more than 25 atom percent of Tl also move in the direction of negative values as the thallium concentration increases, although the fact that the interfacial tension increases in this region shows that thallium is here negatively adsorbed in the surface layer. It can be supposed, however, that the concentration of thallium in the surface layer will continually rise as the bulk concentration increases, always remaining less than the latter.

We will now confirm these qualitative considerations through suitable calculations. The work of [4] suggests that the displacement of the null-charge potential of a metal, $\Delta\varphi^0$, resulting from the addition of a second component is to be determined from the relation* $\Delta\varphi^0 = (\varphi_2^0 - \varphi_1^0)\,\theta_2$, in which φ_1^0 and φ_2^0 are the

* Supposing the capacity of the electrical double layer to be independent of the composition of the alloy.

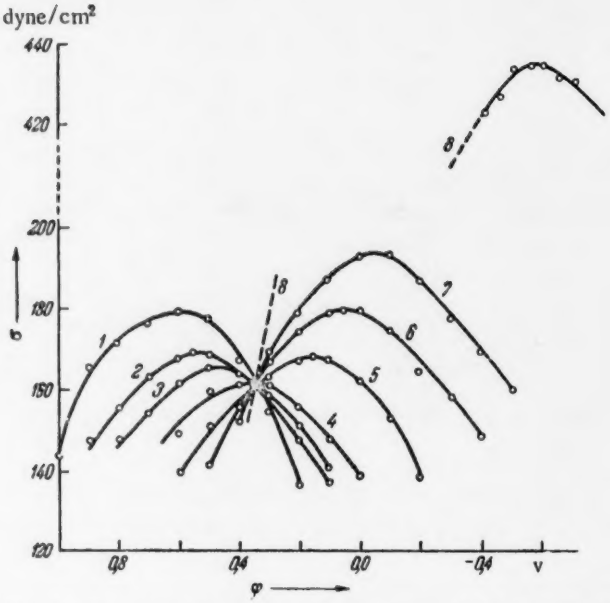

Fig. 1. Electrocapillary curves for Te, Tl, and the Te–Tl alloys: 1) Te, 2) 3.83 at.%, 3) 10.9; 4) 22.1; 5) 42.3; 6) 53.7; 7) 65.2 at. % Tl; 8) Tl.

null-charge potentials of the components 1 and 2 and θ_2 is the proportion of the surface layer which is occupied by the particles of the second component. The index 1 will refer to tellurium in this and the following expressions, and the index 2, to thallium.

The quantity θ_2 can be determined in the following manner. When the electrolyte concentration is constant, as in our experiments, the differential equations for the family of electrocapillary curves can be written as [4]: $d\sigma = -\Gamma_1 d\mu_1 - \Gamma_2 d\mu_2 - \epsilon\, d\varphi$, where Γ_1 and Γ_2 are the Gibbs surface concentrations of the components 1 and 2, μ_1 and μ_2 are the chemical potentials of these components, and ϵ is the charge density of the electrical double layer.

At the maximum of the electrocapillary curve, $\epsilon = 0$, and a small variation in the surface tension, $d\sigma_{max}$, can be expressed as:

$$d\sigma_{max} = -\Gamma_1 d\mu_1 - \Gamma_2 d\mu_2,$$

Selecting the Gibbs surface of separation so that $\Gamma_1 = 0$ and designating the corresponding surface concentration of the second component as $\Gamma_2^{(1)}$, we find:

$$\Gamma_2^{(1)} = \frac{d\sigma_{max}}{d\mu_2}.$$

The value of $\Gamma_2^{(1)}$ corresponding to the maximum on the electrocapillary curve can thus be found by graphical differentiation of the curve $\sigma_{max} = f(\mu_2)$. Guggenheim and Adams have shown convincingly, however, [5] that these quantities cannot be used for a direct determination of the composition of the surface layer. For this reason the method of [5] passes from the surface concentration $\Gamma_2^{(1)}$ over to the quantity Γ_2^{v}. This latter represents the difference between the number of moles of the second component in equal volumes of the surface layer and of the bulk of the alloy, and can be defined as:

$$\Gamma_2^{v} = (C_2^1 - C_2)\,\delta,$$

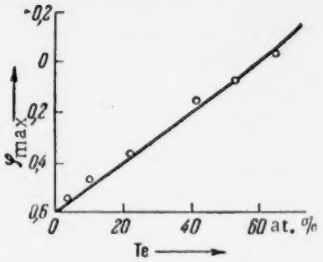

Fig. 2. The relation between the null-charge potentials of Te–Tl alloys and the concentration of Tl in the alloy.

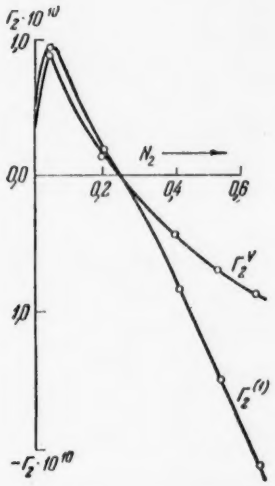

Fig. 3. The relation between the Tl adsorption and the alloy composition.

C_2^1 and C_2 being the concentrations of the component 2 in the surface layer and in the bulk of the alloy, respectively, and δ, the depth of the surface layer. θ_2 can be found readily when the value of C_2^1 is known since elementary considerations show that $\theta_2 = C_2^1 A_2 / d_2$, A_2 being the atomic weight and d_2, the density of the second component.

The activity of Tl in the alloy is needed for the evaluation of $\Gamma_2^{(1)}$; we have determined such activities from emf measurements on concentration cells of the type: Tl, eutectic mixture LiCl–KCl + 2 weight % TlCl, Tl–Te alloy. The results of these calculations are compiled in Table 1; from them it is seen that the Tl–Te alloys deviate markedly from Raoult's law. Figure 3 shows $\Gamma_2^{(1)}$ plotted as a function of the alloy composition; the thallium adsorption is positive ($\Gamma_2^{(1)} > 0$) in alloys whose Tl content does not exceed 25 atom percent and negative ($\Gamma_2^{(1)} < 0$) in alloys of higher concentration. This same figure also shows the variation of Γ_2^{ν} with the alloy composition.

These quantities were used in evaluating the fraction of the surface layer which is occupied by the thallium particles. It was necessary to make an assumption as to the depth of the surface layer before such calculations could be carried out. The comparatively low absolute value of Γ_2^{ν} suggests a monomolecular surface layer. On the other hand, the large negative deviations of these alloys from Raoult's Law, which have been pointed to above, indicate a strong interaction between the particles of the components. There is no doubt that there is a similar interaction between the particles which enter into the surface layer, with the result that dipoles, oriented perpendicularly to the surface of separation, will be formed here. Analogous effects have been noted in the work of A. N. Frumkin and N. S. Polyanovskaya [6] on thallium amalgams. Thus, there is reason to presume that the surface layers in the tellurium – thallium alloys are thicker than monomolecular layers and it can assumed that they will be approximately two molecules deep. The calculations which are reported below have for this reason been carried out for a monomolecular surface layer, and for a surface layer two molecules deep.

The crystallographic diameter of the thallium atom is 3.4 A [7] and the diameter calculated from the density of liquid thallium (10.98 g/cm^3 at 475 °C) is 3.2 A. The so-called covalent diameter of the tellurium atom is 2.7 A [7] and the diameter calculated from the density of liquid tellurium (5.763 g/cm^3 at 465°C) is 3.3 A. These figures show that the diameters of the thallium and tellurium atoms are each approximately 3 A. For this reason, calculations were made for a monomolecular layer 3 A deep and for a dimolecular layer 6 A deep. The results are shown in Table 2. Column 3 of this table gives the observed displacement of the null-charge potentials of the tellurium – thallium alloys with respect to the null-charge potential of pure tellurium. Columns 4 and 6 give the fraction of the surface layer which is occupied by the thallium atoms, these values being obtained on the assumption that this layer is 3 A or 6 A deep respectively. Columns 5 and 7 give the displacement of the null-charge potentials of the alloys, as calculated from the equation $\Delta\varphi_2^0 = (\varphi_2^0 - \varphi_1^0)\theta_2$. Our measurements show the null-charge potential for tellurium to be +0.6 v with respect to the molten lead electrode, and that of thallium to be −0.58 v. The quantity $(\varphi_2^0 - \varphi_1^0)$ was thus equal to −1.18 v in these calculations.

The figures of Table 2 show the calculated results to be in satisfactory agreement with the experimental observations. The data of the present work thus support A. N. Frumkin's conclusion [4] that the displacement of the null-charge potential of an alloy is directly proportional to the fraction of the surface layer which is

TABLE 1

Activities and Activity Coefficients in Te – Tl Alloys

Mole fraction of Tl in alloy	a_1	f_1
1,00	1,00	1,00
0,652	$1,90 \cdot 10^{-2}$	$3,92 \cdot 10^{-2}$
0,537	$5,37 \cdot 10^{-3}$	$1,00 \cdot 10^{-2}$
0,423	$1,44 \cdot 10^{-3}$	$3,40 \cdot 10^{-3}$
0,221	$1,35 \cdot 10^{-4}$	$6,12 \cdot 10^{-4}$
0,109	$3,47 \cdot 10^{-5}$	$3,18 \cdot 10^{-4}$
0,038	$1,17 \cdot 10^{-5}$	$3,08 \cdot 10^{-4}$

TABLE 2

The Fraction of the Surface Layer Occupied by Thallium Atoms and the Displacement of the Null-Charge Potential

N_2	$-\Delta\varphi^0_{expt}$	$\delta = 3$		$\delta = 6$	
		θ_2	$-\Delta\varphi^0_{cal}$	θ_2	$-\Delta\varphi^0_{cal}$
0,038	0,06	0,09	0,11	0,06	0,07
0,109	0,14	0,12	0,13	0,106	0,13
0,220	0,24	0,23	0,27	0,19	0,22
0,423	0,44	0,32	0,38	0,34	0,40
0,537	0,52	0,40	0,47	0,43	0,51
0,652	0,63	0,50	0,59	0,53	0,63

occupied by the atoms of the added metal. If similar results could be obtained for other binary alloys, this would then be considered a general statement of the relation between the composition of the surface layer and the null-charge potentials of alloys.

The data of Table 2 shows that the values of θ_2, or $\Delta\varphi^0$, are approximately the same, regardless of whether δ is assumed to be 3 A or 6 A. On the other hand, the values of $\Delta\varphi^0_{cal}$ calculated from δ = 6 A are in better agreement with the experimental data than are those from δ = 3 A. This indicates indirectly that the surface layers in the Te–Tl alloys are more than one molecule deep.

We conclude by expressing our deep thanks to Academician A. N. Frumkin for his unflagging interest in this work and for his valuable advice.

LITERATURE CITED

[1] C. Karpachev and A. Stromberg, J. Phys. Chem. 18, 47 (1944).

[2] V. A. Kuznetsov, V. P. Kochergin, et al., Proc. Acad. Sci. USSR 92, 1197 (1953).

[3] Khansen, The Structure of Binary Alloys [in Russian], 2, Moscow-Leningrad, 1941.

[4] A. Frumkin and A. Gorodetskaya, Zs. Phys. Chem. A136, 451 (1928).

[5] E. A. Guggenheim and N. K. Adams, Proc. Roy. Soc. A139, 218 (1933).

[6] A. N. Frumkin and N. S. Polyanovskaya, J. Phys. Chem. 32, 157 (1958).

[7] B. V. Nekrasov, A Course in General Chemistry [in Russian], Moscow-Leningrad, 1952.

Received March 5, 1959

THE RAPID ADDITION OF CHLORINE TO A DOUBLE BOND AT LOW TEMPERATURES

V. A. Lishnevskii and G. B. Sergeev

The M. V. Lomonosov State University, Moscow

(Presented by Academician N. N. Semenov, May 25, 1959)

The rapid addition of chlorine to ethylene in a low temperature condensed phase was first observed by Chaikin [1] in 1955. It can be assumed that diminishing steric hindrances facilitate the union of chlorine with unsaturated compounds under such conditions, and it was for this reason that we decided to study the interaction of chlorine with various compounds which contain a double bond. The addition of chlorine to ethylene, propylene, isobutylene, cyclohexene, styrene, and thiophene has been studied in this work.

Reaction proceeds almost instantaneously in each of these cases. The interaction of equimolar amounts of chlorine, and ethylene, propylene, isobutylene, cyclohexene, or styrene, is quantitative (see Table 1) and only addition products are formed. The formation of substitution products is not observed. This makes the low-temperature chlorination of the double bond a very satisfactory method for preparing the dichloro derivatives of various unsaturated compounds.

TABLE 1

The Results of Low-Temperature Equimolar Chlorination of Compounds Containing a Double Bond

Compound	Addition product	Yield, % of theo.	B. p., °C	n_D^{20}
Ethylene	1,2-Dichloroethane	92	83-84	1.4443
Propylene	1,2-Dichloropropane	98	97-98	1.4387
Isobutylene	1,2-Dichloro-2-methylpropane	87	38.6–39.2/70 mm	1.4372
Styrene	α,β-Dichloroethylbenzene	95	114.5–115.5/15 mm	1.5525 (n_D^{15} = 1.5547)
Cyclohexene	1,2-Dichlorocyclohexane	86	87–90/30 mm	1.4815

Chlorine evidently reacts with thiophene since the mixture changes color, but it is difficult to separate the reaction products.

The ethylene, propylene, and isobutylene were prepared by the dehydration of the corresponding alcohols and were carefully dried and purified by low-temperature distillation in vacuum. The constants of the cyclohexene, styrene, and thiophene agreed with the values reported in the literature. The chlorine was first passed through a trap containing concentrated sulfuric acid and a tube containing calcium oxide, and was then subjected to low-temperature distillation in vacuum.

The experiments were carried out in a vacuum system. Definite amounts of chlorine and the organic compound were frozen out in layers on a trap cooled with liquid nitrogen. The Dewar flask with the liquid nitrogen was then removed, the mixture was melted, and the reaction products analyzed. The extent of reaction was estimated from the final pressure as read on a membrane manometer. The 1,2-dichloroethane and the 1,2-dichloropropane were distilled off in a glass-packed column which had an efficiency of 19 theoretical plates; the 1,2-dichloro-2-methylpropane, the 1,2-dichlorocyclohexane, and the α, β-dichloroethylbenzene were distilled off under vacuum. It is to be seen from Table 1 that the constants of the products were in good agreement with the data of the literature. A study of the data of this same table shows that it is products from addition at the double bond which formed under these conditions and that the reaction yields are good. These results point to the possibility of a new method for the synthesis of the dichloro derivatives of various compounds.

A detailed study of the mechanisms of these reactions is planned for the future.

LITERATURE CITED

[1] A. M. Chaikin, Master's Dissertation, Moscow, 1955.

Received May 23, 1959

THE ADSORPTION CHARACTERISTICS OF HIGH-MOLECULAR HYDROCARBONS OF COMPOSITE STRUCTURE

S. R. Sergienko, L. N. Kvitkovskii, Yu. T. Gordash, and Al. A. Petrov

The Institute for Geology and the Treatment of Minerals, Academy of Sciences, USSR

(Presented by Academician M. M. Dubinin, May 25, 1959)

Processes centering around the properties of solid surfaces are widely employed in both research and industry. Such highly porous adsorbents as aluminum oxide and silica gel have large specific surface areas and are thus able to take up large amounts of gaseous and liquid substances. Selective adsorption usually occurs, however, when an adsorbent is brought into contact with a mixture, and such adsorption depends on the structures and chemical compositions of the individual components. This fact lies at the basis of the widely used method of adsorptional chromatography for the separation of mixtures of hydrocarbons. The adsorption of a hydrocarbon is a completely reversible physical process so that the adsorption isotherm is one of the best criteria for characterizing the adsorptional characteristics of such a compound. A study of the adsorptional characteristics of the hydrocarbons which make up the benzene-kerosene fractions of petroleum has shown that the adsorptional activity of these compounds increases in the order: saturated hydrocarbons < olefins < diolefins < monocyclic aromatic hydrocarbons < polycyclic aromatic hydrocarbons. The chromatographic method has been widely used in recent years for studying the higher fractions of petroleum in which molecules of composite (hybrid) structures predominate. The above classification could scarcely serve as a basis for evaluating the selective adsorption of complex hydrocarbon molecules which contain both phenyl and polymethylene rings, and even rings of higher complexity. Interest thus attaches to the elucidation of the effect of the type and the number of the aromatic units, and the influence of other structural factors, on the adsorptional characteristics of complex hydrocarbons. This problem is treated in the present work.

Adsorption isotherms have been developed for a large number of specially synthesized high-molecular hydrocarbons of various structures [1] in an attempt to arrive at a quantitative evaluation of the adsorbability of hybrid hydrocarbon molecules. The isotherms were developed under static conditions by bringing solutions of the test hydrocarbon in n-dodecane of various concentrations in contact with a definite amount of the adsorbent. Silica gel of the "ASK" type and aluminum oxide of the "for chromatography" grade were used as adsorbents since these are most widely employed in studies of petroleum and petroleum products. The accuracy of the refractometric analyses was increased by using the low-volatile n-dodecane as solvent. At the same time, the adsorbability of n-dodecane is approximately the same as that of the n-hexane or dearomatized petroleum ether which are commonly employed in chromatography.

The "apparent" adsorption isotherms were obtained from 10-13 experimental points and had the form which is characteristic for the case of completely miscible liquids. The "apparent" adsorption isotherm of one hydrocarbon is given in Fig. 1, 12.* The remaining "apparent" isotherms were of the same type and, for this reason, they have not been included in the figure. The total amount of a component in the adsorbed volume was determined from Gibbs' adsorption isotherm (apparent) and the adsorbed volume, v_a, following the method which has been employed by Shcherbakova and Kiselev [2, 3].

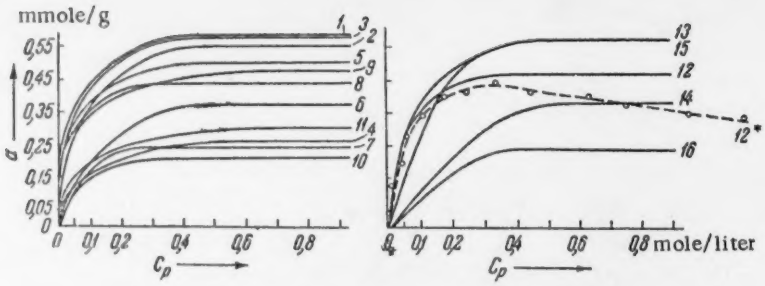

Fig. 1. Adsorption isotherms for hydrocarbons on silica gel.

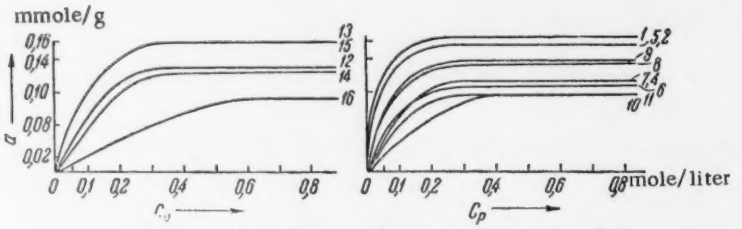

Fig. 2. Adsorption isotherms on aluminum oxide.

Figures 1 and 2, and Table 1 contain the values of those quantities which are most characteristic in fixing the adsorption of any one hydrocarbon on a given adsorbent, namely, the total amount of this substance corresponding to an equilibrium concentration of 0.1 mmole/liter, the maximum adsorption, a_M, in mmoles/g, and the adsorbed volume, v_a, in cm^3/g.

These data show that the value of the maximum adsorption increases with an increase in the proportion of those carbon atoms of the molecule which are found in the aromatic structural units, the adsorbability of complex high-molecular hydrocarbons depending, within wide limits, on the number of aromatic, or other, rings in the system, and especially on the ratio of the number of carbon atoms in aromatic rings to the number in paraffin chains. The character of the aromatic structural units (whether benzene or naphthalene), and their mutual distribution in the hydrocarbon molecules have only little effect on the adsorbability.

The introduction of decalin or cyclohexane structures into a hydrocarbon molecule which already contains benzene or naphthalene rings noticeably increases the adsorbability; this effect is quite pronounced when two new rings are introduced into cyclohexane structures. The adsorbability of the saturated hydrocarbons on these adsorbents, and from this solvent, is practically zero, but the introduction of a cycloparaffin structure into an alkyl aromatic hydrocarbon considerably increases the adsorbability. We believe that this increase in the adsorbability is related to the alteration in the ratio of the aromatic to the paraffin carbon atoms, since this has already been pointed out as the most important of the factors determining the adsorbability of such a compound. A comparison of the adsorbabilities of a single hydrocarbon on silica gel and on aluminum oxide shows the former to be somewhat the more selective in its adsorption of those compounds which contain two aromatic groups in the molecule. On the other hand, relative values from the adsorption isotherms of the various hydrocarbons on these two adsorbents are approximately the same, the aluminum oxide showing the higher adsorbability for each hydrocarbon.

The essential difference between these two adsorbents is that the isotherms for the adsorption of the benzene derivatives on aluminum oxide are flatter than those for adsorption on silica gel; this would undoubtedly influence the rate of desorption of these hydrocarbons and would thus effect the results of chromatographic analysis.

An analysis of the adsorption isotherms of the various hydrocarbons indicates that it should be possible to chromatographically separate mixtures of hydrocarbons which have the same molecular weight but different

TABLE 1

Compound No.	Hydrocarbon	Silica gel			Aluminum oxide		
		$a_{0,1}$, mmoles/g	a_M, mmoles/g	v_a, cm³/g	$a_{0,1}$, mmoles/g	a_M, mmoles/g	v_a, cm³/g
1		0,440	0,5900	0,295	0,146	0,170	0,0860
2		0,370	0,5700	0,280	0,134	0,160	0,0763
3		0,420	0,5825	0,235	—	—	—
4		0,160	0,2650	0,180	0,074	0,116	0,0490
5		0,385	0,5100	0,235	0,134	0,160	0,0763
6		0,195	0,3755	0,175	0,078	0,108	0,0526
7		0,175	0,2475	0,035	0,074	0,116	0,0546
8		0,360	0,4450	0,190	0,101	0,136	0,0690
9		0,345	0,4750	0,260	0,108	0,142	0,0690
10		0,145	0,2300	0,094	0,038	0,098	0,0364
11		0,195	0,3075	0,140	0,062	0,098	0,0440
12		0,360	0,4850	0,135	0,066	0,132	0,0308
13		0,390	0,5825	0,229	0,099	0,164	0,0495
14		0,120	0,3950	0,100	0,053	0,124	0,0357
15		0,280	0,5825	0,217	0,099	0,164	0,0495
16		0,095	0,2500	0,045	0,014	0,093	0,0328

numbers of aromatic rings in the molecule. The actual chromatographic separation of prepared binary mixtures of C_{24}, or C_{32}, hydrocarbons has proved that the adsorption isotherm (or, more exactly, the value of the adsorption maximum) is a good criterion for evaluating the possibility of separating hydrocarbon mixtures.

LITERATURE CITED

[1] S. R. Sergienko, L. N. Kvitkovskii, et al., Proc. Acad. Sci. USSR 120, No. 3, 541 (1958).*

[2] K. D. Shcherbakova and A. V. Kiselev, Coll. Papers on Phys. Chem., Acad. Sci. USSR, Press, 1947, p. 225.**

[3] A. V. Kiselev, Prog. Chem. 25, 705 (1956).

Received May 23, 1959

*Original Russian pagination. See C. B. Translation.

**In Russian.

A STUDY OF THE RATES OF SIMULTANEOUS ELECTROCHEMICAL REACTIONS

T. A. Fatueva and A. T. Vagramyan

The Institute of Physical Chemistry of the Academy of Sciences, USSR

(Presented by Academician V. I. Spitsyn, May 25, 1959)

The modern theory of the simultaneous discharge of metallic ions is based on the assumption that the rules applying to reduction of the individual ions remain valid for joint deposition [1]. Numerous investigations on joint ionic reduction have shown, however, that the experimental results are essentially different from those which would be expected from studies on individual discharge [2]. We have shown in an earlier paper [3] that the simultaneous discharge of cobalt and nickel ions is a composite electrochemical reaction. A mutual interaction between discharging ions has also been observed in a study of the simultaneous discharge of nickel and iron, and cobalt and iron. Here, the rate of discharge of the ion which separates out at the more negative potential (in the individual reduction) proves to be greater than the rate of discharge of the more positive component. Figures 1 and 2 show the rates of ionic reduction in the electrodeposition of nickel, iron, and cobalt, and in the simultaneous deposition of nickel and iron, and cobalt and iron, from sulfuric acid solutions as functions of the electrode potential.

It should be noted that hydrogen ion discharge accompanies the electrodeposition of nickel, iron, and cobalt, individually, and the simultaneous deposition of these metals, and that this makes for difficulties in elucidating the mechanism of joint discharge. For orientation, we will now consider some of the data which are presented in Table 1.

These data indicate a rate of discharge of iron (expressed as the current density at φ = 970 mv) of 13.6 ma/cm^2 for simultaneous deposition with nickel, and a rate of 4.5 ma/cm^2 for deposition of the iron alone, the rate of discharge of the iron being thus increased by a factor of 3 in the joint separation with nickel; at the same time, the rate of discharge of nickel falls from 20.8 to 2.6 ma/cm^2 and thus diminishes to approximately one eighth. The rate of discharge of hydrogen ions is 7.9 ma/cm^2 in a simultaneous separation with nickel, 4.4 ma/cm^2 in a simultaneous separation with iron, and 4.5 ma/cm^2 in a simultaneous discharge with both iron and nickel. These figures indicate that the low value of the hydrogen overvoltage on nickel is responsible for a more rapid separation of hydrogen with nickel than with iron, or with iron and nickel together.

The curves of Fig. 2 show that there is an increase in the rate of reduction of iron, and retardation in the discharge of cobalt, in a simultaneous reduction of ions of these metals, comparison being made with the rates of the individual depositions. Thus the rate of reduction of iron in a simultaneous electrodeposition of nickel and iron, or cobalt and iron, is much greater than would be anticipated from a study of individual polarization curves.

It can be seen from the accumulated data [4] that the rate of an electrochemical process can be altered by: 1) an alteration in the nature and state of the cathode surface, 2) an alteration in the structure of the double layer, and 3) an alteration in the electrolyte concentration and the state of the ions in solution. It seems to us that it is impossible to explain the increase in the rate of discharge of iron ions and the diminution in the rate of discharge of nickel ions in a combined deposition of these metals in terms of an alteration in the states of these ions in solution, that is to say, this explanation cannot be had by assuming diminished dehydration of the iron ions and increased hydration of the nickel ions when these are present simultaneously in a solution.

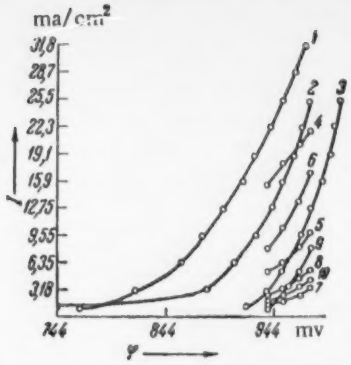

Fig. 1. The relation between the rate of reduction in simultaneous electrochemical reactions and the electrode potential (with respect to the saturated calomel electrode) of Ni, Fe, and H at pH 1.9 and 25°: 1) total polarization curve for the separation of Ni and H from a 1 N $NiSO_4$ solution; 4,5) the rates of reduction of Ni and H, respectively, as functions of the electrode potential, based on the data of 1; 2) total polarization curve for the simultaneous discharge of Fe, Ni, and H in a 1 N $NiSO_4$ + 1 N $FeSO_4$ solution; 6-8) the rates of reduction of Fe, Ni, and H, respectively, as functions of the electrode potential, based on the data of 2; 3) total polarization curve for the separation of Fe and H from a 1 N $FeSO_4$ solution; 9, 10) the rates of reduction of Fe and H, respectively, as functions of the electrode potential, based on the data of 3.

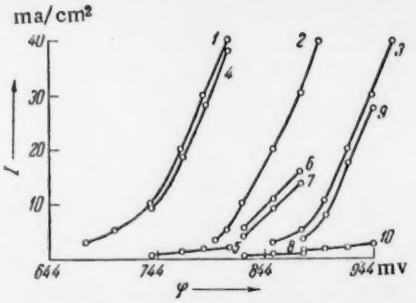

Fig. 2. The relation between the rate of reduction in simultaneous electrochemical reactions and the electrode potential of Co, Fe, and H at pH 3.2 and 25°: 1) total polarization curve for the separation of Co and H from a 1 N $CoSO_4$ solution; 4,5) the rates of reduction of Co and H, respectively, as functions of the electrode potential, based on the data of 1;2) total polarization curve for the simultaneous discharge of Co, Fe,and H in a 1 N $CoSO_4$ + 1 N $FeSO_4$ solution; 6-8) rates of reduction of Fe, Co, and H, respectively, as functions of the electrode potential, based on the data of 2;3) total polarization curve for the simultaneous discharge of Fe and H in a 1 N $FeSO_4$ solution; 9,10) rates of reduction of Fe and H, respectively, as functions of the electrode potential, based on the data of 3.

Hydration is known to result from the attraction of the polar water molecules, the hydration being the greater the higher the charge of the ion and the smaller its radius. The radii of iron, nickel, and cobalt ions are almost exactly equal, so that these ions would seem to act uniformly on the ionic state when they are present in a single solution and the reduction should thus be facilitated to a certain degree. This is not observed, however. Furthermore, addition to the electrolyte of considerable quantities of a salt whose metal carries a high specific charge ($MgSO_4$) should also increase the rate of reduction of the metals of the iron group at fixed electrode polarization, but the observed effect is just the reverse. From what has been said, it can be concluded that it is impossible to explain the change in the rate of discharge (as compared with the rates of the individual separations) of iron and nickel in the joint reduction of these metals as resulting from an alteration of the states of the ions in solution, in general, or from an alteration of the degree of hydration of the ions, in particular.

An alteration in the structure of the electrical double layer has been shown to affect the rates of electrode processes in the case of the deposition of nickel and cobalt. The work of A. N. Frumkin [5] has proved that it is the ionic concentration in the double layer which fixes the rate of reduction of an ion, and not the concentration in the body of the solution. Two ions introduced into an electrolyte will partially displace one another from the electrical double layer, so that the concentration of the discharging ion in this layer is diminished. Thus there should be a reduction in the rate of reduction of the ions in the joint deposition of nickel and cobalt at a fixed potential drop in the Helmholtz double layer, comparison being made with the rates for the individual depositions. The electrodeposition of nickel and iron, or cobalt and iron, show, however, that there is not only a retardation in the reduction of the nickel ions but also sharp acceleration in the discharge of the iron ions, so that it is clearly impossible to fully explain the alteration in the rate of reduction in terms of a change in ionic concentrations in the double layer.

TABLE 1

The Current Distribution in Individual, and Combined, Electrodeposition of Metals at a Cathode Potential, φ, of 970 mv

Current density	Current consumption, ma/cm²		
	in electrodeposition of iron	in electrodeposition of nickel	in discharge of nickel and iron
I_{tot}	8.9	28.7	20.7
I_{Fe}	4.5		13.6
I_{Ni}		20.8	2.6
I_{H_2}	4.4	7.9	4.5

It has been repeatedly shown [6] that the rate of reduction of ions is altered considerably by a change in the condition of the cathode surface. There are two competing processes at play in the electrodeposition of metals: the increase in the active surface and the passage of this surface into a passive state as a result of adsorption of foreign particles such as those of hydrogen, hydroxides, and surface active substances. The actual retardation of an electrochemical reaction will depend on the ratio of the rates of these two processes.

The investigations of Yu. S. Petrova on the electrodeposition of the metals of the iron group have shown that the rate of adsorption, and eventual inclusion, of hydrogen and hydroxides varies from metal to metal. Thus, there is also a variation in the retarding action of the adsorbed hydrogen and hydroxides. Considerably more hydrogen than hydroxide is included in a deposit of nickel, whereas the reverse is true in the case of iron where the hydrogen bonding is stronger. A study of the electrodeposition of nickel has shown that the electrode polarization rapidly increases as the layer adjacent to the electrode is made alkaline, the indication being that the retardation of this reaction is due to the adsorption of hydroxides on the nickel surface.

V. N. Kuznetsova, working in our laboratory, has proven that the rate of reduction of iron ions increases as the extent of codeposition of hydrogen diminishes; i.e., the separation of iron proceeds more readily on an iron surface that is free of hydrogen than on one which is covered with hydrogen. Thus, it can be supposed that the marked retardation of the electrodeposition of nickel is due to the adsorption of hydroxides, whereas the retardation of the deposition of iron is due to the adsorption of the evolved hydrogen. The rate of reduction of the iron ions should then be found to increase in the discharge of iron and nickel since the ability of the alloy to adsorb hydrogen is less than that of iron. The marked retardation of the reduction of nickel ions which is observed in codeposition with iron must result from an increased adsorbability of the hydroxides on the alloy (in comparison with the separation of the individual metals), the formation of iron hydrate beginning at a higher acidity than that of nickel.

The observed anomalous acceleration of the reduction of iron ions and retardation of the discharge of nickel ions are thus related to the alteration in the state of the electrode surface and to the change in the concentrations of the components in the layer adjacent to the electrode.

LITERATURE CITED

[1] S. Glasstone, An Introduction to Electrochemistry [Russian translation], Foreign Lit. Press, 1951; V. I. Lainer and N. T. Kudryatsev, Principles of Electroplating [in Russian], chapt. 2, Moscow, 1957; R. Kremann, and R. Müller, Elektromotorische Kräfte, Elektrolyse und Polarisation 2, 1931. O. A. Esin, J. Appl. Chem. 6, 795, 1935; Proc. S. M. Kirov Ural Industrial Institute, No. 27, 29 (1947); V. L. Kheifets and A. L. Rotinyan, Proc. Acad. Sci. USSR 82, 423 (1952); A. I. Rotinyan, V. L. Kheifets, et al., Proc. Acad. Sci. USSR 88, 301 (1953); V. L. Kheifets and L. S. Reishakhrit, Annals Leningrad Univ., chem. ser., v. 13, No. 169, 173 (1953); V. L. Kheifets and A. I. Rotinyan, Proc. Planning and Scientific Research Ins. Gipronikel', vol. 1, Leningrad, 1958; Yu. V. Baimakov, Proc. Kalinin Polytech. Ins., Leningrad, No. 188, 162 (1957).

[2] A. I. Krasovskii, Proc. Fourth Conference on Electrochemistry, Acad. Sci. USSR, Press, 1959; N. V. Korovin, J. Inorg. Chem. 2, No. 9, 2259 (1957); B. I. Skirstymonskaya, J. Appl. Chem. 31, No. 3, 408;* No. 4, 638 (1958);* T. F. Frantsevich-Zabludovskaya and A. I. Zayats, J. Appl. Chem. 31, No. 2, 234 (1958);* G. A. Tsyganov, Proc. Fourth Conference on Electrochemistry, Acad. Sci. USSR, Press, 1959.

[3] A. T. Vagramyan and T. A. Fatueva, J. Inorg. Chem., No. 6 (1959).

[4] A. T. Vagramyan, Proc. Fourth Conference on Electrochemistry, Acad. Sci. USSR, Press, 1959; A. T. Vagramyan, Prace Konferencji Elektrochemicznej Warszawa, 1957; V. A. Kistyakovskii, Yu. V. Baimakov, and I. V. Krotov, Bull. Acad. Sci. USSR, math.-phys. sec. 771 (1929); V. V. Mikhailov, J. Phys. Chem. 28, vol. 6 1067 (1954).

*Original Russian pagination. See C. B. Translation.

[5] A. N. Frumkin, Zs. phys. Chem. (A), 164, 121 (1933); A. N. Frumkin, V. S. Bagotskii, et al., Kinetics of Electrode Processes [in Russian], Moscow, 1952.

[6] N. T. Vagramyan and A. T. Vagramyan, J. Phys. Chem. 23, 78 (1949); A. T. Vagramyan and Z. A. Solov'eva, J. Phys. Chem. 26, 910 (1952); A. T. Vagramyan and Z. A. Solov'eva, J. Phys. Chem. 18, 1153 (1954); A. T. Vagramyan and Z. A. Solov'eva, Methods of Investigating the Electrodeposition of Metals [in Russian], Acad. Sci. USSR, Press, 1955.

Received May 22 , 1959

THE INFLUENCE OF SURFACE ACTIVE LUBRICANTS ON FRICTIONAL SHEAR RESISTANCE

I. S. Avetisyan and G. I. Epifanov

The Institute of Physical Chemistry of the Academy of Sciences, USSR

(Presented by Academician P. A. Rebinder, May 18, 1959)

It has been shown in [1] that external friction between clean metallic surfaces is essentially a process of plastic shear in comparatively thin surface layers of the weaker of the two rubbing materials. It is for this reason that such frictional characteristics as the frictional force and the coefficient of friction are largely determined by the shear resistance of the weaker material of the frictional pair and by the total area of the surface which is developed in frictional movement.

The frictional shear moves out of the surface layers of the contacting metals into a lubricating film when the frictional surfaces are covered by a thin layer ($\sim 0.1\mu$) of a solid "molded" lubricant of low shear resistance (graphite, soft plastic metals, etc.). At the same time, frictional paths develop, just as before, in the material of the contacting bodies, these being due to a "furrowing" of the content surfaces by penetrating microprojections. Frictional movement under the lubricating action of such films is quantitatively described by the equation [2]

$$F_N = F_c + F_a = S_c\tau_f + S_a\theta. \tag{1}$$

in which F_N is the force of friction under the normal load N, F_c is the surface shear component of this force, S_c is the shear area in the film material, τ_f is the shear resistance of this film, S_a is the cross-sectional area of the frictional paths and θ is the resistance of the material to plastic extrusion during formation of these paths.

Equation (1) shows that the shear component of the specific force of friction, $f_c = F_c/S_c$, must be equal to the shear resistance of the film material

$$f_c = \tau_f \tag{2}$$

This conclusion has been confirmed by experiments on the lubricating action of films of graphite, tin, lead, cadmium, zinc, and copper on steel surfaces [2].

From this point of view, there is a need for study of the influence of solid and liquid organic lubricants on the frictional characteristics of metallic surfaces and, especially, the effect of these substances on the shear resistance of the surfaces of contact of rubbing bodies. Experiments were carried out with a semispherical slide of tempered steel which moved over a plane surface obtained by cutting off fine shavings from a specimen. This slide was 12 mm in diameter. These experiments were performed with normal loads of 12.5 kg for lead, cadmium and zinc, 25 kg for aluminum and tin, 50 kg for iron and copper, and 62.5 kg for the alloy EI-437.

The first series of experiments studied the effect of layers of the solid lubricants paraffin, cetyl alcohol,

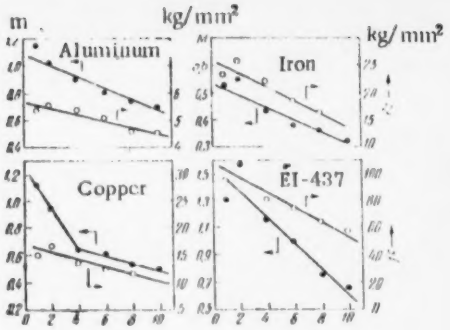

Fig. 1. The effect of the length of the hydrocarbon chain of a liquid lubricant (alcohol) on the frictional characteristics.

and palmitic acid on the frictional characteristics. Paraffin was selected as a nonpolar aliphatic hydrocarbon, and cetyl alcohol and palmitic acid served as typical surface active substances which differ in chemical activity. Each of these substances was deposited on the frictional surface from solution in a volatile solvent. This solvent was allowed to evaporate and the lubricated surface carefully rubbed with clean gauze until a thin film, firmly adhering to the frictional surface, was obtained. This technique of applying the lubricant led to the highly reproducible results which are shown in Table 1.

The data of Table 1 show that solid organic films are capable of bringing about a considerable diminution in the shear component of the specific force of friction, f_c (reduction to one-sixtieth of the original value) and in the coefficient of friction, μ, (reduction to one-twentieth of the original value). In this respect there is no marked difference in the lubricating ability of the nonpolar paraffin and of such highly polar compounds as cetyl alcohol and palmitic acid.

The shear component of the specific force of friction is practically independent of the mechanical properties of the rubbing metals, just as in the case of the molded solid lubricants. The value of this component is considerably greater (approximately 10 times) than the shear resistance of the lubricating material, however. These results could be explained by assuming that an external film, or "surface phase," is produced when the lubricant is applied to the frictional surface in the manner described and that it is in this region that frictional shear occurs. The difference between f_c and τ_f for the lubricant would be considerable since the values of the mechanical characteristics of such phases are much greater than those of matter in bulk [3]. This explanation is not, however, consistent with the results obtained with the nonpolar paraffin, which, according to the data of [4], does not form surface phases. On the other hand, the lubricating action of a paraffin film is practically identical with that of a film of cetyl alcohol or palmitic acid. If, however, adsorptional plasticizing of the surface layers of the contacting metals played a fundamental role in the lubricating action of solid films [5], the nonpolar paraffin would be a much poorer lubricant than either cetyl alcohol or palmitic acid and the shear component of the specific force of friction would be quite dependent on the characteristics of the metal whose surface layers were subjected to adsorptional plasticizing. The data of Table 1 show that neither of these effects is actually observed.

It is thus to be concluded that the lubricating action of films of solid lubricants is the result of a screening of the frictional surfaces [6]. This screening can never be complete so that the shear component of the specific force of friction is considerably in excess of the τ_f value for the lubricant. Table 1 gives calculated values of the percentage of screening, ϑ, which were obtained from the experimental data on f_c. ϑ is greater than 90% for effective lubricants.

The experimental results do not, of course, indicate that there is no adsorptional plasticizing in such a situation. They only show that this effect is a minor one in fixing the lubricating action of solid films. Adsorptional plasticizing must become increasingly important as the depth of the lubricating layer diminishes and it is likely that this is one of the principal factors determining the lubricating action of invisibly thin surface films of surface active media [7].

It is interesting to note that the liquid oleic acid cannot form a stable surface film which will completely screen the frictional surface so that it is a much less effective lubricant than palmitic acid although it has approximately the same length of hydrocarbon chain. The data of [8] shows, however, that oleic acid is more effective than, say, stearic acid when there is considerable plastic deformation and the flow in thin surface layers of the metals themselves becomes important.

The lubricating action of nonpolar liquid aliphatic hydrocarbons (from hexane to cetane) and their derivative acids (from acetic to pelargonic) and alcohols (from methyl to decyl) was investigated in a second series of experiments. The results of these experiments are shown in Table 2. The data of this table indicate,

TABLE 1

The Influence of Surface Films of Solid Lubricants on the Coefficient of Friction, μ, the Shear Component of the Specific Force of Friction, f_c, (kg/mm^2), and the Degree of Screening of the Surface, ϑ, (%)

Lubricant	Iron			Copper			Zinc			Aluminum			Tin			Lead			Shear resistence kg/mm^2
	μ	f_c	ϑ	μ	f_c	ϑ	μ	f_c	ϑ	μ	f_c	ϑ	μ	f_c	ϑ	μ	f_c	ϑ	
Dry	1,6	48	—	1,3	32	—	0,8	12	—	1,7	8,0	—	0,5	2,9	—	1,0	3,0	—	—
Paraffin	0,11	1,7	97	0,08	1,5	95	0,08	0,63	94,7	0,16	1,1	86	0,25	0,64	78	0,22	0,3	90	0,13
Cetyl alcohol	0,1	1,1	98	0,08	1,5	95	0,07	0,8	93,4	0,1	0,36	95	0,31	0,89	69,5	0,19	0,2	93	0,07
Palmitic acid	0,09	0,82	98	0,08	1,6	95	0,08	0,8	93,4	0,08	0,6	93	0,2	0,31	89,3	0,37	0,8	73	0,04
Oleic acid	0,16	4,3	—	0,11	5,0	—	0,21	5,0	—	0,26	2,1	—	0,4	1,0	—	0,16	0,2	—	—

TABLE 2

The Influence of Liquid Hydrocarbons and Their Derivatives on the Coefficient of Friction, μ, and on the Shear Component of the Specific Force of Friction, f_c (kg/mm^2)

		Dry	Nonpolar hydrocarbons				Alcohols						Acids						
			hexane	heptane	octane	decane	methyl	ethyl	butyl	hexyl	octyl	decyl	acetic	propionic	n-butyric	n-valeric	caprionic	enanthic	pelargonic
Copper	μ	1,32	0,7	0,48	0,45	—	1,12	0,95	0,64	0,61	0,53	0,5	0,71	0,67	0,51	—	0,38	0,21	0,17
	f_c	31,5	19,8	13,5	12,7	—	15,2	16,7	13,8	12,2	12,0	—	12,2	13,1	11,3	7,9	8,2	—	6,2
Aluminum	μ	1,64	1,07	1,16	1,1	—	1,15	1,02	0,89	0,8	0,73	0,69	1,32	1,18	1,09	—	0,9	0,8	0,65
	f_c	9,6	8,20	7,9	7,7	—	5,35	5,6	5,45	5,1	4,55	4,5	7,0	6,4	6,3	—	4,8	—	3,6
Iron	μ	1,9	—	—	—	—	0,52	0,54	0,43	0,38	0,36	0,32	0,55	0,49	0,48	—	0,42	0,39	0,3
	f_c	49	—	—	—	—	22,6	25,9	22,1	18,3	16,6	—	14,3	13,2	14,8	11,8	9,7	—	10,8
Alloy EI-437	μ	1,43	1,53	1,16	1,15	—	1,31	1,58	1,16	1,05	0,76	0,67	1,16	1,0	0,83	0,76	—	0,69	0,58
	f_c	126	125	122	110	108	95	108	81	75	64	59	79	—	59	54	—	—	40,2

first of all, that the liquid hydrocarbons and their derivatives are much less effective lubricants than are surface films of the solid hydrocarbons and their derivatives. Their ability to diminish μ and f_c is less than that of the solid films by a factor of $1/5 - 1/2$. Furthermore, the lubricating ability of the liquid compounds is markedly dependent on their polarity, being at a maximum in the acids, somewhat lower in the alcohols and lower still in the nonpolar hydrocarbons. In addition, Fig. 1 shows the shear component of the specific force of friction and the coefficient of friction to steadily diminish as the chain length of the liquid hydrocarbons and their derivatives is increased. And finally, the magnitude of the shear component of the specific force of friction is markedly dependent on the mechanical properties of the rubbing surfaces when liquid hydrocarbons or their derivatives are present. This last shows the mechanical properties of the surface layers of the rubbing bodies to be of direct significance in fixing the frictional characteristics in this case.

All of this gives reason to suppose that the lubricating action of liquid surface active media differs from that of solid media in so far as screening is accompanied by a significant adsorptional plasticizing of the metallic surface layers, which leads to a reduction of the shear resistance and a diminution in the values of the frictional characteristics.

This conclusion is confirmed by the fact [9] that the effect of the steel spherical slide in moving over the surface of an iron specimen is intensified by the presence of surface active substances, even though the tangent of the frictional force is reduced.

LITERATURE CITED

[1] G. I. Epifanov, Proc. Acad. Sci. USSR 114, No. 4 (1957);* G. I. Epifanov, Collected Papers Dedicated to Academician V. D. Kuznetsov on his 70-th Birthday, Acad. Sci. USSR Press, 1957;** G. I. Epifanov, Proc. Acad. Sci. USSR 118, No. 6 (1958).*

[2] G. I. Epifanov and N. I. Minaev, Bull. Higher Ed. Inst., Physics, No. 1 (1959); G. M. Bartenev and G. I. Epifanov, J. Eng.-Phys., No. 12 (1958); G. I. Epifanov and I. S. Avetisyan, Abstract of Reports, Third All-Union Conference on Friction and Wear in Machines, Moscow, 1957.

[3] B. V. Deryagin, Friction and Lubricating Action [in Russian], Moscow, 1938; B. V. Deryagin and M. M. Kuskakov, Bull. Acad. Sci. USSR, chem. ser., 5, 741 (1936).

[4] V. V. Karasev, Dissertation, Moscow, 1955.

[5] P. A. Rebinder, Collected Papers Dedicated to the 30-th Anniversary of the Great Socialistic Revolution of October,** Acad. Sci. USSR Press, 1947; V. I. Likhtman, P. A. Rebinder and G. V. Karpenko, The Influence of Surface Active Substances on the Deformation of Metals [in Russian], Acad. Sci. USSR Press, 1954.

[6] F. P. Bowden and D. Tealbor, cited in Friction and Surface Lubrication [in Russian], Moscow, 1953.

[7] S. Ya. Veiler, V. I. Likhtman and P. A. Rebinder, Proc. Acad. Sci. USSR 110, No. 6 (1956); S. Ya. Veiler and V. I. Likhtman, Proc. Acad. Sci. USSR 114, No. 6 (1957).*

[8] V. M. Korbut, Proc. Acad. Sci. USSR 124, No. 1 (1959).*

[9] G. I. Epifanov, N. I. Glagolev and P. A. Rebinder, Proc. Acad. Sci. USSR 123, No. 4 (1958);* N. I. Glagolev and G. I. Epifanov, J. Eng.-Phys. 2, No. 3 (1959).

Received April 27, 1959

* Original Russian pagination. See C. B. Translation.
** In Russian.

THE MECHANISM OF THE VAPORIZATION OF BERYLLIUM IN HIGH VACUUM

V. M. Amonenko, L. N. Ryabchikov, G. F. Tikhinskii, and V. A. Finkel'

The Khar'kov Physicotechnical Institute of the Academy of Sciences, UkSSR

(Presented by Academician G. V. Kurdyumov, June 6, 1959)

Oxygen lowers the plasticity of beryllium [3] even more than do other contaminants [1, 2] and thus limits the technical application of the metal at the present time. There is usually about 0.1% of oxygen in beryllium which has been prepared by electrolysis or distillation [4].

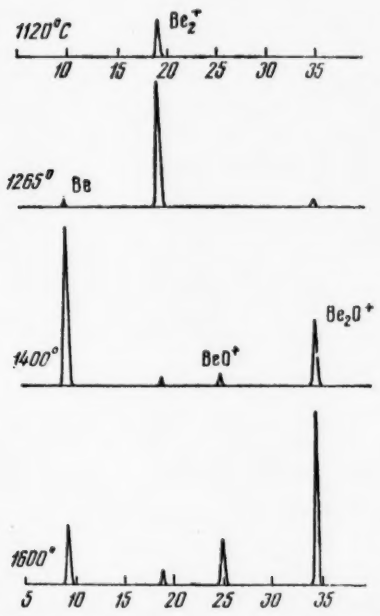

Fig. 1. Mass spectra of the vapors in the Be–BeO system at various temperatures.

The mechanism of the vaporization of Be has been studied in the present work in order to obtain an explanation of the presence of oxygen in the distilled metal. The MS-1 mass spectrometer which was used in this study was equipped with a standard ion source and a beryllium oxide crucible which was heated with a tungsten spiral. This crucible was loaded with 20-30 mg of high-quality distilled Be. Vaporization was carried out through collimating orifices in molybdenum screens which surrounded the crucible. The temperature was determined to within ± 5° from the power input. A vacuum ~ 10^{-6} mm of Hg was maintained in the neighborhood of the ionizer. The vapors were passed into the ionizing chamber of the mass-spectrometer source and the resulting ions were detected and analyzed in the usual manner. The intensities of the ionic currents were measured with an electrometric amplifier.

Figure 1 shows the mass spectra which were obtained at various temperatures. The mass number 18, corresponding to the dimer Be_2, predominated in the spectrum obtained by vaporizing solid Be. It is clear that there are molecules in the vapors of Be, the situation here being similar to that observed earlier in the case of Si, C, Bi and Cu, Ag, Au [5, 6]. A mass-spectrometric study of the sublimation of Be from a tantalum boat showed that the formation of the dimer Be_2 was not due to the presence of beryllium oxide. The only ion current observed in these latter experiments at 850-1150° was that of Be_2. The ratio of the ionic intensities Be^+/Be_2^+ began to alter above the melting point and the peak corresponding to mass 9 predominated. Loss of the metal through vaporization led to a decrease in the intensity of the beryllium peaks as time progressed.

The peak corresponding to the mass number 34, which appeared in addition to the ion peaks of Be, Be_2

TABLE 1

(hkl)	d	Intensities	
		calculated	Observed
(111)	3,1050	100	100
(220)	1,9028	77,2	74
(311)	1,6210	23,2	21
(400)	1,3415	9,3	9
(331)	1,2374	6,0	6
(422)	1,1018	18,9	23
(332),(511)	1,0380	4,3	6
(440)	0,9535	7,2	13
(531)	0,9126	4,7	4
(620)	0,8545	15,8	20
(533)	0,8242	3,2	very weak
(622)	0,8154	19,2	18

and BeO at temperatures above 1300°, can only be explained as resulting from formation of the lower oxide Be_2O. It is essential to note that this oxide of beryllium was detected in the mass spectra only when metallic beryllium was present.

The lower oxide was not formed when BeO was heated without the metal. X-ray studies confirmed the existence of the compound Be_2O. The dark gray deposit which condensed on the collimator screens (the temperature of these screens reached 1200-1250° in the course of the experiments) was removed and subjected to x-ray analysis.

The x-ray diagrams showed two line systems, a weak one belonging to BeO and another arising from a phase with a CaF type of cubic lattice which had a parameter of a = 5,402 ± ± 0,001 kX and was identified as Be_2O. Satisfactory agreement with the experimental data was obtained when the x-ray interference intensities of the BeO were calculated on the basis of a lattice having:

Be at $\left(\frac{1}{4}\frac{1}{4}\frac{1}{4};\ \frac{1}{4}\frac{1}{4}\frac{3}{4};\ \frac{1}{4}\frac{3}{4}\frac{1}{4};\ \frac{3}{4}\frac{1}{4}\frac{1}{4};\ \frac{1}{4}\frac{3}{4}\frac{3}{4};\ \frac{3}{4}\frac{1}{4}\frac{3}{4};\ \frac{3}{4}\frac{3}{4}\frac{1}{4};\ \frac{3}{4}\frac{3}{4}\frac{3}{4}\right)$, O at $\left(000;0-\frac{1}{2}\frac{1}{2};\ \frac{1}{2}0\frac{1}{2};\ \frac{1}{2}\frac{1}{2}0\right)$ (Table 1).

The data of Table 1 apply to CuK α radiation. Satisfactory agreement with the calculated intensity values was also obtained with FeK$_\alpha$ and with NiK$_\alpha$ radiation.

Thus it has been shown that beryllium which vaporizes from the solid phase is principally in the form of the dimer Be_2, whereas that which vaporizes from the liquid phase is principally in the form of the monomer Be. The reaction Be + BeO → Be_2O proceeds in vacuum at temperatures of ~ 1400° and above, the product Be_2O being stable at normal conditons. The lower oxide of beryllium is more volatile than BeO and is one of the sources of the oxygen contamination in the metal obtained by distillation from BeO crucibles.

The authors consider it their pleasant duty to express their thanks to B. G. Lazarev for his interest in this work and for his valuable advice.

LITERATURE CITED

[1] R. I. Garber, I. A. Gindin, et al., Physical Metallurgy and Metalworking, 1, 529 (1955).

[2] R. I. Garber, I. A. Gindin, and Yu. V. Shubin, J. Exp. Theo. Phys. 36, 376 (1959).

[3] H. A. Sloman, J. Inst. Met. 49, 365 (1932).

[4] V. M. Amonenko, Dissertation, Phys.-Tech. Inst., Acad. Sci. UkSSR, Khar'kov, 1952.

[5] W. A. Chupka and M. G. Inghram, J. Phys. Chem. 59, 100 (1955)

[6] J. Drowat and R. E. Honig, J. Chem. Phys. 25, 581 (1956).

Received June 3, 1959

MEASUREMENTS OF THE VAPOR PRESSURE OF SOLID BERYLLIUM OXIDE

L. P. Belykh and A. N. Nesmeyanov

The M. V. Lomonosov State University, Moscow

(Presented by Academician V. I. Spitsyn, June 5, 1959)

The pioneer work of Fichter [1] and Brunner and Ruff [2], showed beryllium oxide to undergo evaporation even below the melting point of 2450 ± 50°C but Tiede and Birnbrauer [3] were not able to observe vaporization at temperatures of this same order (2400 ± 100°C). Mott [4] used the order of volatility of various substances and the separation of the condensation bands in estimating a normal boiling point of 3900°C for the oxide. The papers which have appeared more recently [5, 6] have been principally concerned with the increase in the volatility of the oxide which results from the presence of water vapor. Erway and Seifert [5] have measured the vapor pressure of pure beryllium oxide using the radioisotope $_4Be^7$ and a differential variant of the effusion method. These authors employed the vapor pressure – temperature relation to find a boiling point of 4120 ± 170°C for the oxide. Their results stand in need of confirmation, however, since their work involved effusion of beryllium oxide vapors out of tungsten chambers and it has been established that this metal is especially effective in reducing the oxide when the two are heated together in vacuum [8].

The pressure of the vapors in equilibrium with solid beryllium oxide has been measured over the temperature interval 2103-2573°K in the present work. These measurements were carried out by the method of vacuum evaporation from a free surface and by an integral variant of the effusion method.

The beryllium oxide was prepared from basic beryllium acetate which was distilled three times in vacuum, treated with sulfuric acid, and then heated in vacuum to temperatures ranging from 1300 to 2600°K. Quantitative analyses showed the resulting material to contain no less than 99.93% of the oxide. Spectral analysis indicated the presence of very minute amounts of alloying magnesium, titanium, and silicon.

Hot pressing without addition of a binder was used in obtaining dense specimens. This pressing was carried out in graphite molds at 1600-1700°C and pressures of 25-35 kg/cm^2. The molded forms were mechanically separated from the surface and then heated in vacuum at 2600°K. Quantitative analysis showed the mean oxide content of these specimens to be 99.5%.

Vapor pressure measurements were made in the vacuum units of the assembly of the high-frequency MVP-3M furnace used for heating the effusion chambers and the containers with the specimens.

Tungsten cups were used to hold the pressed or powdered specimens in the experiments which were carried out by the Langmuir method; the chambers employed in the effusion measurements were of the usual construction, the external parts being of tantalum and the internal, of tungsten. The possibility of reduction of beryllium oxide by the metal of the chamber was eliminated in many instances by loading the chamber cups with beryllium oxide inserts which were ground to diaphragms whose inner surfaces were covered with thorium oxide or zirconium oxide.

The temperature of the vaporizing specimen surface was determined with the aid of an OPPIR-09 optical pyrometer which had been calibrated under the working conditions.

The material which vaporized out of the containers was condensed on a water-cooled quartz collector.

TABLE 1

Rates of Vaporization and Vapor Pressures of Beryllium Oxide

Temperature, °K	Area of orifice, cm^2	Duration of experiment, sec	Weight of condensate, g	Rate of vaporization, $g/cm^2 \cdot sec$	Pressure, atmos
2573	$1,37 \cdot 10^{-3}$	2640	$2,42 \cdot 10^{-4}$	$7,181 \cdot 10^{-5}$	$1,53 \cdot 10^{-5}$
2508	$1,03 \cdot 10^{-3}$	3600	$1,30 \cdot 10^{-4}$	$3,507 \cdot 10^{-5}$	$7,94 \cdot 10^{-6}$
2463	$1,03 \cdot 10^{-3}$	1200	$2,25 \cdot 10^{-4}$	$1,820 \cdot 10^{-5}$	$4,07 \cdot 10^{-6}$
2453	$2,74 \cdot 10^{-3}$	3900	$1,39 \cdot 10^{-4}$	$1,301 \cdot 10^{-5}$	$2,91 \cdot 10^{-6}$
2378	$1,03 \cdot 10^{-3}$	3900	$3,24 \cdot 10^{-5}$	$8,066 \cdot 10^{-6}$	$1,78 \cdot 10^{-6}$
2373	$2,74 \cdot 10^{-3}$	1800	$3,33 \cdot 10^{-5}$	$6,752 \cdot 10^{-6}$	$1,49 \cdot 10^{-6}$
2333	$2,74 \cdot 10^{-3}$	2700	$4,44 \cdot 10^{-5}$	$6,002 \cdot 10^{-6}$	$1,31 \cdot 10^{-6}$
2308	$1,13 \cdot 10^{-1}$	1500	$5,82 \cdot 10^{-4}$	$3,434 \cdot 10^{-6}$	$7,45 \cdot 10^{-7}$
2293	$2,74 \cdot 10^{-3}$	2760	$2,38 \cdot 10^{-5}$	$3,147 \cdot 10^{-6}$	$6,80 \cdot 10^{-7}$
2263	$2,74 \cdot 10^{-3}$	2700	$4,16 \cdot 10^{-6}$	$5,623 \cdot 10^{-7}$	$1,21 \cdot 10^{-7}$
2203	$1,13 \cdot 10^{-1}$	3600	$2,77 \cdot 10^{-4}$	$6,814 \cdot 10^{-7}$	$1,45 \cdot 10^{-7}$
2213	$2,74 \cdot 10^{-3}$	4200	$6,10 \cdot 10^{-6}$	$5,301 \cdot 10^{-7}$	$1,13 \cdot 10^{-7}$
2183	$1,13 \cdot 10^{-1}$	4200	$1,94 \cdot 10^{-4}$	$4,088 \cdot 10^{-7}$	$8,61 \cdot 10^{-8}$
2163	$2,74 \cdot 10^{-3}$	18300	$1,66 \cdot 10^{-5}$	$3,311 \cdot 10^{-7}$	$6,95 \cdot 10^{-8}$
2153	$1,13 \cdot 10^{-1}$	1200	$3,33 \cdot 10^{-5}$	$2,456 \cdot 10^{-7}$	$5,14 \cdot 10^{-8}$
2128	$1,13 \cdot 10^{-1}$	1500	$3,17 \cdot 10^{-5}$	$1,870 \cdot 10^{-7}$	$3,89 \cdot 10^{-8}$
2103	$1,13 \cdot 10^{-1}$	3600	$3,33 \cdot 10^{-5}$	$8,186 \cdot 10^{-8}$	$1,70 \cdot 10^{-8}$

It was necessary to coat the inner surface of this collector with polystyrene, or with polyethylene, since it is very difficult to wash beryllium oxide off of quartz. The film and the oxide were washed from the surface of the receiver together and the dry residue left after distillation of the solvent was treated and analyzed for beryllium by a method using "berillon-11 IREA."

The rate of evaporation and the pressure of the vapors in equilibrium with solid beryllium oxide were determined from the amount of material vaporized (Table 1). The equation $\log P_{atmos} = 8.156 - 3.324/T \cdot 10^4$ was obtained by applying the method of least squares to the experimental data; from this it follows that the heat of sublimation is $\Delta H_0^0 = 157.6$ kcal/mole. This treatment of the experimental data gives no more than an upper limit for the vapor pressure of the beryllium oxide since it does not allow for thermal dissociation of the oxide in vaporization.

Analysis shows the results of the present work to be in agreement with those of Erway and Seifert; the reduction of beryllium oxide by tungsten is obviously insignificant over the investigated temperature interval and does not markedly affect the experimental results. The condensation coefficient of beryllium oxide can be assumed to be approximately equal to unity since the results of the effusion experiments agree with those obtained by the Langmuir method.

LITERATURE CITED

[1] F. Fichter, Zs. anorg. chem. 93, 84 (1915).

[2] O. Ruff, Zs. anorg. chem., 82, 373 (1913).

[3] E. Tiede and E. Bimbrauer, Zs. anorg. chem. 87, 129 (1914).

[4] W. Mott, Trans. Am. Electrochem. Soc. 34, 255 (1918).

[5] C. Hutchison and J. Malm, J. Am. Chem. Soc. 71, 1338 (1949).

[6] L. Glossweiner and R. Seifert, J. Am. Chem. Soc. 74, 2701 (1952).

[7] N. Erway and R. Seifert, Electrochem. Soc. J. 98, 83 (1951).

[8] J. Askerman and R. Thorn, Congr. Pure and Appl. Chem., Paris, 1957.

Received June 2, 1959

AN INVESTIGATION OF THE INTERACTION OF CROSSED POLARIZED METALLIC FILAMENTS IN ELECTROLYTIC SOLUTIONS FOR THE SIMULATION OF COAGULATION EFFECTS, AND THE DETERMINATION OF NULL-CHARGE POTENTIALS AND THE VAN DER WAALS' FORCE CONSTANT

T. N. Voropaeva, Corresponding Member Acad. Sci. USSR
B. V. Deryagin, and B. N. Kabanov

The Institute of Physical Chemistry and the Institute of Electrochemistry of the Academy of Sciences, USSR

The modern theory of the stability of lyophobic colloids [2, 3] and direct experimental observations [1] both show that the force between charged surfaces in an electrolytic solution is one of repulsion at the larger, and the smaller, distances of separation and one of molecular attraction at distances of the order of magnitude of the depth of the ionic atmosphere. In order to break through the film of liquid and establish direct contact between crossed metallic filaments it is thus necessary that the driving force exceed the force barrier marked out by the maximum, N_m, on the curve showing net interaction as a function of distance (Fig. 1).

The appearance of a force of adhesion equal to the minimum on the force of interaction vs distance curve can serve as a criterion for the establishment of contact. This type of trial and error procedure is not suitable for determining the height of the force barrier since two driving forces, sufficiently close to one another in value, will not give different results in regard to the eventual appearance of the force of adhesion. A rapid and successful method for this determination can be based on the discontinuous alteration in the electrical resistance which occurs at the instant of contact of the two filaments.

The force barrier can be measured as a function of the composition and concentration of the electrolyte, used as a function of the potential of the filament surface, these surfaces being polarized by a current so that the potential is uniform, or almost so (see below).

Technique of Measurement. Smooth platinum wires, 300 μ in diameter, were used as filaments. The filament 1 was affixed to the elastic torsion suspension 3 (Fig. 2). The angle of twist of this suspension was measured with the aid of the attached mirror 4. The twist angle of the suspension was recorded on an automatic recorder through a signal passed from the solution by a photorelay [4]. Filament 2 was firmly attached to the moving part of the apparatus and could be gradually and smoothly brought up to filament 1, or withdrawn from it, by a small motor-driven transmission system. Filaments 1 and 2 were set in hermetically sealed vessel 5 at an angle of approach of 90°; this vessel could be fed with the electrolytic solution from the reservoir 6. This vessel could also be connected with the comparison electrode 7 through an electrolytic bridge.

The circuit of Fig. 3 allowed each of the filaments to be charged to any desired potential. These potentials were measured with respect to a saturated calomel electrode. The platinum wires 3 and 4 served as auxiliary electrodes for polarizing the filaments. A small difference of potential was established between the filaments (0.01 v) and measured with the potentiometer π_2, in order to mark the instant of contact in determining the force barrier. These potentials were equalized at contact and the compensating system was thrown out of balance. Vibrational effects were eliminated by mounting the apparatus on a shock-adsorbing plate which was affixed to a concrete pillar driven into the earth.

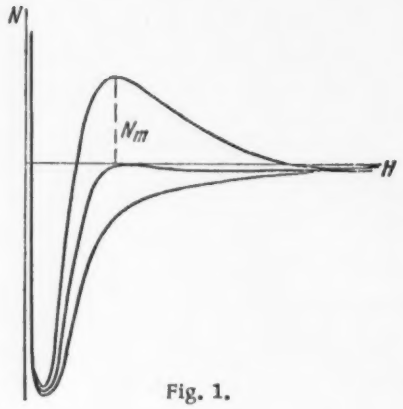

Fig. 1.

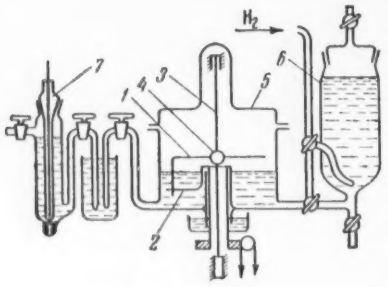

Fig. 2.

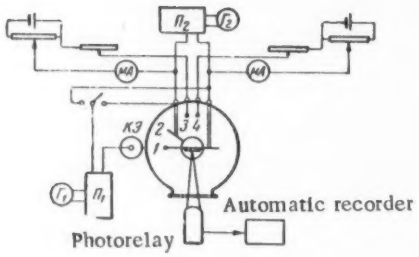

Fig. 3.

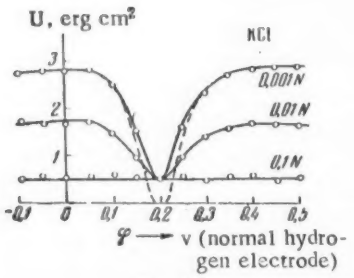

Fig. 4.

The filaments were cleansed prior to measurement by being immersed for 3 minutes in concentrated H_2SO_4 and then cathodically polarized for 3-4 hours in 1 N H_2SO_4 solution, after which they were repolarized, first cathodically, and then anodically, for 15 minutes in fresh 1 N H_2SO_4 under hydrogen. The H_2SO_4 solution was then displaced by hydrogen, the vessel and the filaments were washed out with the solution which was to be used in the measurements, and final loading with the solution then carried out. The solution was freed of organic contaminants by placing a platinized platinum gauze in the vessel and flushing it out with hydrogen for 12 hours.

The desired potentials were then applied to the filaments. These filaments were separated from one another at the beginning of the experiment and the zero position of filament 1 (the one attached to the elastic suspension) was marked on the scale of the automatic recorder. Filament 2 was then brought up gradually to filament 1. When filament 2 had come sufficiently close to 1, the latter began to rotate in the same direction as 2, twisting the suspension through an angle which was proportional to the force of interaction (driving force) of the filaments; this angle was registered on the recorder. There was sharp deflection on the needle of the potentiometer galvanometer at π_2, when direct contact was established between the filaments as a result of surmounting the force barrier and penetrating through the electrolyte film. The magnitude of the force barrier, N_m, between the filaments was determined from the reading of the recorder at this instant.

EXPERIMENTAL RESULTS

With various potentials on the filaments, the value of N_m was measured in three KCl solutions at the concentrations 10^{-3}, 10^{-2} and 10^{-1} N. The results are shown in Fig. 4, where the potential, φ, has been expressed in terms of the normal hydrogen electrode. This figure shows a minimum, N_m, at 0.2 volts which is independent of the solution concentration. This potential ($\varphi_n = 0.2 \pm 0.02$) falls between the values found by other workers for the null-charge potential of platinum. Curves showing the potential barrier as a function of the potential are symmetric about this minimum point; far from the minimum each of these curves asymptotically approaches a constant value which increases as the dilution of the solution rises. To all intents and purposes, these constant values are already reached at $\pm$ 0.15 volts from φ_n.

DISCUSSION OF RESULTS

A theory of the interaction in electrolytic solution of hydrophobic convex surfaces uniformly charged to the potential $\psi = \varphi - \varphi_n$ has been developed by one of us in [3]; the case of the symmetric electrolyte is there covered by the equation

$$\frac{N}{2\pi r} \equiv U = I - \frac{A}{12\pi}\frac{1}{H^2}, \qquad (1)$$

$$I = \frac{8\gamma nRT}{\varkappa}\left[\frac{2}{k}E - \left(\frac{1}{k} - k\right)K - 2\right];$$
$$H = \frac{2kK}{\varkappa}. \qquad (2)$$

in which N is the force of interaction of the convex surfaces at their distance of nearest approach, H; U and I are, respectively, the total interaction and the electrostatic interaction for unit surfaces of the same type separated by a plane-parallel layer of this same electrolyte of thickness H; A is the Hamaker constant of molecular attraction [5]; γ is the electrolyte concentration in moles per 1 cm^3; $\underline{n}$ is the number of anions or cations per molecule of the electrolyte; R is the molar gas constant; T is the absolute temperature; $\varkappa^{-1}$ is the Debye depth of the ionic atmosphere; K and E are elliptic integrals of the first and second kinds with modulus $\underline{k}$ and limits $u_1 = \frac{1}{k}\ \mathrm{sch}\ \frac{F\psi}{2RT}$, $u_2 = 1$; and $\underline{r}$ is the filament radius.

By giving all possible values to the parameter $\underline{k}$, the corresponding values of H and U can be calculated and their relation thus expressed in parametric form. The maximum value of N, N_m, and the value H_m corresponding to it, can be found by the well known rule for locating maxima. Theory shows that the electrostatic repulsion increases from zero to a certain asymptotic value* as absolute value of ψ rises, whereas the van der Waal's attraction remains constant, to within a first degree approximation. From this it follows that the force of attraction should predominate at all distances and N_m be equal to zero when the value of $|\psi|$ is less than a certain δ (which is in contradiction with experiment, see Fig. 4); $N_m > 0$ when $|\psi| > \delta$. The value of δ can be found readily by making use of the simultaneous equations in H: $(dN(H)/dH) = 0$ and $N(H) = 0$. N_m should increase with a further rise in $|\psi|$, tending asymptotically to a definite limit when $|\psi| >> kT/ne$, as is observed experimentally. The symmetry of the N_m vs φ curves around the abscissas φ_n is also in agreement with experiment. The radius of action of the repulsive force diminishes as the concentration rises, so that the N_m vs φ curve should fall (as experiment shows to be the case) and finally coincide with the axis of abscissas when the concentration reaches a certain critical value (which is in contradiction with experiment, see Fig. 4).

Having obtained N_∞ and U_∞, the asymptotic values of N_m and U_m, from experiment, solution of the equations

$$\frac{dU(H)}{dH} = 0, \qquad (3)$$

$$U(H) = U_\infty, \qquad (4)$$

makes it possible to evaluate the constant of molecular attraction, A, which is then the single unknown. Equations (1) and (3) give the condition for maxima in N and U in the form: $\frac{dI}{dH} = -\frac{A}{6\pi H^3}$; here, the right member expresses the specific force (per 1 cm^2) of van der Waals' attraction between surfaces separated by a plane-parallel layer of electrolyte of thickness H and the left member 3: $\frac{dI}{dH} = P(H) = 4\gamma nRT\left(\frac{1}{k^2} - 1\right)$, the specific electrostatic repulsion of these same surfaces. We finally obtain the equation: $4\gamma nRT\left(\frac{1}{k^2} - 1\right) = -\frac{A}{6\pi H^3}$ as a statement of the condition for unstable equilibrium between these two forces. An equation in $\underline{k}$ results when the unknown A is eliminated from this last result (1) and (4)

$$\frac{1}{k}\left[4E - 4k - (1-k)K\right] = \frac{U_\infty \varkappa}{4\gamma nRT}, \qquad (5)$$

and the right member of this equation will contain only experimentally determined quantities. Values of $\underline{k}$

* For wetting films, this was first shown by A. N. Frumkin [6].

and K = K (k) can be obtained from (5) and substituted in (1) and (2) to give the following results:

$C \equiv 10^3\ \gamma$, mole/liter	10^{-3}	10^{-2}
H, cm	$4 \cdot 10^{-7}$	$5 \cdot 10^{-7}$
A, erg	$6{,}6 \cdot 10^{-12}$	$7{,}3 \cdot 10^{-12}$

The good agreement between the two values of A, and the fact that these values are of a reasonable order of magnitude, can serve as strict confirmation of the applicability of the theory to the concentration interval from 0.001 to 0.01 N. Once A is known, theoretical N_m, $\varphi = \psi + \varphi_n$ relations can be developed by solving Eq. (3) for H at various values of ψ and γ and substituting in (1). Such relationships are shown in Fig. 4 in the form of dotted curves. The concordance and the divergence between the experimental data and the theoretical results are obvious. The divergences arise from repulsive forces which are unaccounted for by theory (forces of the "third type"), the existence of such forces being reflected in the fact that the relation $\varphi - \varphi_n = 0$ is independent of the concentration in the interval 0.001 – 0.1 N and independent of the potential and surface charge at an electrolyte concentration of 0.1 N.

The abscissa of the axis of symmetry of the N vs φ curve, $\varphi_n = 0.2 \pm 0.02$ volts, is the null-charge potential of platinum. Thus a study of the interaction of crossed filaments has given a new method for evaluating the null-point of metals, and one which has many advantages. Satisfactory results on the null-charge point of platinum cannot be obtained by the usual method of determining the minimum point in the double-layer capacity in dilute electrolytic solutions. There is a considerable divergence among the results which have been obtained by other methods [7]. The proposed method gives a value which is close to that obtained electrokinetically [8].

LITERATURE CITED

[1] B. V. Deryagin and E. V. Obukhov, Coll. J. 1, 385 (1935); Acta phys. chim. URSS 5, 1 (1936); B. V. Deryagin and A. S. Titievskaya, Proc. Acad. Sci. USSR 89, 104 (1953); B. V. Deryagin and A. S. Titievskaya, Discuss. Farad. Soc. No. 18, 24 (1954); M. van den Tempel, J. Colloid Sci. 13, 125 (1958); G. I. Fuks, Coll. J. 20, 748 (1958).

[2] B. V. Deryagin, Bull. Acad. Sci. USSR, chem. ser., 6, 1153 (1937); Acta phys. chim. URSS 10, 333 (1939); Trans. Farad. Soc. 36, 203 (1940); 36, 730 (1940).

[3] B. V. Deryagin and L. Landau, J. Exp. Theo. Phys. 11, 802 (1941); J. Exp. Theo. Phys. 15, 663 (1945); Acta phys. chim. URSS 14, 633 (1941).

[4] B. V. Deryagin, I. I. Abrikosova, and E. M. Lifshits, Prog. Phys. Sci. 3, 493 (1958).

[5] H. C. Hamaker, Physica 4, 1058 (1937).

[6] A. N. Frumkin and A. V. Gorodetskaya, J. Phys. Chem. 4, 529 (1933).

[7] A. N. Frumkin, A. Shlygin, and V. Medvedovskii, Bull. Acad. Sci. USSR, chem. ser., 5, 773 (1936); Acta phys. chim, URSS 6, 911 (1936); A. V. Gorodetskaya and B. N. Kabanov, J. Phys. Chem. 4, 529 (1933); N. A. Balasheva, Proc. Acad. Sci. USSR 103, 639 (1955).

[8] N. A. Balasheva and A. N. Frumkin, Proc. Acad. Sci. USSR 20, 449 (1938).

Received June 30, 1959

CONSECUTIVE ELECTROCHEMICAL REACTIONS IN OSCILLOGRAPHIC POLAROGRAPHY

Ya. P. Gokhshtein and A. Ya. Gokhshtein

The V. I. Vernadskii Institute of Geochemistry and Analytical Chemistry of the Academy of Sciences, USSR

(Presented by Academician A. N. Frumkin, June 1, 1959)

The lack of quantitative relations for the case of consecutive waves has been noted in the literature [1]. Equations of this type would relate the consecutive currents to the constants of the reaction steps and would be a means through which the kinetics of these reactions could be studied. The relations which have been derived below are ones which allow currents to be evaluated from constants and, at the same time, permit a solution of the inverse problem.

We will consider $\underline{m}$ ions σ_i of charge z_i which are related through reactions of the type

$$n_{ip}\ominus + \sigma_i \rightleftarrows \sigma_p \quad (i,\ p = 1,\ 2,\ \ldots,\ m); \tag{1}$$

where $n_{ip} = z_i - z_p$ is the number of electrons involved in a given step and $n_{ip} = -n_{pi}$.

The rate constants for the forward and the reverse reactions can be given the symmetrical form [2]:

$$\Phi_{ip} = k_{ip} \exp\left[-\alpha_{ip}\frac{n_{ip}F}{RT}E(t)\right], \qquad \alpha_{ip} + \alpha_{pi} = 1. \tag{2}$$

It is customary in polarography to use a large excess of a foreign electrolyte and, under these conditions, the flow of matter to the electrode is maintained by diffusion. A system of $\underline{m}$ equations applying at the electrode – solution boundary can be obtained by making use of Fick's Law:

$$D_i\varphi_i = \sum_{p=1}^{m}(C_i\Phi_{ip} - C_p\Phi_{pi}), \qquad \sum_{i=1}^{m} D_i\varphi_i = 0, \qquad \varphi_i(t) = \frac{\partial C_i(0,\ t)}{\partial x}. \tag{3}$$

Further operations will aim at an evaluation of the quantities $\varphi_i(t)$ since these are the factors which completely determine the polarographic currents:

$$I(t) = SF\sum_{i=1}^{m} z_i D_i\varphi_i(t) = SF\sum_{i=1}^{m-1}(z_i - z_m)\,D_i\varphi_i(t) = SF\sum_{k=1}^{m-1} n_{k,k+1}\sum_{i=1}^{k} D_i\varphi_i(t); \tag{4}$$

S is here the area of the electrode and each term in the last sum over $\underline{k}$ refers to an individual wave. It is only necessary to combine the System (3) with the diffusion equations and the initial conditions in order to find $\varphi_i(t)$. The diffusion layer in oscillographic polarography is a shallow one and this makes it possible to neglect the

effect of the curvature of the electrode. This, in turn, permits the problem to be reduced to the one-dimensional case.

Each problem of the type ($0 \leq x < \infty$; $0 < t < \infty$)

$$\partial C_i/\partial t = D_i \partial^2 C_i/\partial x^2, \quad C_i(x, 0) = \phi_i(x), \quad \partial C_i(0, t)/\partial x = \varphi_i(t). \tag{5}$$

can be solved separately as soon as the $\varphi_i(t)$ are known.

For each of the m ions a relation between the concentration and the current to the electrode surface can be obtained by passing to the limit $x \to 0$ in the solution of this standard problem:

$$C_i(0,t) = \Psi_i(t) - \sqrt{\frac{D_i}{\pi}} \int_0^t \frac{\varphi_i(\tau)\, d\tau}{\sqrt{t-\tau}} \left(\Psi_i(t) = \frac{1}{\sqrt{\pi D_i t}} \int_0^\infty \phi_i(\xi)\, d\xi \right). \tag{6}$$

A useful relation between the concentrations on the electrode surface results from a combination of (3) and (6):

$$\sum_{i=1}^{m} \sqrt{D_i} C_i(0, t) = \sum_{i=1}^{m} \sqrt{D_i} \Psi_i(t). \tag{7}$$

Equation (7) simplifies to

$$\sqrt{D_1} C_1(0, t) + \sqrt{D_2} C_2(0, t) + \ldots + \sqrt{D_m} C_m(0, t) = \sqrt{D_1} C. \tag{8}$$

when $\phi_1(x) \equiv C$, $\phi_{i+1} \equiv 0$, as is frequently the case.

Substitution of the expressions for the $C_i(0, t)$ from (6) into the System (3) leads to a system of integral equations in the functions $\varphi_i(t)$

$$\begin{aligned} D_i \varphi_i + \sum_{p=1}^{m} \sqrt{\frac{D_i}{\pi}}\, \Phi_{ip} \int_0^t \frac{\varphi_i(\tau)\, d\tau}{\sqrt{t-\tau}} - \sqrt{\frac{D_p}{\pi}}\, \Phi_{pi} \int_0^t \frac{\varphi_p(\tau)\, d\tau}{\sqrt{t-\tau}} = \\ = \sum_{p=1}^{m} \Psi_i \Phi_{ip} - \Psi_p \Phi_{pi} \quad (i = 1, 2, \ldots, m). \end{aligned} \tag{9}$$

Setting the solution of this system into (4) gives the desired result, namely, the time dependence of the polarographic current in a stepwise reaction.

In an actual determination of the $\varphi_i(t)$, it is useful to represent the integrals of (9) in the form [3]

$$\int_0^t \frac{\varphi_i(\tau)\, d\tau}{\sqrt{t-\tau}} = \sqrt{\delta} \int_0^n \frac{\varphi_i(\delta\nu)\, d\nu}{\sqrt{n-\nu}} = \frac{4}{3} \sqrt{\delta} [\varphi_i(n) + \beta_i(n)], \tag{10}$$

where $\varphi_i(t) = \varphi_i(\delta n)$ is arbitrarily represented by $\varphi_i(n)$ and $\beta_i(n) = 0{,}5\ \varphi_i(n-1) +$

$$+ 0{,}75\ S_i(n) + 0{,}25\ \widetilde{S}_i(n),\ S_i(n) = \sum_{\nu=1}^{n-1} \rho(n-\nu) [\varphi_i(\nu) + \varphi_i(\nu-1)];$$

$$\widetilde{S}_i(n) = \sum_{\nu=1}^{n-1} \rho^3(n-\nu)[\varphi_i(\nu) - \varphi_i(\nu-1)]; \quad \rho(m) = \sqrt{m+1} - \sqrt{m}.$$

The arbitrary time unit δ is here fixed by dividing the time covered by the experiment, θ, into a suitable number, N, of equal intervals such that $t = \delta n = \frac{\theta}{N} n$. The arc $\varphi_i(t)$ is replaced by the chord in each of these intervals. The sums $S_i(n)$ and $\widetilde{S}_i(n)$ involve only those φ_i values which refer to preceding instants of time: $\varphi_i(1), \varphi_i(2), \ldots, \varphi_i(n-1)$. This makes it possible to approximate (9) by a system of algebraic equations in $\varphi_i(n)$:

$$\varphi_i\left(D_i + \sum_{p=1}^{m} \overline{\Phi}_{ip}\right) - \sum_{p=1}^{m} \overline{\Phi}_{pi}\varphi_p = \sum_{p=1}^{m} (\beta_p - \overline{\Psi}_p)\overline{\Phi}_{pi} - (\beta_i - \overline{\Psi}_i)\sum_{p=1}^{m} \overline{\Phi}_{ip},$$
$$\overline{\Phi}_{ip} = \frac{4}{3}\sqrt{\frac{\delta}{\pi}}\sqrt{D_i}\Phi_{ip}, \quad \overline{\Psi}_i = \frac{3}{4}\sqrt{\frac{\pi}{\delta}}\frac{\Psi_i}{\sqrt{D_i}} \quad (i = 1, 2, \ldots, m). \tag{11}$$

The argument n is the same for all the functions of system (11) and it has been omitted from the notation for brevity. It is now possible to evaluate $\varphi_1(1), \varphi_1(2), \ldots, \varphi_1(\theta)$ for $i = 1, 2, \ldots, m$ by setting up a system of the type of (11) for each instant of time and using at each point the results which were obtained in the preceding step.

System (11) will consist of three and four equations, respectively, for the practically important 2-step and 3-step reactions (m = 3 or m = 4). In addition, it is usually true that $\psi_1(x) \equiv C$ and $\psi_2(x) = \ldots = \psi_m(x) = 0$. Thus $\Psi_1(t) \equiv C$, $\Psi_2(t) \equiv \ldots \equiv \Psi_m(t) = 0$. Finally, a truly consecutive series of reactions will be such that $\sigma_1 - \sigma_2 - \ldots - \sigma_m \Phi_{ip} = 0$ when $|i - p| > 1$. With these conditions m = 3, Eq. (3) can be used to bring System (11) into the form:

$$a_{11}\varphi_1 + a_{12}\varphi_2 = b_1, \quad a_{21}\varphi_1 + a_{22}\varphi_2 = b_2;$$
$$a_{11} = D_1 + \overline{\Phi}_{12}, \quad a_{12} = -\overline{\Phi}_{21}, \quad a_{21} = \frac{D_1}{D_3}\overline{\Phi}_{32} - \overline{\Phi}_{12},$$
$$a_{22} = D_2 + \overline{\Phi}_{21} + \overline{\Phi}_{23} + \frac{D_2}{D_3}\overline{\Phi}_{32}, \quad b_1 = \bar{c}\,\overline{\Phi}_{12} - \overline{\Phi}_{12}\beta_1 + \overline{\Phi}_{21}\beta_2,$$
$$b_2 = -\bar{c}\,\overline{\Phi}_{12} + \left(\overline{\Phi}_{12} - \frac{D_1}{D_3}\overline{\Phi}_{32}\right)\beta_1 - \left(\overline{\Phi}_{21} + \overline{\Phi}_{23} + \frac{D_2}{D_3}\overline{\Phi}_{32}\right)\beta_2,$$
$$\overline{\Phi}_{ip} > 0 \text{ when } |i - p| = 1, \quad \bar{c} = {}^3/_4\sqrt{\pi/\delta}\, c/\sqrt{D_1}.$$

The same can also be done for the case m = 4.

Direct test proves that the determinants of these two systems are different from zero. The successive wave currents can be shown to be proportional to D_1, whatever the degree of reversibility of the reactions, and to be only weakly dependent on the remaining diffusion coefficients. It is thus possible to make the calculations on the basis of the same value for all the diffusion coefficients, $D_1 = D_2 = D_3 = \ldots$.

We will now consider the actual case of the reduction of Nb^{5+} in 23 N H_2SO_4. The mechanism of this reaction has been explained only recently [4]. An experimentally developed oscillogram is shown in Fig. 1. The first wave passes through a maximum at $E_1 = -0.334$ volts (normal hydrogen electrode) and the second through a maximum at $E_2 = -0.524$ volts. The difference in curvatures of these waves forces the conclusion that the first step is irreversible and the second step, nearly reversible. The α_{12} coefficient for the first wave was calculated from the Matsuda equation [5] and had the value 0.44. The boundary conditions (3) for this case take the form:

$$D_1\varphi_1(t) = C_1(0, t)\,\Phi_{12}(t) = C_1(0, t)\,e^{p(t-0)},$$
$$\frac{C_2(0, t)}{C_3(0, t)} = \frac{\sqrt{D_3}C_2(0, t)}{\sqrt{D_1}C - \sqrt{D_1}C_1(0, t) - \sqrt{D_2}C_2(0, t)} - b_1 e^{-at} \tag{12}$$
$$(C_1(x, 0) = C, \quad C_2(x, 0) = C_3(x, 0) = 0),$$

TABLE 1

First wave	Second wave	
	reversible	irreversible
Reversible	$\frac{0,087}{n_{12}}+\frac{0,146}{n_{23}}$	$\frac{0,087}{n_{12}}+\frac{0,153}{\alpha_{23}n_{23}}$
Irreversible	$\frac{0,024}{\alpha_{12}n_{12}}+\frac{0,146}{n_{23}}$	$\frac{0,024}{\alpha_{12}n_{12}}+\frac{0,153}{\alpha_{23}n_{23}}$

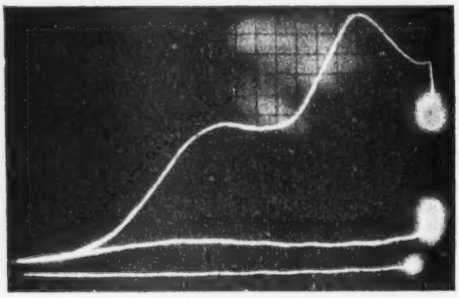

Fig. 1. Oscillogram of Nb^{5+} in 23 N H_2SO_4; cathode polarization, V = 3.10 v/sec; maxima, $E_1 = -0.334$ v, $E_2 = -0.524$ v, relative to the normal hydrogen electrode; t = 21°. Zero line and background current below.

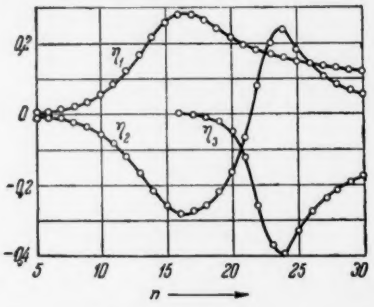

Fig. 2. The theoretically evaluated functions η_1, η_2, and η_3 which are proportional to the Nb^{5+}, Nb^{4+}, and Nb^{3+} currents to the electrode.

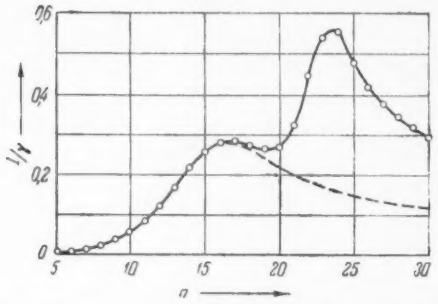

Fig. 3. Currents calculated for the reaction $Nb^{5+} - Nb^{4+} - Nb^{3+}$; $\gamma = CSF\sqrt{p\pi D_1}$.

where $p = \alpha_{12}\frac{n_{12}F}{RT}v$; $\theta = \frac{\bar{E}}{v} - \frac{RT}{n_{12}F}\frac{\ln k_{12}}{\alpha_{12}v}$;

$a = \frac{n_{23}F}{RT}v$; $b = e^{at_{1/2}}$, $\bar{E}$ is the initial potential;

and v is the rate of change of the potential. It will be supposed further that $n_{12} = n_{23} = 1$ ($Nb^{5+} - Nb^{4+} - Nb^{3+}$) and $D_1 = D_2 = D_3$. Setting (6) into the conditions (12) representing the integrals according to (10) and introducing the change of variables

$$\varphi_i = C\sqrt{\pi p}/D_i\eta_i, \quad t = \delta n/p \tag{13}$$

gives

$$\eta_{i1}(n) = \left\{1 - \frac{\sqrt{\delta}}{3}[2\eta_{i1}(n-1) + 3S_1(n) + \tilde{S}_1(n)]\right\} \Big/ \left(e^{\omega-\delta n} + \frac{4}{3}\sqrt{\delta}\right),$$
$$\eta_{i2}(n) = -[0,5\,\eta_{i2}(n-1) + 0,75S_2(n) + 0,25\,\tilde{S}_2(n)] - \tag{14}$$
$$-[\eta_{i1}(n) + 0,5\,\eta_{i1}(n-1) + 0,75\,S_1(n) + 0,25\,\tilde{S}_1(n)] \Big/ \left[1 + e^{\frac{\delta}{\alpha_{12}}(n-n_{1/2})}\right].$$

The portion of the axis of potentials corresponding to the period of observation was divided into 30 equal sections, so that $\delta = 0.4605$; $\omega = \ln 10^3$ and $n_{1/2} = 22.5$. The calculated results are shown in Fig. 2.

An expression for the current was obtained from (10)

$$I(n) = SF[2D_1\varphi_1(n) + D_2\varphi_2(n)] = CSF\sqrt{\pi pD_1}[2\eta_1(n) + \eta_{i2}(n)]. \quad (15)$$

A graph of the current is given in Fig.3. A dashed curve has been used to distinguish the currents for the first and the second steps in the reduction. Theoretically, the ratio of the currents at the first and second maxima should be equal to 0.51 (Fig. 3) and this is close to the experimentally observed ratio of 0.52 (Fig. 1). The currents of Fig. 1 are measured from the background line which is the second curve from the bottom. The good agreement between theory and experiment supports the mechanism which has been proposed for this reaction. The height of the second curve, as measured from the dotted line of Fig. 3, is 1.40 times greater than the height of the first wave and that despite the fact that the same number of electrons is involved in each of the two steps. Equation (15) shows that the height of each wave should be proportional to the square root of the rate of alternation of the potential.

The waves corresponding to the individual steps can be considered as independent in the event that the difference between the successive peak potentials exceeds a certain value. The values D_1 and C can then be used as the coefficient of diffusion and the initial concentration.

The minimal distances between peaks which are given in Table 1 have been calculated on the basis of a 1% error in the maximum of the second wave. Lack of space makes it impossible to justify these conclusions or derive the equation for the current at the maxima of successive independent waves.

LITERATURE CITED

[1] Delahaye, New Apparatus and Methods in Electrochemistry [Russian translation], IL, 1957, p. 160.

[2] S. Glasstone, K. Laidler and H. Eyring, The Theory of Absolute Reaction Rates [Russian translation], IL, 1948, p. 548.

[3] Ya. P. Gokhshtein, Proc. Acad. Sci. USSR 126, 598 (1959)*.

[4] Ya. P. Gokhshtein, Ind. Lab., No. 1, 38 (1956).

[5] H. Matsuda and J. Ayabe, Zs. Elektrochem. 59, 494 (1955).

Received April 16, 1959

*Original Russian pagination. See C. B. Translation.

THE DETONATION WAVE PARAMETERS OF TROTYL, HEXOGEN, NITROGLYCERIN AND NITROMETHANE

A. N. Dremin and P. F. Pokhil

The Institute of Chemical Physics of the Academy of Sciences, USSR

(Presented by Academician V. N. Kondrat'ev, April 27, 1959)

The present work presents the results of an experimental determination of the mechanical parameters of detonation waves in the Chapman-Jouguet plane.

The modern hydrodynamic theory of detonation predicts that the profile of the plane detonation wave will be of the form shown in Fig. 1.

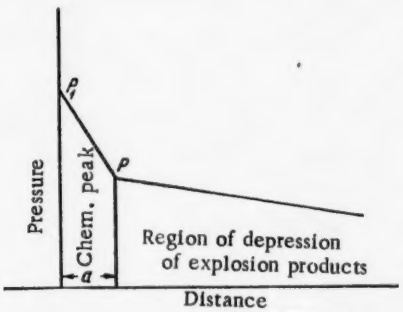

Fig. 1. Pressure profile in a plane detonation wave: a) depth of zone of chemical reaction; P_1) pressure on shock front; P) pressure in Chapman-Jouguet plane.

The five unknown mechanical parameters of the detonation wave (D – the detonation velocity; ρ – the density of the explosion products; U – the velocity of the explosion products; C – the velocity of sound in the explosion products; and, P – the pressure of the explosion products in the Chapman-Jouguet plane) are related by the system obtained by combining the equations for conservation of mass (1) and momentum (2) in passing from the initial state into the Chapman-Jouguet state

$$\rho_0 D = \rho (D - U), \tag{1}$$

$$P = \rho_0 DU \tag{2}$$

with the Chapman-Jouguet condition

$$D = U + C. \tag{3}$$

Two of these parameters must be determined experimentally if all five are to be evaluated without a knowledge of the equation of state of the explosion products. D and P have been measured in the present work. The velocity D was determined with the aid of ionization gauges separated by ~ 20 mm, the accuracy of measurement being ~ 0.5%.

P was determined indirectly by measuring the initial velocity, W, of the free surface of metallic plates of various thicknesses, these plates being firmly embedded into the ends of the explosive charges. It has been shown that $W = 2U_M$ [3, 4], where U_M is the mass velocity behind the shock wave in the metal. D_M and $P_M = \rho_{0M} D_M U_M$ can be found from U_M if the shock adiabat of the metal is known. The equality of pressures and rates of mass flow at the boundary surface between the explosive and the metal can be used to obtain a relation between the pressure in the incident detonation wave and the pressure in the shock wave which is propagated with velocity D_M through the metal of initial density ρ_{0M}:

TABLE 1

Explosive	ρ_0, g/cm³	D, km/sec	U, km/sec	$P \cdot 10^{-6}$, bar	C, km/sec	ρ, g/cm³
Hexogen	1,755	8,66	2,41	366	6,25	2,43
	1,59	8,10	2,23	287	5,87	2,19
	1,40	7,44	2,05	213	5,31	1,96
	1,20	6,75	1,87	152	4,88	1,66
Trotyl	1,59	6,94	1,83	202	5,11	2,16
	1,45	6,50	1,72	162	4,78	1,97
	1,30	6,04	1,59	125	4,45	1,77
	1,14	5,57	1,45	92	4,12	1,54
	1,00	5,10	1,30	64	3,80	1,34
Nitroglycerin	1,60	7,65	2,06	253	5,59	2,19
Nitromethane	1,14	6,30	1,80	129	4,50	1,60

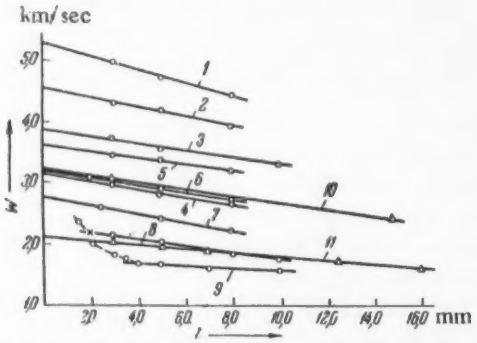

Fig. 2. The relation between the initial velocity, W, of the free surface of the metallic plate and the plate thickness. 1-4, hexogen: 1) ρ_0 = 1.755, 2) ρ_0 = 1.59, 3) ρ_0 = 1.40, 4) ρ_0 = 1.20 g/cm³; 5-9, trotyl: 5) ρ_0 = 1.59, 6) ρ_0 = 1.45, 7) ρ_0 = 1.30, 8) ρ_0 = 1.14 and 9) ρ_0 = 1.00 g/cm³; 10, nitrogycerin, ρ_0 = = 1.60 g/cm³. 11, nitromethane, ρ_0 = 1.14 g/cm³.

$$P = \frac{P_M}{2}\left(1 + \frac{\rho_0 D}{\rho_{0M} D_M}\right). \quad (4)$$

The acoustical approximation was used in deriving Eq. (4) [2].

We have developed the shock adiabat of magnesium, one of the metals used in this experiment, by following the method of [3] and determining D_M and U_M indirectly:

$$D_{Mg} = (4{,}78 + 1{,}16U_{Mg}) \text{ km/sec}, \quad \rho_{0Mg} = 1{,}72 \text{ g/cm}^3 \quad (5)$$

The shock adiabat of aluminum was taken from [5]:

$$D_{Al} = 5{,}190 + 20{,}77 \log_{10}\left(\frac{2U_{Al} + 10{,}895}{10{,}895}\right) \text{ km/sec}, \quad (6)$$

$$\rho_{0Al} = 2{,}70 \text{ g/cm}^3.$$

Experimental data are shown in the graph of Fig. 2, detonation wave parameters calculated from this data being compiled in Table 1.

The data on trotyl and hexogen were obtained with magnesium plates and those on nitroglycerin and nitromethane, with aluminum plates. The total height of the charge and the explosion lens which formed the plane wave front was 85 mm in each case and the diameter 40 mm. The charges of trotyl and hexogen were prepared from pressed cubes, 20 mm in height; the charges of nitromethane and nitroglycerin were fired in metallic casings, 3 mm thick. Each graph point represents the mean of the results from 2-5 experiments. The relative mean experimental error was 1.0-1.5%. It is to be noted that this error was least for the liquid explosives, nitroglycerin and nitromethane.

It has been shown in [6] that ~ 1-2 mm of metal will damp out the zone of chemical reaction in the detonation wave from a substance of medium strength. On this basis calculation of the detonation wave parameters in the Chapman-Jouguet plane could be carried out in the following manner. The W = f (l) relation was first extrapolated to zero plate thickness. The resulting W_0 (the value of W at l = 0) was then diminished by 2%, this being the difference between W_0 and W at that depth of metal where the chemical peak is damped out. The detonation wave parameters obtained in this way are accurate to within ~ 2-3%.

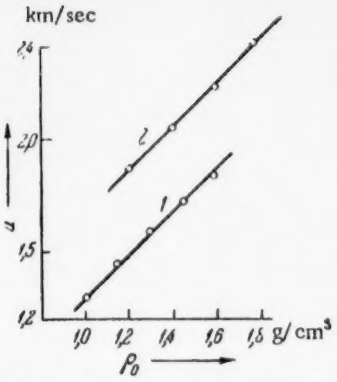

Fig. 3. The relation between the mass velocity on the detonation wave front of trotyl (1), and hexogen (2), and the initial density.

The mass velocity–initial density relations for trotyl and hexogen are shown in Fig. 3. These relations are seen to be linear over the investigated range of densities. Thus $(D/U) - 1$, the index of polytropy in the explosion products in the neighborhood of the Chapman-Jouguet plane, remains constant when the initial density is varied. This quantity can be assumed to remain constant even at high dispersion of the explosion products obtained from detonating explosives of high initial density. The index values of trotyl and hexogen are constant over the entire investigated pressure range.

LITERATURE CITED

[1] Ya. B. Zel'dovich, J. Tech. Phys., No. 10, 542 (1940).

[2] R. E. Duff and E. Houston, J. Chem. Phys. 23, No. 7 (1955).

[3] L. V. Al'tshuler, K. K. Krupinikov, et al., J. Exp. Theo. Phys., 34, No. 4, 874 (1958).

[4] J. M. Walsh and R. H. Christian, J. Phys. Rev. 97, No. 6 (1955).

[5] J. M. Walsh and Rice, J. Chem. Phys. 26, No. 4 (1957).

[6] Report, Institute of Chemical Physics of the Acad. of Sci. of the USSR, 1956 [in Russian].

Received April 24, 1959

THE ZINC TUNGSTATE, HYDROGEN EQUILIBRIUM AND THE THERMODYNAMIC PROPERTIES OF $ZnWO_4$

L. A. Zharkova, Corresponding Member Acad. Sci. USSR
Ya. I. Gerasimov, T. N. Rezukhina, and Yu. P. Simanov

Yu. P. Simanov

The M. V. Lomonosov State University, Moscow

The present paper is a continuation of work on the thermodynamic properties of the tungstates and molybdates of divalent metals which has been in progress in our laboratories since 1944.

EXPERIMENTAL

All of the earlier work employed a circulating method for the measurement of equilibrium constants [1-6]. This method is unsuitable for the case at hand since the zinc which is formed in reduction has a considerable vapor pressure at high temperatures and is carried completely out of the reaction zone by the circulating gas mixture. The reverse reaction occurs in the condensation zone to change the composition of the equilibrium gases and render circulation inapplicable.

It was for this reason that a dynamic flow method was used in measuring the equilibrium constant for the reduction of zinc tungstate. This method has been described in detail in the literature [7-11].

The apparatus employed in measuring the equilibrium constant by the flow method was similar to that of Kitchener and Ignatowicz [10] and is represented schematically in Fig. 1. Measurement was made of the concentration of hydrogen in the equilibrium gases rather than of the amount of volatile product carried away by the gas stream. The zinc vapors formed in the reaction were adsorbed in the hot portion of the reactor by copper filings. This procedure was necessary in order to eliminate the reverse reaction ($Zn + H_2O = ZnO + H_2$) which would alter the composition of the equilibrium gases. The copper had no effect on the water vapor–hydrogen ratio in the equilibrium gaseous mixture since Kp for the $Cu_2O + H_2 = 2Cu + H_2O$ reaction is much greater than this ratio over the interval of working temperatures.

Special experiments showed the equilibrium constant for the $ZnWO_4$ reduction to be independent of the rate of gas flow when this rate fell within the limits 2-5 liters/hour. The rate of gas flow in all subsequent experiments was approximately 2.5 liters/hour. The adsorption of the zinc vapors by copper was complete at this velocity.

The zinc tungstate was prepared by precipitation from stoichiometric volumes of K_2WO_4 and $ZnCl_2$ solutions; analysis by the method of Hillebrand and Lundell [12] (accuracy, 0.5%) showed the composition to correspond to the formula $ZnWO_4$.

The hydrogen was prepared by electrolysis of a 20% NaOH solution; it was freed of oxygen by being passed over paladinized silica gel, and of water, by being passed over $CaCl_2$ and P_2O_5. The argon was of "Pure" grade and was passed through a purifying-drying system composed of columns containing: 1) copper turnings (300°), 2) finely dispersed copper on silica gel (170°), 3) KOH, 4) $CaCl_2$, and 5) and 6) P_2O_5. Electrolytic copper was used in preparing the copper filings for adsorption of the zinc vapors.

The concentration of hydrogen in the mixed gases, α, was determined from the emf between two hydrogen electrodes, one saturated with pure hydrogen and the other, with the $H_2 + A$ mixture.

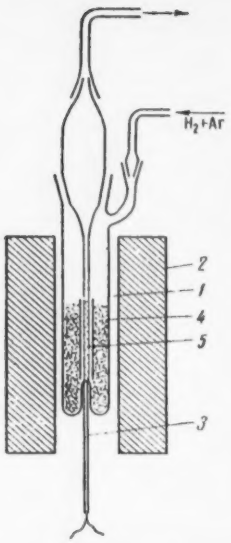

Fig. 1. Diagram of apparatus: 1) quartz reactor, 2) furnace, 3) thermocouple, 4) $ZnWO_4$, 5) capillary, the hot part of which is filled with copper filings.

$$E = \frac{RT}{2F} \ln \frac{P_0}{P},$$

where P^0 is atmospheric pressure plus a small correction (according to a water manometer) and P is the partial pressure of hydrogen in the gas mixture. The accuracy of the emf measurements was ± 0.01-0.02 mv. The furnace temperature was held constant to within ± 1°.

The accuracy of the results obtained with our apparatus was checked by making several determinations of the equilibrium constant for the reduction of zinc oxide. Figure 2, I shows the data of Kitchener and Ignatowicz on this equilibrium [10] and our own data, which is in good agreement with theirs.

The equilibrium constant for the reaction

$$ZnWO_4 + 4\,H_2 = Zn_{gas} + W + 4\,H_2O \qquad (1)$$

was evaluated from the equation

$$K_P = \frac{\left(\frac{\alpha}{1-\alpha} - \frac{\alpha'}{1-\alpha'}\right)^5 P}{\left(\frac{\alpha'}{1-\alpha'}\right)^4 \left(\frac{\alpha+4}{1-\alpha} - \frac{\alpha'}{1-\alpha'}\right)},$$

in which α and α' are the mole fractions of hydrogen in the initial gases and equilibrium gases, respectively, and P is the pressure in the reaction zone.

X-ray analysis was used to fix the phase composition of the reaction products. The experimental data is given in Table 1.

The log K_P, 1/T relation is shown in Fig. 2, II.

The method of least squares led to the equation $\log K_P = -\frac{17{,}769}{T} + 10.21$ which is capable of reproducing the experimental data with an accuracy of ± 16%.

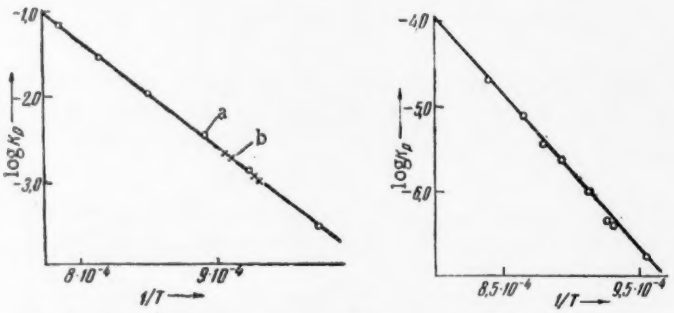

Fig. 2. The relation between the temperature and the equilibrium constant for reduction of: 1) ZnO, a) data of [10], b) experimental data; II) $ZnWO_4$.

$$\Delta Z^0_{(1)} = 81\,310 - 46{,}74\,T.$$

Reaction (1) can be combined with the reaction for the formation of water vapor

$$H_2 + \frac{1}{2}O_2 = H_2O, \qquad (2)$$

to give the reaction for the formation of zinc tungstate from the elements

$$Zn_{gas} + W + 2O_2 = ZnWO_4, \qquad \Delta Z^0_{(3)} = 4\,\Delta Z^0_{(2)} - \Delta Z^0_{(1)}. \qquad (3)$$

The Chipman Equation [13]:

$$\Delta Z^0_T = -59251 + 0{,}871\,T \ln T - 7{,}5\cdot10^{-5}T^2 + \frac{408\,000}{T} + 6{,}8085\,T.$$

was used for reaction (2).

TABLE 1

t, furnace, °C	emf. initial mixture		emf, equilibrium mixture		$P_{H_2} = P_{H_2+A}$, in electrodes mm	α	α′	P, in reactor, mm	Kp, atmos
	mv	t °C	mv	t °C					
768	45,60	21,5	47,10	21,8	762,7	$2{,}75\cdot10^{-2}$	$2{,}46\cdot10^{-2}$	764,3	$1{,}7\cdot10^{-7}$
802	38,95	20,0	40,45	20,0	753,9	$4{,}54\cdot10^{-2}$	$4{,}03\cdot10^{-2}$	756,8	$4{,}1\cdot10^{-7}$
807	35,70	20,0	37,18	20,0	754,0	$5{,}86\cdot10^{-2}$	$5{,}22\cdot10^{-2}$	756,8	$4{,}6\cdot10^{-7}$
819	45,60	20,0	47,70	20,0	762,7	$2{,}75\cdot10^{-2}$	$2{,}35\cdot10^{-2}$	764,3	$9{,}7\cdot10^{-7}$
845	35,60	20,0	37,60	20,0	752,6	$5{,}91\cdot10^{-2}$	$5{,}05\cdot10^{-2}$	755,4	$2{,}4\cdot10^{-6}$
864	38,95	20,0	41,20	20,0	753,4	$4{,}54\cdot10^{-2}$	$3{,}80\cdot10^{-2}$	756,3	$3{,}4\cdot10^{-6}$
878	35,55	20,0	38,10	20,0	752,3	$5{,}94\cdot10^{-2}$	$4{,}93\cdot10^{-2}$	754,0	$6{,}2\cdot10^{-6}$
918	42,27	21,5	45,60	21,7	754,4	$3{,}49\cdot10^{-2}$	$2{,}68\cdot10^{-2}$	756,1	$2{,}1\cdot10^{-5}$

The following equation for ΔZ^0_T was obtained by the method of Temkin and Shvartsman [16], account being taken of the temperature variation of the heat capacities of O_2, W, Zn_g, and $ZnWO_4$ [14, 15]:

$$\Delta Z^0_T\ (\pm 0{,}1 \text{ kcal}) = -327\,043 + 110{,}66\,T - T\,(1{,}4195\,M_0 + 7{,}2952\cdot10^{-3}M_1 + 1{,}80\cdot10^5\,M_{-2}),$$

from this it follows that $\Delta H^0_{298} = -327.0$ kcal/mole, $\Delta S^0_{298} = -110.66$ cal/mole · deg, $\Delta Z^0_{298} = -285.1$ kcal/mole.

The standard entropy of $ZnWO_4$, $S^0_{298} = 33.8$ cal/mole · deg, was obtained from the standard entropies [14], O_2: $S^0_{298} = 49.00$, W: $S^0_{298} = 8.00$ and Zn: Zn_g: $S^0_{298} = 38.41$.

LITERATURE CITED

[1] T. N. Rezukhina, Ya. I. Gerasimov, and Yu. P. Simanov, Bull. Moscow Univ. 6, 103 (1949).

[2] T. N. Rezukhina, Ya. I. Gerasimov, and V. A. Morozova, J. Phys. Chem. 25, 93 (1951).

[3] T. N. Rezukhina, G. M. Dugacheva, and Yu. P. Simanov, J. Phys. Chem. 31, 2206 (1957).

[4] I. A. Vasil'eva, Ya. I. Gerasimov, and Yu. P. Simanov, J. Phys. Chem. 31, 682 (1957).

[5] Yu. P. Simanov, T. N. Rezukhina, et al., J. Phys. Chem., 25, 357 (1951).

[6] I. A. Vasil'eva, Ya. I. Gerasimov, Yu. P. Simanov, and T. N. Rezukhina, J. Phys. Chem. 31, 825 (1957).

[7] F. Pollitzer, Zs. anorg. Chem. 64, 121 (1909).

[8] R. N. Pease and R. S. Gook, J. Am. Chem. Soc. 48, 1199 (1926).

[9] K. Ellinek and G. A. Rosner, J. phys. Chem. (A), 143, 51 (1929).

[10] J. A. Kitchener and S. Ignatowicz, Trans. Farad. Soc. 47, 1278 (1951).

[11] J. F. Gilbert and J. A. Kitchener, J. Chem. Soc. 1956, 3919.

[12] W. Hillebrand and G. Lundell, A Practical Guide to Inorganic Analysis [in Russian] 1957.

[13] I. Chipman, Trans. Am. Soc. Metals 22, 385 (1934).

[14] Brief Handbook of Physical Chemical Constants, K. P. Mishchenko and A. A. Ravdelya, editors, Leningrad, 1957 [in Russian].

[15] L. A. Zharkova and T. N. Rezukhina, J. Phys. Chem. 32, No. 10, 2233 (1958).

[16] M. I. Temkin and L. A. Shvartsman, Prog. Chem. 17, 2, 259 (1948).

Received July 2, 1959

THE THEORY OF THERMAL CHAIN FLAME PROPAGATION IN SYSTEMS WITH BRANCHING CHAIN REACTIONS

L. A. Lovachev

The Institute of Physical Chemistry of the Academy of Sciences, USSR

(Presented by Academician V. N. Kondrat'ev, May 22, 1959)

Preceding papers have treated processes of flame propagation in systems with nonbranching [1-3] or degenerative-branching [4] reactions. The agreement between theory and experiment was satisfactory in the case of hydrogen – chlorine flames [2, 3].

The present article will deal with the combustion of hydrogen [5], which will be assumed to proceed by the branching-chain reaction

$$H_2 + O_2 \rightarrow 2OH, \qquad \Phi_1 = h_{R1}R_1(T'); \tag{0}$$
$$H_2 + M \rightarrow 2H + M, \qquad \Phi_2 = h_{R2}R_2(T'); \tag{0'}$$
$$O_2 + O_2 \rightarrow O_3 + O, \qquad \Phi_3 = h_{R3}R_3(T'); \tag{0''}$$
$$OH + H_2 \rightarrow H_2O + H, \qquad Q_1n_1 = h_1F_1n_1 = h_1K_1(T')\,n_An_1; \tag{1}$$
$$H + O_2 \rightarrow OH + O, \qquad Q_2n_2 = h_2F_2n_2 = h_2K_2(T')\,n_Bn_2; \tag{2}$$
$$O + H_2 \rightarrow OH + H, \qquad Q_3n_3 = h_3F_3n_3 = h_3K_3(T')\,n_Cn_3. \tag{3}$$

The expressions written on the right are those for the rates of evolution or absorption of heat; in them, h_i is the heat of reaction (cal/mole); n_1, n_2, and n_3 are the concentrations of OH, H and O (moles/g of mixture); n_A, n_B, and n_C are the concentrations of H_2, O_2, and H_2O (moles/g of mixture); K_i is a velocity constant ($g^2/cm^3 \cdot mole \cdot sec$); R_i is the rate of chain initiation ($mole/cm^3 \cdot sec$) and T' is the temperature in °K. The diffusion coefficients of H_2, O_2 and H_2O will be supposed equal to the coefficient of thermal diffusivity ($\lambda = c\rho D_A = c\rho D_B = c\rho D_C$) so that $R_i = R_i(T')$ and $F_i = F_i(T')$. Processes of chain rupture have been omitted from the reaction scheme since [1, 2, 3] have shown that reactions proceeding through three-body collisions can be neglected at high temperatures.

With the reaction scheme which has been adopted, the assumed conditions reduce the system of equations for a laminar plane flame to four members:

$$\lambda pp' - Bcp + \Phi + Q_1n_1 + Q_2n_2 + Q_3n_3 = 0, \tag{4}$$
$$D_1p^2n_1'' - pn_1'(B - D_1p') + R_1 + F_2n_2 + F_3n_3 - F_1n_1 = 0, \tag{5}$$
$$D_2p^2n_2'' - pn_2'(B - D_2p') + R_2 + F_1n_1 + F_3n_3 - F_2n_2 = 0, \tag{6}$$
$$D_3p^2n_3'' - pn_3'(B - D_3p') + R_3 + F_2n_2 - F_3n_3 = 0, \tag{7}$$

here $\underline{x}$ is a coordinate (cm); $\underline{u}$ is the flow rate (cm/sec); ρ is the density (g/cm^3); λ is the thermal conductivity of the mixture ($cal/cm \cdot sec \cdot °C$); $\underline{c}$ is the heat capacity ($cal/g \cdot °C$); D_{P_1}, D_{P_2}, and D_{P_3} are the diffusion coefficients of OH, H and O (cm^2/sec); $B = u\rho$; $D_i = \rho D_{Pi}$; $T = T' - T_0'$; $p = dT/dx$; $p' = dp/dT$; $n_i' = dn_i/dT$;

$n_i'' = d^2 n_i / dT^2$ and $\Phi = \Phi_1 + \Phi_2 + \Phi_3$. The index zero designates the initial state of the mixture ($T' = T_0'$), the index $\underline{b}$, the state at the combustion temperature ($T' = T_b'$) and the index $\underline{m}$, the state corresponding to maximum temperature gradient $p = p_m$ ($T' = T_m'$) [1].

Equations (5), (6) and (7) can be used [1] to give an approximation for the concentration of active centers at $T = T_m$.

$$n_{1m} = t_1 + (R_{1m} + F_{2m} n_{2m} + F_{3m} n_{3m} - F_{1m} n_{1m} - B l_1 p_m) N_1, \tag{8}$$
$$n_{2m} = t_2 + (R_{2m} + F_{1m} n_{1m} + F_{3m} n_{3m} - F_{2m} n_{2m} - B l_2 p_m) N_2, \tag{9}$$
$$n_{3m} = t_3 + (R_{3m} + F_{2m} n_{2m} - F_{3m} n_{3m} - B l_3 p_m) N_3, \tag{10}$$

in which $l_i = \frac{n_i\ b - n_{i0}}{T_b}$, $N_i = \frac{r}{2D_{im} p_m^2}$, $t_i = n_{i0} + l_i T_m$. $r = T_m (T_b - T_m)$, $T_m = 0{,}5 T_b$ [1], $B = \eta p_m = \eta p_*$ [1] and $\eta = 4\lambda_0 / c_0 T_m$.

Solution of the system (8), (9) and (10) gives

$$n_{1m} = \Delta_1 / \Delta, \quad n_{2m} = \Delta_2 / \Delta, \quad n_{3m} = \Delta_3 / \Delta, \tag{11}$$

where

$$\Delta = 1 + F_{1m} N_1 + F_{2m} N_2 + F_{3m} N_3 + F_{1m} F_{3m} N_1 N_3 - 2 F_{1m} F_{2m} F_{3m} N_1 N_2 N_3$$
$$\Delta_1 = \varepsilon_1 (1 + F_{2m} N_2 + F_{3m} N_3) + \varepsilon_2 F_{2m} N_1 (1 + 2 F_{3m} N_3) + \varepsilon_3 F_{3m} N_1 (1 + 2 F_{2m} N_2)$$
$$\Delta_2 = \varepsilon_1 (1 + F_{3m} N_3) F_{1m} N_2 + \varepsilon_2 (1 + F_{1m} N_1)(1 + F_{3m} N_3) + \varepsilon_3 F_{3m} N_2 (1 + 2 F_{1m} N_1),$$
$$\Delta_3 = \varepsilon_1 F_{1m} F_{2m} N_2 N_3 + \varepsilon_2 F_{2m} N_3 (1 + F_{1m} N_1) + \varepsilon_3 (1 + F_{1m} N_1 + F_{2m} N_2),$$
$$\varepsilon_i = t_i - B l_i p_m N_i + R_{im} N_i = t_i \omega_i + R_{im} \delta_i \frac{1}{p_*^2}, \quad \delta_i = \frac{r}{2 D_{im}}$$
$$\omega_i = 1 - \frac{2 q_i}{\varkappa_i}, \quad q_i = \frac{\mu_0}{\mu_m} \left(\frac{T_0'}{T_m'} \right)^{a_i - 1} \text{ when } D_{pi} \sim (T')^{a_i} \text{ and } \varkappa_i = \frac{c_0 D_{i0}}{\lambda_0}.$$

An equation for the determination of p_* at $T = T_m$ (here, $p = p_m$ and $p' = 0$) is obtained by setting (11) into (4)

$$A_1 p_*^5 + A_2 p_*^6 + A_3 p_*^4 - A_4 p_*^2 - A_5 = 0, \tag{12}$$

where

$$A_1 = c\eta,$$
$$A_2 = c\eta (F_{1m}\delta_1 + F_{2m}\delta_2 + F_{3m}\delta_3) - (Q_{1m} t_1 \omega_1 + Q_{2m} t_2 \omega_2 + Q_{3m} t_3 \omega_3) - \Phi_m,$$
$$A_3 = c\eta F_{1m} F_{3m} \delta_1 \delta_3 - t_1 \omega_1 (Q_{1m} F_{2m} \delta_2 + Q_{1m} F_{3m} \delta_3 + Q_{2m} F_{1m} \delta_2) - t_2 \omega_2 (Q_{1m} F_{2m} \delta_1 +$$
$$+ Q_{2m} F_{1m} \delta_1 + Q_{2m} F_{3m} \delta_3 + Q_{3m} F_{2m} \delta_3) - t_3 \omega_3 (Q_{1m} F_{3m} \delta_1 + Q_{3m} F_{1m} \delta_1 +$$
$$+ Q_{2m} F_{3m} \delta_2 + Q_{3m} F_{2m} \delta_2) - \Phi_m (F_{1m}\delta_1 + F_{2m}\delta_2 + F_{3m}\delta_3) -$$
$$- (Q_{1m} R_{1m} \delta_1 + Q_{2m} R_{2m} \delta_2 + Q_{3m} R_{3m} \delta_3),$$
$$A_4 = F_{1m} F_{2m} F_{3m} [2c\eta \delta_1 \delta_2 \delta_3 + t_1 \omega_1 \delta_2 \delta_3 (h_2 + h_3) + t_2 \omega_2 \delta_1 \delta_3 (2h_1 + h_2 + h_3) +$$
$$+ t_3 \omega_3 \delta_1 \delta_2 2 (h_1 + h_2)] + \Phi_m F_{1m} F_{3m} \delta_1 \delta_3 + R_{1m} \delta_1 (Q_{1m} F_{2m} \delta_2 +$$
$$+ Q_{2m} F_{1m} \delta_2 + Q_{1m} F_{3m} \delta_3) + R_{2m} \delta_2 (Q_{1m} F_{2m} \delta_1 + Q_{2m} F_{1m} \delta_1 + Q_{3m} F_{2m} \delta_3 +$$
$$+ Q_{2m} F_{3m} \delta_3) + R_{3m} \delta_3 (Q_{1m} F_{3m} \delta_1 + Q_{3m} F_{1m} \delta_1 + Q_{2m} F_{3m} \delta_2 + Q_{3m} F_{2m} \delta_2),$$
$$A_5 = F_{1m} F_{2m} F_{3m} \delta_1 \delta_2 \delta_3 [R_{1m} (h_2 + h_3) + R_{2m} (2h_1 + h_2 + h_3) +$$
$$+ R_{3m} 2 (h_1 + h_2) - 2\Phi_m].$$

The rate of flame propagation is found from [3, 4]

$$u_0 = \frac{1}{\rho_0}\eta p_*, \tag{13}$$

once p_* has been determined from (12).

Equation (11) permits the OH, H and O concentrations to be expressed as functions of the temperature $T = T' - T_0'$ [1] after each $\underline{r}$ is replaced by $T(T_b - T)$ and the expression for $p_m = p_*$ is introduced from (12).

The low values of A_1 and A_2 justify the assumption that $A_1 \cong A_2 \cong 0$ in (12). An approximation for p_* is obtained by supposing the rate of chain initiation to be relatively low [1-3] ($R_1 \cong R_2 \cong R_3 \cong 0$) and neglecting all members of A_3 and A_4 which contain $t_i\,\omega_i$ (for systems with branching reactions this is permissible when the concentration of the active centers in the reaction zone exceeds the equilibrium concentration at the combustion temperature).

$$p_*^2 = 2\delta_2 F_{2m}. \tag{14}$$

Numerical calculations show that the assumptions involved in the derivation of (14) are justified for the case of the combustion of hydrogen.

A very simple but approximate [in distinction to (13)] expression for the rate of flame propagation can be obtained by introducing (14) into (13):

$$u_0 = \frac{4\lambda_0}{\rho_0 c_0}\sqrt{\frac{\overline{K_{2m} n_{Bm}}}{D_{2m}}} = \frac{4\lambda_0}{\rho_0 c_0}\sqrt{\frac{\overline{K_{2m}^0 \rho_m n_{Bm}}}{D_{P2m}}}, \tag{15}$$

here $K_2 / \rho^2 = K_2^0$ (cm^3/mole·sec).

Calculations on the combustion of hydrogen have shown that values obtained from (15) are very close to those resulting from (13). It is obvious that the terms containing $t_i\,\omega_i$ can always be neglected in A_3 and A_4 unless the pressure is so very low that there is considerable dissociation.

Equation (15) opens the possibility of determining the frequency factor and the energy of activation of reaction (2) from the experimentally developed relation between the combustion temperature and the rate of flame propagation. This relation was developed from data on two mixtures:

1. Mixture composition 0.72 H_2 + 0.2795 O_2 + 0.0015 N_2: $\lambda_0 = 2.6 \cdot 10^{-4}$, $D_{P20} = 1.35$ (atom H), $a_2 = 1.9$, $T_0' = 293°K$ and $T_b' = 3045°K$.

2. Mixture composition 0.43 H_2 + 0.57 air: $\lambda_0 = 1.6 \cdot 10^{-4}$, $D_{P20} = 1.15$ (atom H), $a_2 = 1.9$, $T_0' = 293°K$ and $T_b' = 2126°K$.

Dissociation was taken into account in calculating the combustion temperature. The value of the effective radius of the hydrogen atom was taken from [6] and used in calculations on the diffusion coefficients. The thermal conductivities were determined from the experimental data of [7] on H_2, O_2 mixtures.

Data from two sources were used in arriving at experimental K_2^0 values for these two mixtures: 1) the value 3.39 which Jahn [8] gives for the ratio of the flame propagation rates, which with (15) leads to $K_2^0 = 1.32 \cdot 10^{14} \exp(-14{,}000/RT')$($cm^3$/mole·sec) as the expression for the rate constant; and 2) the more recent value of Bartolomé for this ratio [10] which with (15) gives $K_2^0 = 4.72 \cdot 10^{14} \exp(-16{,}300/RT')$ (cm^3/mole·sec).

The resulting values of the rate constant K_2^0 are in satisfactory agreement with values obtained from $K_2^0 = 5.66 \cdot 10^{13} \exp(-15{,}100/RT')$, an expression which was developed independently of flames by the kinetic methods of L. V. Karmilova, A. B. Nalbandyan, and N. N. Semenov [10, 11].

K_2^0 can be determined more exactly from Eq. (13) but, in that case it is well to first increase the precision of all data used in the calculations, find the rate of flame propagation by numerical integration of the system

of equations (4)-(7) and, finally, compare this last result with that calculated from (13) in order to fix the divergence between predictions based on this equation and the results obtained by numerical integration. A comparison of this type was carried out for a system with nonbranching chain reactions [1-3] where the same method of solution was employed as in the present paper [1]. Use of this previously tested method of solution gives assurance that the resulting errors will be of an acceptable magnitude (in systems with branching-chain reactions, the exact values of these errors can only be determined exactly by numerical integration).

Equation (15) shows that the rate of flame propagation is directly proportional to the thermal conductivity of the mixture and inversely proportional to the square root of the diffusion coefficient of the hydrogen atom. The ratio of the rates of flame propagation in two 0.21 H_2 + 0.11 O_2 mixtures, one containing 0.68 He and the other, 0.68 A, is given in the paper of Mellish and Linnett [12]. The experimental value of this ratio proves to be equal to 2.40. The ratio of the thermal conductivities of these same mixtures, 3.76, is found in [12], together with the square root of the ratio of the diffusion coefficients of the hydrogen atom, 1.32. When calculated from (15), the theoretical ratio of the rates of flame propagation (3.76/1.32 = 2.85) proves to be somewhat larger than the experimental. Such agreement is satisfactory, however, in view of the difficulties involved in determining the transfer coefficients, the possibility of errors in the theoretical approximation equations, and the inaccuracy in the experimental data.

A theoretical relation between the rate of flame propagation and the pressure P_Σ in a system with branching-chain reactions can be derived from (15). The combustion temperature, T_b, will diminish with diminishing P_Σ in mixtures of high heating value; according to (15), there will be an accompanying diminution in the rate of flame propagation which will be principally determined by the energy of activation of reaction (2). The combustion temperature is almost independent of P_Σ in mixtures of low heating value so that the rate of flame propagation in these mixtures remains unaltered as the pressure changes. The only experimental data is that of [13] for hydrogen – oxygen mixtures where the rate of flame propagation diminishes as the pressure decreases.

LITERATURE CITED

[1] L. A. Lovachev, Proc. Acad. Sci. USSR 120, No. 6, 1287 (1958).*

[2] L. A. Lovachev, Proc. Acad. Sci. USSR 124, No. 6, 1271 (1959). * **

[3] L. A. Lovachev, Proc. Acad. Sci. USSR 125, No. 1, 129 (1959).*

[4] L. A. Lovachev, Proc. Acad. Sci. USSR 123, No. 3, 501 (1958).*

[5] V. N. Kondrat'ev, The Kinetics of Gaseous Chemical Reactions [in Russian] Moscow, 1958, p. 514.

[6] W. H. Clingman, R. S. Brokaw, and R. N. Pease, Fourth Symposium on Combustion, Baltimore, 1953, p. 310.

[7] J. O. Hirschfelder, C. F. Curtiss, and R. B. Bird, Molecular Theory of Gases and Liquids, N. Y., 1954.

[8] G. Jahn, Der Zündvorgang in Gasgemischen, Karlsruhe, 1934.

[9] E. Bartolomé, Zs. f. Elektrochem. 54, No. 3, 169 (1950).

[10] L. V. Karmilova, A. B. Nalbandyan, and N. N. Semenov, J. Phys. Chem. 32, vol. 6, 1193 (1958).

[11] N. N. Semenov, Certain Problems in Chemical Kinetics and Reactivity [in Russian], Moscow 1958 .

[12] C. E. Mellish and J. W. Linnett, Fourth Symposium on Combustion, Baltimore, 1953, p. 407.

[13] Physical Measurements in Gas Dynamics and Combustion [in Russian], Foreign Lit. Press, 1957, p. 462.

Received May 18, 1959

* Original Russian pagination. See C. B. Translation.

** The word "pier" (mol) was mistakenly printed for the word "mole" (mol') in designating the dimensions of the quantities on page 1271 (lines 9, 10, and 11 from the top) and page 1273 (line 19 from the top) of [2].

THE THEORY OF CATALYTIC SELECTIVITY AND BOND ENERGIES

V. Kh. Matyushenko

(Presented by Academician A. A. Balandin, May 23, 1959)

The problems of the theory of catalytic selectivity occupy a central position in theoretical and applied catalytic chemistry [1]. The modern theory has reached a stage in which the most important task is that of accumulating information on the nature of the bond between the catalyst and the adsorbed molecule and its relation to the chemical properties of the catalyst and the lattice substituents.

A method of evaluating bond energies from energies of sublimation and electronegativities is proposed below. A starting point is found in the Pauling and Sherman [2] proportionality between the bond energy, Q_{A-A}, and the square of the bond strength, S_A

$$Q_{A-A} \sim S_A^2. \tag{1}$$

Pauling and Sherman have used Eq. (1) to obtain an expression for the energy, Q_{A-B}, of the bond between the A and B atoms

$$Q_{A-B} = \frac{1}{n}\sqrt{Q_{A-A}\cdot Q_{B-B}} + \frac{1}{n}\Delta Q_{A-B}; \tag{2}$$

here ΔQ_{A-B} is a correction for the difference in electronegativity, X, which is expressed by $23.06\,(X_A - X_B)^2$ and n is a constant which they set equal to unity. A number of authors [3, 4, 5] have used Eqs. (1) and (2) successfully for evaluation of the bond energy Q_{A-B}. We have carried on calculations with Eq. (2) by setting Q_{B-B} equal to the mean binding energy in organic molecules (Q_{H-H}, Q_{C-C}, Q_{O-O}, $Q_{C=C}$, first ruptured bond, etc.) and writing

$$Q_{A-A} = \frac{k_0 - k_s}{k_0} L, \tag{3}$$

using k_0 and k_s to designate the coordination number of the A atom in the body of the catalyst and on the catalyst surface, respectively, and L to designate the energy of sublimation.

Equation (3) can be derived by starting from the assumption that the catalytically active center, or multiplet, is a portion of the crystal lattice of the catalyst, or a nucleus of such a lattice, on the catalyst surface. The surface atoms of the catalyst differ from the atoms in the interior insofar as a part of their valence shell remains free and does not participate in chemical bonding with neighboring atoms. From this point of view, the surface atoms can be said to have a certain amount of "free valence." The atoms of the active center have enhanced chemical and adsorptional potentials because of this unsaturation. The less a surface atom of the catalyst A is saturated, the greater will be its contribution to the bond energy Q_{A-B}, i.e.,

$$Q_{A-A} = \frac{1}{2}(k_0 - k_s)\,Q'_{A-A}, \tag{4}$$

TABLE 1

Energies of Bonding of Organogens with Catalyst Surfaces (kcal/mole)

Catalyst	Energy of sublimation (kcal/g-at)	$f=\frac{k_0-k_S}{k_0}$	Electronegativity (ev)	H	C	N	O	S	F	Cl	Br	I
Be	76,63	$\frac{12-9}{6+6}$	1,5	54,4	15,7	29,9	62,9	29,2	164,9	85,1	70,9	56,5
Mg	35,9	$\frac{12-9}{6+6}$	1,2	50,0	16,5	33,5	75,4	31,4	192,3	97,3	80,7	63,4
Ca	46,04	$\frac{12-9}{12}$	1,0	65,0	20,7	40,6	85,0	39,5	221,1	118,1	99,3	79,5
Sr	39,2	$\frac{12-9}{12}$	1,0*	61,7	20,1	39,8	84,0	38,4	219,4	116,1	97,4	77,6
Ba	41,96	$\frac{8-6}{8}$	0,9	69,1	22,1	43,1	90,4	42,4	227,6	126,1	106,9	85,8
Al	75,0	$\frac{12-9}{12}$	1,5	54,0	15,6	29,8	62,8	28,6	164,6	84,8	70,6	56,2
Sc	93	$\frac{12-9}{12}$	1,3	65,9	19,3	36,1	74,4	35,9	191,4	103,1	87,1	70,5
Y	103	$\frac{12-9}{6+6}$	1,2	72,5	21,0	39,5	83,9	39,8	205,1	103,1	95,9	78,1
Ti	112	$\frac{12-9}{6+6}$	1,6	61,0	16,7	30,4	62,0	30,5	159,7	85,5	71,8	57,9
Zr	125	$\frac{8-6}{8}$	1,5	67,0	18,5	33,9	67,7	33,6	172,4	94,4	79,6	65,2
Hf	72	$\frac{12-9}{12}$	1,4	56,3	16,6	31,9	66,9	30,9	175,7	91,2	76,3	60,8
Th	177	$\frac{12-9}{12}$	1,4	80,9	22,1	38,9	76,3	40,6	192,9	109,6	93,8	78,0
V	120	$\frac{8-6}{8}$	1,9	57,3	14,6	25,1	50,6	26,0	130,1	69,6	58,7	48,9
Nb	184,5	$\frac{8-6}{8}$	1,7	74,1	19,1	32,6	63,5	34,5	157,9	90,5	77,5	65,1
Ta	185	$\frac{8-6}{8}$	1,7	74,2	19,2	32,7	63,5	34,6	157,9	90,7	77,6	65,2
Cr	80,5	$\frac{12-9}{6+6}$	2,2	54,8	10,7	17,9	36,7	19,0	97,7	48,8	41,1	34,8
Mo	155,5	$\frac{8-6}{8}$	1,6	70,6	18,9	33,1	65,6	34,2	165,5	92,7	78,5	65,3
W	201,6	$\frac{8-6}{8}$	2,0	73,0	17,6	28,2	53,3	31,3	130,9	77,1	66,5	57,6
U	125	$\frac{8-6}{8}$	1,9	58,4	14,1	25,5	51,0	26,5	130,8	70,5	59,5	49,7
Mn	68,34	$\frac{12-9}{8+4}$	1,5	52,0	15,2	29,2	61,6	28,1	163,5	83,3	68,9	54,3
Re	189	$\frac{12-9}{6+6}$	2,2	70,3	16,1	24,8	45,9	28,5	112,4	67,0	58,7	53,0
Fe	96,68	$\frac{8-6}{8}$	1,8	53,1	14,0	25,3	52,1	25,3	136,0	70,7	59,0	48,1
Ru	160	$\frac{12-9}{6+6}$	2,0	65,0	15,9	25,9	50,3	28,2	126,0	71,2	60,9	52,1
Os	174	$\frac{12-9}{6+6}$	2,0	67,9	16,4	26,8	51,3	29,2	127,7	73,3	62,9	54,1
Co	105	$\frac{12-9}{12}$	1,7	57,0	15,4	27,8	57,0	27,8	147,6	77,7	65,3	53,2
Rh	138	$\frac{12-9}{12}$	2,1	60,1	14,3	23,2	45,3	25,3	114,5	63,4	54,2	46,6
Ir	165	$\frac{12-9}{12}$	2,1	65,7	15,5	24,8	47,3	27,5	117,9	67,6	58,2	40,5
Ni	101,61	$\frac{12-9}{12}$	1,8	54,2	14,3	25,6	52,6	25,8	136,7	71,6	60,0	49,0
Pd	93	$\frac{12-9}{12}$	2,0	49,7	12,4	21,6	44,5	22,2	116,9	59,8	49,9	41,3
Pt	121,6	$\frac{12-9}{12}$	2,1	56,3	13,5	22,2	43,8	23,9	112,2	60,2	51,6	44,0
Cu	81,52	$\frac{12-9}{12}$	2,0	46,5	11,7	20,7	43,3	20,9	115,0	57,5	47,7	[illegible]
Ag	69,12	$\frac{12-9}{12}$	1,8	45,2	12,3	23,1	49,3	22,3	131,3	64,9	53,5	42,7
Au	82,29	$\frac{12-9}{12}$	2,3	46,8	10,6	16,9	34,0	18,6	90,5	45,9	38,9	33,8
Zn	31,19	$\frac{12-9}{6+6}$	1,5	38,3	12,2	25,3	56,9	22,7	155,2	73,1	59,3	45,2
Cd	26,97	$\frac{12-9}{6+6}$	1,5	36,3	11,7	24,8	56,1	21,9	154,0	71,6	57,9	43,9

TABLE 1 (continued)

Catalyst	Energy of sublimation (kcal/g-at)	$f=\frac{k_o-k_s}{k_o}$	Electronegativity (ev)	H	C	N	O	S	F	Cl	Br	I
In	58,2	$\frac{12-9}{8+4}$	1,5	48,7	14,4	28,8	60,8	26,8	151,5	80,9	66,8	52,6
Tl	43,34	$\frac{12-9}{12}$	1,9	35,0	9,6	18,8	42,2	17,3	116,7	53,0	42,8	33,3
Sn	72	$\frac{6-5}{4+2}$	1,8	38,2	10,7	21,1	46,5	19,5	127,0	59,6	48,4	37,7
Pb	46,34	$\frac{12-9}{12}$	1,8	37,6	10,1	20,9	46,3	19,2	126,7	59,1	47,9	37,3
Ge	78,44	$\frac{4-3}{4}$	1,8	48,1	12,9	23,9	50,3	23,4	127,8	66,9	55,5	44,7

Values of Q_{B-B} and X_B

	H	C	N	O	S	F	Cl	Br	I
Bond energy, kcal/mole	104,18	82,87	75,33	59,5	64	37,6	58	53,4	51
Electronegativity, ev	2,15	2,5	3,0	3,5	2,5	3,95	3,0	2,8	2,55

TABLE 2

Bonding Energies (kcal/mole) of the Carbon Atoms of Organic Molecules with Metallic Catalysts ($f = 1/4$)

	$H_2C=CH_2$	$H_2C=CH$ (R)	In β, γ olefins, C=C	In olefins which are not α branching C=C	HC≡CH	C≡C (R, R)		HC—CH (H_2C, CH_2)	△C	□C	
X_C, ev	3,589	3,42	3,368	3,285	4,127	3,953	4,01	3,72	3,587	3,56	3,004
Q_{B-B}, kcal/mole	57,9	63,33	65,43	68,65	51,6	50,9	121,3	67,0	82,87	82,87	82,87
Ni	28,0	25,0	24,3	23,1	40,1	35,5	41,9	31,4	29,8	29,3	19,8
Co	30,2	27,1	26,3	25,1	43,1	38,3	44,7	33,9	32,1	31,5	21,4
Fe	27,6	24,8	24,0	22,8	39,9	35,4	41,5	31,2	29,5	29,0	19,5
Pt	23,3	21,0	20,4	19,5	33,6	29,4	36,2	26,4	25,3	24,8	17,3
Pd	23,6	21,2	20,5	19,5	34,7	30,5	36,3	26,8	25,4	25,0	16,8
Cu	23,0	20,5	19,8	18,8	34,1	29,9	35,4	26,2	24,7	24,3	16,0

where Q'_{A-A} is the energy of binding of A-A atoms in the body of the catalyst.

Q'_{A-A} is readily expressed in terms of the sublimation energy

$$Q'_{A-A} = \frac{2}{k_o} L. \tag{5}$$

Equation (3) results when (5) is introduced into (4). We have set n equal to the valence of the atom which is bound directly to the catalyst surface since a surface atom of the catalyst interacts with all of the valence electrons of the adsorbed radical and not merely with the free electrons. Such a procedure is justified by the agreement between experimental data and the results of calculations based on Eq. (6). The final result is

$$Q_{A-B} = \frac{\sqrt{\frac{k_o - k_s}{k_o} L Q_{B-B} + 23{,}06\,(X_A - X_B)^2}}{n_B}. \tag{6}$$

The quantities Q_{A-B}, Q_{B-B} and L are expressed in kcal/mole in this equation and X is in electron volts.

Tables 1 and 2 give results obtained from Eq. (6) for definite values of $f = \frac{k_0 - k_s}{k_0}$. The sublimation energies used in these calculations were taken from the circular of the National Bureau of Standards of the USA [6] and the bond energies, from the data of Kondrat'ev [7].

Electronegativities were taken principally from the compilation of Gordy and Thomas [8], although values for the atoms =C, ≡C, C_{ar}, C_{dien}, ΔC, □C and ▽C were calculated from the equation

$$X_i = X_C + \frac{a}{23{,}06}, \qquad (7)$$

where a is the absolute value of the difference between the actual heat of formation and the heat of formation determined additively from bond energies. Values of $X_{=C}$ ranging from 3.589 to 3.285 were obtained for =C and values of $X_{\equiv C}$ ranging from 4.127 to 3.953, for ≡C. Bykov, using an entirely different method, has found $X_{=C} = 3.56$ and $X_{\equiv C} = 3.81$ [9].

By way of a preliminary discussion of the results, it can be pointed out that the data of Table 1 show a rather clear periodicity in the catalytic properties of the elements, these properties being dependent, in turn, on the physical state of the surface (Q_{A-B} is rather markedly affected by alteration of f). There is a wide variation in the bond energy, Q_{A-B}, a quantity which depends on the catalyst ($Q_{Cd-H} = 36.3$ and $Q_{Th-H} = 80.9$; $Q_{Tl-C} = 9.6$ and $Q_{Ba-C} = 22.1$; $Q_{Au-O} = 34.0$ and $Q_{Ba-O} = 90.4$, etc.) and the valence state of the atom (see Table 2). The strength of binding on a single catalyst, Q_{A-B}, increases in the sequence $Q_{A-C} < Q_{A-N} < Q_{A-S} < Q_{A-I} < Q_{A-O} < Q_{A-H} < Q_{A-Br} < Q_{A-Cl} < Q_{A-F}$; no account is taken here of differences in the valence state of the carbon and there is a possibility of a transposition of neighboring entries in various cases. The bond energies are such that $Q_{A-N} \approx Q_{A-S}$; $Q_{A-H} \approx Q_{A-O} \approx Q_{A-I}$ and $Q_{A-Cl} \approx Q_{A-Br}$.

In a paper which is to appear in the Journal of Physical Chemistry (in press) S. L. Kiperman and A. A. Balandin have treated the data of the literature by a kinetic method to obtain energies of binding of the reacting atoms of organic molecules with Ni, Fe, Pt and Pd catalytic surfaces. All of their results are in good agreement with the data of Tables 1 and 2. Certain discrepancies can be related to inaccuracies in the experimental data due to uncertainties in the choice of limiting state and difficulties of kinetic measurements in the presence of hydrogen, and to alterations in the structural factor of the multiplet, f.

The proposed method can be applied without especial difficulty to other types of catalysts, as well.

LITERATURE CITED

[1] A. A. Balandin, J. Russ. Phys. Chem. Soc. 61, 909 (1929); 62, 703 (1930).

[2] L. Pauling and J. Sherman, J. Am. Chem. Soc. 59, 1454 (1937).

[3] A. V. Savitskii, Proc. Acad. Sci. USSR 87, No. 4, 631 (1952).

[4] D. D. Eley, Disc. Farad. Soc. 8, 34 (1950).

[5] D. P. Stevenson, J. Chem. Phys. 23, No. 1, 203 (1955).

[6] U. S. Nat. Bur. Stand., Circ. 500, Washington, 1952.

[7] V. N. Kondrat'ev, Prog. Chem. 26, 861 (1957).

[8] W. Gordy and W. J. O. Thomas, J. Chem. Phys. 24, 439 (1956).

[9] G. V. Bykov, Bull. Acad. Sci. USSR, Div. Chem. Sci., 1956, No. 12, 1435.*

Received May 12, 1959

*Original Russian pagination. See C. B. Translation.

THE MECHANISM OF THE ACTION OF LOW MELTING ALLOYS ON THE MECHANICAL PROPERTIES OF METALS OF HIGHER MELTING POINT

N. V. Pertsov, Yu. V. Goryunov, L. A. Kochanova, and V. I. Likhtman

The M. V. Lomonosov State University, Moscow

The Institute of Physical Chemistry of the Academy of Sciences, USSR

(Presented by Academician P. A. Rebinder, May 28, 1959)

Shear in a metallic monocrystal is known to result from a displacement of dislocations in the acting system of slip planes. The fact that there is considerable plastic deformation when even small shearing stresses are applied to pure, well annealed, monocrystals indicates that dislocation can be generated in these materials by very low stresses. These shearing stresses rise as the shear increases, the lattice being strengthened by the passage of large numbers of dislocations. Barriers to the movement of the dislocations are thus set up in the slip planes and these are the more difficult to overcome, the more the regenerative processes arising from thermal motion of the atoms are retarded, i.e., the lower the temperature and the higher the rate of deformation. Mott claimed [1] that the accumulation of dislocations before such a barrier leads to a localization of stress concentration and that this, in turn, gives rise to cracking and rupture. It is clear that the first steps here are ones of coalescence of the leading dislocations to form open dislocation nuclei which serve as centers for microfissures; these open dislocation centers then aggregate into wedge-shaped cracks which are in equilibrium under the acting normal strains [7, 8]. The higher the level of the normal strains and the less the significance of the relaxation processes of spontaneous closure of the defects arising from deformation, the more rapidly will the cracks pass out from equilibrium and thereby bring about brittle shearing fracture of the crystal. The higher the temperature, the more intensive will be the relaxation processes, the higher the plasticity of the crystal, and the slower the development of rupture cracking, the danger point for given conditions of normal loading being reached only when there is considerable residual deformation. The role of the deformation rate at fixed temperature is obviously a similar one; the lower this rate, the more plastic the monocrystal, and inversely.

Thus it is that the generation and development of brittle rupture cracking in metallic monocrystals is predetermined by the deformation processes themselves, the temperature and the conditions of shear fixing the more or less early stage of plastic formation in which brittle rupture occurs [12]. Such common surface active substances as organic acids and alcohols can exert no influence on the formation and development of rupture fissures since these processes take place in the body of the solid object; the maximum adsorptional effects of these materials are thus observed under prolonged and favorable conditions of stress in creep, fatigue, and endurance experiments [2, 3, 11].

The situation is different in the case of deformation of a metallic monocrystal of higher melting point in a surface active metallic alloy. The atoms of this alloy can penetrate into the deformed monocrystal by irregular diffusion through the outcropping of dislocations onto a lateral surface. An open dislocation nucleus will form when these dislocations meet a barrier which is strong enough, and atoms of the surface active alloy will then move rapidly along the resulting canal, adsorbing on the walls of nascent cracks and facilitating their further development by considerably reducing the work of formation of a new surface. Under these conditions, the monocrystal will undergo "premature" brittle fracture at a comparatively low value of the normal stress [4, 5, 6].

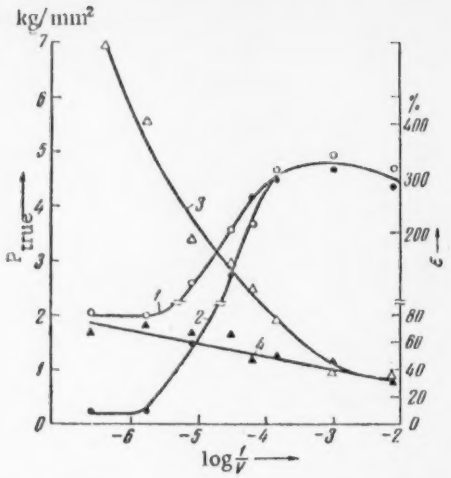

Fig. 1. The relation between the logarithm of the reciprocal deformation rate (V, in % per minute), the true rupture stress (P) and the maximum extension at rupture (ε) for pure (Curves 1 and 3), and amalgamated (Curves 3 and 4), monocrystals of tin ($\kappa_0 = 55°$).

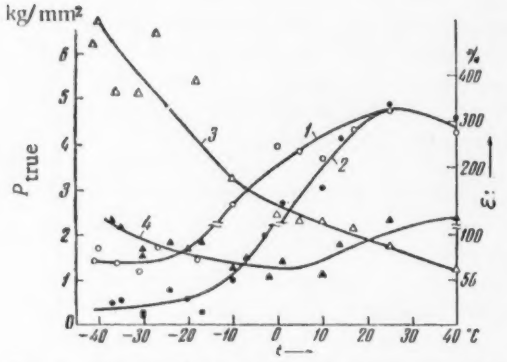

Fig. 2. The relation between the temperature (t°C), the true rupture stress (P) and the maximum extension at rupture (ε) for pure (Curves 1 and 3), and amalgamated (Curves 2 and 4), monocrystals of tin ($\kappa_0 = 55°$).

This theory of the deformation and brittle rupture of metallic monocrystals and the effect of surface active alloys on these processes leads to the formulation of a new quantitative law of brittle fracture which is applicable even when there is no surface active medium [7, 8].

At the same time, this theory makes possible a correct evaluation of the role of temperature and deformation conditions, physicomechanical factors which can favor or oppose the adsorptional effects of embrittlement and strength reduction in metallic monocrystals. The adsorptional effect from a low melting alloy must be most pronounced at those temperatures and rates of deformation where there is the greatest possibility for development of internal fissures and the maximum weakening of those spontaneous processes of relaxation which retard the formation and further development of these equilibrium cracks of brittle rupture.

In this connection, investigation has been made of the action of mercury on monocrystals of very pure tin (99.999%). At room temperature and with low deformation rates, the presence of a thin mercury film on the surface of a tin monocrystal has no effect whatsoever on the mechanical properties of the metal. There are, however, a number of indications that mercury is surface active with respect to tin [9]. The lack of any effect at room temperature can be explained by the fact that tin is then near its melting point and there is an intensive healing of cracks which impedes crack growth even though the adsorbed mercury atoms reduce the work required for the formation of new surfaces. If these conclusions are correct, a decrease in the temperature, or an increase in the deformation rate at room temperature, should promote the action of a surface active mercury covering on a tin monocrystal. Figure 1 gives results from tensile strength experiments on tin monocrystals which were carried out at room temperature with deformation rates ranging from 10^2%/min to 10^6%/min; some of the crystals being bare and some covered with thin mercury films approximately 5 μ thick.

The mercury effect appeared only at comparatively high rates of extension (about 10^4%/min), just as was to be anticipated, and continued to increase as the rate of extension rose.

Exactly similar results were obtained at a fixed deformation rate (7000%/min) but lower temperatures (Fig. 2). The lower the temperature, the more pronounced the adsorptional effect of the mercury film in lowering the strength and plasticity of the tin monocrystals. The adsorptional effect could be observed on the amalgamated tin monocrystals only when the temperature was held above the melting point of the mercury film so as to assure mobility of the mercury atoms. The effect of the mercury film diminished considerably at temperatures below −39° where the mobility of the mercury atoms was low.

These results thus show that there is a possibility of considerable adsorptional effects in the reduction of the strength and plasticity of metals by low melting alloys even in those cases in which this effect cannot be

detected at a given temperature and with given deformation conditions. The lack of an effect under certain conditions does not necessarily indicate an absence of adsorptional activity of the alloy since this may be due to a poor selection of the conditions of deformation. Naturally, this does not mean that reduction of strength and plasticity can be obtained with every high melting metal – low melting alloy pair.

The adsorptional effect, the temperature, and the deformation conditions are interrelated only if the low melting alloy is surface active with respect to the high melting metal. When this necessary condition is fulfilled, it is always possible to find a region of temperatures and deformation rates within which the adsorptional effect will be most pronounced.

It should be noted that these same ideas can be used to explain a rule developed by S. T. Kishkin and his collaborators for steels containing various amounts of carbon [10] which claims that the action of a low melting alloy will increase as the strength of the steel rises. The lighter the steel, the more pronounced should be the action of low melting alloys at the higher rates of deformation (at constant temperature).

LITERATURE CITED

[1] N. F. Mott, Proc. Roy. Soc. A, 220, 1 (1953).

[2] V. I. Likhtman, P. A. Rebinder, and G. V. Karpenko, The Effect of Surface Active Media on the Deformation of Metals [in Russian], Acad. Sci. USSR Press, 1954.

[3] P. A. Rebinder, New Problems of Physicochemical Mechanics, Report, Colloquin on Solid Phases of Variable Composition held conjointly with Moscow Colloquium on Colloid, January 26, 1956 [in Russian].

[4] P. A. Rebinder, V. I. Likhtman, and L. A. Kochanova, Proc. Acad. Sci. USSR, 111, No. 6 (1956).

[5] V. I. Likhtman, L. A. Kochanova, and L. S. Bryukhanova, Proc. Acad. Sci. USSR 120, No. 4 (1958).*

[6] V. N. Rozhanskii, N. V. Pertsov, E. D. Shchukin, and P. A. Rebinder, Proc. Acad. Sci. USSR 116, No. 5 (1957).*

[7] V. I. Likhtman and E. D. Shchukin, Prog. Phys. Sci. 66, 213 (1958).

[8] E. D. Shchukin and V. I. Likhtman, Proc. Acad. Sci. USSR 124, No. 2 (1959).*

[9] N. V. Pertsov and P. A. Rebinder, Proc. Acad. Sci. USSR 123, No. 6 (1958).*

[10] S. T. Kishkin, V. V. Nikolenko, and S. I. Ratner, J. Tech. Phys. 24, 8 (1954).

[11] V. I. Likhtman, P. A. Rebinder, and L. P. Yanova, Proc. Acad. Sci. USSR 56, No. 8 (1947).

[12] E. D. Shchukin, Proc. Acad. Sci. USSR 118, No. 6 (1958).*

Received May 18, 1959

*See C. B. Translation.

THE MECHANISM OF ELECTROREDUCTION OF THE $Fe(CN)_6^{3-}$ ANION OF THE DROPPING MERCURY ELECTRODE

Academician A. N. Frumkin, O. A. Petrii, and N. V. Nikolaeva-Fedorovich

The M. V. Lomonosov State University, Moscow

A. N. Frumkin and G. M. Florianovich [1] have developed an approximation equation for curves covering the $S_2O_8^{2-}$ anion reduction in the presence of various concentrations of KCl by assuming the slow step to be that of combining electrons with anions which have been repelled by the surface charge of the electrode. The polarization curves which we have obtained in our study of the reduction of $Fe(CN)_6^{3-}$ differ from those for the $S_2O_8^{2-}$ reduction insofar as there is no increase in the reaction rate after passing through the minimum in the region of high negative potentials. This suggests that the slow step in the $Fe(CN)_6^{3-}$ reduction is of a different type, possibly a slow penetration of the anion into the double-layer field such as is described by the theory of V. G. Levich [2, 3]. Other hypotheses concerning the reduction of this anion have been advanced recently [4, 5].

For this reason, we have undertaken a more detailed study of the mechanism of the reduction of the $Fe(CN)_6^{3-}$ anion on the dropping mercury electrode. Measurements were carried out in a Jena glass cell [6] having a capillary with the constants m = 1.25 mg/sec and τ = 6.1 seconds at $\varphi = -0.5$ volts. The curves were corrected for the discharge currents, these being determined by making measurements on a 10^{-3} N $K_4Fe(CN)_6$ solution with an additive in the case of a 10^{-3} N $K_3Fe(CN)_6$ solution containing this same additive at this same concentration and by measurements on solutions of 10^{-3} N concentration in CsCl or LiCl in the case of 10^{-3} N $Cs_3Fe(CN)_6$ and 10^{-3} N $Li_3(CN)_6$. The graph shows only that portion of each curve which is free of distortion from anodic dissolution of mercury and polarographic maxima of the first type. Values of the potential φ are expressed in terms of the saturated calomel electrode.

1. The polarization curve for the $Fe(CN)_6^{3-}$ anion in a 10^{-3} N $K_3Fe(CN)_6$ solution containing $3 \cdot 10^{-2}$ N KCl is normal (Fig. 1, 7). The value of the saturation current is in agreement with that calculated from the Ilkovich equation with $D = 8.9 \cdot 10^{-6}$ cm^2/sec. There is a diminution of the current in the region of the null-charge potential on the reduction curve for $Fe(CN)_6^{3-}$ when the total concentration of the electrolyte decreases (Fig. 1, 1-6). This current reaches a minimum value at $\varphi = -1.2$ and then remains practically constant as the potential changes. This must be a kinetic current since its minimum value is independent of the height of the mercury column. The curves obtained with $2 \cdot 10^{-3}$ N and $3 \cdot 10^{-3}$ N $K_3Fe(CN)_6$, and with 10^{-3} N $Cs_3Fe(CN)_6$* and 10^{-3} N $Li_3Fe(CH)_6$ containing added CsCl and LiCl, respectively, also show this drop in the current and run a similar course. There is an increase in the current in solutions of 10^{-3} N $Li_3Fe(CN)_6$ containing added LiCl as the potential passes to values more negative than -2.0 (Fig. 1).

2. In developing the relation between the potential and the rate of reduction of $Fe(CN)_6^{3-}$, the polarization curves were corrected for concentration polarization by using the exact Meiman-Bagotskii theory [8] of concentration polarization in first order reactions on the dropping electrode. The calculations show the rate of reduction of the $Fe(CN)_6^{3-}$ to increase by 30-40% when the polarization passes beyond the minimum (Fig. 2).

* The $Cs_3Fe(CN)_6$ and the $Li_3Fe(CN)_6$ were synthesized from $K_3Fe(CN)_6$ by the method described in [7].

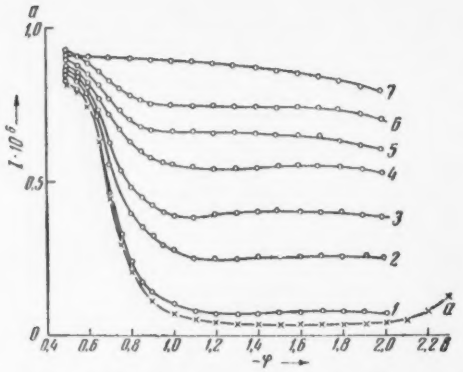

Fig. 1. Polarization curves for the reduction of 10^{-3} N $K_3Fe(CN)_6$ solutions containing KCl at the concentrations: 1) 0, 2) $5 \cdot 10^{-4}$ N, 3) 10^{-3} N, 4) $1.5 \cdot 10^{-3}$ N, 5) $2 \cdot 10^{-3}$ N, 6) $3 \cdot 10^{-3}$ N, 7) $3 \cdot 10^{-2}$ N; a) is a polarization curve for the reduction of 10^{-3} N $Li_3Fe(CN)_6$.

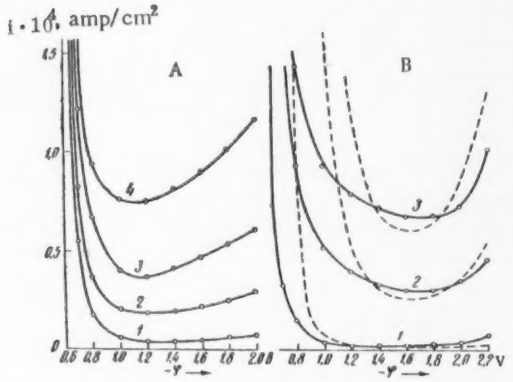

Fig. 2. The relation between the potential and the rate of reduction of $Fe(CN)_6^{3-}$. A) in 10^{-3} N $K_3Fe(CN)_6$ solutions containing KCl at the concentrations: 1) 0, 2) $5 \cdot 10^{-4}$ N, 3) 10^{-3} N, 4) $1.5 \cdot 10^{-3}$ N; B) in 10^{-3} N $Li_3Fe(CN)_6$ solutions containing LiCl at the concentrations: 1) 0, 2) $2 \cdot 10^{-3}$ N, 3) $3 \cdot 10^{-3}$ N. The dotted curves have been developed from Eq. (1).

The absence of an increase in the current on the experimental $Fe(CN)_6^{3-}$ reduction curve at high negative potentials is to be explained by the fact that the reduction rate of this ion increases only slowly as the cathodic potential rises while the drop period and the drop surface, which is proportional to the kinetic current, diminish markedly as the surface charge becomes more negative.

3. Measurements on 10^{-3}N $K_3Fe(CN)_6$, 10^{-3} N $Cs_3Fe(CN)_6$ and 10^{-3} N $Li_3Fe(CN)_6$ solutions containing KCl, CsCl, and LiCl, respectively, show the rate of reduction of $Fe(CN)_6^{3-}$ to be proportional to the 3.0-3.2 power of the concentration, C, of the foreign cation in each case. The relation between C and rate of reduction of $S_2O_8^{2-}$ in the presence of KCl and CsCl is one in which the exponent of C varies from 1.3 at $\varphi = -0.75$ to 2.0 at $\varphi = -1.35$.

4. The rate of reduction of the $Fe(CN)_6^{3-}$ increases by four-fold on replacing K^+ with Cs^+ at the same concentration. The rate of reduction of $S_2O_8^{2-}$ is increased seven-fold by passing from KCl to CsCl.

5. The temperature coefficient of the $Fe(CN)_6^{3-}$ reduction is positive and its value depends on the nature of the background cation, just as in the case of the $S_2O_8^{2-}$ [6, 9]. Over the temperature interval from 0° to 30° the reaction rate increases by 10% in 10^{-3} N $Cs_3Fe(CN)_6 + 10^{-3}$ N CsCl, by 20% in 10^{-3} N $K_3Fe(CN)_6 + 1.5 \cdot 10^{-3}$ N KCl and by two-fold in 10^{-3} N $Li_3Fe(CN)_6 + 3 \cdot 10^{-3}$ N LiCl.

6. At negative surface charges, increase of the background anion charge in the sequence $Cl^- < SO_4^{2-} < Fe(CN)_6^{4-}$ leads to a diminution of the rate of reduction of $Fe(CN)_6^{3-}$ (Fig. 3) and $S_2O_8^{2-}$ while the specifically adsorbed halogen anions ($Cl^- < Br^- < I^-$) increase the rate of reduction of $S_2O_8^{2-}$ at these same potentials [10] and leave the rate of reduction of $Fe(CN)_6^{3-}$ unaltered.

7. The organic cations $[(CH_3)_4N]^+$, $[(C_2H_5)_4N]^+$, $[(C_4H_9)_4N]^{3+}$, $[(C_5H_{11})_4N]^+$ and $[C_6H_{13})_4N]^+$ will increase the rate of reduction of $Fe(CN)_6^{3-}$ if the potential is such that adsorption can occur. The effectiveness of these cations increases with the concentration and the length of the carbon chain. Addition of $[(C_6H_{13})_4N]^+$ exerts a marked effect on the rate of reduction of $Fe(CN)_6^{3-}$ at high negative potentials, the situation being similar to the organic cation effect which we have observed earlier in the reduction of $S_2O_8^{2-}$ in the presence of $[(C_5H_{11})_4N]^+$ and $[(C_6H_{13})_4N]^+$ [11]. This effect can be explained by assuming that a deformation of the organic cation at high negative surface charges leads to an alteration in the relation between the position of the center of the active complex of the discharging anion and the positive charge of the cation [12].

The accumulated experimental data and the various schemes which have been proposed for the electroreduction of anions [1, 2, 4] permit the conclusion that there is no fundamental difference between the reduction of $Fe(CN)_6^{3-}$ and the reduction of $S_2O_8^{2-}$, the rate of reduction being determined in the former case by the delayed anion of electrons and $Fe(CN)_6^{3-}$ ions in the neighborhood of the electrode.

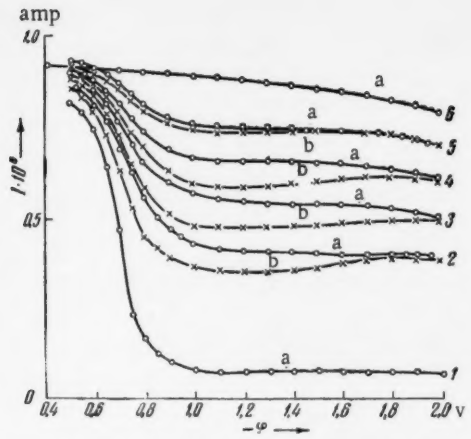

Fig. 3. Polarization curves for the reduction of 10^{-3} N $K_3Fe(CN)_6$ solutions containing KCl (a), or $K_4Fe(CN)_6$ (b) at the concentrations: 1) 0, 2) 10^{-3} N, 3) $1.5 \cdot 10^{-3}$ N, 4) $2 \cdot 10^{-3}$ N, 5) $3 \cdot 10^{-3}$ N, 6) 10^{-1} N.

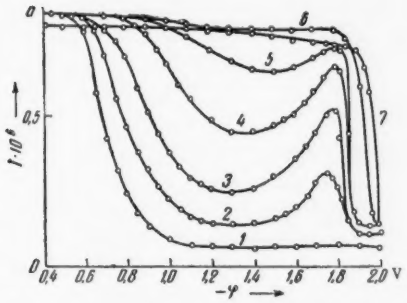

Fig. 4. Polarization curves for the reduction of 10^{-3} N $K_3Fe(CN)_6$ containing $[(C_6H_{13})_4N]$ Br at the concentrations: 1) 0, 2) $5 \cdot 10^{-6}$ N, 3) 10^{-5} N, 4) $1.5 \cdot 10^{-5}$ N, 5) $2 \cdot 10^{-5}$ N, 6) $5 \cdot 10^{-5}$ N, 7) 10^{-4} N.

We have developed reduction curves for $Fe(CN)_6^{3-}$ on this basis, proceeding as in [1] for reduction of $S_2O_8^{2-}$ but calculating the concentration polarization from the Melman-Bagotskii theory [8] rather than from an approximation equation. The constant a was determined from the initial curve segments and proved to be equal to 0.16. Figure 2 shows that theoretical curves developed from the equation

$$i = kC_A \exp \frac{\alpha F}{RT}\left(-\varphi + \frac{3+\alpha}{\alpha}\psi_1\right), \quad (1)$$

(here, C is the bulk concentration of anions and k is a constant which is equal to $1.25 \cdot 10^{12}$ amp·cm/mole in the present case) will reproduce the general form of the experimental curves. Divergences exist, however, and these reach 20% in the region of potentials from −1.2 to −2.2 volts. There is a logarithmic relation between the ψ_1-potential and the concentration of the electolyte at sufficiently high negative potentials so that Eq. (1) shows the discharge rate of a triply charged anion to increase with the $3 + \alpha$ power of the concentration of the singly charged cation of the background and the discharge rate of a doubly charged anion to increase with the $2 + \alpha$ power of this concentration, predictions which are partially confirmed by experiment. This same rate for the reaction–cation concentration relation can also be obtained from other reduction schemes.

Equation (1) gives an approximation to the relation between the rate of reaction, the electrode potential and the background concentration, but the theory lying behind it is in need of fundamental corrections for it has been already pointed out [3, 6] that it is incapable of explaining the observed values of the temperature coefficients and their relation to the cation radius. The derivation of (1) assumes that the ψ_1-potential is constant along the electrode surface; calculations based on the Levich equation [2] show, however, that the rate of penetration of doubly and triply charged anions into the electrical field of the negatively charged electrode would then be many orders less than observed reaction rates at the potentials in question. This dilemma can be avoided by taking account of a nonuniform distribution of potentials in the double layer or, what amounts to the same thing, by considering the interaction of the anion with the nearest neighbor cation or cations. It is also impossible to explain the fact that the $Fe(CN)_6^{4-}$ ion has an effect on the reaction rate at high negative potentials even though it has no pronounced specific adsorbability unless it is considered that the ψ_1-potential can become approximately zero, or even positive in value, at distances from a negatively charged electrode surface which are not too large. Gierst has proposed [4] that the classical theory of double layer structure can be retained in explaining the role of cations in the reduction of anions if it is assumed that it is ionic pairs of the type $MeFe(CN_6)^{2-}$ or $Me_2Fe(CN)_6^-$, which are reduced, these pairs being formed in the body of the solution by such reactions as:

$$Me^+ + Fe(CN)_6^{3-} \rightleftarrows MeFe(CN)_6^{2-}.$$

The calculated rate of penetration of the doubly charged anion proves to be too low when a uniform potential

distribution is assumed; an improbably small a value of α ($\sim$ 0.05) would be required to account for the observed minimum on the curve showing rate as a function of potential in the case of the singly charged anion. In addition, the depth of the reaction layer must clearly be quite small [3] and less than the depth of the diffuse double layer, which leads back to the decisive role played by the interaction of anions and cations, not in the body of the solution, but in the double layer itself.

LITERATURE CITED

[1] A. N. Frumkin and G. M. Florianovich, Proc. Acad. Sci. USSR 80, 907 (1951); J. Phys. Chem. 29, 1827 (1955); A. N. Frumkin, Prog. Chem. 24, 933 (1955).

[2] V. G. Levich, Proc. Acad. Sci. USSR 67, 309 (1949); Proc. Acad. Sci. USSR 124, 869 (1959).*

[3] A. Frumkin, Trans. Farad. Soc. 55, 156 (1959).

[4] L. Gierst, Cinétique d'approche et réactions d'électrodes irréversibles, 1958.

[5] P. Kivalo and H. Laitinen, J. Am. Chem. Soc. 77, 5205 (1955); A. Frumkin and N. Nikolaeva, J. Chem. Phys. 26, 1552 (1957); P. Kivalo, J. Phys. Chem. 61, 1126 (1957).

[6] A. N. Frumkin and N. V. Nikolaeva-Fedorovich, Herald Moscow Univ., chem. ser., 769 (1957).

[7] I. Meyer, Zs. anorg. Chem. 115, 206 (1921).

[8] N. N. Meiman, J. Phys. Chem. 22, 1454 (1948); V. S. Bagotskii, J. Phys. Chem. 22, 1466 (1948).

[9] A. N. Frumkin, Proceedings Fourth Conference on Electrochemistry 1956, Acad. Sci. USSR Press, 1959, p. 21; N. V. Nikolaeva-Fedorovich, ibid, p. 150.

[10] T. V. Kalish and A. N. Frumkin, J. Phys. Chem. 28, 473 (1954); A. Frumkin, N. Nikolaeva-Fedorovich, and R. Ivanova, Canad. J. Chem. 37, 253 (1959).

[11] O. A. Petrii, Diploma Work, Moscow State University, 1959.**

[12] N. V. Nikolaeva-Fedorovich, L. A. Lokina and O. A. Petrii, Proc. Acad. Sci. USSR 122, 639 (1958).*

Received July 28, 1959

*Original Russian pagination. See C. B. Translation.

**In Russian.

THE EQUILIBRIUM DISTRIBUTION OF DEUTERIUM DURING HYDROGEN EXCHANGE WITH LIQUID DEUTERIUM IODIDE

P. P. Alykhanov and Ya. M. Varshavskii

L. Ya. Karpov Physicochemical Scientific Research Institute

(Presented by Academician S. S. Medvedev, June 19, 1959)

The present work is part of a general study of isotope equilibria in various systems of hydrogen-containing substances [1-4]. In this work, the equilibrium distribution of deuterium for the exchange reactions in which hydrogen iodide takes part has been investigated experimentally for the first time. The relevant measurements were made for the system: aromatic C−H bond −HI.

From the point of view of the general law [1] which describes the equilibrium distribution of deuterium in hydrogen exchange reactions, the knowledge of the value of the distribution coefficient (α) of deuterium for systems involving hydrogen iodide is of fundamental interest. According to this law, hydrogen iodide occupies a special position since, in comparison with the remaining hydrogen halides as well as hydrides of any known metals (which have no free valences), it is distinguished by the smallest value of β-factor.* The knowledge of the value of α is also necessary in the study of deuterium exchange between organic compounds and hydrogen iodide.

The most convenient substance for the study of the isotope equilibrium between the aromatic C−H bond and hydrogen iodide should be benzene since all its hydrogen atoms are equivalent; in addition, the value of the equilibrium coefficient, determined experimentally, of the deuterium distribution between benzene and HI could be directly compared with the corresponding value calculated on the basis of the data on oscillation frequencies available in literature [1]. However, it has been found experimentally that the rate of deuterium exchange between benzene and HI is very low. As a result of the study of the exchange rate between some aromatic compounds and liquid deuterium iodide, it was established [7] that the most suitable substance for the study of this equilibrium is diphenyl $(C_6H_5)_2$. When diphenyl is dissolved in liquid hydrogen iodide, the six hydrogen atoms (in ortho- and para-positions) undergo the exchange relatively easily while the remaining four atoms (meta) remain practically unexchanged. The absence of the exchange of meta-atoms of hydrogen can also be confirmed by the fact that such an exchange is not observed when liquid hydrogen bromide is used as the solvent and donor of deuterium [5].

The experiments were carried out in sealed glass ampoules in liquid-phase homogeneous systems under pressure (4-15 atm). After equilibrium had been attained, the hydrogen iodide was evaporated, and the remaining diphenyl was subjected to purification and combustion in an oxygen stream; the deuterium content in the water produced was determined by means of the drop method [6]. The concentration of deuterium in the initial HI was determined by means of analyzing the water produced as a result of the decomposition of HI on copper oxide at 350-400°C in a nitrogen stream.** The isotope equilibrium was approached from both sides in experiments with

*The hydride of astatine, the heaviest and most unstable halogen, which, as is known, does not occur in nature, should have an even smaller value of β-factor.

**Apparently, CuI, and not CuI_2 was formed in the process of HI decomposition and therefore one obtained large quantities of free iodine which was then combined with metallic copper at an elevated temperature.

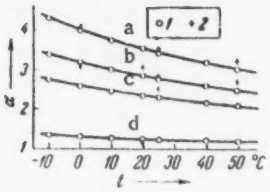

Fig. 1. Temperature curves of the distribution coefficients of deuterium in the systems C−H−H−Hal. a) HI-CH; b) HBr-CH, c) HCl; d) HF-CH; 1) calculated values; 2) experimental values.

direct and reverse exchange. In the latter case, samples of diphenyl with deuterium, substituted in ortho- and para-positions, were used.* For the purpose of reducing the time of attaining the isotope equilibrium, the experiments were carried out in the presence of iodine which acted as a catalyst for the exchange reactions between the hydrocarbons and the liquid deuterium iodide [7]. The concentration of the catalyst was selected in such a way as to achieve a fairly high velocity but not high enough to allow the isotope equilibrium to be displaced toward large values of α in a short time required for the evaporation of hydrogen iodide at a low temperature.

It is interesting to compare the temperature curves of the equilibrium distribution coefficient of deuterium between the aromatic bond C−H and hydrogen halides for various hydrogen halides [2, 3, 4]. This comparison is shown in Fig. 1. The curves were plotted from calculated values [1]; at the same time experimental points were also plotted.

The value of $\alpha_{0°} = 4.07$, $\alpha_{25°} = 3.47$ and $\alpha_{50°}$ 3.13, obtained in the present work, for the isotope equilibrium of hydrogen between diphenyl and liquid hydrogen iodide are in good agreement with the calculated values, and for the temperatures given are the maximum values among all the experimental values of α obtained so far for deuterium exchange.

TABLE 1

Isotope Equilibrium in the Hydrogen Iodide − Diphenyl System

Experimental conditions		Molar ratio of components		Deuterium concentration, at.,%				α	α_{mean}	$\alpha_{calc.}$
				initial		final				
temperature, °C	time, hrs	$\frac{m_{J_2}}{m_{HJ}} \cdot 10^4$	$\frac{m_{(C_6H_5)_2}}{m_{HJ}} \cdot 10^2$	HJ	$(C_6H_5)_2$*	HJ**	$(C_6H_5)_2$			
0	28	25	2,58	—	11,85	1,91	4,44	4,10		
0	28	25	2,46	—	11,85	1,85	4,32	4,12	4,07	4,02
0	43	16	1,51	3,90	—	2,91	6,50	4,06	(±0,1)	(+0,2)
0	43	16	1,55	3,90	—	2,91	6,37	3,99		
25	27	18	1,73	—	11,93	1,52	3,13	3,56		
25	27	21	2,07	—	11,93	1,74	3,50	3,50		
25	50	17	1,97	—	11,93	1,68	3,41	3,52	3,47	3,43
25	43	17	1,70	3,90	—	2,94	5,64	3,43	(±0,1)	(±0,2)
25	43	10	1,47	3,90	—	3,06	5,76	3,36		
50	43	13	2,06	—	11,93	1,79	3,29	3,18		
50	43	14	1,91	—	11,85	1,69	3,09	3,16	3,13	2,97
50	43	10	1,51	3,90	—	3,09	5,36	3,05	(±0,1)	(±0,2)

*Deuterium in ortho- and para-positions in the samples.

**Calculated from the deuterium balance (see equations (4) and (5) in [7]).

LITERATURE CITED

[1] Ya. M. Varshavskii and S. É. Vaisberg, Doklady Akad. Nauk SSSR 100, 97 (1955); Zhur. Fiz. Khim. 29, 523 (1955); Uspekhi Khimii 26, 1355 (1957).

[2] Ya. M. Varshavskii, V. R. Kalinachenko, S. É. Vaisberg, and A. I. Shatenshtein, Zhur. Fiz. Khim. 30, 1647 (1956).

*Samples of ortho- and para-hexadeuterium diphenyl according to [9] were obtained by means of isotope exchange between diphenyl and deuterium bromide under conditions when only ortho- and para-atoms of hydrogens undergo an exchange process. The deuterium content in the samples used was approximately 12%.

[3] Ya. M. Varshavskii and A. I. Shatenshtein, Doklady Akad. Nauk SSSR 95, 297 (1954).

[4] Ya. M. Varshavskii, S. É. Vaisberg, and B. A. Trubitsyn, Doklady Akad. Nauk SSSR 122, 831 (1958).*

[5] A. I. Shatenshtein, V. R. Kalinachenko, and Ya. M. Varshavskii, Zhur. Fiz. Khim. 30, 2093 (1956).

[6] A. I. Shatenshtein and Ya. M. Varshavskii, Zhur. Anal. Khim. 11, 746 (1956). *

[7] A. I. Shatenshtein and P. P. Alikhanov, Zhur. Obsh. Khim. (in press).**

[8] Ya. M. Varshavskii and V. R. Kalinachenko, Zhur. Fiz. Khim. 30, 2094 (1956).

[9] A. I. Shatenshtein, G. V. Peregudov, E. A. Izraelevich, and V. R. Kalinashenko, Zhur. Fiz. Khim. 32, 146 (1958).

Received April 13, 1959

* Original Russian pagination. See C. B. Translation.

** See C. B. Translation.

THE SOLUTION OF METALLIC MAGNESIUM IN FUSED CHLORIDES

N. G. Bukun and E. A. Ukshe

Bereznikov Branch of the All-Union Aluminum and Magnesium Institute

(Presented by Academician A. N. Frumkin, June 22, 1959)

The dissolution of metals in fused salts, a phenomenon discovered by G. Davy more than 150 years ago, [1] plays a very important part in several electrochemical industries such as the production of magnesium, aluminum, sodium, etc. Naturally, this phenomenon has been the subject of a large number of investigations (e.g. [2, 3]). So far, however, neither the kinetics nor the nature and mechanism of the dissolution of metals have been fully elucidated. In view of this fact, as well as in view of the necessity to solve a number of practical problems, we decided to undertake the study of the mechanism of the interaction of liquid metals with a fused electrolyte. In the present paper we report some of the results.

We determined the equilibrium concentration of dissolved metal for fused magnesium in contact with chloride electrolytes of various composition. The method was similar to one used earlier by A. I. Zhurin [4]. The mixture of salts of a given composition was placed in a hermetic steel vessel. The volume of the salt was such as to make the free space in the vessel as small as possible. A lump of magnesium whose surface area was cleaned mechanically before the experiment was placed into the vessel with the salt. The vessel had a thick bottom wall in which an opening for the thermocouple was drilled. The vessel, with the thermocouple, was placed into a tubular tilting furnace ($\frac{1}{2}$ period per sec) so that a uniform mixing of the melt was ensured. The temperature of the furnace was maintained constant ($\pm$ 10°C) by means of an electronic potentiometer, ÉPV-OI. The experiment took 2.5 hours. After the experiment, the oven was set vertically and the vessel was kept for approximately one hour at a given temperature until the salt phases were completely separated. The vessel was then quenched with cold water and the metallic magnesium content in the solid salt was determined from the hydrogen content which separated in the reaction:

$$Mg + 2H_2O = Mg(OH)_2 + H_2.$$

For the determination of the hydrogen content, we used the Lunge flowmeter [5] by means of which we could determine the gas volume reduced to NTP. In the experiments, chemically pure recrystallized salts which were dried throughly by means of ammonium chloride and subsequent remelting were used. The salts were remelted in CO_2 atmosphere and were left standing for 2 hours.

The most important sources of error in the determination of the solubility of magnesium were the contamination of the salt sample with microscopic particles of metal and the evolution of gases resulting from the reaction of water with carbides which formed as a result of the action of magnesium on the walls of the steel vessel. The first source of error could be eliminated by taking sufficient care during the experiments. As regards carbides, special experiments showed that the error due to the carbides corresponds to the solubility of magnesium of $(2\text{-}3)\cdot 10^{-3}$ M% and in the first approximation this error can be ignored. The difference between the results of independent experiments varied from 5-10% of the absolute value of the solubility if the solubility was fairly high and up to 20-25% of the absolute value if the solubility was poor (for instance, in melts of potassium, sodium and barium chlorides).

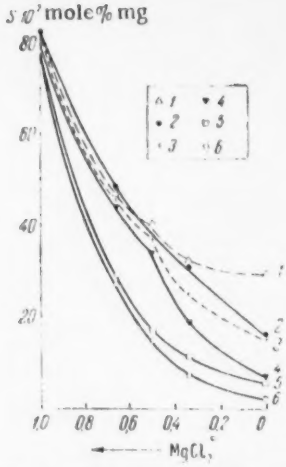

Fig. 1. The solubility of magnesium in the salt phase as a function of its composition at t = 800°C. 1) $MgCl_2$–$CaCl_2$; 2) $MgCl_2$–LiCl; 3) $MgCl_2$–$SrCl_2$; 4) $MgCl_2$–$BaCl_2$; 5) $MgCl_2$–NaCl; 6) $MgCl_2$–KCl.

The results of the determination of magnesium solubility in melts of salts of different compositions are given in Fig. 1. Most of the points were obtained at a temperature of 800°C. The points corresponding to the following composition of the salt phase were exceptions: NaCl (850°); KCl (820°); $CaCl_2$ (830°); 34% $MgCl_2$ + 66% $SrCl_2$ (820°); $SrCl_2$ (920°); 34% $MgCl_2$ + 66% $BaCl_2$ (900°); $BaCl_2$ (1000°).* These deviations in temperature affected somewhat the smoothness of the curves of the solubility vs the composition of the salt phase.

If we consider the dissolution of magnesium in melts as the result of the establishment of equilibrium:

$$MgCl_2 + Mg \rightleftarrows Mg_2Cl_2, \qquad (A)$$

then, obviously, according to the law of mass action

$$k_0 = \frac{x_0\gamma_0}{x_1\gamma_1 x_m^2\gamma_m^2}, \qquad (1)$$

where $\gamma_0, \gamma_1, \gamma_m$ are the activity coefficients, and x_0, x_1, x_m are the concentrations of Mg_2Cl_2, and $MgCl_2$ in the salt phase and of Mg in the metallic phase, respectively. For the system Mg-$MgCl_2$ we can assume $\gamma_0 = 1$ and then, according to the data given above,

$$k_0 = x_0 = 41{,}6 \cdot 10^{-4}. \qquad (2)$$

Close values of k_0 (from $40 \cdot 10^{-4}$ to $49 \cdot 10^{-4}$) are obtained from the results of A. I. Zhurin for the system Mg-Al-$MgCl_2$ at 800°C.

It can be assumed that when the salt phase is diluted with other chlorides, Equation (1) should still be valid. However, the calculation, for instance, for the $MgCl_2$-KCl system, for which the activity coefficient for individual components are known [6], shows that this is not the case and that Equation (1) is valid only for the concentration of $MgCl_2$ of more than 50%. Neither is it possible to explain the solubility of magnesium in foreign-ion melts on the basis of the reaction (A). All this leads to an assumption that at a low concentration of magnesium chloride, exchange reactions of the following type play an important part:

$$Mg + 2Li^+ \rightleftarrows Mg^{2+} + 2Li, \qquad (B)$$

$$2Mg + 4Li \rightleftarrows Mg_2^{2+} + 2Li_2 \qquad \text{etc.} \qquad (C)$$

The specificity of the action of foreign cations on the solubility of magnesium (S) is such that the latter decreases with a decreasing polarizing action of cations of the foreign salt,

Me^{z+}	Ca^{+2}	Li^+	Sr^{+2}	Ba^{+2}	Na^+	K^+
z / R^2	1,76	1,64	1,34	0,98	1,04	0,56
$S \cdot 10^2$%	30	16,2	15,6	7,1	6,0	2,4

This is understandable since the higher the polarizing action (z/R^2) the more the corresponding cation should polarize the Cl^- ion and consequently the more stable should be the bond Mg-Mg, which apparently determines the existence of the Mg_2^{2+} subion [7].

The equilibria of type (A)-(C) are electrochemical equilibria and, therefore, if the above hypothesis is valid, in the systems of the type metal-melted electrolyte one should take into account not only the interaction of metal with its ions but also with the cations of the solvent. This is important since it means that the potential

* The composition is given in molar %.

of liquid metals in dilute melts of their salts are quasi-equilibrium potentials, and apparently, A. N. Frumkin's theory of stationary potentials should be applicable in this case. Other authors (for instance [8, 9]) also point out the significant role of the equilibria of types (B) and (C) so that our interpretation of the results obtained is quite probable. Of course, by using Luther's rule one can evaluate the standard potential of magnesium chloride from the results obtained. Since for the equilibrium system

$$\varphi = \varphi^0_{Mg/Mg^{+2}} + \frac{RT}{2F} \ln a_{Mg^{+2}} = \varphi^0_{Mg^{+2}/Mg_2^{+2}} + \frac{RT}{F} \ln \frac{a_{Mg^{+2}}}{a^{1/2}_{Mg_2^{+2}}} =$$

$$= \varphi^0_{Mg/Mg_2^{+2}} + \frac{RT}{F} \ln a^{1/2}_{Mg_2^{+2}}$$

and since, on the chlorine scale of potentials, one can assume

$$\varphi^0_{Mg/Mg^{+2}} = -2{,}60 \text{ v}$$

at 800°C, then, by using the k_0 value obtained we find

$$\varphi^0_{Mg/Mg_2^{+2}} = -2{,}36 \text{ and } \varphi^0_{Mg_2^{+2}Mg^{+2}} = -2{,}84 \text{ v}$$

LITERATURE CITED

[1] H. Davy, Trans. Roy. Soc., London, 97, 1 (1807).

[2] A. I. Belyaev, E. A. Zhemchuzhina, and L. A. Firsanova, Physical Chemistry of Fused Salts [in Russian] Moscow, 1957.

[3] P. F. Antipin, A. F. Alabyshev, N. A. Belozerskii et al., Electrochemistry of Fused Salts [in Russian] 1937.

[4] A. I. Zhurin, Metallurg, No. 3-4 (1935).

[5] Berl'-Lunge, Khimiko-tekhnicheskie metody issledovaniya, 1, No. 2, 1936, p. 146.

[6] I. L. Reznikov, Zhur. Prikl. Khim. 23, 897 (1950).*

[7] K. Grjotheim, F. Grönvold, and J. Krogh-Moe, J. Am. Chem. Soc. 77, 5824 (1955).

[8] K. Stern, J. Phys. Chem. 62, 385 (1958).

[9] W. Jander and G. German, Zs. anorg. Chem. 239, 65 (1938).

Received May, 19, 1959

*Original Russian pagination. See C. B. Translation.

TURBULENT COMBUSTION IN AN ENCLOSED SPACE

V. P. Karpov, E. S. Semenov, and A. S. Sokolik

Institute of Chemical Physics

(Presented by Academician V. N. Kondrat'ev, June 11, 1959)

The development of the theory of turbulent combustion is seriously hampered by the lack of the fundamental empirical equations relating the main characteristics of the flame, i.e., the velocity and the width of the reaction zone with the turbulent characteristics of the stream and the physical and chemical properties of the burning mixture. This situation has arisen because the method of Guy-Michelson cannot, in principle, be applied to a turbulent flame stabilized either by a pilot flame or by a hydrodynamic stabilizer. The main conditions necessary for the determination of the rate of combustion by means of this method – the presence of a stationary, infinitely thin, continuous surface of ignition with an equal rate of combustion over all its length and hydrodynamic characteristics of the flow – do not obtain in the turbulent flame. With a view of eliminating these difficulties, the possibility of determining the velocity of turbulent combustion, U_T, in a free spherical flame formed as a result of spark ignition in a turbulent stream i.e., under conditions similar to those of the constant-pressure bomb method was investigated in our laboratory in 1950 [1]. The method of a free spherical flame was also applied in the investigations of turbulent combustion in [2] and [3]. However, under these conditions it was found impossible to change from the directly observed velocity of flame propagation, $U_B = dR/dt = U_t\rho_0/\overline{\rho}$, to the actual rate of combustion U_t relating to the fresh gas because the mean value of the density of the gas in a spherical turbulent flame in which the combustion zone is filled with fresh, burning and burnt gas could not be determined. This fact was taken into account in [1 – 2] where the measurements were limited to U_B. On the other hand, in [3], the magnitude $\rho_0/\overline{\rho}$ in a spherical turbulent flame was incorrectly identified as the theoretical degree of propagation corresponding to the adiabatic temperature of the flame. This assumption would be correct only if the width of the zone of turbulent combustion was comparable with the width of the laminar flame. Thus, the application of the method of a free spherical flame for the determination of U_t was found possible only when the mean density of the gas enclosed in the flame could be determined by an independent method. This condition has been realized in the new method of studying the development of a spherical turbulent flame in an enclosed space. The measurements were made in a bomb (shown in Fig. 1) of a nearly spherical shape of R = 70 mm, equipped with four stirrers (2) driven by electric motors (1). It will be shown later that in this way a uniform intensity of the isotropic turbulence in the whole volume is achieved. The mixture was ignited by means of a spark in the center of the bomb. The flame spread was recorded through two parallel glass windows (6) by means of a schlieren camera with objectives of 140 mm diameter, the film speed being 4000 pictures per sec. Two piezo-quartz pressure indicators (7) (only one indicator is shown in Fig. 1) were used for pressure recording; one highly sensitive pressure indicator was used in the initial stage of combustion, and the other for recording the pressure of combustion up to the maximum pressure. The flame recording was made for the initial stage (45 mm radius) in which the increase in pressure $P/P_0 \leq 1.2$, whereas the maximum increase in pressure, corresponding to complete combustion was $P_m/P_0 = 6\text{-}8$. Under these conditions, one could ignore the ignition of the fresh mixture during the combustion process.

Figure 2 shows two specimens of the film of the flame development in a calm gas (upper row, laminar flame) and in turbulent gas (lower row). In the second case, the visible velocity of the flame propagation was determined from the rate of increase of the radius of the circular surface area equal to the projection of the flame. The pressure, recorded as a function of time P(t) directly during the experiment, can be reevaluated as a function of radius, P(R).

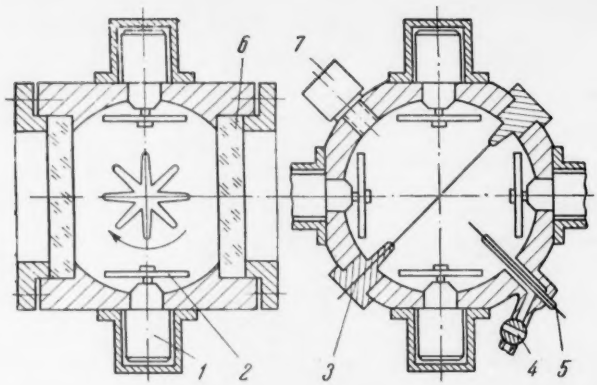

Fig. 1.

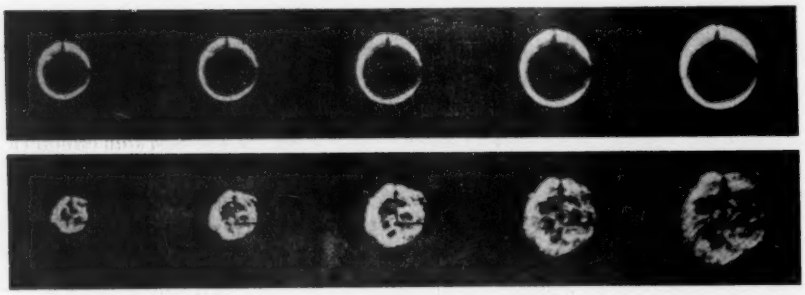

Fig. 2.

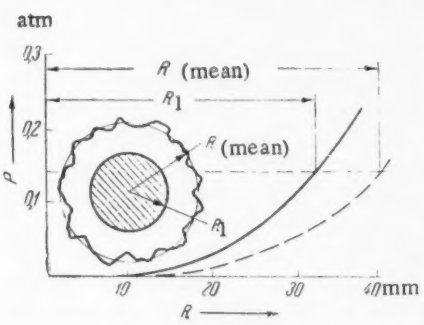

Fig. 3.

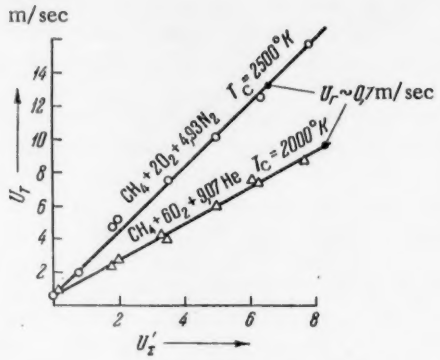

Fig. 4.

It is seen from Fig. 3 that in the turbulent flame the increase in pressure is smaller than in the laminar flame of the same radius and this is directly reflected by the larger extent of the combustion zone in the turbulent flame. Taking into account the fact that the relative pressure increase $\Delta P/(P_m - P_0)$ represents the combusted portion of the sample, one can determine from the material balance of the material enclosed in the spherical envelope of the turbulent flame the degree of expansion in the turbulent flame:

$$\bar{\varepsilon} = \rho_0 / \bar{\rho} = \frac{R_t^3 \rho_0}{R_1^3 \rho_c + (R_t^3 - R_1^3)\rho_0}, \qquad (1)$$

Where R_l and R_t are the respective radii of the laminar and turbulent flame for the same pressure increase; ρ_0 and ρ_c are the densities of the fresh gas and of the combustion products, respectively, at the adiabatic temperature of the flame. By recording the propagation of the laminar and turbulent flames in parallel experiments with the use of the same mixture we can determine directly the actual average expansion ϵ in the turbulent flame and, hence, the velocity of turbulent combustion $U_t = \frac{dR}{dt} / \bar{\epsilon}$. The method of determining the mean density of the gases in the turbulent flame, which is based on comparing the radii of the laminar and turbulent flame for the same pressure increase, is free of errors which occur when $\bar{\rho}$ is determined directly from ΔP and $\Delta P/\Delta R$ as it was done in the determinations in spherical laminar flames [4].

Beginning from the minimum radius suitable for measurements ($R \approx 10$ mm) the value dR/dt remains practically constant within the limits of the field of observation. The ratio R_t/R_l does not vary more than 3% , and the ratio $(R_t/R_l)^3$ not more than 10% . Hence, the value U_t is also constant during the combustion stage when no noticeable pressure increase takes place. This reflects the fact that the combustion proceeds with constant physical and chemical properties of the mixture and under conditions of constant turbulence intensity. The intensity of the turbulence, controlled by the number of revolutions of the stirrers was measured by means of a compensated thermoelectric anemometer, ÉTA 5A [5] at various distances from the center and at various positions of the filament; variations in the turbulence intensity within the field under study constituted ± 20% and the variations in the isotropy constituted ±15%.

The measurements of the mean value of the anemometer current give the magnitude of the mean velocity which represents the result of averaging the absolute values of the projections of the velocity on the plane perpendicular to the filament. Experiments show that this value remains constant for any position of the filament (except at very low speed of the stirrers). It means that in an enclosed space and with a sufficiently vigorous mixing of the gas there is no directional velocity of the flow and that the mean velocity determined is a measure of the mean value of the absolute intensity of the turbulence $|\overline{U'}|$. It is obvious that one cannot, essentially, apply the concept of the relative intensity of the turbulence of these conditions. The analysis of the oscillograms shows that high frequency pulsations, which contribute to the process of turbulent diffusion, are superimposed on the value $|\overline{U}|$. A measure of the intensity of these pulsations is the magnitude $(\overline{u'^2})^{1/2}$, measured as a variable component of the instantaneous velocity recorded. On the average $|\overline{U'}| / (\overline{u'^2})^{1/2} \approx 3$. As a general measure of the intensity of the turbulence, one should take the value

$$U'_\Sigma = \{|\overline{U'}|^2 + \overline{u'^2}\}^{1/2}. \qquad (2)$$

It is seen from Fig. 4 that for various mixtures and at a constant velocity U_c of the laminar combustion, U_t increases linearly with the intensity of the turbulence

$$U_T = a \cdot U'_\Sigma + b, \qquad (3)$$

where the coefficient a increases from 1 to 2 for low temperatures of combustion, and possibly even more for higher temperatures.

LITERATURE CITED

[1] N. N. Zagryazkin, A Study of the Velocity of Flame Propagation in Turbulent Gas Stream [in Russian] Thesis, Moscow, 1952.

[2] H. L. Olsen and E. L. Gayhart, Jet Propuls. 25, No. 6, 276 (1955).

[3] R. E. Bolz and H. Burlage Jr., Jet Propuls. 25, No. 6, 265, 283 (1955).

[4] A. S. Leah, Phil. Mag. 34, 795 (1943).

[5] E. S. Semenov, Pribory i technika eksperimenta, No. 1, 93 (1958).

Received June 5, 1959

THE SPECTRA OF PARAMAGNETIC ELECTRON RESONANCE AND THE KINETICS OF THE ACCUMULATION OF RADICALS FORMED DURING THE IRRADIATION OF FROZEN AQUEOUS SOLUTIONS OF SODIUM NITRATE BY FAST ELECTRONS

Yu. N. Molin, V. A. Sharpatyi, and N. Ya. Buben

L. Ya. Karpov Physicochemical Research Institute

(Presented by Academician V. N. Kondrat'ev, May 27, 1959)

In literature we find assumptions that radicals participate in the processes of radiolytic reduction of nitrate to nitrite. These assumptions are based on the results of the analysis of final products [1, 2, 3] but no attempts have been made to determine the radical products directly. It is also of interest to obtain evidence of the mechanism of the radiolytic transformation of nitrate in frozen solutions. It has been assumed until now that under these conditions the diffusion of the intermediate products is reduced to a minimum and the radiolytic transformation of the dissolved substance is caused mainly by the direct action of the radiation [4, 5, 6].

By means of an apparatus [7] for investigating the spectra of paramagnetic electron resonance (p.e.r.) during the irradiation by fast electrons (1.5 Mev), spectra of frozen aqueous solutions of sodium nitrate (at various concentrations of $NaNO_3$ and various pH of the solution) were taken and the kinetics of the accumulation and disappearance of the radical products was studied by the method described in [8]. The majority of the measurements were made at a temperature of approximately −145°C. At this temperature, radicals formed from water have a fairly high mobility [9, 10, 11] and can enter into the reaction with the dissolved substance. At the same time, radicals which are formed during the irradiation of frozen solutions of $NaNO_3$ are stable under the conditions that were found in our experiments. A rapid disappearance of these radicals takes place only when the temperature is increased to −90°C.

Spectra of p.e.r. of 1 M solutions of $NaNO_3$ in alkaline and neutral media, irradiated at −145°C, are shown in Fig. 1, a and b. The main characteristics of p.e.r. spectra of radicals are given in Table 1. The form of p.e.r. spectra does not change noticeably when the concentration of $NaNO_3$ is changed within the limits within which the kinetics of radical accumulation were investigated (see Fig. 2). Nevertheless, these spectra differ sharply from the p.e.r. spectrum of irradiated polycrystalline sample of dry $NaNO_3$ salt obtained under the same conditions. In the latter case, the spectrum consists of a single asymmetric line with hardly noticeable "branches" (Fig. 1c). The analysis shows that the form of p.e.r. spectra for alkaline and neutral solutions depends on the presence of at least three radicals. Radicals I and II are present in both cases, their spectra have a triplet hyperfine structure (hfs) which is due to the interaction of an unpaired electron with an N^{14} nitrogen nucleus (nucleus spin I = 1). The central components of the triplets are superposed giving a single line, the area under the line being nearly the same as the area of the side components. Apart from the N^{14} nucleus, the nuclei of H and Na^{23} could give hyperfine structure spectra. However, experiments with solutions in which all the H atoms were replaced with D, and experiments with the $Ca(NO_3)_2$ solution showed that there is no change in hfs spectra in those cases. Hence, radicals I and II contain the nitrogen nucleus, i.e., they are formed from the nitrate ion. The magnitude of the hyperfine resolution in radical I is very close to the resolution of the NO_2 molecule frozen in a matrix of argon at 4°K (115.6 oersted) [12]. Similar values were obtained for the NO_2 molecule in the gas phase (approximately 96 oersted) [13]. Therefore, one can assume that radical I is probably NO_2. In the elucidation of the mechanism of the radiolytic reduction of nitrate in aqueous solutions, it is assumed that H atoms

TABLE 1

Radical	Number of component of hyperfine structure	Distance between extreme components (oersted)	g-factor
I	3	110	~2.00
II	3	62	~2.00
III	1	–	2.015
IV	1	–	~2.04

formed from water join the NO_3^- ion and produce an ion of hydronitric acid, HNO_3^- [3]. The nitrogen atom is quadrivalent and carries an unpaired electron. It can be assumed that radical II is HNO_3^-. The absence of an additional hyperfine resolution in the radical on account of the interaction of an impaired electron with an H atom requires special study, since H atoms which are in the β-position with regard to the free valence in alkyl radicals usually take part in the hyperfine resolution. It is not impossible, however, that in the given case the structure of the radical prevents this interaction from taking place.

Fig. 1. Paramagnetic electron resonance spectra of irradiated solutions: a) 1 M $NaNO_3$ solution: the spectra of 0.5 M $NaNO_3$ and 0.5 M HNO_3 solutions are shown by the dotted line: b) 1 M $NaNO_3$ solution in alkaline (1 M NaOH) medium: c) polycrystalline $NaNO_3$ salt at −145°C. A is the intensity of absorption.

It is interesting to note that the lines of radical II disappear completely in an acid medium (0.5 M HNO_3, 0.5 M $NaNO_3$), as was found in our experiments (see dotted line, Fig. 1a). This result can be compared with a well-known fact that the salts of hydronitric acid exist only in an alkaline medium. It would be interesting in this connection to investigate the p.e.r. spectra of the salts of hydronitric acid.

It is seen from Fig. 1 that line III is found in neutral and acid media and line IV in an alkaline medium only. Tests showed that frozen alkaline solutions give very weak p.e.r. signals when irradiated under the same conditions. Therefore, one can assume that in the presence of alkali a transformation of radical III (or any other primary radical producing radical III) into radical IV takes place. The absence of the hyperfine structure of radicals III and IV indicates that the unpaired electron in these radicals is localized on oxygen atoms whose nuclei have no magnetic moment. A considerable difference in g-factors of these radicals from the g-factor of a free electron (2.0023) signifies that extent of the delocalization of the orbit of the unpaired electron in these radicals is small. Apparently, radicals which have these properties could only be the peroxide type radicals

formed from the NO_3^- ion, or radicals O^-, O_2^-, HO_2 and other radicals containing no nitrogen atoms. For the formation of peroxide-type radicals one could suggest, for instance, the following scheme:

$$NO_3^- + OH \rightarrow HON(OO')O^- \left(-O-N\begin{matrix}O-O'\\ \diagdown\\ \diagup\\ O-H\end{matrix}\right).$$

where the presence of the hydroxyl,* formed from a water molecule, is assumed. The narrower line III can be ascribed to this type of radical and the disappearance of the line in the presence of an alkali can be due to the instability of the peroxide radical in the alkaline medium or to the reactions which remove the free radical, for instance: $OH + OH^- \rightarrow O^- + H_2O$. In the latter case, the appearance of a wide line IV in the alkaline medium should be attributed to the formation of a hydrated O^- ion. The presence of the residual orbital moment in such an ion subjected to the action of intracrystal fields could cause a substantial change in the g-factor and a widening of the line. Line IV can be apparently explained, apart from O^-, by the formation of such radicals as O_2^- or HO_2. Unfortunately, there is not enough information in literature on the spectra of radicals of this type and on the effect of intracrystal fields on the form of spectra to identify radicals III and IV unequivocally.

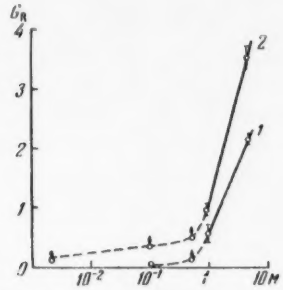

Fig. 2. Radical yield G_R as the function of the $NaNO_3$ concentration: 1) in neutral solution and 2) in alkaline (1 M NaOH) solution at −145°C.

TABLE 2

Sample	G_R	$G_{NO_2^-}$ (equiv)
1*M* $NaNO_3$, 1*M* NaOH, air	1,1	1,0
5*M* $NaNO_3$, 1*M* NaOH, air	2,4	3,2
1*M* $NaNO_3$, 1*M* NaOH, nitrogen	1,0	3,2
1*M* $NaNO_3$, 1*M* NaOH, nitrogen	0,9	2,7
5*M* $NaNO_3$, 1*M* NaOH, nitrogen	3,3	8,7
5*M* $NaNO_3$, 1*M* NaOH, nitrogen	3,8	8,4

To obtain some data on the mechanism of the formation of radicals, we investigated the kinetics of the accumulation of these radicals at various concentrations of nitrate in neutral and alkaline (1 M and 5 M NaOH) solutions. It was established by special tests that the yield of radicals is independent of the nature of the gas dissolved in the solution. Figure 2 shows how the radiation yield of radicals changes with the change in $NaNO_3$ concentration in the solution. In experiments with the solutions of concentration $\leq 10^{-1}$ M, large dimensions of the samples resulted in a certain systematic error in the determination of the dose and hence in too low a value of G_R. One could assume that the rise in G_R at high concentrations of nitrate ion is connected with the predominance of the mechanism of the direct action of the radiation on NO_3^- under these conditions. The fact, however, that the form of the p.e.r. spectra is independent of the concentration of the nitrate indicates that the mechanism of radical formation is the same for all concentrations. This fact as well as the high absolute value of G_R and the sensitizing effect of the alkali (c. f. 1 and 2 in Fig. 2) on the formation of radicals, prompt one to conclude that the indirect action of radiation is predominant. The substantial difference between the p.e.r. spectra of irradiated solid $NaNO_3$ salt (where radicals are formed only due to the direct action of radiation) and those of its aqueous solutions confirm these conclusions indirectly. In the initial experiments, in which carbon dioxide could condense on the samples when the solution was frozen out on the thermocoupole, we observed weak H lines with characteristic resolution $\Delta H \approx 500$ oersted when irradiation was carried out at −180°C [15]. It is possible that the carbon dioxide, like some other acids which contain oxygen [16], stabilizes the H. The intensity of these lines weakens with the increase in the nitrate concentration. The H lines were absent in 5 M $NaNO_3$. These results can be taken as

*M. A. Proskurnin and V. D. Orekhov [14] pointed out the possibility of the reaction of hydroxyl with a number of oxidizing radicals ($Cr_2O_7^{2-}$, MnO_4^-, NO_3^-) resulting, in the formation of higher oxygen compounds of peroxide type.

an indication that H is brought into the reaction with NO_3^- ions. With sufficiently high $NaNO_3$ concentrations, this reaction 'intercepts' practically all the H atoms and thus prevents their stabilization.

To elucidate the role of radicals in the process of NO_2^- formation, we compared the values of G_R and $G_{NO_2^-}$. Table 2 contains the results of the experiments in which G_R and NO_2^- were determined on the same samples. The large difference between the values of G_R and $G_{NO_2^-}$ cannot, apparently, be explained by the fact that the main portion of the nitrite is not formed by the radical mechanism (it is seen from the data in Table 2 and from work [17] that the presence of oxygen in the solution has a strong inhibiting effect on the formation of NO_2^-). Of course, intermediate products which cannot be detected by the p.e.r. method (for instance, radicals which have very wide absorption lines, biradicals, isomerization products of nitrogen compounds) can be formed in the system under study.

The sensitizing action of alkali on the formation of radicals constitutes an interesting experimental result which should be studied in more detail. Experiments showed that an increase in the concentration of NaOH to 5 M in 1 M $NaNO_3$ results in an increase in G_R (up to 2.5) as well as in $G_{NO_2^-}$ (up to ~ 10). Such an action of alkali may be due to the effect of OH^- on the yield of primary products of the radiolysis. On the other hand, if we consider that the oxidizing component of the radiolysis of water, OH, suppresses the process of radical formation, then we could explain the sensitizing action of alkali by the removal of this component from the reversible oxidation reactions. It is possible that the suppression of the reversible reaction of the oxidation of the products of radiolytic transformation of nitrate in the liquid phase depends precisely on these processes [18].

The authors wish to thank V. N. Shamshev and A. T. Koritskii for their assistance in the experimental work, and Corresponding Member of the Academy of Sciences, V. V. Voevodski, Prof. M. A. Proskurnin and V. D. Orekhov for valuable discussions.

LITERATURE CITED

[1] V. A. Sharpatyi, Proceedings of the 1st All-Union Conference on Radiation Chemistry [in Russian], Izd. AN SSSR, 1958, p. 112.

[2] N. A. Bakh, V. I. Medvedovskii, et al., Proceedings of the 1st All-Union Conference on Radiation Chemistry [in Russian], Izd. AN SSSR, 1958, p. 25.

[3] V. A. Sharpatyi, V. D. Orekhov, and M. A. Proskurnin, Effect of Ionization Radiation on Inorganic and Organic Systems [in Russian], Izd. AN SSSR, 1958, p. 43.

[4] M. Cottin, J. Chim. Phys. 53, 915 (1956).

[5] M. Haissinsky and M. Lefort, J. Chim. Phys. 48, 429 (1951).

[6] M. Lefort, J. Chim. Phys. 47, 624 (1950).

[7] Yu. N. Molin, A. T. Koritskii et al., Doklady Akad. Nauk SSSR 123, 882 (1958).*

[8] A. T. Koritskii, Yu. N. Molin et al., Vysokomolekularnye coedineniya, 1, No. 8 (1959).

[9] M. S. Matheson and B. Smaller, J. Chem. Phys. 23, 521 (1955).

[10] B. Smaller, M. S. Matheson, and E. Yasaitis, Phys. Rev. 94, 202 (1954).

[11] J. A. Ghormley and A. C. Stewart, J. Am. Chem. Soc. 78, 2934 (1956).

[12] C. K. Jen, S. N. Foner, et al., Phys. Rev. 112, No. 4, 1169 (1958).

[13] J. G. Castle and R. Beringer, Phys. Rev. 80, 114 (1950).

[14] M. A. Proskurnin, Problemy fizicheskoi khimii, No. 1, 1958, p. 49.

[15] Science, 128, No. 3325, 623 (1958).

[16] R. Livingstone, H. Zeldes, et al., Phys. Rev. 94, 725 (1952); 96, 1702 (1954).

[17] V. A. Sharpatyi, V. D. Orekhov, and M. A. Proskurnin, Doklady Akad. Nauk SSSR 127, 1279 (1959).*

[18] V. D. Orekhov, A. I. Chernova, and M. A. Proskurnin, Collection of articles on radiation chemistry [in Russian] Izd. AN SSSR, 1955, p. 91.

*Original Russian pagination. See C. B. Translation.

A STUDY OF ABSORPTION LAYERS ON LIQUID METAL SURFACES

N. L. Pokrovskii and D. S. Tissen

M. V. Lomonosov Moscow State University

(Presented by Academician M. M. Dubinin, June 6, 1959)

From theoretical considerations, and then experimentally, during the study of the surface tension (σ) of liquid metal solutions it was shown that alkali metals have a significant surface activity on liquid mercury, tin, lead and bismuth [1]. Later on, a high surface activity was detected in the elements of the sixth group of the periodic system, vis.: tellurium on lead [2, 3], sulfur on copper [4], oxygen and sulfur on iron [5].

The object of the present work was to investigate the effect of the elements of the third and fifth groups of the periodic system on liquid tin. From among these elements we selected thallium and arsenic. For measuring the surface tension of metallic solutions, the method of maximum pressure in a drop [6, 7] was used. The solutions were prepared in vacuum ($\sim 1 \cdot 10^{-5}$ mm Hg). The tin used,* purified by zonal melting, contained less than $1 \cdot 10^{-3}$% weight %of impurities. Thallium and arsenic were approximately 99.99% weight %pure.

Measurements of σ of tin-thallium solutions were carried out in a temperature range of 270-400°C and with a thallium concentration from 0.18 to 1.96 at%. The densities of the solutions necessary for calculating σ were determined experimentally. Fig. 1. shows the graph $\sigma = f(N)$, where N is the atomic fraction of thallium. It is seen from Fig. 1 that with an increasing concentration of thallium the isotherms converge. This indicates that the temperature coefficient of the surface tension ($\partial \sigma / \partial T = K$) decreases. The isotherms intersect when thallium concentration is 1.96 at%; K becomes equal to zero. This variation of K is explained by a fall in the value of σ with an increase in temperature and with rise in the value of σ as a result of thallium desorption. All the isotherms, except one at 400°C, are convex toward the concentration axis and are expressed well by the Szyszkowski equation:

$$\sigma_0 - \sigma = \alpha \ln (1 + \beta N). \qquad (1)$$

The values of the constants α and β varied for different temperatures and were determined from experimental curves. The deviation of the values of σ, calculated with this equation, from experimental values did not exceed ± erg/cm^2. By differentiating Equation (1) with respect to N one can find the value of the limiting surface activity of thallium in tin solutions $G_0 = - \partial \sigma / \partial N_{N \to 0}$, equal to the product of the constants α and β. At temperatures of 270, 300, 350 and 400°C, G_0 has the values 2300, 2100, 1800 and 1200 respectively, i.e., it decreases with increasing temperature.

The surface tension of tin-arsenic solutions was studied in a temperature range of 300-450 °C and with an arsenic concentration from 0.50 to 5.90 at %. The density of these solutions was also determined. Figure 2 shows the function $\sigma = f(N)$ (N is the atomic fraction of arsenic). Similar to tin-thallium solutions, the isotherms converge and K decreases with an increase in the concentration of arsenic. One's attention is attracted to the linear character of surface tension isotherms at all the temperatures investigated. The slope of these lines determines the surface activity of arsenic on liquid tin, the activity remaining constant over the whole range of concentrations. At temperatures of 300, 350, 400, and 450°C, G_0 has the values 420, 370, 350 and

* The surface tension of tin, purified by zonal melting, was studied by N. L. Pokrovskii and D. S. Tissen.

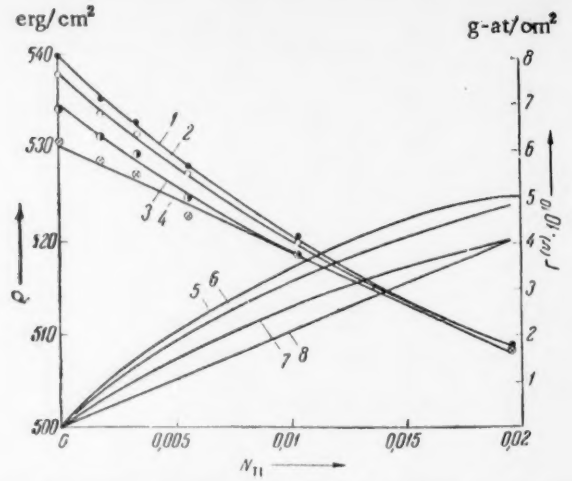

Fig. 1. Surface tension isotherms of tin-thallium solutions: 1) 270°C, 2) 300°C, 3) 350°C, 4) 400°C, and adsorption isotherms of thallium on the surface of liquid tin: 5) 270°C, 6) 300°C, 7) 350°C, 8) 400°C.

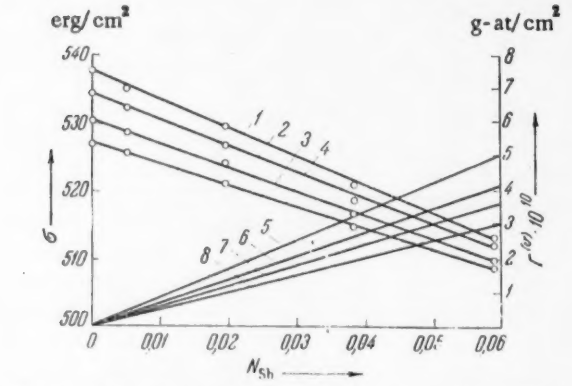

Fig. 2. Surface tension isotherms of tin-arsenic solutions: 1) 300°C, 2) 350°C, 3) 400°C, 4) 450°C; and adsorption isotherms of arsenic on the surface of liquid tin: 5) 300°C, 6) 350°C, 7) 400°C, 8) 450°C.

310 respectively, i.e., it increases with increasing temperature. The value of G_0 for arsenic is several times less than the value of G_0 for thallium, but at the same time both these impurities have a much lower surface activity than sodium [7] and tellurium [3] on tin.

The adsorption ($\Gamma_1^{(2)}$)of thallium and arsenic on liquid tin surfaces was calculated from the Gibbs equation

$$\Gamma_1^{(2)} = -\frac{a}{RT} \cdot \frac{\partial \sigma}{\partial a}.$$

The necessary data on the activity of thallium and arsenic were known for the tin-thallium system [8] as well as for the tin-arsenic system [9]. From the calculated values of $\Gamma_1^{(2)}$, the adsorption $\Gamma^{(\nu)}$ could be determined by the Adam-Guggenheim equation. As a result of the calculations made, it was found that for the solutions under study $\Gamma^{(\nu)} = \Gamma_1^{(2)}$ within the accuracy of the determination of $\Gamma_1^{(2)}$ from the experimental results. This is explained by the fact that the solutions studied were sufficiently dilute.

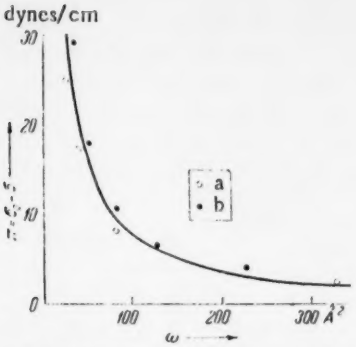

Fig. 3. Ideal isotherm of state of a gaseous two-dimensional layer at 300°C; a) for arsenic, b) for thallium.

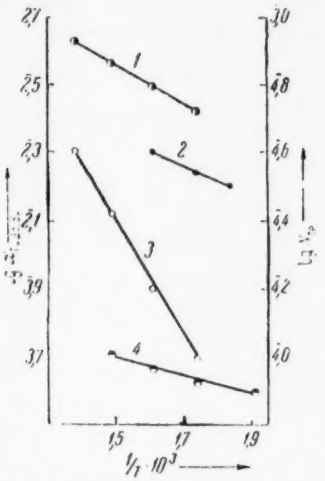

Fig. 4. Adsorption isosteres of arsenic (1), thallium (2), tellurium (3), and bismuth (4) on the surface of liquid tin ($\Gamma = 2 \cdot 10^{-10}$ g-at/cm^2).

The forms of the curves $\Gamma^{(\nu)} = f(N)$ for thallium and arsenic, as shown in Figs. 1 and 2, are different. The adsorption isotherms for tin-arsenic solutions are rectilinear and in this respect they are similar to the adsorption isotherms for tellurium on tin [2]. The adsorption isotherms for tin-thallium solutions are concave toward the abscissa and are similar in shape to the adsorption isotherm of sodium on tin [7]. It is seen from the graphs that the adsorption of thallium and arsenic on tin decreases with increasing temperature and this is in agreement with the established relationships.

From the adsorption value of thallium and arsenic one can calculate the surface areas ω per atom of these metals on the surface of liquid tin. The ω for arsenic was determined from the equation

$$\omega = \frac{1}{\Gamma^{(\nu)} + \delta C},$$

where C is the volume concentration of arsenic in tin solution, δ is the thickness of the surface layer, its value being taken equal to the diameter of an arsenic atom on the assumption of a monoatomic adsorption layer. For thallium $\Gamma^{(\nu)} \gg \delta$ c and $\omega = 1/\Gamma^{(\nu)}$. Figure 3 shows the results plotted in the coordinates π (dynes/cm), the surface pressure, the amount by which the surface tension is less than that of the pure tin, and ω Å^2, calculated values of area per particle of thallium or arsenic in the surface layer. The experimental points lie quite near the ideal isotherm of the gaseous two-dimensional film whose equation is

$$\pi\omega = kT.$$

Therefore the adsorption films of thallium and arsenic on liquid tin within the investigated concentration range can be regarded as the gas-phase type. The small deviations of the experimental points from the ideal isotherm can be explained by the repulsion between the particles in the surface layer in tin-thallium solutions, and by the attraction in the case of tin-arsenic solutions.

The calculation of the heat of adsorption of arsenic, thallium, tellurium,* and bismuth* on the surface of liquid tin. The heat of adsorption, Q_Γ, of impurities on the surface of liquid tin for the solutions being studied can be calculated from the relation $\Gamma = f(a, T)$. In the calculations, we used the equation for dilute solutions [10]

$$Q = -R \left[\frac{\partial \ln a}{\partial (1/T)}\right]_\Gamma.$$

The relation log a = f (1/T) for the adsorption value of $2 \cdot 10^{-10}$ g-at/cm^2 (for other values of adsorption from $1 \cdot 10^{-10}$ to $3.5 \cdot 10^{-10}$ g-at/cm^2 the slope of the isosteres remained constant) is shown in Fig. 4. The heat of adsorption Q_Γ was determined from the slope of the straight lines obtained (see Fig. 4). For tin-bismuth solutions the atomic fractions are identical with the activities since the system is an ideal one [11]. No values for the activities of tellurium in tin could be found in literature. Since, however, the solutions under study were very dilute, the activity of tellurium was taken to be equal to its atomic fraction.

* Data for tellurium and bismuth were taken from earlier papers [2, 15].

The calculated values of G_Γ for bismuth, thallium, arsenic, and tellurium were 1200, 2000, 2700, and 7700 cal/gram-atom respectively. It is interesting to note that the values obtained for the heat of adsorption were found to be comparable with the values for the physical adsorption of gases and vapors on solid surfaces [12]. For tin-arsenic and tin-thallium solutions the values of the heat of adsorption are very similar to the values of the partial molar heat of solution of arsenic and thallium in tin (at corresponding concentrations) viz: the heat of solution for thallium at 350°C is equal to approximately 1800cal/gram atom [8], and for arsenic at 630°C it is equal to approximately 1500 cal/gram atom [13].

The heat of adsorption of tellurium on tin is several times greater than the heat of adsorption of other additions. It is comparable with the heat of formation of an SnTe compound from liquid tin and solid tellurin [14]. At 300°C, the heat of formation of this compound is equal to 16300 cal/gram atom and it is approximately twice the value of the heat of adsorption of tellurium on lead. It is possible that the adsorption process in tin-tellurium solutions involves additional complications due to chemical reactions. It should be pointed out that the curves $\sigma = f(T)$ for tin-tellurium solution pass through a maximum [3]. In a certain temperature range these solutions have a positive temperature coefficient, σ, this fact being probably due not only to the tellurium desorption but also to the dissociation of the SnTe compound. This view is supported by the results of works [4, 5] in which the adsorption of oxygen and sulfur on liquid copper and iron was investigated. The calculated areas per oxygen or sulfur atom at maximum adsorption had values near to the values of areas per atom of these elements in the plane of maximum packing in FeO, FeS, CuS compounds respectively.

The authors wish to thank Prof. V. K. Semenchenko for his tireless interest in this work and Prof. A. V. Kiselev for valuable advice during the discussion of the results.

LITERATURE CITED

[1] V. K. Semenchenko, Surface Phenomena in Metals and Alloys [in Russian] Moscow, 1959.

[2] É. Kristian, Thesis, Moscow, 1954.

[3] N. L. Pokrovskii, Zhur. Inorg. Khim. 1, 1383 (1956).

[4] C. F. Baes and H. H. Kellogg, J. Metals 5, 643 (1953).

[5] F. A. Halden and W. D. Kingery, J. phys. Chem. 59, 557 (1955).

[6] N. L. Pokrovskii and M. Saidov, Fizika Metallov i Metalloved. 2, No. 3, 546 (1956).

[7] N. L. Pokrovskii and N. D. Galanina, Zhur. Fiz. Khimii 23, No. 3, 324 (1949).

[8] Y. H. Hildebrand and Y. N. Sharma, J. Am. Chem. Soc. 51, 462 (1929).

[9] Y. A. Yanko, A. E. Drake, and F. Hovorka, Trans. Electrochem. Soc. 89, 357 (1946).

[10] A. V. Kisilev, Uspekhi Khimii 15, No. 4, 456 (1946).

[11] H. Seltz and J. Dunkerley, J. Am. Chem. Soc. 64, 1392 (1942).

[12] S. Brunauer, Adsorption of Gases and Vapors [in Russian], Moscow (1948).

[13] R. O. Frantik and H. Y. McDonald, Trans. Electrochem. Soc. 88, 243 (1945).

[14] Y. H. McAteer and H. Seltz, J. Am. Chem. Soc. 58, 2081 (1936).

[15] V. K. Semenchenko, N. L. Pokrovskii, and V. B. Lazarev, Doklady Akad. Nauk SSSR 89, 1021 (1953).

Received May 28, 1959

COPOLYMERIZATION OF PARACHLOROSTYRENE WITH α-METHYLSTYRENE AND STYRENE UNDER THE ACTION OF ALKALI CATALYSTS

Ya. L. Spirin, A. R. Gantmakher, and Academician S. S. Medvedev

L. Ya. Karpov Physicochemical Scientific Research Institute

The relative reactivity of chlorine-containing monomers in anionic polymerization has not yet been investigated. We have carried out a study of the copolymerization of these monomers under the action of organic lithium and sodium catalysts in various media. The polymerization was carried out in vacuum and in nitrogen atmosphere under such conditions that air and moisture were prevented from entering the system. The amount of catalysts in the monomer mixture constituted 6% mole % with respect to the chlorine-containing monomer. The composition of copolymers was determined by means of the combustion of a weighed sample of polymer with metallic sodium and Na_2O_2 in a bomb and subsequent titration of Cl^- by the Volhard method.

On carrying out copolymerization we have established that the interaction of monomers which have relatively mobile chlorine atoms with lithium alkyls in accordance with the Würtz reaction proceeds at a high velocity and therefore there is no formation of polymers under these conditions. Thus, during the copolymerization of styrene with vinylchloride in heptane with ethyllithium, the detachment of chlorine is almost instantaneous even at −75°C. Neither is there any polymerization of chloroprene at 20°C.

However, owing to a lower rate of the decomposition of the catalyst during the polymerization and copolymerization of parachlorostyrene, which contains a relatively less mobile chlorine atom, it is possible to achieve the polymerization to the extent of up to 10-20%. The detachment of chlorine in the presence of organic lithium and sodium compounds results in a somewhat lower chlorine content in polymers. Thus, for instance, the polymer obtained from the polymerization of parachlorostyrene in benzene or triethylamine contained 23% chlorine (chlorine content in the monomer was 25.6%). This figure was taken for the calculation of the composition of copolymers.

The results on the composition of copolymers of parachlorostyrene – styrene and parachlorostyrene – α-methylstyrene systems, obtained with various catalysts and in various media, are given in Table 1.

It is seen from Table 1 that the composition of copolymers depends to a large extent on the nature of the catalyst and the medium.

On considering the dependence of the composition of copolymers on the condition of polymerization we came to the conclusion that there are two competing reactions of radical and anionic polymerization in these systems.

During polymerization with ethyllithium in carbon dioxide medium, the radical polymerization is predominant since the velocity of the anionic process is relatively low under these conditions [1] Experiments 1, 2, 3, and 10). The same result is also obtained when the initiation of the anionic polymerization is strongly inhibited Experiment 4). The copolymers obtained under these conditions are very similar in composition to the copolymers which were obtained during the polymerization of the same systems by means of the radical mechanism(γ-radiation, Experiments 9 and 12).

TABLE 1

Composition of Copolymers of Parachlorostyrene– styrene and Parachlorostyrene – α Methylstyrene Systems

Expt. No.	Second component	Parachlorostyrene content, % (weight)		Catalyst	Medium	Temperature of polymerization, °C	Yield, % (weight)
		initial mixture	copolymer				
1	Styrene	56,5	38	Ethyllithium	Benzene	20	9,35
2		56,5	42	Ethyllithium	Benzene	0	8,6
3		56,5	38	Ethyllithium	Benzene	—20	7,7
4		56,5	45	Na-triphenyl methyl	Ether	0	2
5		56,5	58	Ethyllithium	Ether	0	6,5
6		56,5	81	Ethyllithium	Triethylamine	0	9
7		39	75	Ethyllithium	Triethylamine	0	17,5
8		56,5	85	α-Na-naphthalene	Tetrahydrofuran	0	2,3
9		56,5	43	γ-radiation (radical)		0	6
10	α-methyl styrene	17,2	27	Ethyllithium	Benzene	0	1
11		17,2	88	Ethyllithium	Triethyl amine	0	3
12		17,2	31,5	γ-radiation (radical)		0	3

The formation of radicals in these systems takes place as a result of the reaction:

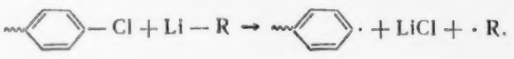

At a relatively low velocity of the reaction the conditions which are necessary for the reaction of polymerization to proceed according to the radical mechanism* may be established.

The polymerization which proceeds via the anionic mechanism is predominant if ethyllithium is used as the catalyst in triethylamine medium (Experiments 6, 7, 11) and also in the presence of α-sodium naphthalene Experiments 8). The relative velocity of polymerization by the radical mechanism is low under these conditions and the composition of copolymers indicates the reactivity of monomers with respect to corresponding carbanions.

The polymerization with ethyllithium in ether constitutes an intermediate case when the velocities of the polymerization by the radical and the anionic mechanisms are of the same order.

The copolymerization constants for the copolymerization by anionic mechanism were determined for the sytrene-parachlorostyrene system (methyllithium catalyst in triethylamine). Their values, α (styrene) = 0.1 ± ± 0.1 and β (parachlorostyrene) = 6.5 ± 0.1, indicate that the introduction of a chlorine atom in para-position in styrene causes a sharp increase in the reactivity of the monomer in anionic polymerization.

LITERATURE CITED

[1] Yu. L. Spirin, A. R. Gantmakher, and S. S. Medvedev, Zhurn. Vysokomolekul. Soed. 1, No. 8 (1959).

[2] T. L. Brown and M. T. Rogers, J. Am. Chem. Soc. 79, 1959 (1957).

Received July 6, 1959

* The low velocity of Reaction (1) can, apparently, be explained by the fact that the reaction is endothermic. If we assume that D(LiCl) = 115 kcal, D(Cl-phenyl) = 88 kcal, then the heat of reaction Q = 27-D(Li-R). The bond energy of Li-C in ethyllithium is estimated to be 57 kcal [2]. In the given system, Reaction (1) is, apparently, less endothermic owing to the formation of an organic lithium compound of a lower bond energy, the compound being formed when the monomer is attached to the catalyst. That the latter reaction takes place can be deduced from the appearance of coloration corresponding to the formation of carbanions which are conjugated with the phenyl ring and which appear when the catalyst is introduced into the mixture of monomers.

MOLECULAR ORBITALS OF $Cr(C_6H_6)_2$ (DIBENZENECHROMIUM) $Fe(C_5H_5)_2$ (FERROCENE OR BISCYCLOPENTADIENYLIRON) AND $Co(C_5H_5)_2^+$ (BISCYCLOPENTADIENYLCOBALT ION)

E. M. Shustorovich and M. E. Dyatkina

Institute of General and Inorganic Chemistry, Academy of Sciences, USSR

(Presented by Academician I. I. Chernyaev, June 5, 1959)

The electronic structure of the aromatic complex compounds of metals can be elucidated only on the basis of the method of molecular orbitals. In this way, a qualitative scheme for the molecular orbitals of $Fe(C_5H_5)_2$ and other aromatic complexes has been given [1]. We know of only one attempt at a quantitative evaluation of molecular orbitals of this type of molecules viz: $Fe(C_5H_5)_2$; the results of this work were published by Yamazaki [2] in the form of a letter to the editor in 1956.

In our systematic study of the aromatic complexes of metals we attempted to calculate molecular orbitals in other molecules of this type, such as dibenzenechromium $Cr(C_6H_6)_2$ and biscyclopentadienylcobalt ion $Co(C_5H_5)_2^+$. Since, however, we did not know the details of Yamazaki's calculation for ferrocene, $Fe(C_5H_5)_2$, we could not compare our results with the results obtained by Yamazaki for this molecule. Therefore, we calculated the molecular orbitals for $Fe(C_5H_5)_2$ too. All the calculations were carried out by Roothaan's [3] SCF LCAO-MO method (self-consistent field linear combination of atomic orbitals-molecular orbitals). It was assumed in the calculations that molecular orbitals of molecules are formed from the molecular orbitals of the C_5H_5 and C_6H_6 rings composed of $2p\pi$ orbitals of the carbon atoms and of nine $3d^5$ $4s$ $4p^3$ atomic orbitals of the central atom. One takes the combination of molecular orbitals of the rings and atomic orbitals of the central atom of the same symmetry. There result nine bonding molecular orbitals on which are accomodated 18 bonding electrons of the complex and several antibonding molecular orbitals (10 in ferrocene and in biscyclopentadienylcobalt, and 12 in dibenzenechromium) are located. In all the molecules the orbitals of types a_{1g}, a_{1u} and e_{1u} correspond to donor-acceptor bond owing to the electron pairs in the molecular orbitals of the rings and the free atomic orbitals of the central atoms; orbitals of type e_{2g} correspond to the dative bond owing to the electron pairs of the atomic orbitals of the central atom and the free molecular antibonding orbitals of the rings; the orbitals of the e_{1g} type in $Fe(C_5H_5)_2$ and $Co(C_5H_5)_2^+$ are formed from the molecular orbitals of the rings and the atomic orbitals which contain unpaired electrons (covalent bond), and in $Cr(C_6H_6)_2$ these orbitals correspond to the donor-acceptor bond. The following simplifying assumptions were made in the calculations: 1) the eighteen bonding electrons of the complex were assumed to be in the field of the positive core of the central atom (Cr^{6+}, Fe^{8+} and Co^{9+}) and of the core of the rings in which each carbon atom constitutes a single positive charge; 2) all the eighteen electrons were expressed by Slater wave functions with the effective charges given in Table 1; 3) in the nonorthogonal matrix all the nondiagonal terms S_{ij} ($i \neq j$) were assumed to be equal to zero; 4) in the calculations of the elements of the matrix H_{ij} (operator which includes single-electron terms only) all resonance integrals between the nonneighboring carbon atoms were assumed to be equal to zero for the neighboring atoms the value of $\beta_{cc} = 2.39$ ev was assumed. The matrix elements H_{ij} between atomic orbitals of the central atom and molecular orbitals of the rings of the same symmetry were assumed to be proportional to nonorthogonality integrals (see Table 2). In the calculations of the diagonal elements of the matrix H_{ij} corresponding to $2p\pi$ atomic orbitals of C atoms, the energy of the valence state ($W_{2p} = -11.28$ ev) was taken into account as is usually done in calculations of π-electron systems in conjugate hydrocarbons [4]; 5) in the electron-electron interaction matrix, only the integrals of the form

$$\int \frac{\varphi_i^2(1)\,\varphi_j^2(2)}{r_{12}}\,d\tau_1\,d\tau_2;$$

were taken into account; 6) it was assumed that the interaction between the $3d_{z^2}$ atomic orbitals with the molecular orbitals of the rings of the same symmetry could be neglected. The calculated values of the nonorthogonality integrals given in Table 2 confirm that such an assumption is permissible. The majority of the integrals were evaluated by the formulas which we obtained earlier [5], as well as with the use of Kotani tables [6]. The calculated energies of the molecular orbitals are given in Table 3.

TABLE 1

Effective Charges of Slater's Atomic Orbitals

Charge	C	Cr	Fe	Co^+
ζ_{2p}	1,6	—	—	—
$\zeta_{4s,\ 4p}$	—	0,8	1,0	1,1
ζ_{3d}	—	1,6	2,0	2,2

TABLE 2

Nonorthogonality Integrals

	$Cr(C_6H_6)_2$	$Fe(C_5H_5)_2$	$Co(C_5H_5)_2^+$
$s \mid a_{1g},\ 4s \mid$	0,242	0,359	0,443
$s \mid a_{1g},\ 3d_z2 \mid$	—0,078	0,023	0,066
$s \mid a_{1u},\ 4p_z \mid$	—0,081	0,063	0,209
$s \mid e_{1g},\ 3d_{xz} \mid$	0,397	0,339	0,276
$s \mid e_{1u},\ 4p_x \mid$	0,319	0,380	0,409
$s \mid e_{2g},\ 3d_{xy} \mid$	0,270	0,192	0,140

It is seen from Table 2 that the nonorthogonality integrals for donor-acceptor bonds of types a_{1g}, a_{1u} and e_{1u} increase in the order $Cr(C_6H_6)_2 < Fe(C_5H_5)_2 < Co(C_5H_5)_2^+$ and the nonothogonality integrals for dative bonds of type e_{2g} decrease in the same order, corresponding to the increase in the electronegativity of the central atom. The following conclusions can be drawn from the values of the energies of the molecular orbitals given in Table 3.* The lower bonding molecular orbitals for all molecules are placed in the following order according to their energy $a_{1g} < a_{1u} < e_{1u} < e_{1g}$. Then follow the e_{2g} and a_{1g}^* (atomic orbitals d_{z^2}) orbitals in $Cr(C_6H_6)_2$, and a_{1g}^* and e_{2g} in $Fe(C_5H_5)_2$ and $Co(C_5H_5)_2^+$. The calculated values of energies of higher occupied orbitals, which determine the ionization potentials of the molecules, are: 4.19 ev for $Cr(C_6H_6)_2$, 6.39 ev for $Fe(C_5H_5)_2$ and 11.13 ev for $Co(C_5H_5)_2$. Experimental results are available for $Fe(C_5H_5)_2$ only (7.05 ev) and they are in good agreement with the calculated values. The large values for the ionization potentials of $Co(C_5H_5)_2$ are natural since in this case the electron is detached from the cation. It is of interest to check the prediction that the ionization potential of $Cr(C_6H_6)_2$ is lower than that of $Fe(C_5H_5)_2$.

From the data on the bonding molecule orbitals given in Table 3 it follows that the coefficients of a atomic orbitals of the central atom are almost always smaller than those of the molecular orbitals of the rings. The coefficients of atomic orbitals for all types of bond increase in the order $Cr(C_6H_6)_2 < Fe(C_5H_5)_2 < Co(C_5H_5)_2^+$ together with the lowering of the orbits. This corresponds to a high force pulling the electron pairs from occupied molecular orbitals of the rings into free atomic orbitals of the central atom in donor-acceptor bonds, and a lower force pulling the electron pairs from occupied atomic orbitals of the central atom to free molecular orbitals of the rings in the dative bond in accordance with the increase in the electronegativity of the central atoms. One finds here the same regularity as in the nonorthogonality integrals.

* The energies of the molecular orbitals which we determined for $Fe(C_5H_5)_2$ differ from those obtained by Yamazaki in the following ways. While the energy which we obtained for the antibonding orbitals are positive (except for the a_{1g}^* orbital which has a small negative energy), all the antibonding orbitals calculated by Yamazaki have high negative energies (from −7.07 ev to −3.64 ev). The energy range for the binding orbitals which we determined is in agreement with the value determined by Yamazaki, and so is the position of the deepest a_{1g} orbital (−16.80 ev according to Yamazaki) of the second bonding symmetric orbital a_{1g} (−8.57 ev according to Yamazaki), although according to Yamazaki this is a hybrid orbital, and according to our calculations it is a pure d_{z^2} orbital. At the same time, the positions and the sequence of the remaining orbitals differ slightly. We are not in a position to consider the reasons for these differences since the details of Yamazaki's calculations have not been published.

TABLE 3

Molecular Orbitals of Complex Compounds and the Energies of Molecular Orbitals

Symmetry	Compound	Bonding molecular orbitals		Antibonding molecular orbitals,***
		orbitals	energy (ev)	energy (ev)
a_{1g}	$Cr(C_6H_6)_2$	$0,98a_{1g} + 0,22s$	−13,31	+3,21
	$Fe(C_5H_5)_2$	$0,87a_{1g} + 0,49s$	−16,05	−1,50
	$Co(C_5H_5)_2^+$	$0,79a_{1g} + 0,62s$	−20,84	−5,33
a'_{1g}	$Cr(C_6H_6)_2$	d_{z^2}	−4,19**	—
	$Fe(C_5H_5)_2$	d_{z^2}	−8,44	—
	$Co(C_5H_5)_2^+$	d_{z^2}	−13,20	—
a_{1u}	$Cr(C_6H_6)_2$	$0,998a_{1u} - 0,062p_z$	−12,73	+2,15
	$Fe(C_5H_5)_2$	$0,99a_{1u} + 0,10p_z$	−13,74	+0,54
	$Co(C_5H_5)_2^+$	$0,91a_{1u} + 0,41p_z$	−18,04	−5,20
e_{1u}	$Cr(C_6H_6)_2$	$0,94e_{1u} + 0,36p_x$	−10,72	+3,84
	$Fe(C_5H_5)_2$	$0,81e_{1u} + 0,59p_x$	−12,62	+1,52
	$Co(C_5H_5)_2^+$	$0,77e_{1u} + 0,64p_x$	−16,65	−1,96
e_{1g}	$Cr(C_6H_6)_2$	$0,96e_{1g} + 0,30d_{xz}$	−10,61	+10,12
	$Fe(C_5H_5)_2$	$0,93e_{1g} + 0,37d_{xz}$	−11,02	+6,20
	$Co(C_5H_5)_2^+$	$0,90e_{1g} + 0,44d_{xz}$	−14,20	+0,19
e_{2g}	$Cr(C_6H_6)_2$	$0,78e_{2g} + 0,63d_{xy}$	−4,76	+6,97
	$Fe(C_5H_5)_2$	$0,52e_{2g} + 0,85d_{xy}$	−6,39**	+4,92
	$Co(C_5H_5)_2^+$	$0,32e_{2g} + 0,95d_{xy}$	−11,13**	+0,57
e_{2u}	$Cr(C_6H_6)_2$	—	—	+2,19
	$Fe(C_5H_5)_2$	—	—	+2,23
	$Co(C_5H_5)_2^+$	—	—	−0,27

* We do not give the form of antibonding molecular orbitals since, if the nonorthogonality of normalized atomic orbitals φ_1 and φ_2 is neglected, the bonding and antibonding molecular orbitals are expressed as $\psi_{bond} = c_1\varphi_1 + c_2\varphi_2$ and $\psi_{bond} = c_2\varphi_1 - c_1\varphi_2$ ($c_1^2 + c_2^2 = 1$) respectively.

** The absolute value of the energy of this orbital, which is the outer occupied molecular orbital, corresponds to the first ionization potential.

*** $Cr(C_6H_6)_2$ has yet another two antibonding orbitals b_{1g} and b_{2u} which, however, are of no importance for our purpose.

TABLE 4

Distribution of Electron Density

Compound	Effective charge				Dipole moments (D)	
	central atom	both rings	one ring	each C atom	metal-C bond	metal-ring
$Cr(C_6H_6)_2$	+1,470	−1,470	−0,735	−0,122	0,27	1,23
$Fe(C_5H_5)_2$	+0,682	−0,682	−0,341	−0,068	0,14	0,55
$Co(C_5H_5)_2^+$	−0,118	+1,118	+0,559	+0,112		

The calculated effective charges of individual atoms in the molecules are given in Table 4. It follows from the calculations that the Cr atom in $Cr(C_6H_6)_2$ has a positive charge equal to +1.47, the Fe atom in $Fe(C_5H_5)_2$ has a charge of +0.68, and the Co atom in $Co(C_5H_5)_2$ has a negative charge equal to −0.118. This

indicates that the electrons in $Cr(C_6H_6)_2$ were displaced, as compared with neutral Cr and C_6H_6, from the metal to the ring and so the dipole moment of the metal-ring bond equal to ~ 1.2 D appeared. For $Fe(C_5H_5)_2$, the displacement is of the same sign but considerably smaller and the dipole moment of the metal-ring bond is reduced to 0.55 D. The effective charge of the Fe atom is much smaller than that which would correspond to ionic structure of the molecule ($Fe^{2+}2C_5H_5^-$). Unlike in neutral molecules, in $Co(C_5H_5)_2^+$ the electrons are pulled away from the ring toward the central atom to such an extent that they balance the initial positive charge of the cobalt: the positive charge of the total $Co(C_5H_5)_2^+$ cation is in the rings and is distributed between 10 C atoms. This arrangement of effective charges is also reflected by the strengthening of donor-acceptor bonds and the weakening of dative bonds in the order $Cr(C_6H_6)_2$, $Fe(C_5H_5)_2$, $Co(C_5H_5)_2^+$. The distribution of electron densities obtained is the consequence of the characteristics of donor-acceptor and dative bonds in aromatic complex compounds of metals. It follows from the form of molecular orbitals that the formation of donor-acceptor bonds of the central atom with the rings is established without a significant displacement of the π-electrons of the ring. At the same time, the corresponding bonding molecular orbitals are the deepest and make a substantial contribution to the stability of the complex compounds of the $Fe(C_5H_5)_2$ type. The orbitals which correspond to the dative bonds, e_{2g}, are most significant in complex compounds of the $Cr(C_6H_6)_2$ type and they provide for the resulting excess of π-electron density in rings in neutral complex compounds. The preservation of and even an increase in π-electron density in rings in complexes as compared with isolated rings may be the reason for the aromatic character of the complexes. The conclusions as regards the relative contributions of donor-acceptor and dative bonds to the stability of the molecule make it possible to improve the results which were obtained previously from the calculations of the energy of the valence state of the central atoms [7].

LITERATURE CITED

[1] H. H. Jaffé, J. Chem. Phys. 21, 156 (1953); W. Moffitt, J. Am. Chem. Soc. 76, 3386 (1954); E. Ruch and E. O. Fischer, Zs. Naturforsch., 7b, 1952 (1952); M. E. Dyatkina, Izv. AN SSSR, Otd. Khim. Nauk, 1959, 1025.*

[2] M. Yamazaki, J. Chem. Phys. 24, 1260 (1956).

[3] C. C. J. Roothaan, Revs. Modern Phys. 23, 69 (1951).

[4] R. G. Parr and R. S. Mulliken, J. Chem. Phys. 18, 1338 (1950).

[5] E. M. Shustorovich and M. E. Dyatkina, Zhur. Fiz. Khim. (in press).

[6] M. Kotani, M. Amemiya, et al., Table of Molecular Integrals, Tokyo, 1955.

[7] E. M. Shustorovich and M. E. Dyatkina, Zhur. Neorg. Khim. 3, 2722 (1958); M. E. Dyatkina and E. M. Shustorovich, Zhur. Neorg. Khim. 4, 402 (1959); E. M. Shustorovich and M. E. Dyatkina, Zhur. Neorg. Khim. 4, 553 (1959).

Received May 22, 1959

* Original Russian pagination. See C. B. Translation.

CRITICAL CONDITIONS FOR THE THERMAL EXPLOSION OF TETRYL

A. G. Merzhanov, V. G. Abramov, and F. I. Dubovitskii

(Presented by Academician V. N. Kondrat'ev, June 1, 1959)

Thermal explosion in condensed systems is a complex but little-studied phenomenon. Characteristic features of this phenomenon consist in the presence of various transformations of the state of aggregation and related processes (the removal of gaseous products from the zone of reaction, the dissolution of initial solid substance in liquid products of decomposition, etc.). These processes have a substantial effect on the kinetic relationships (heat evolution) as well as on the heat transfer. Some problems connected with the particular features of the kinetics of decomposition and thermal explosion of condensed substances have been discussed theoretically [1, 2, 3].

The present work was carried out as an experimental study of the main characteristics of the thermal explosion of melted tetryl and to explain the mechanism of heat transfer during the thermal explosion in the liquid phase.

A diagram of our apparatus for the study of the thermal explosion is shown in Fig. 1. The charge of the material was placed in a glass vessel of cylindrical shape with double walls between which the heat carrier (glycerol), heated in the thermostat to the experimental temperature, was circulated. The vessel and the tubes were insulated thoroughly with asbestos. The temperature difference between the thermostat and the glycerol in the vessel did not exceed 0.3°C. The temperature of the substance was measured by means of a copper-constantan thermocouple with one junction in a thin small-bore glass tube immersed in the substance and the other placed in the thermostat. The position of the thermocouple junction in the substance was not strictly fixed. The process of heating was recorded by means of an ÉPP-09 potentiometer. From the recordings of the instrument the conditions of the decomposition (above or below critical) were determined, as well as the induction period and the maximum pre-explosion temperature. By means of a rapid replacement of hot glycerol by cold, the reaction could be stopped at any chosen moment. The extent of the decomposition was determined by means of weighing the charge.

Our experiments were designed for the determination of the critical state* of the thermal explosion of melted tetryl. For a given size of the charge, we selected "by trial" two thermostat temperatures corresponding to explosion and nonexplosion conditions of decomposition. The mean value was taken as the critical temperature, T_{cr}. T_{cr} in our experiments was determined to an accuracy of ± 0.5°C. The induction period t_{ind}, was calculated from the formula

$$t_{ind} = t_{expl} - t_h + \eta_1 / W_0,$$

where t_{expl} is the time period from the beginning of the circulation of the heat-transfer medium to the time of explosion; t_h is the time of preheating; η_1 is the degree of decomposition during the time of preheating; W_0 is the initial velocity of the reaction at the experimental temperature T_0. The maximum temperature, t_{max}, for

* The critical state is the relationship between the temperature, size, and constants of the substance; this relationship defines the boundary between the two manners of decomposition (explosion and nonexplosion).

TABLE 1

Experimental Data on the Critical Conditions of Thermal Explosion of Melted Tetryl

Diameter of the charge, d, cm	Weight of the charge, m, g	Wall thickness of the vessel, d_w, cm	Experimental characteristics of the critical conditions				Calculated* values of critical temperature	
			temperature, T_{cr}, °C	induction period, t_{cr} min	preheating ΔT_{cr}, °C	degree of pre-explosion decomposition, η_{cr}	for conduction heat transfer, T, °C	for convection heat transfer, T, °C
4,04	434	0,15	136	378	50	—	120	152
4,35	296	0,165	138,5	300	44	0,56	122	152
3,72	186	0,21	142	170	45	0,47	125	150
3,22	120	0,12	145	116	50	—	127	158
3,11	108	0,135	145	124	34	—	128	157
3,09	106	0,11	143,5	169	42	—	128	159
3,04	101	0,11	145	111	40	0,53	129	160
2,60	60	0,15	149	62	48	0,50	131	158
2,55	60	0,15	148,5	67	28	—	132	158
2,11	33	0,145	155	31	48	0,55	135	160
2,10	33	0,145	152,5	39	39	—	135	161
2,0 (мет)	29	0,12	164	9	35	—	136	207
1,96	27	0,135	156,5	24	32	—	136	162
1,77	20	—	160,5	15	46	0,46	138	—
1,74	19	—	157,5	21	34	—	139	—
1,54	13	—	160,5	16	—	—	140	—
1,53	13	—	159	21	30	—	141	—
1,40	10	—	166,5	8	44	0,49	142	—

* The calculations were made with the use of equations given in work [3]. The values of the constants used were: heat of reaction [4], Q = 20 cal/cm^3: autocatalysis factor $\eta_0 = 0.2$; effective autocatalytic constant of the velocity of decomposition $K_2 = 10^{15.6} e^{-38000/RT}$ sec^{-1}; the degree of volume change $\mu = 0.23$; thermoconductivity of tetryl $\lambda_t = 3.5 \cdot 10^{-4}$ cal/cm·sec·°C; thermoconductivity of glass $\lambda_g = 1.9 \cdot 10^{-3}$ cal/cm·sec·°C; thermoconductivity of steel $\lambda_s = 1 \cdot 10^{-1}$ cal/cm·sec·°C.

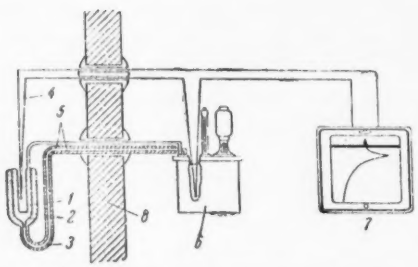

Fig. 1. Diagram of the apparatus for the study of the thermal explosion of condensed materials: 1) material charged; 2) reaction vessel; 3) heat insulation; 4) differential thermocouple; 5) tubes; 6) thermostat; 7) potentiometer; 8) shielding.

nonexplosion decomposition was calculated from a similar formula. The mean value between t_{ind} and t_{max} at temperatures near T_{cr} was taken as t_{cr}. The degree of preexplosion decomposition η_{cr} for the critical conditions was determined by stopping the reaction at the maximum heating temperature. The accuracy, however, of such a method of determining η_{cr} is not high.

The experiments were carried out in vessels of approximately 1.5-5.0 cm diameter in a temperature range of approximately 135-165°C (the melting temperature of tetryl is approximately 130°C). The ratio of the length of the charge to its diameter was 3 in all experiments. The weight of the substance was chosen accordingly (the density of the melted tetryl is approximately 1.53 g/cm^3). Measurements showed that the degree of decomposition during the time of preheating is small (about 1%). This fact indicates that our experiments on thermal explosion were designed correctly.

The main experimental results are shown in Table 1 and they allow us to draw the following conclusions.

1. The experimental values of T_{cr} lie between the values calculated on the assumption of purely conductive and purely convective heat transfer. This indicates that under our experimental conditions a complex heat transfer involving conduction and convection takes place. Special experiments showed that side by side with the temperature distribution in the reaction zone there is a significent temperature gradient across the wall of the

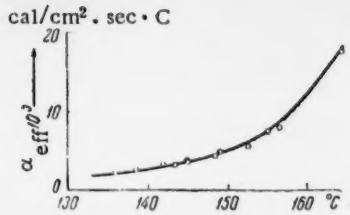

Fig. 2. Dependence of the effective heat transfer coefficient, α_{eff} on the experimental temperature, T_0.

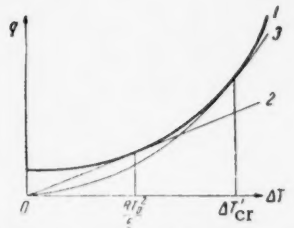

Fig. 3. A graphical interpretation of the cause of too-high critical preheating: 1) heat absorption curve; 2) heat removed at a constant heat transfer coefficient; 3) heat removed at an increasing heat transfer coefficient.

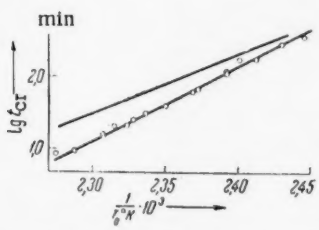

Fig. 4. Dependence of the induction period (for critical conditions) on the temperature, plotted on a semilog graph. The upper line was calculated on the assumption of a constant effective heat transfer coefficient during the decomposition process.

vessel. This fact is also confirmed by experiments carried out in a vessel made of stainless steel (see Table 1). Figure 2 shows the relationship between the effective heat transfer coefficient, α_{eff}, obtained by substituting the experimental results in the equation of critical state and the experimental temperature. With the increase in temperature the contribution of the convection heat transfer increases. Observation carried out by means of a PTUOM television apparatus showed that the convection heat mixing of the liquid phase by transfer mixed by the bubbles of the gaseous products.

2. The critical values of ΔT_{cr} are several times larger than the value calculated on the assumption of Semenov's theory [5] ($\Delta T_{cr} = RT_0^2/E \sim 10^0$. The too-high values of ΔT_{cr} can be explained by the increase in the effective heat transfer coefficient during the decomposition process. It is seen from the diagram (Fig. 3) that the curvature of the heat removal line displaces the tangential point to the region of higher temperatures. The increase in the effective heat transfer coefficient takes place due to an increase in the degree of mixing by means of gaseous products during the process of decomposition. This phenomenon is due to the fact that the rate of gas evolution and the viscosity change rapidly with temperature.

3. The relationship between the induction period and the temperature for the critical conditions is shown in Fig. 4 and may be expressed in the form

$$t_{cr} = 10^{-21,5} e^{49000/RT} \text{ sec.}$$

The experimental values of the induction period are smaller than the values calculated on the assumption of a constant heat transfer coefficient because the decomposition takes place at higher temperatures and consequently at a higher velocity. The value (equal to 49000 cal/mole) which determines the relationship between t_{cr} and the temperature is larger than the energy of activation (E = 38000 cal/mole). This is also explained by the dependence of α_{eff} on temperature.

4. The experimental values of the degree of the preexplosion decomposition are close to the value $\eta_{cr} = 0.48$ calculated theoretically (for constant α_{eff}).

5. It should be pointed out that in all the experiments the explosion was of a "soft flare" type, i.e., was not accompanied by a shock wave.

Thus, the study of the characteristics of the thermal decomposition of tetryl made it possible to conclude that the effective heat transfer coefficient increases during the decomposition process owing to the liquid phase being mixed by the evolving gaseous products. Apparently, this phenomenon is characteristic for all liquid and melted explosive substances.

LITERATURE CITED

[1] F. I. Dubovitskii, G. B. Manelis, and A. G. Merzhanov, Doklady Akad. Nauk SSSR 121, 668 (1958).*

*Original Russian pagination. See C. B. Translation.

[2] G. B. Manelis and F. I. Dubovitskii, Doklady Akad. Nauk, SSSR 126, No. 4 (1959).*

[3] A. G. Merzhanov and F. I. Dubovitskii, Doklady Akad. Nauk SSSR 124, 364 (1959).*

[4] F. I. Dubovitskii, Yu. I. Rubtsov, and G. B. Manelis, Izv. AN SSSR, Otd. Khim. Nauk (in press).**

[5] N. N. Semenov, Chain Reactions [in Russian] Leningrad, 1934.

Received May 28, 1959

*Original Russian pagination. See C. B. Translation.
**See C. B. Translation.